MODELING OF SMART COMPOSITE STRUCTURES

by

Krishna Sri Challagulla

Submitted
in partial fulfilment of the requirements
for the degree of

DOCTOR OF PHILOSOPHY

Major Subject: Mechanical Engineering

at

DALHOUSIE UNIVERSITY

Halifax, Nova Scotia August, 2006

Your file Votre référence
ISBN: 978-0-494-27638-9
Our file Notre référence
ISBN: 978-0-494-27638-9

DALHOUSIE UNIVERSITY

To comply with the Canadian Privacy Act the National Library of Canada has requested that the following pages be removed from this copy of the thesis:

Preliminary Pages
- Examiners Signature Page
- Dalhousie Library Copyright Agreement

Appendices
- Copyright Releases (if applicable)

DEDICATION

This work is dedicated to my mother Sanjeeva Rani and father Srinivasa Rao. Without their prayers and blessing, reaching this milestone so quickly with such satisfying results would have been impossible. I love you always.

TABLE OF CONTENTS

LIST OF TABLES

LIST OF FIGURES

LIST OF ABBREVIATIONS AND SYMBOLS

ABBREVIATIONS

BaTio3	Barium Titanate
CCC	Carbon-Carbon Composite
CFRP	Carbon Fiber Reinforced Polymer
CMC	Ceramic Matrix Composite
ER	Electrorheological Fluids
FFT	Fast Fourier Transform
FP	Fabry-Perot
FRP	Fiber Reinforced Polymer
GFRP	Glass Fiber Reinforced Polymer
GPa	Giga Pascal
IMC	Intermetallic Composites
kN	Kilo Newton
LVDT	Linear Variable Displacement Transformer
MEM	Micro-electro-mechanical
MMC	Metal Matrix Composite
MPa	Mega Pascal
MR	Magnetorheological Fluids
NiTi	Nickel-Titanium
PEEK	Polyetheretherketone
PEK	Polyetherketone
PEKK	Polyetherketoneketone
PMC	Polymer Matrix Composite
PMN	Lead-Magnesium-Niobate
PPS	Polyphenylene sulfide

PVA	Polyvinyl Alcohol
PVDF	Piezoelectric Material
PZT-4	Piezoelectric Material
PZT-5A	Piezoelectric Material
RTM	Resin Transfer Molding
SHM	Structural Health Monitoring
SMA	Shape Memory Alloy

SYMBOLS

P_{ijk}	Actuation or piezoelectric stress tensor
A_{ft}	Austenite finish temperature
A_{st}	Austenite start temperature
P_i	Body force
S^-	Bottom surface of smart composite plate
Θ	Change in temperature
R_k	Control Signal
A	Cross-sectional area of tendon
^oC	Degrees Celsius
u	Displacement field
G	Domain of a smart composite structure
e'	Eccentricity of ellipse
$\tilde{P}_{ijk}$	Effective actuation tensor
$\tilde{C}_{ijkl}$	Effective elastic tensor
$\tilde{K}_{ij}$	Effective thermal expansion tensor
$\tilde{P}_{ij}$	Effective actuation coefficients in contracted notation
$\tilde{C}_{ij}$	Effective elastic coefficients in contracted notation
$\tilde{K}_i$	Effective thermal expansion coefficients in contracted notation
$\langle b_{ij}^{\alpha\beta} \rangle$	Effective elastic coefficients for smart composite plate
$\langle b_{ij}^{*\alpha\beta} \rangle$	Effective elastic coefficients for smart composite plate
$\langle zb_{ij}^{\alpha\beta} \rangle$	Effective elastic coefficients for smart composite plate
$\langle zb_{ij}^{*\alpha\beta} \rangle$	Effective elastic coefficients for smart composite plate

$\left\langle d_{ij}^{k} \right\rangle$	Effective piezoelectric coefficients for smart composite plate
$\left\langle d_{ij}^{*k} \right\rangle$	Effective piezoelectric coefficients for smart composite plate
$\left\langle zd_{ij}^{k} \right\rangle$	Effective piezoelectric coefficients for smart composite plate
$\left\langle zd_{ij}^{*k} \right\rangle$	Effective piezoelectric coefficients for smart composite plate
$\left\langle \Theta_{ij} \right\rangle$	Effective thermal expansion for smart composite plate
$\left\langle \Theta_{ij}^{*} \right\rangle$	Effective thermal expansion for smart composite plate
$\left\langle z\Theta_{ij} \right\rangle$	Effective thermal expansion for smart composite plate
$\left\langle z\Theta_{ij}^{*} \right\rangle$	Effective thermal expansion for smart composite plate
C_{ijkl}	Elasticity tensor
S_f	Fatigue Strength
M_r	Factored moment strength
N_{ij}^{k}	Homogenization function
δh_2	Length of unit cell of smart composite plate
$\sigma_{ij}^{(k)}$	kth term in asymptotic expansion of stress field
P	Load
M_{ft}	Martensite finish temperature
M_{st}	Martensite start temperature
x_i	Macroscopic variable
y_i	Microscopic Variable
M_f	Moment due to factored loads
$d_{ijk}^{(r)}$	Piezoelectric strain tensor
d_{ij}^{*k}	Piezoelectricity unit cell function for smart composite plate
υ	Poisson's ratio

ε	Strain
e_{ij}	Strain tensor
σ	Stress
p_i	Surface traction vector along tangential plate direction
T_r	Tension force
$\alpha_{kl}^{(\theta)}$	Thermal expansion coefficients
K_{ij}	Thermal expansion stress tensor
Θ_{ij}	Thermal expansion unit cell function for smart composite plate
Θ_{ij}^{*}	Thermal expansion unit cell function for smart composite plate
δ	Thickness of smart composite plate
S^{+}	Top surface of smart composite plate
n	Unit normal vector
δh_1	Width of unit cell of smart composite plate
E	Young's Modulus

ACKNOWLEDGEMENTS

There are many people I would like to thank for their help and support during my research.

I would like to thank my supervisor Dr. Anastasis V. Georgiades for his support, and guidance throughout my research, as well as Dr. Alex Kalamkarov and Dr. Guy Kember for serving on the guidance committee.

Further, I would like to thank all my friends and well-wishers who have given me wonderful advice, support and friendship over the years.

Lastly, I would like to thank my loving family Dad (Srinivasa Rao), Mom (Sanjeeva Rani), and Brothers (Uday Bhaskar, Rama Krishna, and Gopi Krishna)) for their support. I love you always.

ABSTRACT

The method of asymptotic homogenization is used to develop three comprehensive micromechanical models pertaining to (i) thin smart composite plates reinforced with a network of orthotropic bars that may exhibit piezoelectric behavior; (ii) prismatic smart composite structures and (iii) three-dimensional composite structures with an embedded periodic network of isotropic reinforcements, the spatial arrangement of which renders the behavior of the given structures macroscopically anisotropic.

The models developed in this thesis allow the transformation of the original boundary value problems for the regularly non-homogeneous composite structure into simpler ones that are characterized by some effective coefficients. These coefficients are calculated from so-called 'unit cell' or periodicity problems and are shown to depend solely on the geometric and material characteristics of the unit cell and are completely independent of the global formulation of the problem. As such, the effective elastic, piezoelectric and thermal expansion coefficients are universal in nature and can be used to study a wide variety of boundary value problems associated with a structure of a given geometry. The models are illustrated by means of several examples of practical importance and it is shown that the effective properties of a given composite structure can be tailored to meet the requirements of a particular application by changing certain material or geometric parameters such as the type, size and relative orientation of the reinforcements. For models (i) and (ii), if the thermal and piezoelectric behavior of the materials is ignored and if the orthotropic nature of the constituents is reduced to that of isotropy, then the results converge to those of previous models obtained by either asymptotic homogenization, or stress-strain relationships in the reinforcements. For model (iii), if the 3-D arrangement of the reinforcements is reduced to a 2-D one then the model again is shown to converge to previous models.

1. INTRODUCTION

1.1. Introduction

Over the last few decades manufacturers, designers, and engineers recognized the ability of composite materials to produce high-quality, durable, and cost-effective advanced smart composite products. In the modern world, composites are used in many critical industrial applications such as the aerospace and military fields where weight, strength and durability are a big concern. Additionally, composite materials can also be found in our day-to-day lives, from the cars we drive, to the boats, railway coach interiors, and sporting goods.

In the present market where demands for product performance are ever increasing, composite materials have proven to be the best choice in terms of reducing costs and improving performance. Composites solve problems, raise performance levels, and enable the development of many new products.

Unlike traditional materials such as steel, composite materials have different mechanical properties in different directions, and can be custom designed to have the required strength in a specific direction. Composite properties (e.g. stiffness, thermal expansion etc.) can be varied to a high degree depending on the materials selected and the spatial orientation of the reinforcing materials within the expanse of the composite. The ability of composites to be adapted to wide range of applications often makes them the most attractive choice.

1.2. What are Composites?

A composite material may be defined as a material composed of two or more constituents combined on a macroscopic scale by mechanical and chemical bonds. The most commonly used composites, the polymeric ones, consist of a controlled distribution of reinforcing fibers in a continuous polymeric resin matrix. The fibers, by virtue of their high strength and stiffness, are the reinforcing components of the composite and are responsible for practically all the load-carrying characteristics of the composites. Due to the cohesive and adhesive characteristics of the matrix, it is responsible for holding the fibers in place and for transferring stress and strain to the reinforcing fibers. The matrix also protects the fibers from harsh environmental conditions. The fiber orientation as maintained by the matrix determines the properties of the composites.

Composites can be classified as fiber-reinforced, particle-reinforced, and laminated composites. The fiber-reinforced composites may contain continuous (long) or discontinuous (short) fibers. Composite properties such as strength and stiffness depend on the orientation and length of the reinforcements. Short fibers or whiskers can be embedded in a preferred orientation so that the composite behaves in an orthotropic fashion, or they can be randomly oriented so that the composite behaves like a quasi-isotropic material. Continuous fiber composites contain long fibers along which the stress is distributed. The continuous fibers may be all oriented in one direction or different families of fibers may be oriented in different directions. Depending on the spatial orientation of the fibers, continuous fiber composites may behave in an orthotropic, or a transversely-isotropic manner. Particle-reinforced composites consist of particles of different shape and size (spheres, flakes, rods) randomly embedded within the matrix. Due to the random nature of the dispersion of these particles in the matrix, the particle-reinforced composites are macroscopically homogeneous and quasi-isotropic. Laminated composites are those composites made of two or more layers of the reinforcements with each layer having two of its dimensions much larger than the third.

From a structural viewpoint, composites may also be classified as polymer matrix composites (PMC), metal matrix composites (MMC), ceramic matrix composites (CMC), carbon-carbon composites (CCC), intermetallic composites (IMC), or hybrid composites [Schwartz 1997a, 1997b].

1.3. Constituents

1.3.1. Reinforcing Materials

Although whiskers and particulate reinforcements are available for the manufacture of structural polymeric composites, the focus of attention in the recent years has been directed towards fibrous reinforcements. Both organic and inorganic fibers are used as reinforcements. The most common inorganic fibers include glass, and carbon, while aramid and asbestos are examples of natural/organic fibers. The type, amount, and orientation of fibers should be properly selected because they influence the following characteristics of a composite structure:

- Specific gravity
- Tensile strength and modulus
- Compressive strength and modulus
- Fatigue strength
- Electric and Thermal conductivity
- Cost

1.3.1.1. Inorganic Fibers

Inorganic fibers such as glass and carbon account for over 90% of the reinforcements used in today's composite industry.

1.3.1.1.1. Glass Fibers

Glass fibers are the most common reinforcing fibers for polymeric composites. In the 1930's the "Owens-Illinois Glass Company" developed a fiberglass manufacturing facility [Schwartz, 1992]. Glass is produced from silica sand, limestone, boric acid, and other elements. The principal advantages of glass fibers are low cost, high tensile strength, high chemical resistance, good processability, increased design flexibility and excellent insulating properties. Glass fibers are available in several types, the most common of which are E-glass, and S-glass. Typical values for the tensile modulus and strength are given in Table 1-1 [Daniel, 1994]. The main disadvantages are low tensile modulus, relatively high specific gravity, and relatively low fatigue resistance. E-glass is the cheapest of all commercially available reinforcing fibers. S-glass has the highest tensile strength among all the fibers in use. However the higher manufacturing cost of S-glass makes it unattractive for many applications and led to the manufacture of a less expensive form, S-2 glass fiber.

1.3.1.1.2. Graphite (Carbon) Fibers

The terms carbon and graphite fibers are typically used interchangeably, although graphite refers to fibers that have greater than 99% carbon composition. Carbon fibers, more than all other fibrous reinforcements, have provided the basis for the development of PMCs as advanced structural engineering materials. Carbon fibers are available with a variety of tensile moduli ranging from 207 GPa to 1035 GPa [Mallick, 1998]. Carbon fibers have high strength and stiffness, and a good resistance against stress rupture. As well, they exhibit good compressive strength and corrosion resistance. Due to their low coefficient of thermal expansion, carbon fibers are the best candidates for high temperature applications. The major limitations of this material are high cost, high thermal and electrical conductivities, and low impact resistance.

1.3.1.2. Organic Fibers

The most common organic fibers are Aramid, and Polyethylene. Table 1-2 [Mallick, 1988] illustrates some of the important physical and mechanical properties of various organic fibers. The main advantages of organic fibers include high strength, stiffness, and specific strength, excellent impact properties, and good corrosion resistance.

Table 1-1: Mechanical properties of typical fibers [Daniel, 1994]

Fiber	Fiber density, g/cc	Tensile Strength, GPa	Tensile Modulus, GPa
E-glass	2.54	3.45	72.4
S-glass	2.49	4.58	86.2
Polyethylene	0.97	2.70	87
Kevlar 49	1.44	3.62	130.0
HS Carbon, T300	1.76	3.53	230
Carbon, AS4	1.81	3.730	235
Carbon, HTS	1.82	2.83	248
Boron	2.60	3.44	407
Steel	3.08	0.58	207
Graphite, T-50	1.67	2.070	393
Silicon carbide	3.05	4.140	400
Silica	2.19	5.8	72.5

1.3.1.2.1. Aramid Fibers

DuPont first commercially introduced Aramid fibers in the early 1970's [Schwartz, 1997a]. There are a number of commercially available aramid fibers, the most common of which are Kevlar (DuPont), Twaron (Akzo) and Technora (Teijin). Among the properties that make aramid fibers attractive for a variety of engineering applications are high impact resistance, and low thermal and electrical conductivities. The main disadvantage of aramid fibers is that they are sensitive to compression.

1.3.1.2.2. Polyethylene Extended-Chain Fibers

Polyethylene fibers are commercially available in many forms and trade names such as Spectra, and Dyneema [Schwartz, 1997a]. Spectra PE fibers have the highest strength-to-weight ratio of all commercial fibers available. However, they only exhibit average strength and stiffness characteristics. PE has a very low melting point (135^0C) and is also susceptible to creep at temperatures above 100^0C. As a consequence, PE fibers are limited to low temperature applications.

Table 1-2: Properties of organic fibers [Mallick, 1988]

Material	Specific Gravity, g/cm^3	Typical diameter, µm	Tensile modulus, GPa	Tensile strength, GPa	Strain to Failure, %
Kevlar 29	1.44	12	83	3.6	4.0
Kevlar 49	1.45	11.9	131	3.62	2.8
Kevlar 149	1.47	12	179	3.45	1.9
Spectra900	0.97	38	117	2.59	3.5
Spectra1000	0.97	27	172	3.0	2.7

1.3.2. Matrices

The main function of the matrix in a fiber-reinforced composite is to transfer stress to and distribute stress between the fibers. The matrix also provides a barrier against adverse environmental conditions and protects the fiber surface from mechanical abrasions. It plays only a minor role in the tensile load-carrying capacity of a composite structure. However, the shear properties of a composite are largely influenced by the selection of the matrix. As mentioned before, matrices can be of the polymeric, metallic or ceramic type.

1.3.2.1. Polymeric Matrix

A polymer is defined as a long-chain molecule containing one or more repeating units of atoms joined together by physical or chemical bonds. These polymers are joined by a process called crosslinking. Polymers are divided into two major categories, thermoplastic and thermoset.

1.3.2.1.1. Thermoplastic Polymers

In a thermoplastic polymer, individual molecules are linear in structure with no chemical covalent bonds between them. Instead, weak physical bonds such as Van der Waals Forces hold them together. Thermoplastics are not crosslinked. Due to these weak bonds, any application of heat and pressure will result in these bonds breaking and subsequent motion of the pertinent molecules relative to each other. When a polymer cools down, the molecules freeze in their new positions and this results in a new solid shape. Thus the characterizing feature of a thermoplastic resin is that it can be melted and reshaped in a reversible manner. Some common types of thermoplastics include polyetheretherketone (PEEK), polyphenylene sulfide (PPS), polysulfone, polyetherketoneketone (PEKK), and polyetherketone (PEK) [Matthews and Rawlings, 1994].

1.3.2.1.2. Thermoset Polymers

In a thermoset polymer, the molecules are held together by means of strong chemical bonds, which form a cross-linked, rigid and three-dimensional network structure. Once these cross-links are formed, any application of heat or pressure cannot melt or reshape the thermoset polymer. The main advantage of thermosets is that they can be used at higher temperatures than thermoplastics and have better creep properties. Table 1-3 [Schwartz, 1997] compares some of the properties of thermosets and thermoplastics. The different types of thermoset resins available for composites include polyester, vinyl ester, epoxy, polyurethane, acrylic, phenolic, polyimide, and bismaleimide [Kaw, 1997].

1.3.2.1.2.1. Polyester Resin

Polyester resins are the most common and least expensive resins used in polymeric composite fabrication and when cured the resulting physical properties meet many of the needs of the commercial composite industry. They generally have a low viscosity and exhibit good processability. The most common applications of polyester resins are boat hulls, shower stalls, bath tubs, car bodies, molded furniture, and pipes. Depending on the chemical designation of the polymer backbone, polyester resins are categorized as orthophthalic, isophthalic, dicycolentadiene, chlorendics, and bisphenol-A [American Composite Manufacturers Association, 2006].

Orthophthalic acid based resins are also called general purpose resins. These resins are generally used where high mechanical, temperature, and corrosion resistance are not required. The main advantage of these resins is their low manufacturing cost.

Unlike orthophthalic acid based resins, their isophthalic counterparts have better mechanical, thermal and corrosion-resistance properties. The main disadvantages of isophthalic resins are that they have high styrene contents and are 10-20% costlier than orthophthalic resins.

Dicyclopentadiene-based resins are generally used where cosmetic finishes are critical and this is due to the low volumetric shrinkage. Like orthophthalic acid based resins these resins exhibit good mechanical and corrosion-resistance behaviour. Their other positive attribute is that the associated styrene content is usually in the 35-38% range. The main disadvantages are that these resins tend to be very rigid and lack the toughness of other resins.

1.3.2.1.2.2. Epoxy Resin

Epoxy resins are relatively expensive and take a long time to cure but exhibit low shrinkage and have excellent resistance to chemicals and solvents. Epoxy resins have been widely used in commercial applications such as aircraft components, pressure vessels and car bodies. Other advantages of epoxy resin include good mechanical properties (strength and stiffness), excellent chemical and weather resistance, and good fatigue strength. Their less attractive attributes include poor high temperature capabilities, the associated toxicity of the unused resin and relatively high manufacturing costs.

1.3.2.1.2.3. Vinyl Ester

Vinyl ester resins have excellent chemical resistance and tensile strength. Vinyl esters are formulated by reacting epoxy resin with methacrylic acid, forming a polymer that has characteristics similar to both polyester and epoxy.

Table 1-3: Properties of thermoset and thermoplastic polymers [Schwartz, 1997]

Property	Thermosets	Thermoplastics
Young's modulus (GPa)	1.3-6.0	1.0-4.8
Tensile strength (MPa)	20-180	40-190
Fracture toughness K_{Ic} (MPa $m^{1/2}$) G_{Ic} (KJ m^{-2})	 0.5-1.0 0.02-0.2	 1.5-6.0 0.7-6.5
Maximum service temperature (^{0}C)	50-450	25-230

1.4. Composites Manufacturing Processes

A wide range of manufacturing processes are available for the fabrication of composite structures. The examples include hand lay-up, chopped laminate process, filament winding, compression molding, pultrusion, reinforced reaction injection molding, resin transfer molding, vacuum bag molding, vacuum infusion processing, centrifugal casting and continuous lamination.

These manufacturing techniques can be classified, depending on the volume of production, as low, medium, or high volume production. The selection of manufacturing process depends on the resin and reinforcements used, complexity of the job, volume of production and cost. In the following section, three common manufacturing processes, namely hand lay-up, filament winding and pultrusion are briefly explained.

1.4.1. Hand Lay-up

Hand lay-up is the simplest and oldest of all composite fabrication processes. Hand lay-up method is suitable for making a wide variety of composite products including tanks, trucks, boats, housing, bathware and many others. In the manufacturing process, the first step is to apply a gel coat to the mold using a spray gun for a high quality finish. Once the gel coat is cured sufficiently, the reinforcements are manually placed on the mold followed by applying resin by pouring, brushing, spraying or using a paint roller (Figure 1-1). After removing excess resin by using FRP rollers, paint rollers, or squeegees, the laminate is cured at room temperature or in an autoclave. The autoclave is a special pressure vessel wherein complex chemical reactions take place, which in turn initiate and complete the consolidation of the composites. Before the autoclave curing, the part should be carefully processed and prepared. This involves the use of special equipment such as separators, bleeders, vacuum bags and others. This process is called vacuum bagging. A typical vacuum bag assembly is shown schematically in Figure 1-2 [Gibson, 1994]. Instead of applying resin after the fibers are laid-up on the mold, it is sometimes common to use prepregs.

The major advantages of hand lay-up include low-cost tooling, simple processing, and the ability to fabricate a wide range of parts. As well, sensors or actuators can be easily embedded into the composites to produce smart composite structures. The main disadvantages of hand lay-up are that it is a low-volume and labor intensive fabrication method.

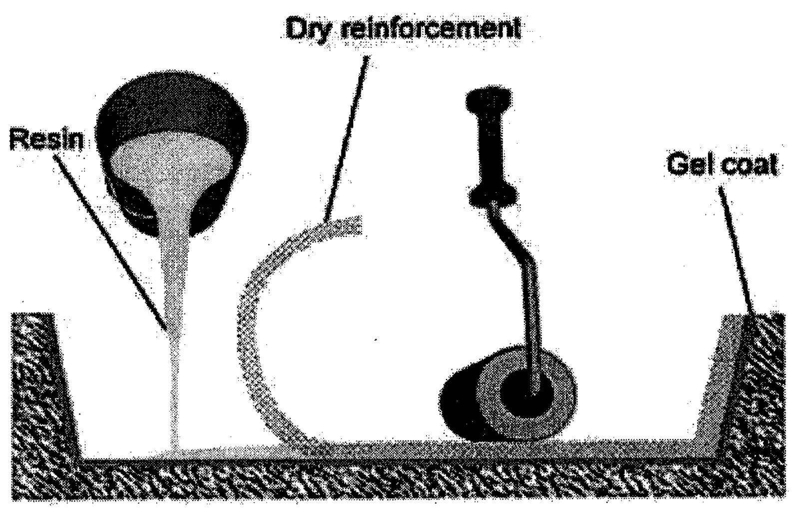

Figure 1-1: Hand Lay-Up process [Design inSite, 2006]

1.4.2. Filament Winding

The basis of the filament winding method is the high-speed precise lay-down of continuous reinforcements in a predescribed pattern over a rotating mandrel. Filament winding is an automated open molding process. It is used to produce hollow cylindrical products such as chemical and fuel storage tanks, pipes, stacks, pressure vessels, and rocket motor cases. A continuous strand roving is pulled from a series of creels into a liquid resin bath containing resin, catalyst, and other ingredients (Figure 1-3). Once the fibers exit from the bath, the resin-impregnated rovings are pulled through a wiping device that removes excessive resin from the rovings and controls resin coating thickness

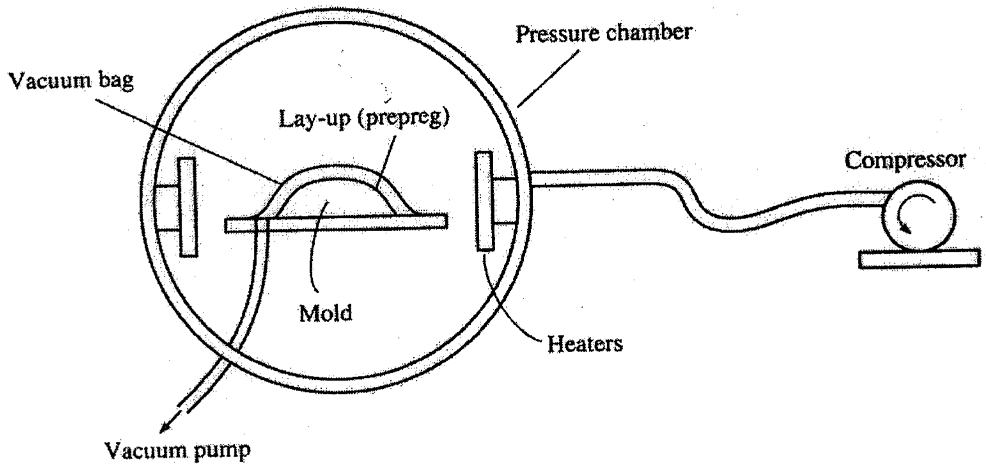

Figure 1-2: Autoclave molding [Gibson, 1994]

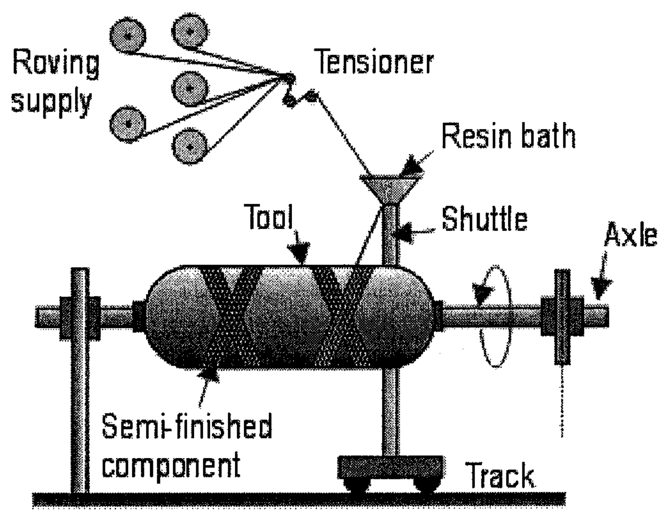

Figure 1-3: Filament winding process [AZoM™, 2005]

around each roving. Once the rovings are thoroughly wiped, they are subsequently placed onto a flat carrier and then positioned into a rotating mandrel. The filament is laid down in a predefined geometric pattern to provide maximum strength in the direction required.

The winding speed of the mandrel and transverse speed of the carriage are controlled to create the desired winding angle pattern. After sufficient layers of fibers have been applied, the structure is cured on the mandrel. Once the composite is cured, the structure is stripped from the mandrel. The molds are available in different shapes and sizes depending on the shape of the part to be build. The molds are usually made of steel or aluminum but in some cases they are made of wax to facilitate part removal. The main advantages of this process are that it produces high strength-to-weight ratio laminates and provides a high degree of control over structural uniformity and fiber orientation. Because this process is automated, it is not as labor intense as hand lay-up.

1.4.3. Pultrusion

Pultrusion is one of the fastest and most cost effective composites manufacturing processes. It is well suited to produce prismatic products such as prestressing tendons, reinforcing bars, structural shapes, beams, channels, pipes, tubing, and fishing rods. Pultrusion produces structures with a high degree of axial reinforcement and this makes it a prime candidate for manufacturing high quality low cost components for structural engineering applications. Fiber optic and other types of sensors as well as actuators can readily be embedded in a composite part during pultrusion and this renders the process ideal for the fabrication of smart composites.

In a pultrusion process, the first step is to pull the fibers from a series of creels into a resin bath containing the liquid resin together with appropriate amounts of catalyst and promoters. These resin-impregnated fibers are subsequently guided to the pultrusion die, which has the profile of the part to be manufactured. Strip heaters attached to the die provide the necessary thermal zones needed to initiate and complete the consolidation process. The product coming out of the die cools in ambient air, or forced air, as it is continuously being pulled by a set of rollers. A schematic of the pultrusion process is shown in Figure 1-4 [Kalamkarov et al., 2000a]. Figure 1-5 shows the overall pultrusion setup at Dalhousie University.

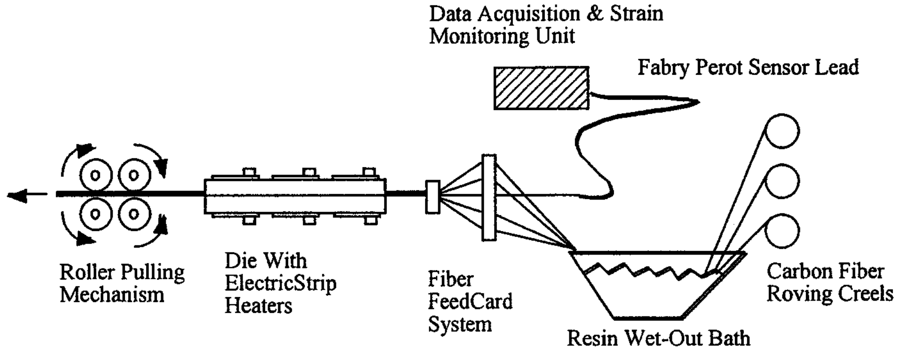

Figure 1-4: Schematic of pultrusion line for embeddement of fiber optic sensors [Kalamkarov et al., 2000a]

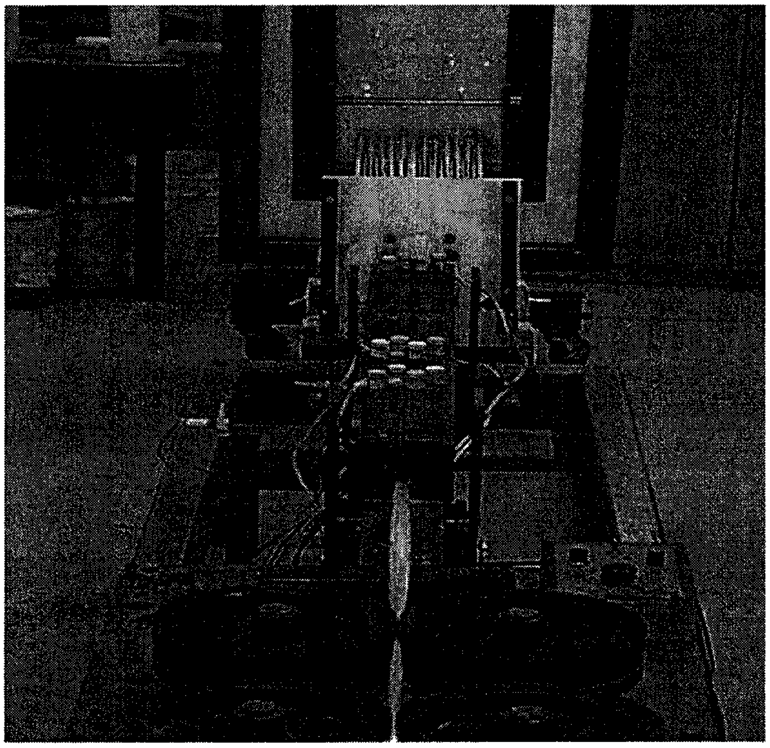

Figure 1-5: Schematic of pultrusion setup at Dalhousie University

1.5. Advantages of Composites

Composites offer a number of advantages over traditional materials like steel. When judiciously selected, composites usually offer one or more of the following advantages:

- High Specific strength
- Ability to fabricate complex profiles
- High degree of integration with other materials
- Inherent durability
- Tailorability of mechanical and physical properties
- Excellent fatigue strength
- Excellent impact resistance
- Excellent thermal resistance
- Reduced assembly time
- Ease of fabrication and shorter fabrication time

1.6. Contributions to Research

The author's contributions to research are as follows:

- Development of micromechanical model pertaining to prismatic smart composite structures with orthotropic reinforcements
- Development of micromechanical model pertaining to thin smart composite plates reinforced with a network of orthotropic bars
- Development of micromechanical models pertaining to general three-dimensional composite reinforced with a network of isotropic bars

2. SMART MATERIALS

2.1. Introduction

The high maintenance cost and limited service life condition often associated with traditional structural materials like concrete and steel can be significantly offset by the application of composites in the areas of civil engineering, aerospace, transportation industry, oil and gas, and marine engineering. At the same time, significant advancements in MEMS, telecommunications, and other fields, significantly facilitates the development of new and highly effective sensors and actuators. Their merge with the field of composites gave birth to the so-called smart composite materials. There are many definitions characterizing smart materials; a) adaptive structures, which incorporate sensors and actuators, b) materials which produce multiple responses to one input in a coordinate fashion, c) passive smart materials that provide information on their state and integrity, and active smart materials that can perform self-adjustment or self-repair as conditions change, d) smart materials and systems reproducing biological functions in load bearing structural systems.

The necessary characteristics of actuators and sensors have been expressed by (Jain 94) as follows: "Sensor materials should have the ability to feedback stimuli such as thermal, electrical, and magnetic signals, to the motor system in response to changes in the thermomechanical characteristics of the smart structures. On the other hand, actuator materials should have the ability to change the shape, stiffness, position, natural frequency, damping and/or other mechanical characteristics of the smart structures in response to changes in temperature, electric field and/or magnetic field. The most popular material systems being used for sensors and actuators are

1. Piezoelectric materials
2. Magnetostrictive and Electrostrictive materials
3. Shape memory alloys
4. Electrorheological and Magnetorheological fluids
5. Carbon nanotubes
6. Optical fibers
7. Electrochromic materials
8. Fullerenes
9. Smart Gels

Magnetostrictive materials, shape memory alloys, and electrorheological fluids are mostly used as actuator materials. Whereas, optical fibers are used as sensor materials. Among all these active materials, piezoelectric materials are most widely used because of their fast electromechanical responses, low power requirements, and relatively high generative forces.

In the following sections an overview of some of these smart materials is presented including definition, applications etc as reported in the literature.

2.2. Piezoelectric

The phenomenon of piezoelectricity describes the ability of the material (crystals) to generate electric voltage when subjected to mechanical stress or conversely, to get deformed when an electric field is applied. In the former case they work as sensors and in the latter case they work as actuators. Piezoelectrics have been the backbone of smart materials research since World War II and are manufactured around the world. To better understand the behavior of piezoelectric ceramics, a basic understanding of these ceramics should not be overlooked. To this end, next section gives a brief introduction of the history, the poling process, and piezoelectric effect.

2.2.1. History of Piezoelectric ceramics

Piezoelectricity is derived from the Greek word "piezo", meaning "pressure". In 1880, Jacques and Pierre Curie discovered a group of materials that exhibit unusual characteristics: when subjected to pressure, the crystals generate an electrical charge. W. Hankel in 1881 first suggested the term "piezoelectricity" and Lipmann deduced the converse effect which states that when this crystal was exposed to an electric field it lengthens or shortens according to the polarity of the fields. The major breakthrough in this field came with the discovery of barium titanate and lead zirconate titanate (PZT) in the 1940s and 1950s which enabled designers to employ the piezoelectric and the inverse piezoelectric effect in many engineering applications. The main advantage of these materials is that the composition, shape and dimensions of piezoelectric ceramics can be tailored to meet the requirements of a specific application.

2.2.2. Poling

In the basic form, the domains within a piezoelectric material are randomly oriented and hence the effect from individual domains cancels each other out. Consequently, they exhibit no piezoelectric properties and are isotropic. Since the direction of polarization among the neighboring domains is random, ceramic elements exhibit no overall polarization characteristics. (Figure 2-1) [APC International, 1999].

Poling is the common process used to orient the domains within a piezoceramic element. In the poling process, a strong direct electric field, usually at a temperature slightly below the curie point is applied to rotate and orient the domains in the direction of electric field (Figure 2-2) [APC International, 1999]. When the electric field is removed most of the dipoles are locked into a configuration of near alignment (Figure 2-3) [APC International, 1999] and the ceramic exhibits the piezoelectric effect. In the polarization process the element lengthens along the poling axis and contracts in both directions perpendicular to it, as a direct consequence of the piezoelectric effect.

2.2.3. Piezoelectric Effect

When mechanically stressed, poled piezoceramic elements (Figure 2-4(a)) generate a voltage. When the piezoelectric element is mechanically compressed along the direction of polarization, or stretched in the direction perpendicular to the direction of polarization, a voltage is developed across the electrodes that have the same polarity as the poling voltage (Figure 2-4(b)). If the applied load causes tension along the direction of polarization, and/or compression along the direction perpendicular to the polarization, the resulting voltage has polarity opposite to the poling voltage (Figure 2-4(c)) and this behavior is called direct piezoelectric effect. Conversely, the converse piezoelectric effect defines the change in shape of the piezoelectric elements, when a voltage is applied. When a voltage that has the same polarity as the poling voltage is applied to a piezoelectric element, the element gets stretched in the direction of poling voltage and as a consequence of Poisson's effect its diameter is reduced (Figure 2-4(d)). If a voltage of polarity opposite to that of poling voltage is applied, the piezoelectric element will become shorter in the poling direction and wider in the perpendicular direction (Figure 2-4(e)). If an alternating voltage is applied to the ceramic element, the element will lengthen and shorten cyclically, at the frequency of the applied voltage.

2.2.4. Application of Piezoelectric Ceramic

The availability of piezoelectric materials in many forms such as thin films, patches and rods, and their light weight has made them the strong candidates for smart composite

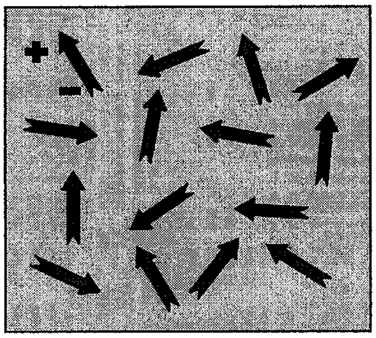

Figure 2-1: Random orientation of domains prior to polarization [APC International, 1999]

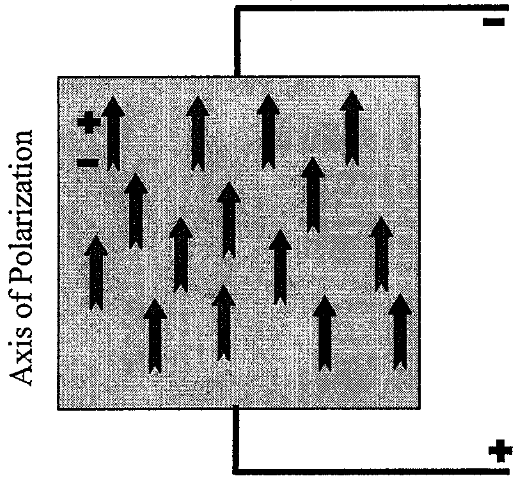

Figure 2-2: Polarization at high DC electric field [APC International, 1999]

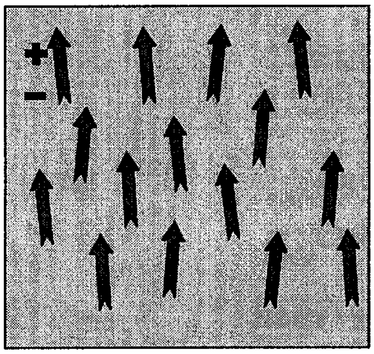

Figure 2-3: Orientation of domains after electric field is removed [APC International, 1999]

applications. Their ability to be easily integrated into structures makes them very attractive in structural control. Recent uses of piezoelectric ceramics in numerous applications have illustrated the feasibility of these materials in improving the performance of smart structures both as sensors and actuators. Piezoelectric ceramic patches can be used as multiple sensors to detect damages in composite structures using a variety of methods. Recently, piezoelectric ceramic patches have been considered for the in-situ monitoring of strains in composite structures. Rees et al. suggested the use of piezoelectric patches as sensors to monitor the crack growth in boron/epoxy repair sites [Rees et al. 1992]. Adali et al. [2000] considered a beam problem where the maximum vertical deflection of a laminated beam is to be minimized using one pair of actuators. Bruant et al. [2001] optimized both sensor and actuator locations, but considered them separately. Bent and Hagood [1997] have considered the use of piezoelectric fiber composites for structural actuation applications. Stack actuators have been studied among others, by Flint et al. [1994]. Samak and Chopra [1994], Song and Librescu [1994], Chen and Chopra [1994], and Haverly et al. [2001], studied the active vibration control of helicopter blades using stack actuators. Other researchers who have considered the use of piezoelectric ceramic patches for the purpose of strain monitoring, actuation and active vibration control include Barboni et al. [2000], Song et al. [2002], Bob et al. [2002], Fukunaga [2002], Kevin and Liangsheng [2004], Park et al. [2005], Kim et al. [2005], Sumant and Maiti [2006], and Seunghee [2006].

Currently, piezoceramic materials are used in military (hydrophones and sonobuoys, depth sounders, targets, telephony, sonar pingers, and adaptive optics), commercial (ultrasonic cleaners, welders, degreasers, thickness gauging, flaw detection, level indicators, geophones, delay lines, ignition systems, fans, relays, ink jet printers and strain guages), medical (ultrasonic cataract removal, ultrasonic therapy, insulin pumps, flow meters, ultrasonic imaging, and vaporizers), automotive (knock sensors, wheel balancers, radio filters, seat belt buzzers, thread wear indicators, air flow, fuel atomization, tire pressure indicator, and audible alarms), and consumer (Humidifiers, gas grill igniters, telephones, smoke detectors, microwave ovens, sneakers, cigarette lighters, lighting security, and ultrasonic sewing) products [Technical Insights, 1999].

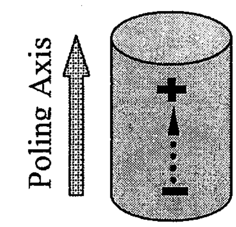

(a) Piezoceramic fiber after polarization

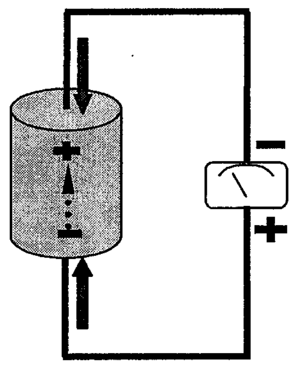

(b) Disk compressed along poling direction, generated voltage has same polarity as the poling voltage

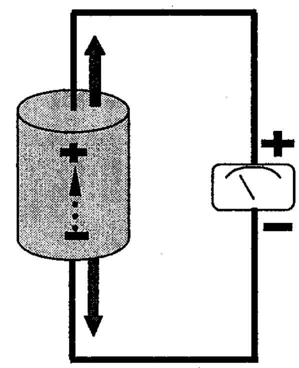

(c) Disk stretched along poling direction, generated voltage has polarity opposite to the poling voltage

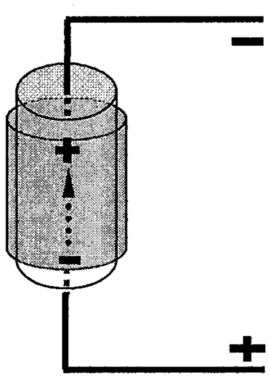

(d) Applied voltage has the same polarity as poling voltage, disk gets lengthen in the direction of polarization

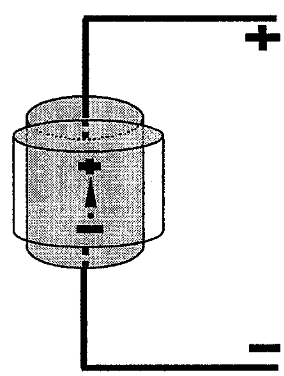

(e) Applied voltage has the polarity opposite to that of poling voltage, disk gets shortens in the direction of polarization

Figure 2-4: Piezoelectric effects in a cylinder of PZT material

2.3. Magnetostrictives and Electrostrictives

Magnetostriction is observed in materials which experience strain under the influence of a magnetic field, and conversely generate a magnetic field when strained. The strength of the magnetic field is proportional to the material's rate of strain [Shakeri et al. 2001]. Early magnetostrictive materials were studied extensively but few practical applications existed because the force and strain they generated were much less than piezoelectric and electrostrictive materials. This fundamental disadvantage changed drastically with the development of Terfenol-D (an alloy of iron, terbium, and dysprosium), a so-called giant magnetostrictor. These materials are capable of generating strains an order of magnitude larger than conventional piezoceramics with similar force output. Unlike piezoelectric materials, Terfenol-D has high endurance and has no time-or cycle-dependent lifetimes.

The phenomenon of magnetostriction results due to the re-orientation of small magnetic domains as a result of application of a magnetic field. With an increase in the applied field, more domains rotate and align until a magnetic saturation is reached. These magnetic domain rotations caused by the application of the external field, create internal strain in the material resulting in elongation (positive magnetostriction) or shortening (negative magnetostriction) of the material depending on the direction of the magnetic field.

Kannan and Dasgupta [1994] performed finite element analysis on the behavior of multi-functional composites with embedded magnetostrictive devices. Fenn [1994] discussed the passive damping and velocity sensing using magnetostrictive transducers. Bi and Anjanappa [1994] examined the feasibility of implementing embedded magnetostrictive miniactuators for smart-structures applications, such as control of beam vibrations. Marcelo [2000] discussed the modeling of strains generated using magnetostrictive transducers in response to an applied magnetic field. Figure 2-5 illustrates the cross-section of a prototypical Terfenol-D magnetostrictive transducer [Marcelo, 2000]. Hao et al. [2006] studied the nonlinear constitutive model-based vibration control system for giant magnetostrictive actuators (Terfenol-D). Chen and Anjanappa discussed the method of detecting delaminations in a composite structure embedded with magnetostrictive particulate sensors. Krishnamurthy et al. [1999] considered health-monitoring of delaminations in composite materials using an excitation coil and a sensing coil. Other researchers include Trovillion et al. [1999], Saidha et al. [2003], Heyliger [2004], and Ghosh and Gopalakrishnan [2005].

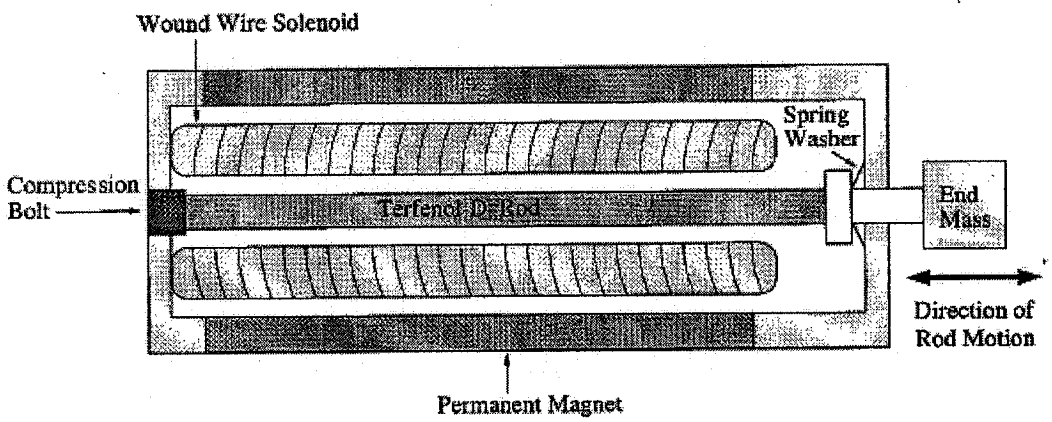

Figure 2-5: Cross section of a typical Terfenol-D magnetostrictive transducer [Marcelo, 2000]

Magnetostrictive materials like Terfenol-D can be incorporated in multifunctional composites for controlling of mechanical deformations as well as for the sensing of deformations and forces. When distributing the magnetostrictive particles in a composite structure as microscale devices in a host material, they can act as distributed sensors. Alternatively, they can act as distributed actuators that are capable of vibration suppressions, micro positioning, damage mitigation, and shape control. Terfenol-D can potentially replace conventional aircraft parts and reduce weight resulting in a lower annual fuel consumption rate.

Electrostrictives are another class of materials that are similar in function to piezoelectric materials but generate more strain and have a nonlinear strain to field dependence [Technical Insights, 1999]. As well, these materials also exhibit less hysteresis which implies a more efficient actuation. The electrostrictive effect can be found in all materials although it is usually too small (approx 10E-5 to10E-7 strain %) to utilize practically. One class of materials known as relaxor ferroelectrics exhibits the electrostrictive effect, and shows strains comparable to those pertinent to piezoelectrics (10E-1strain %) and has already found applications in many commercial platforms. The main concern with electrostrictives is that their behavior is very dependent on operating temperature and applied stress conditions.

Electrostrictive materials produce elastic deformation or change in shape when subjected to an electric field similar to magnetostrictives where deformation is produced due to a magnetic field. Electrostrictive materials are dielectric and typical examples include ceramics like lead-magnesium-niobate (PMN). Electrostrictive materials can be used as transducers, actuators, or sensors.

2.4. Shape Memory Alloys (SMA's)

Shape memory alloys are a unique group of inter-metallic materials that exhibit two very interesting properties, shape memory effect and pseudo-elasticity. Commonly, these materials are referred to as adaptive materials which can convert thermal energy directly to mechanical work. The shape memory effect comes in two forms; in the one-way shape memory effect the alloy is mechanically deformed at a low temperature and when heated above a critical transition temperature, it restores the original memory shape of the specimen. In the two-way shape memory effect, heating (even without application of external loads) the SMA results in one "memorized" shape while cooling results in second different shape [Shahin et al. 1994]. The most popular and effectively used alloys include NiTi (Nickel - Titanium), CuZnAl, and CuAlNi.

The unique properties of shape memory alloys are due to the solid state phase change that is accompanied by a molecular rearrangement. In most shape memory alloys, a temperature change of only about 10°C is necessary to initiate this phase change. The SMA alloys are characterized by two distinct solid phases, a low temperature phase (martensite) and a high temperature phase called austenite. In the martensite phase these alloys can be easily bent into various shapes. To regain the original shape, these alloys should be heated to about 500°C. At this high temperature the atoms rearrange themselves into the most compact and regular pattern possible resulting in a rigid cubic arrangement known as the austenite phase. The nature of shape memory alloy can be better understood by considering the phase diagram shown in Figure 2-6. When heated, martensite starts transforming into austenite at a point called Austenitic Start Temperature (As), and completely transforms into austenite at a temperature Af, know as Austenitic Finish Temperature. Subsequent cooling of the SMA alloy transforms austenite to martensite. This process starts at a temperature Ms called Martensite Start Temperature and completely reverts to martensite at a point Mf (Martensite Finish Temperature).

Shape memory alloys have the potential to be used in a number of applications. More recently, Nagai and Oishi [2006] investigated the use of Shape memory alloys as strain sensors in composites and Ogisu et al. [2006] studied the damage in quasi-isotropic CFRP laminates with embedded pre-strained SMA foils under quasi-static uniaxial tensile loads. One of the most popular areas of application of SMA actuators is noise and vibration control. Some examples can be found in Adachi et al. [1999], Saadat et al. [2001], Humbeeck and Kustov [2005] and many others.

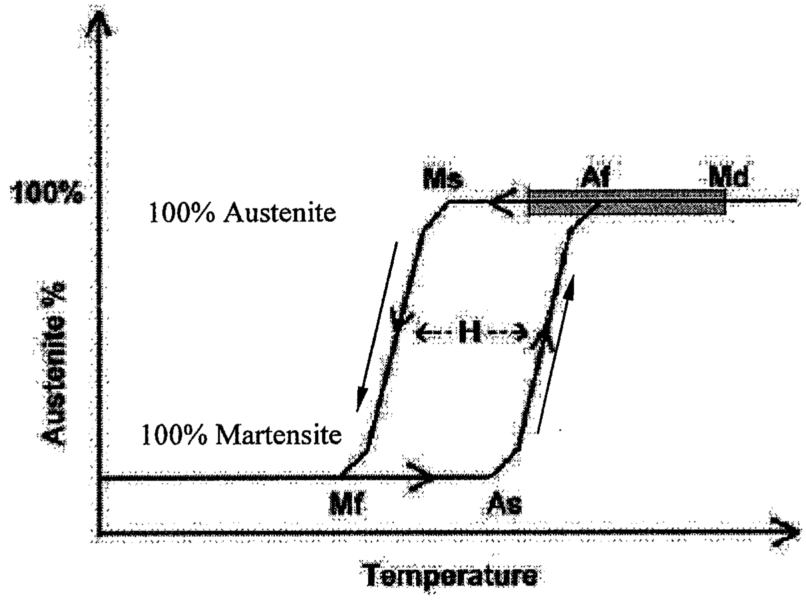

Figure 2-6: SMA behavior [AEROFIT$_{INC}$, 2002]

2.5. Electrorheological (ER) and Magnetorheological (MR) Fluids

Electrorheological and magnetorheological fluids are substances that contain micro particles suspended in an inert carrier fluid that align with an applied electric or magnetic field, respectively. When an external field is applied, these particles join to form semi-rigid chains that can significantly alter the fluid properties.

Electrorheological (ER) fluids transform from the liquid state into the gel state (Figure 2-7) with a yield stress of some kPa in milliseconds by applying an electric field. This reversible change is due to the controllable interaction between micro-sized dielectric particles within the ER suspensions. The polarization of these particles leads to configuration changes, which in turn results in significant changes in rheological properties. In the absence of an electric field, ER fluids behave like Newtonian fluids with shear stress proportional to shear strain. When a field is applied and increased, ER fluids develop a yield stress that must be overcome before there can be any motion between the electrodes. Because of this observed behavior, smart fluids are often modeled as Bingham plastic with a field-dependent yield stress. The main disadvantage of ER fluids is that they require large amount of electrical current to change state.

ER fluids applications can be categorized in two classes, controllable devices and adaptive structures. ER fluid-based controllable devices include valves, mounts, clutches and brakes. Adaptive structures are structures which incorporate ER fluids that have the ability to tune structural properties. Pinkos [1994] studied the utilization of ER fluids in car suspension systems. Wereley [1994] analyzed the feasibility of using ER fluids for active control of flexible rotor blades. Lee and Choi [2005] studied the dynamic properties of an ER fluid under shear and flow modes. Chen and Wei [2006] conducted experimental work on the rheological behavior of ER fluids under a variety of electric fields. ER fluids are mostly used in the automotive and aerospace industries for vibration control and variable torque transmission. Nowadays many additional avenues are being explored, for example civil engineering structures, and robotics. Other applications include residual vibration damping, servo stiffening of DC motors etc.

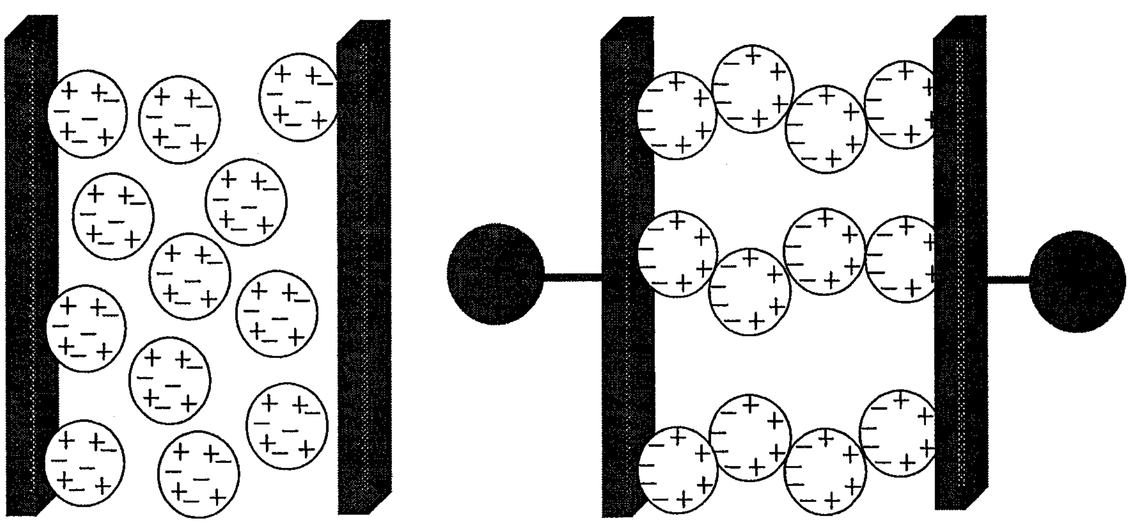

Figure 2-7: Particles chaining between electrodes when subjected to electric field

Similar to electrorheological fluids, magnetorheological fluids change viscosity and other properties as an external magnetic field is applied. When the magnetic field is removed they transform back to liquid. As the external magnetic field strength increases so does the magnetorheological fluid viscosity. Magnetorheological fluids are made up of very small iron particles (typically 3-5 μm) dispersed in a low volatility carrier fluid, usually a synthetic hydrocarbon. Oil, glycol, silicone and even water can be used as the MR fluid medium. Table 2-1 provides typical MR fluid properties [Technical Insights, 1999]. Applications of magnetorheological fluids can be found in automotive shocks, mounts and bushings, vibration dampers for vehicular seats and home appliances, precision lens grinding processes, pneumatic motion control systems, and seismic dampers for buildings and bridges.

2.6. Fiber Optic Sensors

Fiber optic sensors embedded in or attached to composites and other structures provide structural health monitoring and detect the onset of structural degradation and damage. Optical sensors have a number of specific advantages over other type of sensors which include easy embedment into host structures like composite laminates and rods, immunity to electromagnetic interference due to their dielectric nature, lightweight characteristics, corrosion resistance, high bandwidth, an enhanced resistance to environmental conditions, and low cost. The main disadvantages of these sensors are that their associated fiber leads are fragile and they also have a very small diameter which makes them difficult to handle. In addition to strain sensing, fiber optic sensors can be used to monitor a large number of other parameters such as linear and angular position, pressure, flow, liquid-level, temperature, strain, degree of cure etc. Measurements of such variables generally depend on changes in the manner that light is transmitted along the optical fiber.

Table 2-1: Typical MR Fluids Properties [Technical Insights, 1999]

Property	**Typical Value**
Maximum Yield Strength	500-100 kPa
Maximum Field	Approximately 250 kA/m
Plastic Viscosity	0.1-1.0 Pa-s
Operable Temperature Range	40-150^{0}C (limited by carrier fluid)
Susceptibility to Contaminants	Highly resistant to most impurities
Response Time	A few milliseconds
Density	3-4 g/cm^3
Maximum Energy Density	0.1 J/cm^3
Power Supply	2-25 V @ 1-2 A (2-50W)

Fiber optic sensors are categorized into (a) intrinsic sensors and (b) extrinsic sensors. Extrinsic sensors consist of an optical fiber, which carries light to a separate device that modulates it in response to an environmental effect. Intrinsic sensors on the other hand monitor light modulation within the fiber itself. An example of an extrinsic type of sensor used extensively in structural health monitoring applications is the Fabry Perot Sensor. It works on the principle of measuring a gap shift, or cavity length, between two facing fiber ends contained in a glass capillary. As external force (stress) is applied to the sensor, the length of the air gap changes and so does the phase difference between the two reflections. The change in phase between the two reflections is represented on a read-out screen. A schematic of a Fabry Perot sensor is shown in Figure 2-8 [Kalamkarov et al., 2000] and a photograph of an actual sensor is shown in Figure 2-9. Fabry perot sensors are very attractive for smart composite applications because their small size allows them to be easily embedded in composite materials, such as pultruded glass and carbon fiber reinforced tendons [Kalamkarov et. al, 1998, 2000].

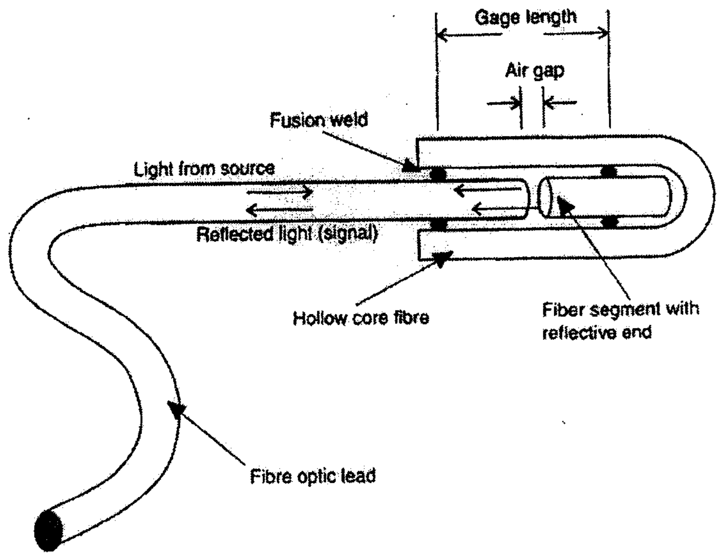

Figure 2-8: Fabry Perot sensor [Kalamkarov et al., 2000]

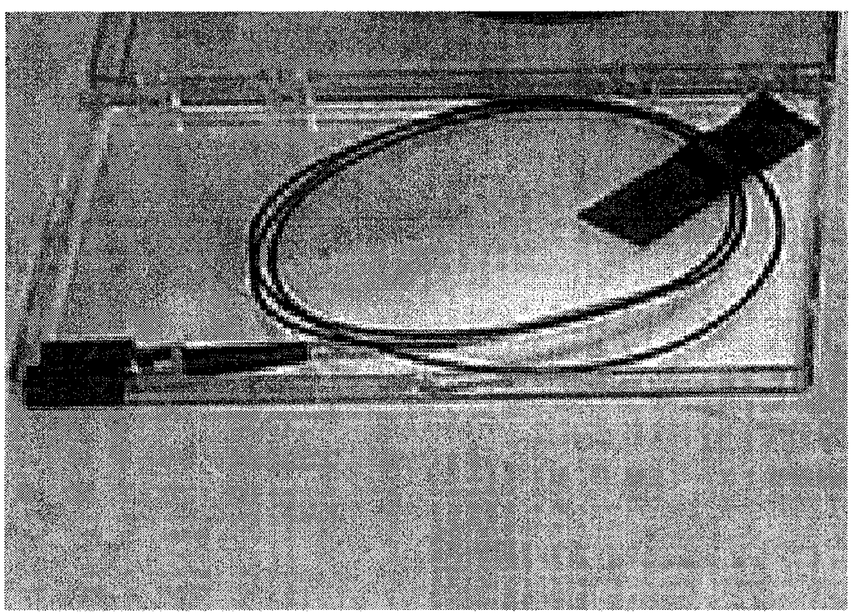

Figure 2-9: Fabry Perot sensor

3. INTRODUCTION TO ASYMPTOTIC HOMOGENIZATION MODELS FOR SMART COMPOSITE STRUCTURES

3.1. Introduction

Significant increase in the popularity of advanced composites and smart composites has seen their incorporation in the areas of mechanical, aerospace, civil, transportation, marine engineering, medicine, recreation and sports goods, etc. The continuous integration of these materials into new engineering platforms largely depends on the correct prediction of their mechanical properties and coefficients such as elastic, actuation, thermal conductivity, hygro-thermal expansion etc., through the development of appropriate models. The actuation coefficients characterize the intrinsic transducer nature of active smart composites that can be used to induce strains and stresses in a coordinated fashion. The micromechanical modeling of smart composite structures however, can be rather convoluted because of the inherent inhomogeneity of the composite materials themselves, and the local interaction between the different constituents. Therefore, it is important to develop mathematical models which are neither too complicated to be described and used, nor too simple to reflect the real properties and characteristics of the structures. In this thesis three different models pertaining to different structures are established and analyzed. The first model pertain to a thin smart composite plate reinforced with orthotropic bars, the second model analyses prismatic smart composite structures, and the third model developed is applied to three-dimensional network reinforced composite structures. Although the three models are fundamentally different because they deal with different structures, they all have some common features. The following sections provide a brief explanation of these features. The detailed modeling of the three structures is given in the subsequent chapters.

3.2. Micromechanical Modeling

The mathematical modeling of composite structures made up of reinforcements embedded in a matrix has been the focus of investigation for many years. Due to the multi-constituent nature of the composite structure, most micromechanical models employ some variant of an 'averaging' technique to determine their overall or 'effective' properties and predict their mechanical behavior. Hashin [1962] developed a composite spheres model to determine the effective properties of a heterogeneous medium. In this model, the inclusions are treated as spherical particles of radius 'a', and are embedded in a spherical region of matrix of radius 'b' in such a manner that the ratio of the radius of the particle to that of the encompassing matrix is constant and independent of the actual particle size. This model was developed to analyze shear and bulk moduli of macroscopically isotropic composites. Hashin and Rosen [1964] developed a composite cylinder model for the analysis of microscopically anisotropic composite materials. This model treats the reinforcing fibers as cylindrical inclusions of radius 'a' associated with a region of matrix of radius 'b'. Similar to the previous model, this model also allows the variation of the absolute size of the reinforcements in order to cover all the available continuous material, keeping however, the ratio a/b constant. Hill [1965] and Budiansky [1965] extended a self-consistent scheme previously developed for modeling the mechanical behavior of polycrystalline materials by Hershey [1954], to analyze multiphase media. Hashin and Shtrikman [1963a, 1963b] developed micromechanical models pertaining to multiphase materials, which exhibit macroscopically quasi-isotropic behavior. In this model, the authors employed a variational approach to determine upper and lower limits for the effective elastic properties as well as electric and thermal conductivity of the multiphase materials. It was discovered that if the properties of the different constituents were of comparable magnitude, then the upper and lower bonds are close to one another. Other mathematical models related to composite structures can be found in Eshelby [1957], Hill [1963], Russel [1973], Mori and Tanaka [1973], Sendeckyj [1974], Berryman [1980], Torquato and Stell [1985], and more recently in Torquato [1991], Tsai [1992], Jansson [1992], Vasiliev [1993], Kalamkarov and Liu [1998c], Zeman and Sejnoha [2001], Sevostianov et al. [2005, 2002], Sevostianov and Kachanov [2003] and others. Christensen [1990], Milton and Kohn [1988], Vinson [1993], and Nemat-Naser and Hori [1993] are among the researchers who employed analytical averaging schemes.

The characteristics of adaptive smart structures of a periodic nature (see Figure 3-1) can be described by means of partial differential equations expressed in terms of two largely different scales; a microscopic scale (fast scale) which reflects the periodic nature of the structure and is of same order of magnitude as the size of the "unit cell" or periodicity unit (Figure 3-1), and a macroscopic scale (slow scale) which is a manifestation of the global formulation of the problem. The macroscopic scale has an order of magnitude similar to a characteristic dimension of the composite structure. The presence of two different scales in the pertinent differential equations makes their analytic or even numerical solution a very difficult task. So, we look for alternative approximate techniques. One such technique is the asymptotic homogenization method. The asymptotic homogenization decouples the microscopic and the macroscopic variations, so that each can be solved independently or sequentially. The general mathematical framework can be found in Bensoussan et al. [1978], Bakhvalov and Panasenko [1984], Sanchez-Palencia, [1980], Kalamkarov [1992], Cioranescu and Donato [1999] etc. This method is mathematically rigorous and when applied to the smart composite structures, it enables the determination of both local and global averaged properties of the structures. Many problems in the framework of elasticity and thermoelasticity have been solved using such models. Kalamkarov and Georgiades [2002a, 2002b] developed general micromechanical models pertaining to smart composite structures with homogeneous and non-homogeneous boundary conditions as well as micromechanical model for thin smart composite layers with wavy boundaries. Other works can be found in Adrianov et al. [1985], Artola and Duvaut [1977], Lene and Leguillon [1982], Caillerie [1984], Kohn and Vogelius [1984], Devries et al. [1989], Ciarlet [1990], Kolpakov and Kolpakova [1995], and Kalamkarov and Kolpakov [1997, 2001]. The main objective of asymptotic homogenization technique is to transform a general anisotropic composite material made of a periodic array of reinforcements and other inclusions such as actuators (Figure 3-1) into a set of simpler problems, often referred to as unit cell problems. It is precisely these unit cell problems that lead to the determination of the aforementioned effective coefficients.

The three essential features characterizing asymptotic homogenization are asymptotic or perturbation expansions, two-scale expansions, and the homogenization process. These features are explained in subsequent sections.

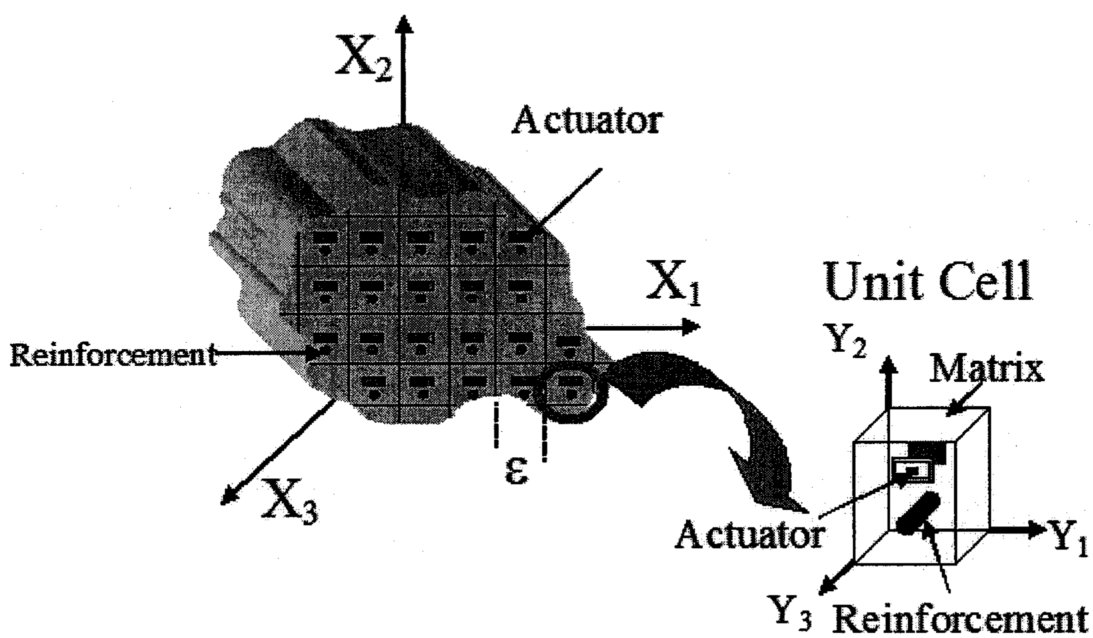

Figure 3-1: Smart Composite with periodically arranged actuators and its periodicity cell

Before explaining these features it is worth explaining briefly what we mean by asymptotic approximations. Most of the physical problems that arise in all branches of science and engineering have some inherent characteristics associated with them that make the exact closed-form solution an impossible or very difficult task. Some examples of these characteristics include, but are not limited to, non-linearity, geometric uncertainties, rapidly oscillating coefficients, and changing boundary conditions. The advances in computer technology helped to solve or deal with such complex problems but strictly numerical solutions come with their share of disadvantages the most important of which is that the insight often gained from exploring the relationships between a solution and the various problem parameters is lost. One way of compensating for this is to construct an *approximate* solution from which the analyst and designers can assess or partly assess the significance of the various parameters. It is therefore important to discuss what exactly we mean by an asymptotic approximation. The best way to explain this is to consider an example as given in Holmes [1995].

Let us consider a problem given by:

$$f(\alpha) = \alpha^2 + \alpha^5, \text{ where } \alpha \text{ is close to zero} \tag{3.1}$$

In this problem we are interested in finding an approximation. To begin solving this problem first let us approximate the above function as:

$$f(\alpha) \approx \alpha^2 \tag{3.2}$$

This approximation is reasonable for α close to zero because $\alpha^5 << \alpha^2$. On the other hand, a lousy approximation would be

$$f(\alpha) \approx \frac{3}{5}\alpha^2 \tag{3.3}$$

We can easily observe that the above approximation is lousy even though the error $f(\alpha)-\frac{3}{5}\alpha^2$ goes to zero as $\alpha \downarrow 0$. The problem with this approximation is that the error is of the same order of magnitude as the quantity being approximated. Thus,

"Given $f(\alpha)$ and $\phi(\alpha)$, we say that $\phi(\alpha)$ is an asymptotic approximation to $f(\alpha)$ as $\alpha \to \alpha_0$ whenever $f = \phi + o(\phi)$ as $\alpha \to \alpha_0$. In this case, we write $f \sim \phi$ as $\alpha \to \alpha_0$". [Holmes, 1995]

In the above definition $\phi(\alpha)$ serves as an approximation to $f(\alpha)$, for α close to α_0, when the error is of higher order than the approximating function. In particular, $f \sim \phi$ as $\alpha \to \alpha_0$ if

$$\lim_{\alpha \to \alpha_0} \frac{f(\alpha)}{\phi(\alpha)} = 1 \qquad [3.4]$$

It is worth mentioning that the asymptotic approximation is not unique and it does not say much about the accuracy of the approximation. To overcome these disadvantages, we need to introduce more structure into the problem formulation.

3.3. Asymptotic Expansion

The differential equations describing the behavior of real structures or systems are often characterized by the presence of certain parameters, which even though small in relation to the other parameters and variables, may have too important of an effect to be ignored. The presence of such parameters makes the differential equations difficult to solve. A particularly useful technique is dealing with any differential equation is to nondimensionlise the variables in a differential equation i.e. normalize them with respect to other suitable characteristic variables so that these transformed variables are approximately of order 1. Thus in such situations, a "small" parameter say ε, implies that ε is much smaller than $1(\varepsilon << 1)$. An approximate solution to the problem is then obtained by expanding it in terms of an infinite series in powers of the small parameter and by subsequently truncating this series after a few terms. The most common methods used to find asymptotic expansions are (a) Taylor's theorem, (b) L'Hospital's rule (c) Educated guess. More information on these methods can be found in Nayfeh [1993]. Typically, but not always, these series are in the form

$$y_{solution} = y_0 + \varepsilon y_1 + \varepsilon^2 y_2 + \varepsilon^3 y_3 + \ldots \qquad [3.5]$$

where the symbol ... stands for higher order terms. Once the series is defined it is inserted into the governing equations and respective boundary conditions, and coefficients of like powers of ε are then grouped to obtain a series of equations for the coefficient functions, which are then solved in a sequential manner. It must be mentioned that the resulting series need not converge for any value of ε; nevertheless, the solution can be still useful in approximating the given function when ε is small.

The general features of an asymptotic expansion will be illustrated by means of a simple example. Consider,

$$\begin{gathered} \frac{dy}{dx} - y^2 = \varepsilon y \\ y(0) = 1 \end{gathered} \qquad [3.6]$$

The first step in solving this problem is to assume that the solution is expressed as:

$$y = y_0(x) + \varepsilon y_1(x) + \varepsilon^2 y_2(x) + O(\varepsilon^3) \quad [3.7]$$

where "O" is the so called Landau symbol and means "order of". The error incurred by truncating the series after the ε^2 is of order ε^3. It should also be noted in Equation [3.7] that the $y_i(x)$ terms are all functions of the independent variable x, and do not depend on ε.

The next step in the process of solving this problem is to substitute the assumed expression into the governing equations and boundary conditions to obtain, after neglecting higher-order terms:

$$\frac{dy_0}{dx} + \varepsilon \frac{dy_1}{dx} - (y_0 + \varepsilon y_1)^2 = \varepsilon y_0 + \varepsilon^2 y_1 \quad [3.8a]$$

$$y_0(0) + \varepsilon y_1(0) + \varepsilon^2 y_2(0) = 1 \quad [3.8b]$$

Collecting the like powers of ε gives two sets of questions:

$$\frac{dy_0}{dx} - y_0^2 = 0 \quad [3.9a]$$

$$y_0(0) = 1 \quad [3.9b]$$

$$\frac{dy_1}{dx} - 2y_0 y_1 - y_0 = 0 \quad [3.10a]$$

$$y_1(0) = 0 \quad [3.10b]$$

From Equation [3.9]

$$y_0 = \frac{1}{1-x} \qquad [3.11]$$

Substituting Equation [3.11] in [3.10a] and solving using Equations [3.10b] gives

$$y_1 = \varepsilon \frac{x}{2}\left\{\frac{2-x}{(1-x)^2}\right\} \qquad [3.12]$$

Combining Equations [3.11] and [3.12] gives the total expression for the asymptotic solution of the problem at hand as follows:

$$y(x) = \frac{1}{1-x} + \varepsilon \frac{x}{2}\left\{\frac{2-x}{(1-x)^2}\right\} + O(\varepsilon^2) \qquad [3.13]$$

To assess the accuracy of the approximate solution obtained, one must compare with an exact solution. Thus, from Equations [3.6] and after some algebraic manipulations, the exact solution for x is given by:

$$y(x) = \frac{\varepsilon . e^{\varepsilon x}}{\varepsilon + 1 - e^{\varepsilon x}} \qquad [3.14]$$

As a final step let us plot the asymptotic and analytic solutions given in Equations [3.13], [3.14] respectively. From Figure 3-2, we observe that they conform very well to one another. The value of $\varepsilon = 0.01$ was used for this plot.

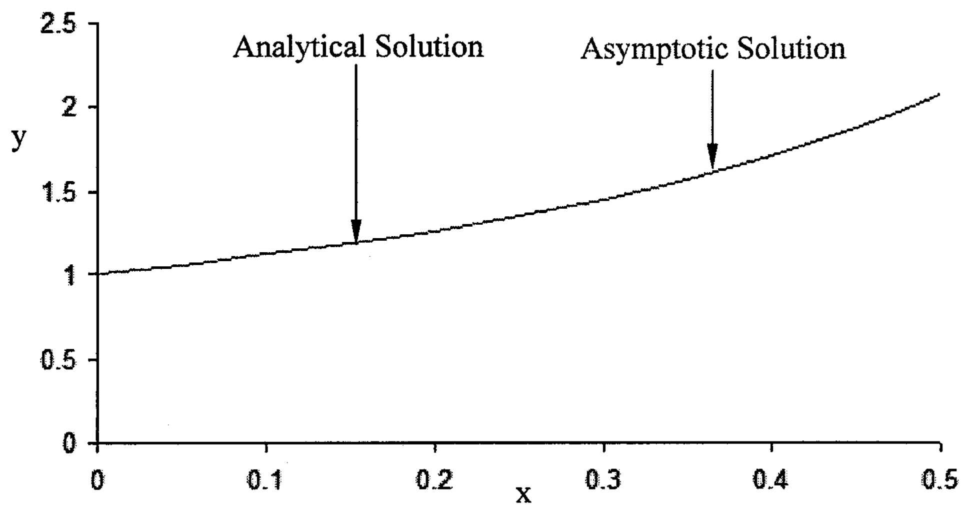

Figure 3-2: Comparison of asymptotic and analytical solutions for the example in Equation [3.6]

3.4. Multi-Scale Expansion

The second characteristic feature of the method of asymptotic technique is the two scale expansion. Unlike matched asymptotic expansion where the solution is constructed in different regions that are then patched together to form a composite expansion [Nayfeh, 1973], the method of multiple-scale expansion essentially starts with a generalized version of a composite expansion. In doing this, one introduces separate coordinates for each region of the problem under consideration. These new variables are considered independent of one another. The result is a transformed partial differential equation which is, surprisingly perhaps, easier to solve rather than the problem described in the original ordinary differential equation.

For illustrative purposes, let us consider a weak spring-mass-damping system with a weak damping coefficient. The problem of this nature is given by the following differential equation and boundary conditions:

$$\frac{d^2y}{dt^2}+\varepsilon\frac{dy}{dt}+y=0 \quad [3.15a]$$

$$y(0)=1, \quad \dot{y}(0)=0 \quad [3.15b]$$

Here ε is the viscous damping coefficient.

We will try to solve this problem by using a regular asymptotic expansion like the one described in Section [3.3]. We start with:

$$y=y_0(t)+\varepsilon y_1(t)+\varepsilon^2 y_2(t)+O(\varepsilon^3) \quad [3.16]$$

Substituting Equation [3.16] into Equations [3.15a], [3.15b] gives

$$\frac{d^2y_0}{dt^2}+\varepsilon\frac{d^2y_1}{dt^2}+\varepsilon^2\frac{d^2y_2}{dt^2}+\varepsilon\frac{dy_0}{dt}+\varepsilon^2\frac{dy_1}{dt}+y_0(t)+ \varepsilon y_1(t)+\varepsilon^2 y_2(t)=0 \quad [3.17a]$$

$$y_0(0)+\varepsilon y_1(0)=1 \quad [3.17b]$$

$$\dot{y}_0(0)+\varepsilon\dot{y}_1(0)=0 \quad [3.17c]$$

Equating equal powers of ε gives the following two sets of equations

$$O(0): \frac{d^2 y_0}{dt^2} + y_0(t) = 0 \quad [3.18a]$$

$$O(0): \; y_0(0) = 1 \quad [3.18b]$$

$$O(0): \; \dot{y}_0(0) = 0 \quad [3.18c]$$

$$O(\varepsilon): \frac{d^2 y_1}{dt^2} + \frac{dy_0}{dt} + y_1(t) = 0 \quad [3.19a]$$

$$y_1(0) = 0 \quad [3.19b]$$

$$\dot{y}_1(0) = 0 \quad [3.19c]$$

Solving the above equations in conjunction with boundary conditions gives the solutions for y_0 and y_1. Combining the two solutions gives the final expression for y as:

$$y(t) = \cos(t) + \frac{1}{2}\varepsilon(\sin t - t\cos t) \quad [3.20]$$

Finally we will derive the analytical solution for the same problem and compare with the approximate solution calculated above. The exact solution for this problem is given by:

$$y(t) = e^{-\frac{\varepsilon}{2}t}\left(\cos\left(\frac{\sqrt{4-\varepsilon^2}}{2}\right)t - \frac{\varepsilon}{\sqrt{4-\varepsilon^2}}\sin\left(\frac{\sqrt{4-\varepsilon^2}}{2}\right)t\right) \quad [3.21]$$

Figure 3-3 compares the approximate solution and the exact solution. For illustration purposes we assume that ε (viscous-damping coefficient) = 0.05. It is observed that the approximate solution agrees with exact solution for times up to about 20 seconds and then the error becomes progressively larger. The reason is that after 20 seconds the second term in the Equation [3.20] becomes as large as first term and the approximation collapses. In any valid asymptotic expansion, each term of the series must always be a small correction to the previous term [Nayfeh, 1973, Holmes, 1995].

From the Figure 3-3 we observe that problems of this nature are actually characterized by two quite different scales. The first one is the "rapid" or fast sinusoidal scale and superimposed on that is a slow exponential scale. Thus, the actual solution decays slowly, but the asymptotic solution can only capture the fast variation in this case. In its attempt to correct the first term, the second term in the asymptotic expansion becomes progressively larger and eventually even larger than the first term. The term $t\cos t$ is called a "secular" term.

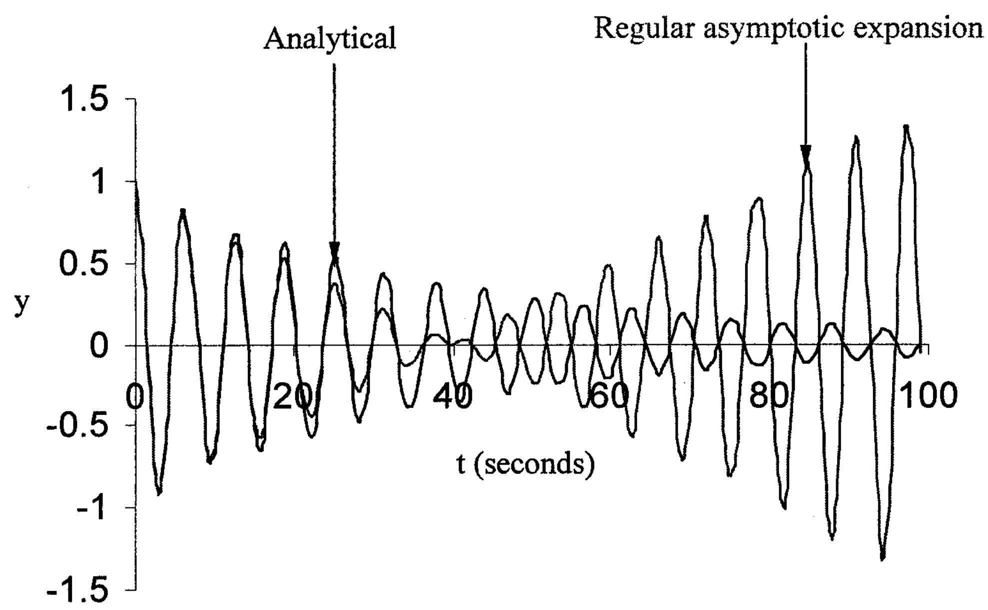

Figure 3-3: Comparison of regular asymptotic and analytical solutions for a weakly damped spring-mass system

The large mismatch between two different scales means that our asymptotic expansion can only capture the slow scale and not the fast scale. One way of solving this problem is to "speed up" the slow variation by introducing a new variable $t_2 = \varepsilon t$. Thus the two variables are defined as:

$$t_1 = t$$
$$t_2 = \varepsilon t \qquad [3.22]$$

In Equation [3.22], t_1 is commonly referred to as the fast variable and t_2 is referred as slow variable. Subsequently, the asymptotic expansion given in Equation [3.16] can be written as:

$$y(t_1, t_2) = y_0(t_1, t_2) + \varepsilon y_1(t_1, t_2) + \varepsilon^2 y_2(t_1, t_2) + O(\varepsilon^3) \qquad [3.23]$$

The introduction of new variables transforms the ordinary differential equations to partial differential equation as

$$\frac{d}{dt} \to \frac{\partial}{\partial t_1}\frac{\partial t_1}{\partial t} + \frac{\partial}{\partial t_2}\frac{\partial t_2}{\partial t} \qquad [3.24]$$

Substituting Equations [3.22] into Equation [3.24] gives

$$\frac{d}{dt} \to \frac{\partial}{\partial t_1} + \frac{\partial}{\partial t_2}\varepsilon \qquad [3.25]$$

and

$$\frac{d^2}{dt^2} = \frac{\partial}{\partial t}\left(\frac{\partial}{\partial t}\right) = \frac{\partial^2}{\partial t_1^2} + 2\varepsilon \frac{\partial^2}{\partial t_1 \partial t_2} + \varepsilon^2 \frac{\partial^2}{\partial t_2^2} \qquad [3.26]$$

Let us now try to solve the above problem using the asymptotic expansion given by Equation [3.23]. The procedure is similar to the one before but the only difference is that the two variables are treated separately. The differential equation and the pertinent boundary conditions now become:

$$\frac{\partial^2 y}{\partial t_1^2} + 2\varepsilon \frac{\partial^2 y}{\partial t_1 \partial t_2} + \varepsilon^2 \frac{\partial^2 y}{\partial t_2^2} + \varepsilon \frac{\partial y}{\partial t_1} + \varepsilon^2 \frac{\partial y}{\partial t_2} + y = 0$$

$$y\big|_{t_1=t_2=0} = 1 \qquad [3.27]$$

$$\left.\frac{\partial y}{\partial t_1} + \varepsilon \frac{\partial y}{\partial t_2}\right|_{t_1=t_2=0} = 0$$

It should be noted that even though Equation [3.27] is 2nd order with respect to t_1 and t_2, only two initial conditions are given. These can be expanded to 4 in an infinite number of ways. To make the solution unique, one needs to impose certain restrictions so as to avoid secular terms [Holmes, 1995].

Substituting Equation [3.23] into Equation [3.27] gives two sets of problems:

$$O(1): \frac{\partial^2 y_0}{\partial t_1^2} + y_0 = 0$$

$$y_0\big|_{t_1=t_2=0} = 1 \qquad [3.28a]$$

$$\left.\frac{\partial y_0}{\partial t_1}\right|_{t_1=t_2=0} = 0$$

and

$$O(\varepsilon): \frac{\partial^2 y_1}{\partial t_1^2} + y_1 = -2\frac{\partial^2 y_0}{\partial t_1 \partial t_2} - \frac{\partial y_0}{\partial t_1}$$

$$y_1\big|_{t_1=t_2=0} = 0 \qquad [3.28b]$$

$$\left.\frac{\partial y_1}{\partial t_1} + \frac{\partial y_0}{\partial t_2}\right|_{t_1=t_2=0} = 0$$

Let us concentrate on first set of equations given by Equation [3.28a]. The solution can readily be obtained to be:

$$y_0 = A(t_2)\sin t_1 + B(t_2)\cos t_1$$

$$A(0) = 0,\ B(0) = 1 \qquad [3.29]$$

Substituting Equation [3.29] into Equation [3.28b] leads, after some manipulations to:

$$y_1 = D(t_2)\cos t_1 + E(t_2)\sin t_1 - \frac{1}{2}\left(2\frac{dA}{dt_2} + A\right)t_1 \sin t_1 - \frac{1}{2}\left(2\frac{dB}{dt_2} + B\right)t_1 \cos t_1 \qquad [3.30]$$

It is obvious that to avoid secular terms, we need to impose the following conditions on A and B:

$$2\frac{dA}{dt_2} + A = 0$$

$$2\frac{dB}{dt_2} + B = 0 \qquad [3.31]$$

Solving Equation [3.31] in conjunction with Equation [3.29] leads to:

$$A = 0 \text{ and } B = e^{-\frac{t_2}{2}} \tag{3.32}$$

Substituting values of A and B into Equation [3.28] gives the solution for y_0 as:

$$y_0 = e^{-\frac{t_2}{2}} \cos t_1 = e^{-\varepsilon\frac{t}{2}} \cos t \tag{3.33}$$

Substituting Equation [3.33] into Equation [3.23] gives the final asymptotic solution as:

$$y = e^{-\varepsilon\frac{t}{2}} \cos t + O\left(\varepsilon^2\right) \tag{3.34}$$

Note that the procedure outlined here simply amounts to letting $t_2 = \varepsilon t$ be a new variable and substituting it into the model. The next term in the series will be of order $\varepsilon t_1 = O\left(\varepsilon^2\right)$, which explains the form of Equation [3.34]. Figure 3-4 shows the plot of new asymptotic solution along with the analytic solution. The two solutions are virtually indistinguishable.

3.5. Asymptotic Homogenization Model

The physical behavior of a composite medium with a regular arrangement of fibers, sensors and/or actuators is governed by differential equations with rapidly oscillating coefficients. The presence of such coefficients makes the solution difficult and sometimes even impossible to solve analytically. One approach to solve such a problem is to consider a "continuum approximation" concept that assumes the material to be continuously distributed. If the characteristic dimensions of the structural elements are small in comparison to the overall dimensions of the structure, then the original inhomogeneous body can be replaced, in an asymptotic sense, by a homogeneous structure with similar mechanical behavior. In other words, we can replace the periodically varying (inhomogeneous) composite structures with a homogeneous structure that has similar mechanical properties (to be referred to as effective properties) as the original composite structure. The problem begins with the basic differential equation and boundary conditions representing the inhomogeneous medium and reduces to a simpler set of problems called the unit cell problems representing the approximately equivalent homogeneous medium. It is precisely these unit cell problems that enable the determination of the effective coefficients.

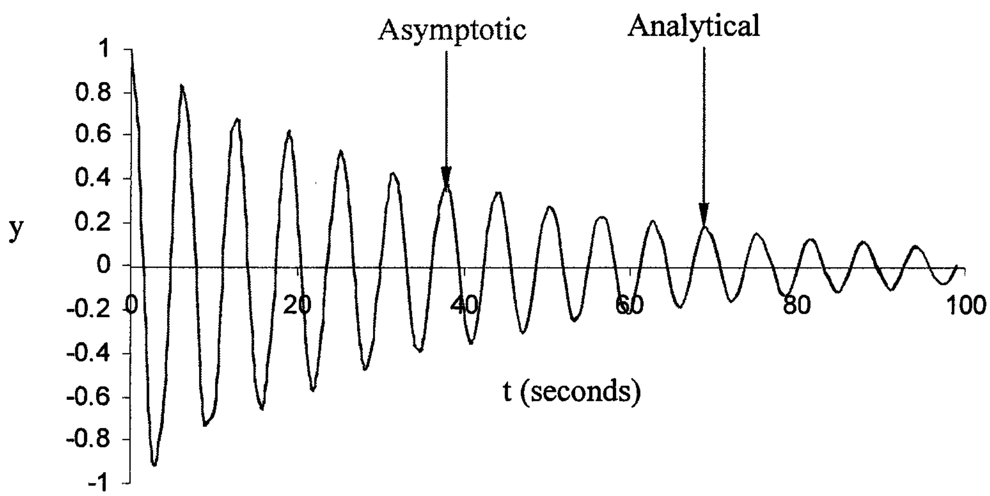

Figure 3-4: Comparison of two-scale asymptotic and analytical solution for a weakly damped spring-mass system

To better understand the concepts of the method of homogenization, let us consider a typical fiber reinforced composite that occupies a domain G with boundary conditions ∂G. Figure 3-5 shows the cross-sectional view of such a composite structure. From the figure, it is evident that the composite structure can be thought of as a regular arrangement of what one might justifiably call unit cells. Let us assume that the unit cell in this case has both length and width equal to a non-dimensional parameter ε, where ε is obviously a very small number. This can be justified from the fact that the magnitude of ε is of the same order as the diameter of the reinforcing fibers or the spacing between the fibers.

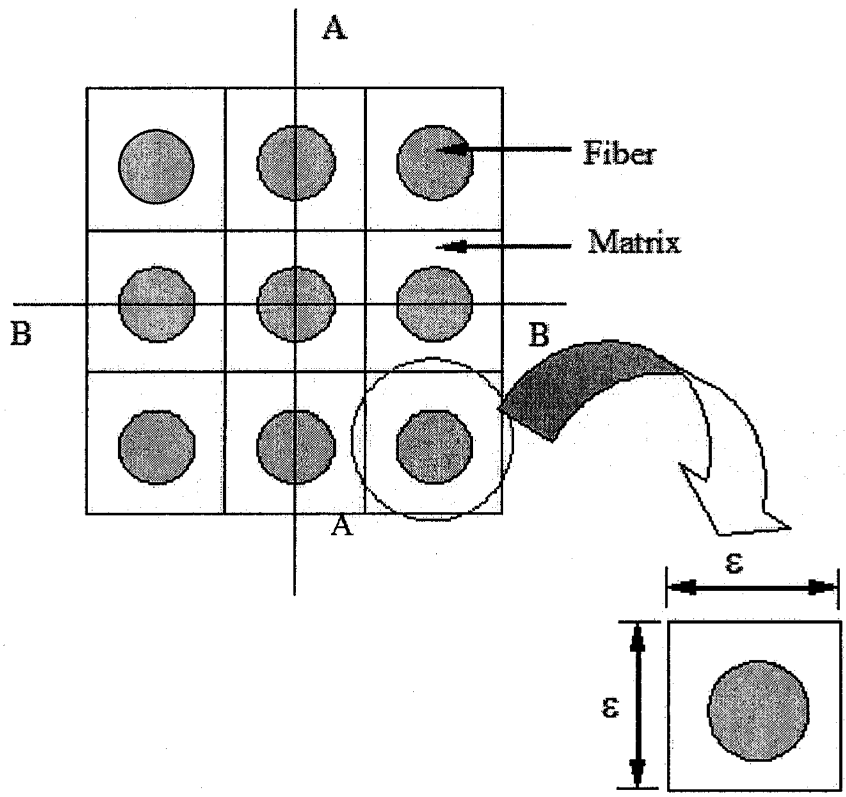

Figure 3-5: Cross-section of a composite Structure

Assume that we are interested in finding, say, the steady state temperature distribution due to some thermal input. During our work, we will inevitably come across material properties like thermal conductivity. Let us plot the variation of thermal conductivity along direction AA or BB direction (Figure 3-5). The result is shown in Figure 3-6. From this figure we observe that the thermal conductivity (as well as other material properties) varies from low to high with a small period ε as we go from fiber to matrix. This periodic variation of material properties is a consequence of the periodic nature of the structure as discussed above. Hence, the differential equations characterizing heterogeneous media (such as composite materials) with a periodic structure, have rapidly oscillating coefficients which depend on the physical properties of the various constituents such as reinforcing fibers, actuators and matrix. In other words, these coefficients are periodic with an extremely small period ε where ε is of the order of the diameter of the reinforcing fibers. The dependent variables such as the stress and strain fields will consequently also have a periodic component with the same period ε. In addition to this periodic component however, the dependent variables have a superimposed non-periodic component as well because they depend not only on material properties, but also on external loads, boundary conditions etc. which are, in general, non-periodic. To better understand this concept, let us consider our example a little further. We assume that the upper surface of this structure (Figure 3-5) is maintained at 0^0C and the lower surface is maintained at 100^0C. At steady state it is natural to expect that the temperature near the lower side is higher than the temperature near the upper surface and hence temperature distribution will not be periodic. Based on these arguments, two important observations are apparent:

The material properties like thermal conductivity, elastic moduli, poisons ratios etc. are strictly periodic with a (small) period ε.

The dependent variables like stress, strain, temperature are characterized by both a periodic and a coupled non-periodic component.

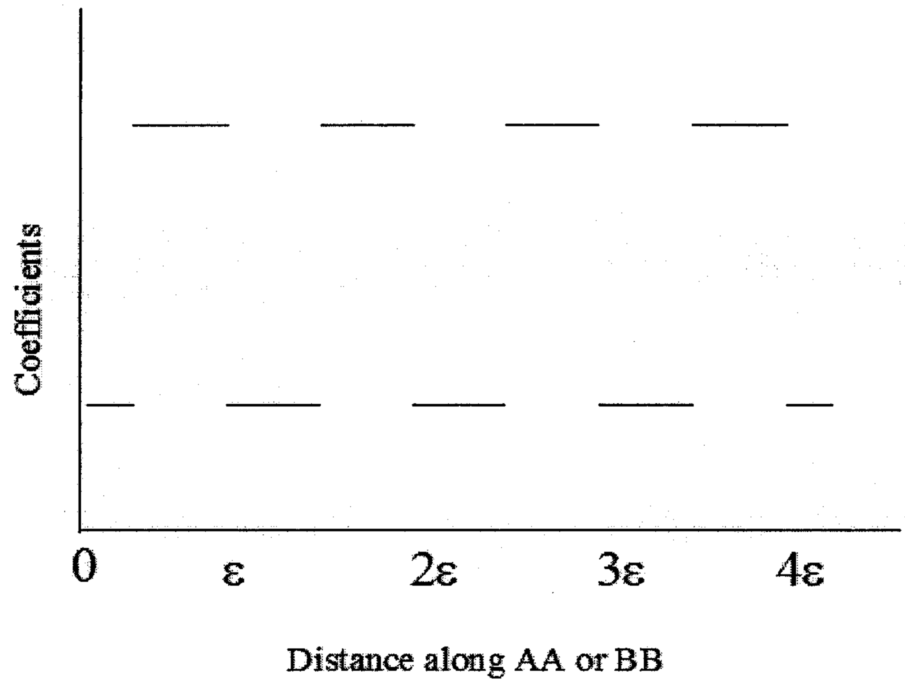

Figure 3-6: Plot of variation of coefficients vs. distance

To illustrate these notations even further let us consider the example shown in Figure 3-7 [Sanchez-Palencia, 1980].

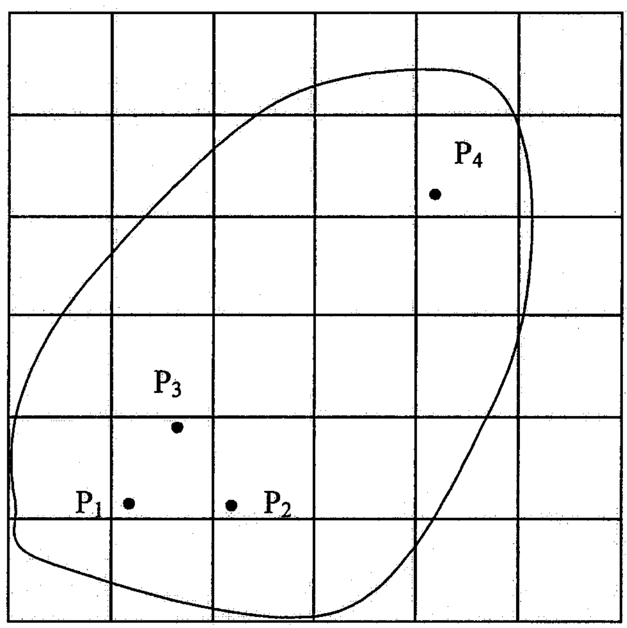

Figure 3-7: A periodic medium [Sanchez-Palencia, 1980]

Suppose that we are interested in finding the temperature distribution, T, in the periodic composite structure of Figure 3-7. Because of the assumed periodicity, and because the points P_1, P_2, and P_4 represent corresponding points in different unit cells, the thermal conductivity at these points will be the same. However, the thermal conductivity at point P_3 will be different. Consider now points P_1 and P_2. At steady state, both the periodic and the non-periodic components of the temperature are same because the two points are close to one another and macroscopically this represents a small distance. Hence the temperature at these points will be (for a very good approximation) same. For points P_1 and P_4 however, the situation is different. The periodic component of the temperature at these points will be the same, but the non-periodic component will be different because these two points are rather far apart. Consequently, the temperature at these points is different.

Thus, from the discussions so far, it is apparent that the problem of a periodic structure is characterized by two vastly different scales, a microscopic or fast scale, and, superimposed on it, a macroscopic scale. The presence of these two scales means that we can not obtain a regular perturbation expansion to our problem, much like we could not find a regular perturbation expansion to the weak spring-mass-damping system considered before. In that case, the difficulty was the mismatch between a rapidly oscillating scale and the slow exponential scale. We solved that problem by "speeding up" the slow scale. A similar technique will be employed for the case of periodic composite structures. Here we solve the problem by simply expanding the domain of the unit cell so that it is now of the same order of magnitude (i.e. ~ 1) as the macroscopic variables. Accordingly, we introduce a new set of variables called "fast" or microscopic variables y_i (in addition to the existing macroscopic variables x_i), such that

$$y_i = \frac{x_i}{\varepsilon}; \qquad i = 1, 2, 3 \tag{3.35}$$

In view of the introduction of the microscopic variables, the unit-cell now gets transformed as in Figure 3-8 and, as a consequence, the material coefficients of the composite medium will now be periodic in y_i with period 1, the size of the transformed unit cell. This will eventually lead to the determination of effective or homogenized coefficients which as we will see later, are independent of the macroscopic scale. Once the effective coefficients are obtained, the global (macroscopic) problem can be solved. More details on the applications of the method of homogenization for the case of smart structures can be found in Kalamkarov [1992, 1997] Kalamkarov and Kolpakov [2001], Kalamkarov and Georgiades [2002a, 2002b] Kalamkarov et al., [2003a, 2003c], Georgiades and Kalamkarov [2004], Georgiades et al. [2003].

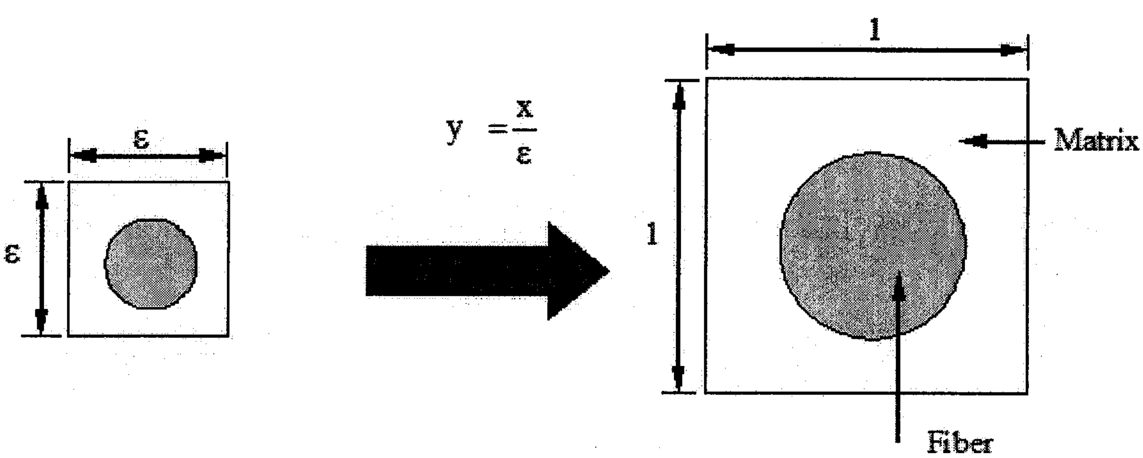

Figure 3-8: Introduction of fast variable

3.6. Developed Models

In the subsequent chapters, three different models will be presented. A number of examples were used to illustrate these models. In these examples, the materials selected are transversely isotropic simply because they are more commonly encountered. The validity of the models however is much more general and they apply without modification to orthotropic materials.

4. ASYMPTOTIC HOMOGENIZATION MODEL FOR NETWORK REINFORCED SMART COMPOSITE PLATES

4.1. Introduction

Smart composites are used in the form of plates and shells in increasingly more applications. In many cases these structures have a periodic configuration with a period much smaller than their characteristic dimensions. Consequently, asymptotic homogenization is the best candidate for analysis. For thin plates and shells where the thickness of the structure is of a similar order of magnitude as the size or spacing of the actuators/reinforcements, the modified methodology first proposed by Caillerie in his heat conduction studies (Caillerie, 1984) should be used. In this technique, two sets of 'fast' variables are introduced; one for the tangential directions which exhibit periodicity and one for the transverse direction for which periodicity do not apply. Such an approach has been used by Kohn and Vogelius (1984, 1985) for the problem of pure bending of a thin homogeneous plate, Kalamkarov (1992), and Kalamkarov and Kolpakov (1997) for three-dimensional elasticity and thermoelasticity problems of thin curvilinear composite layers, Georgiades and Kalamkarov (2003, 2004) for piezoelastic deformations of wafer- and rib-reinforced smart composite structures and others.

In this work, a general 3-dimensional micromechanical model pertaining to smart composite layers with wavy boundaries is applied to the case of thin smart plates reinforced with a network of orthotropic bars that may also exhibit piezoelectric behavior. The method used for the development of the structural model is that of asymptotic homogenization which reduces the original boundary value problem into a set of three decoupled problems, each problem characterized by two differential equations. These three sets of differential equations, referred to as "unit cell problems", deal, independently, with the elastic, piezoelectric, and thermal expansion behavior of the network reinforced smart composite plates. The solution of the unit cell problems yields expressions for effective elastic, piezoelectric and thermal expansion coefficients which, as a consequence of their universal nature, can be used to study a wide variety of boundary value problems associated with a smart structure of a given geometry. It will be shown that these models can readily be used to tailor the effective properties of any smart network structure, to meet the requirements of any particular application by changing some material or geometric parameters such as the size or nature of the reinforcements. For illustration purposes, the methodology is applied to network-reinforced smart structures with generally orthotropic reinforcements and actuators forming spatial rectangular, triangular, or rhombic arrangements. In the limiting case of purely elastic behavior and isotropic reinforcements, the above general orthotropic model converges to results that are consistent with those of Kalamkarov (1992) who also used asymptotic homogenization and Pshenichnov (1982) who used a different approach based on stress-strain relationships in the reinforcements.

4.2. Objective and Synopsis

The objective of this work is to determine the effective elastic, piezoelectric and thermal expansion coefficients of thin smart composite plates with networks of bars made of orthotropic material. A simple network consisting of only one family of actuators/reinforcements is shown in Figure 4-1. A general form of composite plate with networks of more than one family of actuators/reinforcements will be considered in Section 4.5.

The micromechanical modeling of thin composite network structures begins with the basic problem formulation and model development as presented in Section 4.3, followed by the analysis of network reinforced smart composite plates in Section 4.4. Finally, the effective coefficients of the homogenized structures are obtained in sections 4.4.1, 4.4.2, and 4.4.2. Section 4.5 considers specific examples pertaining to rectangular, triangular and rhombic configurations.

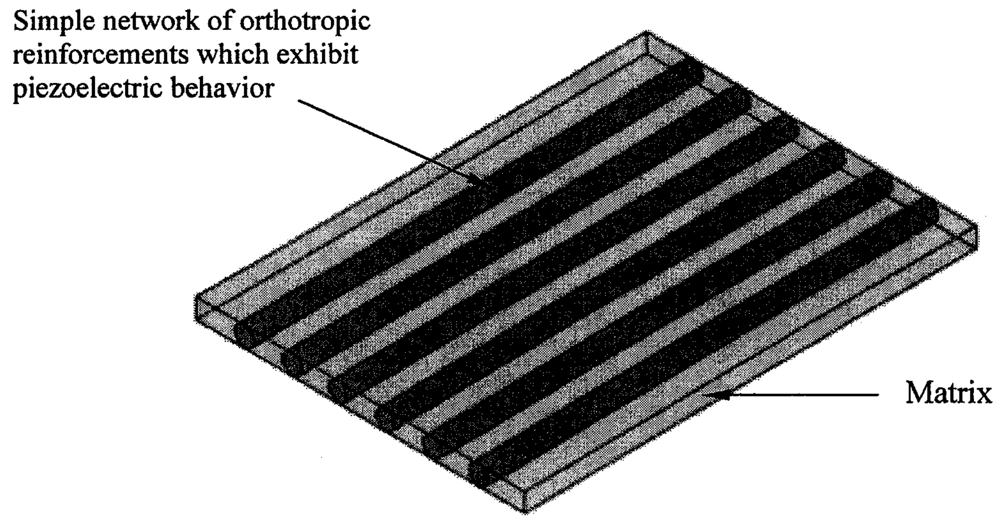

Figure 4-1: Smart composite plate with a network of orthotropic actuators/reinforcements

4.3. Homogenization Model for Network and Framework Reinforced Plates

4.3.1. General Problem Formulation

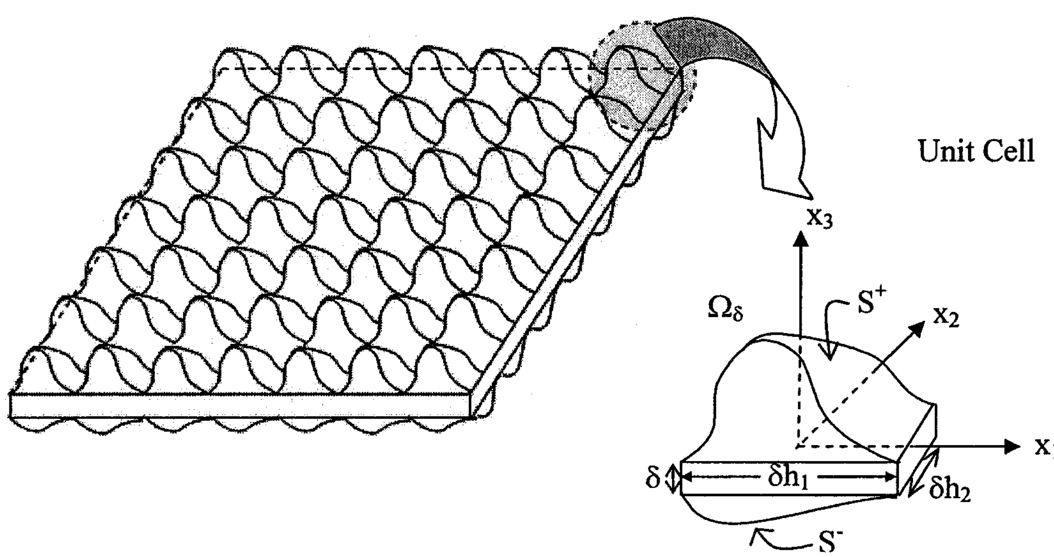

Figure 4-2: Periodic smart composite layer reinforced and its unit cell

The micromechanical model for a network-reinforced smart composite plate will be developed starting from a general model pertaining to a thin smart composite layer with wavy surfaces [Kalamkarov and Georgiades, 2004]. In this section, only the salient features of this latter model will be given in so far as they represent the starting point of the current model.

Consider a thin smart composite layer with wavy surfaces as shown in Figure 4-2. It is assumed that the thin smart composite layer containing a large number of periodically arranged actuators. This periodic structure is obtained by repeating a certain small unit cell Ω_δ in the x_1-x_2 plane but not in transverse direction. All three coordinates in Figure 4-2 are assumed to have been made dimensionless by dividing the unit cell by a certain characteristic dimension of the body, L. The shape of the top and bottom surfaces of this structure is determined by the nature of the reinforcements used (rib or stiffener). Clearly, in the absence of any surface reinforcements, the composite layer will be flat.

The unit cell of the problem under consideration is characterized by the following inequalities:

$$\left\{-\frac{\delta h_1}{2} < x_1 < \frac{\delta h_1}{2},\quad -\frac{\delta h_2}{2} < x_2 < \frac{\delta h_2}{2},\quad S^- < x_3 < S^+\right\},\quad \text{where}$$
$$S^{\pm} = \pm\frac{\delta}{2} \pm \delta F^{\pm}\left(\frac{x_1}{\delta h_1}, \frac{x_2}{\delta h_2}\right) \qquad [4.1]$$

Here, the parameters h_1, and h_2 characterize the ratio of the tangential to thickness dimensions of the unit cell and δ represents the thickness of the plate. The functions $F^{\pm}$ characterize the geometric profiles of the top and bottom surfaces and are assumed to be piecewise smooth and periodic in x_1 and x_2 plane with respective periods δh_1 and δh_2.

The elastic deformation of this smart periodic structure can be represented by means of following expressions:

$$
\begin{aligned}
&\frac{\partial \sigma_{ij}}{\partial x_j} - P_i = 0 \quad \text{where,} \\
&\sigma_{ij} = C_{ijkl}\left\{e_{kl} - d^{(r)}_{klm} R_m - \alpha^{(\theta)}_{kl} T\right\} \quad \text{and} \\
&e_{ij} = \frac{1}{2}\left(\frac{\partial u_i}{\partial x_j} + \frac{\partial u_j}{\partial x_i}\right)
\end{aligned}
\qquad [4.2]
$$

The first expression in Equation [4.2] represents the static equilibrium equation of a body subjected to surface traction and body forces. The second equation is Hooke's law which is modified to include actuation, and thermal expansion effects. The final expression in Equation [4.2] represents the familiar stress-strain relationships.

C_{ijkl} represents the tensor of elastic coefficients, e_{kl} is the strain tensor which is a function of the displacement field **u**, $d^{(r)}_{klm}$ are the actuation coefficients describing the effect of a control signal **R** on the stress field σ_{ij}, $\alpha^{(\theta)}_{kl}$ are the thermal expansion coefficients, and T represents change in temperature with respect to a reference state. Finally, P_i represents body forces. It is assumed in Equation [4.2] that the elastic, piezoelectric and thermal expansion coefficients are periodic in x_1 and x_2 (with respective period's δh_1 and δh_2) but are not periodic in the transverse coordinate x_3. It is further assumed that the top and bottom surfaces of the plate $S^{\pm}$ are subjected to surface tractions p_i (not to be confused with the body force P_i) which are related to stresses by Cauchy's Law as [Holzapfel, 2000]

$$\sigma_{ij} n_j = p_i \qquad [4.3]$$

where **n** is the unit vector normal to the surfaces $x_3 = S^{\pm}(x_1,x_2)$ and is given by [Kalamkarov, 1992]:

$$\mathbf{n}^{\pm} = \left(\mp\frac{\partial S^{\pm}}{\partial x_1}, \mp\frac{\partial S^{\pm}}{\partial x_2}, 1\right) \Bigg/ \sqrt{\left(\frac{\partial S^{\pm}}{\partial x_1}\right)^2 + \left(\frac{\partial S^{\pm}}{\partial x_2}\right)^2 + 1} \qquad [4.4]$$

4.3.2. Asymptotic Analysis, Assumptions and Unit cell Problems

As explained in Chapter 3, we can not obtain a uniformly valid asymptotic expansion of the problem in its existing form, due to the simultaneous presence of the macroscopic and microscopic scales. Thus we need to first introduce the "fast" or "microscopic" variables as

$$y_1 = \frac{x_1}{\delta h_1}, \quad y_2 = \frac{x_2}{\delta h_2}, \quad z = \frac{x_3}{\delta} \qquad [4.5]$$

where δ is the thickness of the composite layer. Therefore, the unit cell Ω_δ is now defined by:

$$\left\{-\frac{1}{2} < y_1 \frac{1}{2}, \quad -\frac{1}{2} < y_2 < \frac{1}{2}, \quad Z^- < z < Z^+\right\}, \text{ where} \qquad [4.6]$$

$$Z^{\pm} = \pm\frac{1}{2} \pm F^{\pm}(\mathbf{y})$$

Similarly, the unit normal vector from Equation [4.4] now becomes:

$$n^{\pm}=\left(\mp\frac{1}{h_1}\frac{\partial F^{\pm}}{\partial y_1},\mp\frac{1}{h_2}\frac{\partial F^{\pm}}{\partial y_2},1\right)\Bigg/\sqrt{\frac{1}{h_1{}^2}\left(\frac{\partial F^{\pm}}{\partial y_1}\right)^2+\frac{1}{h_2{}^2}\left(\frac{\partial F^{\pm}}{\partial y_2}\right)^2+1} \quad [4.7]$$

We subsequently make the following asymptotic assumptions [Kalamkarov and Georgiades, 2002a]:

$$p_\alpha^{\pm}=\delta^2 r_\alpha(x,y), \quad p_3^{\pm}=\delta^3 q_3^{\pm}(x,y) \quad [4.8a]$$

$$P_\alpha=\delta f_\alpha(x,y,z), \quad P_3=\delta^2 g_3(x,y,z) \quad [4.8b]$$

$$d_{ijk}^{(r)}=\delta d_{ijk}(y,z) \quad [4.8c]$$

$$\alpha_{ij}^{(\theta)}=\delta\alpha_{ij}(y,z) \quad [4.8d]$$

It should be noted that unless it is otherwise stated, Greek indices (α, β,….) in Equations [4.8a]-[4.8c] and in subsequent equations, range from 1 to 2 and Latin indices (i, j,…) will vary from 1 to 3.

As well, we assume the following through-the-thickness relationships for temperature, T and electric field R_i:

$$T=T^{(0)}(x)+zT^{(1)}(x)$$

$$R_i=R_i^{(0)}(x)+zR_i^{(1)}(x) \quad [4.9]$$

The next step is to assume asymptotic expansions for the displacement in the form of:

$$u_i=u_i^{(0)}(\mathbf{x},\mathbf{y},\mathbf{z})+\delta u_i^{(1)}(\mathbf{x},\mathbf{y},\mathbf{z})+\delta^2 u_i^{(2)}(\mathbf{x},\mathbf{y},\mathbf{z})+\ldots \quad [4.10]$$

for stress field as:

$$\sigma_{ij} = \sigma_{ij}^{(0)}(\mathbf{x},\mathbf{y},\mathbf{z}) + \delta\sigma_{ij}^{(1)}(\mathbf{x},\mathbf{y},\mathbf{z}) + \delta^2\sigma_{ij}^{(2)}(\mathbf{x},\mathbf{y},\mathbf{z}) + \ldots \qquad [4.11]$$

The solution of this problem is obtained from Equations [4.2], [4.5], [4.10], and [4.11] and results in an equivalent smart composite plate model, see Kalamkarov and Georgiades [2004]. The constitutive relationships of this equivalent model are obtained in terms of the stress resultants, $N_{\alpha\beta}$, the moment resultants, $M_{\alpha\beta}$, and the mid-surface strains, $\varepsilon_{\alpha\beta}$, and curvatures, $\kappa_{\alpha\beta}$. They are given as:

$$\begin{aligned} N_{\alpha\beta} = {} & \delta\left\langle b_{\alpha\beta}^{\lambda\mu}\right\rangle\varepsilon_{\lambda\mu} + \delta^2\left\langle b_{\alpha\beta}^{*\lambda\mu}\right\rangle\tau_{\lambda\mu} - \delta^2\left\langle d_{\alpha\beta}^{k}\right\rangle R_k^{(0)} - \delta^2\left\langle d_{\alpha\beta}^{*k}\right\rangle R_k^{(1)} + \\ & - \delta^2\left\langle \Theta_{\alpha\beta}\right\rangle T^{(0)} - \delta^2\left\langle \Theta_{\alpha\beta}^{*}\right\rangle T^{(1)} \end{aligned} \qquad [4.12]$$

$$\begin{aligned} M_{\alpha\beta} = {} & \delta\left\langle z b_{\alpha\beta}^{\lambda\mu}\right\rangle\varepsilon_{\lambda\mu} + \delta^2\left\langle z b_{\alpha\beta}^{*\lambda\mu}\right\rangle\tau_{\lambda\mu} - \delta^2\left\langle z d_{\alpha\beta}^{k}\right\rangle R_k^{(0)} - \delta^2\left\langle z d_{\alpha\beta}^{*k}\right\rangle R_k^{(1)} + \\ & - \delta^2\left\langle z\Theta_{\alpha\beta}\right\rangle T^{(0)} - \delta^2\left\langle z\Theta_{\alpha\beta}^{*}\right\rangle T^{(1)} \end{aligned} \qquad [4.13]$$

The quantities $< b_{\alpha\beta}^{\lambda\mu} >$, $< b_{\alpha\beta}^{*\lambda\mu} >$, $< zb_{\alpha\beta}^{\lambda\mu} >$, and $< zb_{\alpha\beta}^{*\lambda\mu} >$ are called the effective elastic coefficients, $< d_{\alpha\beta}^{k} >$, $< d_{\alpha\beta}^{*k} >$ are the effective piezoelectric coefficients, and finally, $< \Theta_{\alpha\beta} >$, $< \Theta_{\alpha\beta}^{*} >$ are the effective thermal expansion coefficients. The effective coefficients are obtained through integration over the entire unit cell Ω_δ (with volume equal to $|\Omega|$) according to:

$$\left\langle f(y_1, y_2, z)\right\rangle = \frac{1}{|\Omega|}\int_{\Omega} f(y_1, y_2, z)\,dy_1 dy_2 dz \qquad [4.14]$$

Before expressions [4.12] and [4.13] can be used, the effective coefficients must first be determined from the following problems [Kalamkarov and Georgiades, 2004]:

$$\frac{1}{h_\beta}\frac{\partial}{\partial y_\beta}b_{i\beta}^{\lambda\mu}+\frac{\partial}{\partial z}b_{i3}^{\lambda\mu}=0 \text{ with } \left(\frac{1}{h_\beta}n_\beta b_{i\beta}^{\lambda\mu}+n_3 b_{i3}^{\lambda\mu}\right)=0 \text{ at } z=Z^{\pm} \quad [4.15a]$$

$$\frac{1}{h_\beta}\frac{\partial}{\partial y_\beta}b_{i\beta}^{*\lambda\mu}+\frac{\partial}{\partial z}b_{i3}^{*\lambda\mu}=0 \text{ with } \left(\frac{1}{h_\beta}n_\beta b_{i\beta}^{*\lambda\mu}+n_3 b_{i3}^{*\lambda\mu}\right)=0 \text{ at } z=Z^{\pm} \quad [4.15b]$$

$$\frac{1}{h_\beta}\frac{\partial}{\partial y_\beta}d_{i\beta}^{k}+\frac{\partial}{\partial z}d_{i3}^{k}=0 \text{ with } \left(\frac{1}{h_\beta}n_\beta d_{i\beta}^{k}+n_3 d_{i3}^{k}\right)=0 \text{ at } z=Z^{\pm} \quad [4.16a]$$

$$\frac{1}{h_\beta}\frac{\partial}{\partial y_\beta}d_{i\beta}^{*k}+\frac{\partial}{\partial z}d_{i3}^{*k}=0 \text{ with } \left(\frac{1}{h_\beta}n_\beta d_{i\beta}^{*k}+n_3 d_{i3}^{*k}\right)=0 \text{ at } z=Z^{\pm} \quad [4.16b]$$

$$\frac{1}{h_\beta}\frac{\partial}{\partial y_\beta}\Theta_{i\beta}+\frac{\partial}{\partial z}\Theta_{i3}=0 \text{ with } \left(\frac{1}{h_\beta}n_\beta \Theta_{i\beta}+n_3 \Theta_{i3}\right)=0 \text{ at } z=Z^{\pm} \quad [4.17a]$$

$$\frac{1}{h_\beta}\frac{\partial}{\partial y_\beta}\Theta_{i\beta}^{*}+\frac{\partial}{\partial z}\Theta_{i3}^{*}=0 \text{ with } \left(\frac{1}{h_\beta}n_\beta \Theta_{i\beta}^{*}+n_3 \Theta_{i3}^{*}\right)=0 \text{ at } z=Z^{\pm} \quad [4.17b]$$

The differential equations and pertinent boundary conditions in [4.15a]-[4.17b] are solved entirely on the domain of the unit cell and are called "unit cell problems". It is worth noting that unlike "classical" unit cell problems [see e.g. Bakhvalov and Panasenko, 1984), those defined by Equations [4.15a]-[4.17b] do not depend on periodicity conditions in the z-direction but rather on boundary conditions.

In actual fact, the local functions $b_{ij}^{\lambda\mu}$, $b_{ij}^{*\lambda\mu}$, d_{ij}^{k} etc are not solved directly from Equation [4.15a]-[4.17b]. Instead, the following definitions

$$b_{ij}^{lm} = \frac{1}{h_\beta} C_{ijn\beta} \frac{\partial U_n^{lm}}{\partial y_\beta} + C_{ijn3} \frac{\partial U_n^{lm}}{\partial z} + C_{ijlm} \quad [4.18a]$$

$$b_{ij}^{*lm} = \frac{1}{h_\beta} C_{ijn\beta} \frac{\partial V_n^{lm}}{\partial y_\beta} + C_{ijn3} \frac{\partial V_n^{lm}}{\partial z} + zC_{ijlm} \quad [4.18b]$$

$$d_{ij}^{k} = P_{ijk} - \frac{1}{h_\beta} C_{ijn\beta} \frac{\partial U_n^{k}}{\partial y_\beta} + C_{ijm3} \frac{\partial U_n^{k}}{\partial z} \quad [4.19a]$$

$$d_{ij}^{*k} = zP_{ijk} - \frac{1}{h_\beta} C_{ijn\beta} \frac{\partial V_n^{k}}{\partial y_\beta} + C_{ijm3} \frac{\partial V_n^{k}}{\partial z} \quad [4.19b]$$

$$\Theta_{ij} = K_{ij} - \frac{1}{h_\beta} C_{ijn\beta} \frac{\partial U_n}{\partial y_\beta} + C_{ijm3} \frac{\partial U_n}{\partial z} \quad [4.20a]$$

$$\Theta_{ij}^{*k} = zK_{ij} - \frac{1}{h_\beta} C_{ijn\beta} \frac{\partial V_n}{\partial y_\beta} + C_{ijm3} \frac{\partial V_n}{\partial z}, \quad [4.20b]$$

where

$$P_{ijm} = C_{ijkl} d_{klm}^{(r)}; \quad K_{ij} = C_{ijkl} \alpha_{kl}^{(\theta)} \quad [4.21]$$

are used to relate the local functions with the yet unknown functions $U_n^{lm}(y_1, y_2, z)$, $V_n^{lm}(y_1, y_2, z)$, $U_n^{l}(y_1, y_2, z)$, etc and the material coefficients C_{ijkl}, P_{ijk}, K_{ij}. These functions are periodic in y_α but not in z. Thus, [4.18a]-[4.20b] are first substituted in [4.15a] to [4.17b] to obtain functions $U_n^{lm}(y_1, y_2, z)$, $V_n^{lm}(y_1, y_2, z)$, $U_n^{l}(y_1, y_2, z)$, etc and these are subsequently back substituted in [4.18a]-[4.20b] to evaluate the local $b_{ij}^{\lambda\mu}$, $b_{ij}^{*\lambda\mu}$, d_{ij}^{k} etc coefficients. Finally, the effective elastic, piezoelectric, and thermal expansion coefficients are obtained from the homogenization Equation in [4.14].

When dealing with materials that are periodic in all the three coordinates, Bakhvalov and Panasenko [1984] showed that the symmetry properties of the coefficients involved remain the same after the homogenization process. For this model (Kalamkarov, [1992], and Kalamkarov and Georgiades, [2002a]), there is no periodicity in the transverse direction and so the symmetry properties of the elastic, piezoelectric, and thermal expansion coefficients need some consideration. Although they will not be proved here, the following symmetry relationships are true [Kalamkarov and Georgiades, 2002a]

$$\left\langle b_{ij}^{mn}\right\rangle=\left\langle b_{mn}^{ij}\right\rangle,\left\langle zb_{ij}^{mn}\right\rangle=\left\langle b_{mn}^{*ij}\right\rangle,\left\langle zb_{ij}^{*mn}\right\rangle=\left\langle zb_{mn}^{*ij}\right\rangle \qquad [4.22]$$

$$\begin{gathered}\delta\langle\theta_{mn}\rangle=\left\langle\alpha_{ij}^{(\theta)}b_{ij}^{mn}\right\rangle,\ \delta\langle z\theta_{mn}\rangle=\left\langle\alpha_{ij}^{(\theta)}b_{ij}^{*mn}\right\rangle,\\ \delta\left\langle\theta_{mn}^{*}\right\rangle=\left\langle z\alpha_{ij}^{(\theta)}b_{ij}^{mn}\right\rangle,\ \delta\left\langle z\theta_{mn}^{*}\right\rangle=\left\langle z\alpha_{ij}^{(\theta)}b_{ij}^{*mn}\right\rangle\end{gathered} \qquad [4.23]$$

$$\begin{gathered}\delta\left\langle d_{mn}^{k}\right\rangle=\left\langle d_{ijk}^{(r)}b_{ij}^{mn}\right\rangle,\ \delta\left\langle zd_{mn}^{k}\right\rangle=\left\langle d_{ijk}^{(r)}b_{ij}^{*mn}\right\rangle,\\ \delta\left\langle d_{mn}^{*k}\right\rangle=\left\langle zd_{ijk}^{(r)}b_{ij}^{mn}\right\rangle,\ \delta\left\langle zd_{mn}^{*k}\right\rangle=\left\langle zd_{ijk}^{(r)}b_{ij}^{*mn}\right\rangle\end{gathered} \qquad [4.24]$$

Before closing this section, it is worthwhile to note that there is a direct correspondence between the effective elastic coefficients and the extensional, A_{ij}, bending, B_{ij}, and coupling, D_{ij}, used extensively in the classical composite laminate theory (see e.g. Gibson, [1994]; Reddy, [1997]).

These can be expressed in the following manner:

$$\left[\begin{array}{c|c}A & B\\ \hline B & D\end{array}\right]=\left[\begin{array}{ccc|ccc}\delta\left\langle b_{11}^{11}\right\rangle & \delta\left\langle b_{11}^{22}\right\rangle & \delta\left\langle b_{11}^{12}\right\rangle & \delta^2\left\langle zb_{11}^{11}\right\rangle & \delta^2\left\langle zb_{11}^{22}\right\rangle & \delta^2\left\langle zb_{11}^{12}\right\rangle\\ \delta\left\langle b_{11}^{22}\right\rangle & \delta\left\langle b_{22}^{22}\right\rangle & \delta\left\langle b_{22}^{12}\right\rangle & \delta^2\left\langle zb_{11}^{22}\right\rangle & \delta^2\left\langle zb_{22}^{22}\right\rangle & \delta^2\left\langle zb_{22}^{12}\right\rangle\\ \delta\left\langle b_{11}^{12}\right\rangle & \delta\left\langle b_{22}^{12}\right\rangle & \delta\left\langle b_{12}^{12}\right\rangle & \delta^2\left\langle zb_{11}^{12}\right\rangle & \delta^2\left\langle zb_{22}^{12}\right\rangle & \delta^2\left\langle zb_{12}^{12}\right\rangle\\ \hline \delta^2\left\langle b_{11}^{*11}\right\rangle & \delta^2\left\langle b_{11}^{*22}\right\rangle & \delta^2\left\langle b_{11}^{*12}\right\rangle & \delta^3\left\langle zb_{11}^{*11}\right\rangle & \delta^3\left\langle zb_{11}^{*22}\right\rangle & \delta^3\left\langle zb_{11}^{*12}\right\rangle\\ \delta^2\left\langle b_{11}^{*22}\right\rangle & \delta^2\left\langle b_{22}^{*22}\right\rangle & \delta^2\left\langle b_{22}^{*12}\right\rangle & \delta^3\left\langle zb_{11}^{*22}\right\rangle & \delta^3\left\langle zb_{22}^{*22}\right\rangle & \delta^3\left\langle zb_{22}^{*12}\right\rangle\\ \delta^2\left\langle b_{11}^{*12}\right\rangle & \delta^2\left\langle b_{22}^{*12}\right\rangle & \delta^2\left\langle b_{12}^{*12}\right\rangle & \delta^3\left\langle zb_{11}^{*12}\right\rangle & \delta^3\left\langle zb_{22}^{*12}\right\rangle & \delta^3\left\langle zb_{12}^{*12}\right\rangle\end{array}\right] \qquad [4.25]$$

Similar relationships exist for the effective piezoelectric and thermal expansion coefficients.

4.4. Network Reinforced Smart Composite Plates

Consider a thin smart composite plate reinforced with N families of mutually parallel reinforcements or bars which may also exhibit piezoelectric behavior, see Figure 4-3. The members of each family are made of homogeneous orthotropic material and are oriented at an angle φ_i with the y_1 direction. Furthermore, they are assumed to be much stiffer than the surrounding matrix and as such we may neglect the contribution of the matrix in the ensuing analysis. The nature of the smart structure of Figure 4-3 is such, that it would be more efficient if we first considered a simpler type of unit cell with only a single embedded reinforcement/actuator. Having solved this, the effective elastic, piezoelectric and thermal expansion coefficients of more general structures with more inclusions can readily be determined by superposition. This is the subject of discussion of the next section.

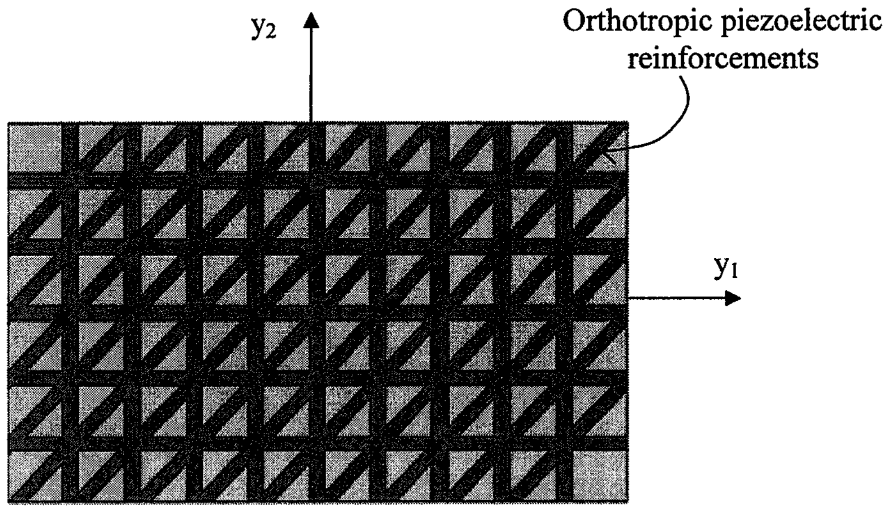

Figure 4-3: Smart composite layer with three families of piezoelectric reinforcements

Before proceeding, we note that the matrices (tensors) of the elastic, piezoelectric, and thermal expansion coefficients of an orthotropic material with respect to a coordinate system which is rotated by an angle φ (in the y_1-y_2 plane) with respect to the principal material coordinate system coincide with those of a monoclinic material and have the following form (Reddy, 1997):

$$[C]=\begin{bmatrix} c_{11} & c_{12} & c_{13} & 0 & 0 & c_{16} \\ c_{12} & c_{22} & c_{23} & 0 & 0 & c_{26} \\ c_{13} & c_{23} & c_{33} & 0 & 0 & c_{36} \\ 0 & 0 & 0 & c_{44} & c_{45} & 0 \\ 0 & 0 & 0 & c_{45} & c_{55} & 0 \\ c_{16} & c_{26} & c_{36} & 0 & 0 & c_{66} \end{bmatrix} \qquad [4.26a]$$

$$[P]=\begin{bmatrix} 0 & 0 & P_{31} \\ 0 & 0 & P_{31} \\ 0 & 0 & P_{33} \\ P_{14} & P_{24} & 0 \\ P_{15} & P_{25} & 0 \\ 0 & 0 & P_{36} \end{bmatrix} \qquad [4.26b]$$

$$[K]=\begin{bmatrix} K_{11} & K_{12} & 0 \\ K_{12} & K_{22} & 0 \\ 0 & 0 & K_{33} \end{bmatrix} \qquad [4.26c]$$

In the following sections the effective elastic, piezoelectric, and thermal expansion coefficients for a network reinforced smart composite plate are derived and specific examples are considered.

4.4.1. Effective Elastic Coefficients

4.4.1.1. Evaluation of b_{ij}^{kl} coefficients for basic unit cell structure

We will begin our analysis with the determination of the effective elastic coefficients of a unit cell with a single inclusion. Consider the unit cell of Figure 4-5 shown both before and after the introduction of the microscopic variables y_1, y_2, and z defined by Equation [4.5]. After this coordinate transformation, the unit cell changes shape and the angle between the reinforcement and the y_1 axis changes from φ to φ' according to:

$$\varphi' = \arctan\left(\frac{h_1}{h_2}\tan\varphi\right) \qquad [4.27]$$

To see how Equation [4.27] is obtained we refer to Figure 4-4, which shows the unit cell in question in both the macroscopic and microscopic variables.

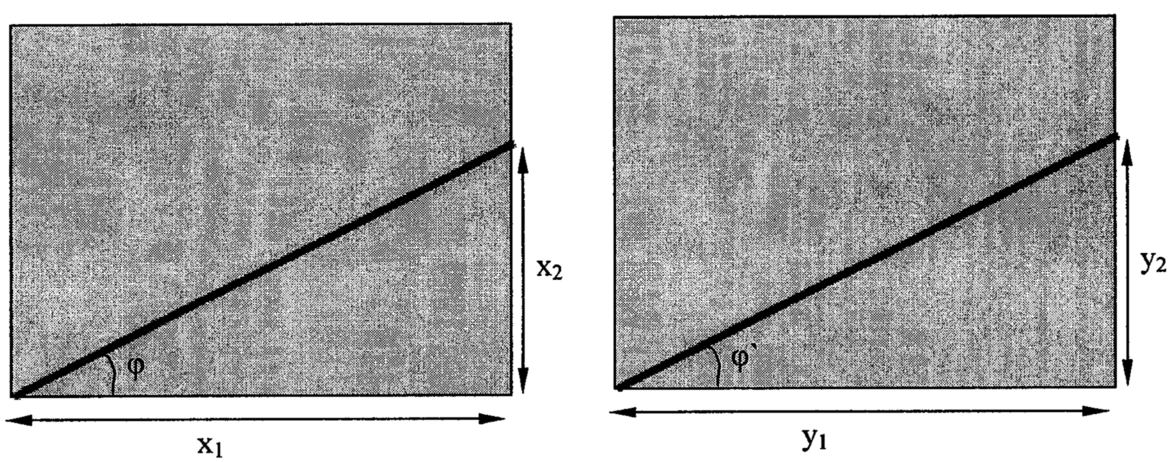

Figure 4-4: Unit cell in both macroscopic and microscopic variables

From Figure 4-4:

$$\tan \varphi = \frac{x_2}{x_1}$$
$$\tan \varphi' = \frac{y_2}{y_1} \qquad [4.28]$$

Equation [4.28] gives, in view of Equation [4.5], the following expression:

$$\tan \varphi' = \frac{h_1}{h_2} \tan \varphi \qquad [4.29]$$

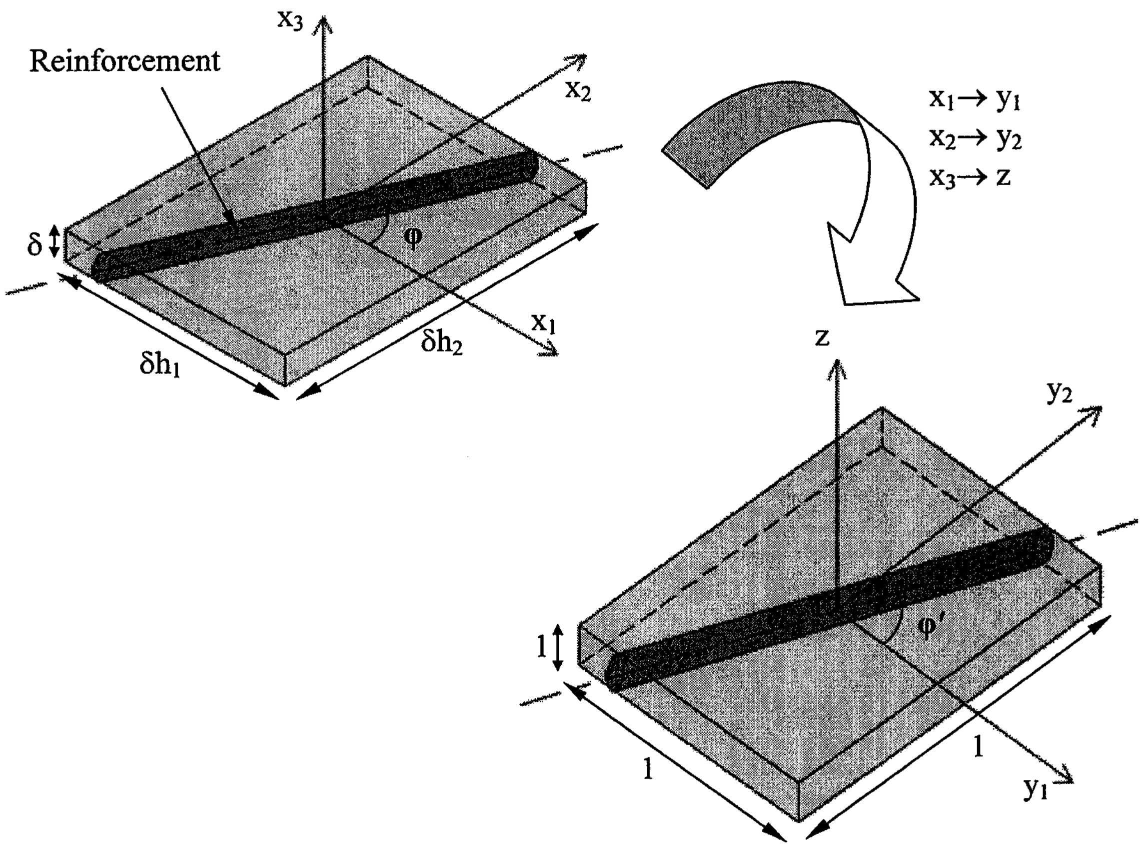

Figure 4-5: Unit cell in the macroscopic and microscopic variables

To determine the effective elastic coefficients, we first solve for the local functions $b_{ij}^{\lambda\mu}$ from Equation [4.18a]. Keeping Equation [4.26a] in mind, the $b_{ij}^{\lambda\mu}$ functions for an off-axis orthotropic reinforcement are obtained as:

$$
\begin{aligned}
b_{11}^{\lambda\mu} &= \frac{1}{h_1}C_{11}\frac{\partial U_1^{\lambda\mu}}{\partial y_1} + \frac{1}{h_2}C_{12}\frac{\partial U_2^{\lambda\mu}}{\partial y_2} + C_{13}\frac{\partial U_3^{\lambda\mu}}{\partial z} + C_{16}\left[\frac{1}{h_1}\frac{\partial U_2^{\lambda\mu}}{\partial y_1} + \frac{1}{h_2}\frac{\partial U_1^{\lambda\mu}}{\partial y_2}\right] + C_{11\lambda\mu} \\
b_{22}^{\lambda\mu} &= \frac{1}{h_1}C_{12}\frac{\partial U_1^{\lambda\mu}}{\partial y_1} + \frac{1}{h_2}C_{22}\frac{\partial U_2^{\lambda\mu}}{\partial y_2} + C_{23}\frac{\partial U_3^{\lambda\mu}}{\partial z} + C_{26}\left[\frac{1}{h_1}\frac{\partial U_2^{\lambda\mu}}{\partial y_1} + \frac{1}{h_2}\frac{\partial U_1^{\lambda\mu}}{\partial y_2}\right] + C_{22\lambda\mu} \\
b_{33}^{\lambda\mu} &= \frac{1}{h_1}C_{13}\frac{\partial U_1^{\lambda\mu}}{\partial y_1} + \frac{1}{h_2}C_{23}\frac{\partial U_2^{\lambda\mu}}{\partial y_2} + C_{33}\frac{\partial U_3^{\lambda\mu}}{\partial z} + C_{36}\left[\frac{1}{h_1}\frac{\partial U_2^{\lambda\mu}}{\partial y_1} + \frac{1}{h_2}\frac{\partial U_1^{\lambda\mu}}{\partial y_2}\right] + C_{33\lambda\mu} \\
b_{12}^{\lambda\mu} &= \frac{1}{h_1}C_{16}\frac{\partial U_1^{\lambda\mu}}{\partial y_1} + \frac{1}{h_2}C_{26}\frac{\partial U_2^{\lambda\mu}}{\partial y_2} + C_{36}\frac{\partial U_3^{\lambda\mu}}{\partial z} + C_{66}\left[\frac{1}{h_1}\frac{\partial U_2^{\lambda\mu}}{\partial y_1} + \frac{1}{h_2}\frac{\partial U_1^{\lambda\mu}}{\partial y_2}\right] + C_{12\lambda\mu} \\
b_{13}^{\lambda\mu} &= C_{55}\left[\frac{1}{h_1}\frac{\partial U_3^{\lambda\mu}}{\partial y_1} + \frac{\partial U_1^{\lambda\mu}}{\partial z}\right] + C_{45}\left[\frac{1}{h_2}\frac{\partial U_3^{\lambda\mu}}{\partial y_2} + \frac{\partial U_2^{\lambda\mu}}{\partial z}\right] + C_{13\lambda\mu} \\
b_{23}^{\lambda\mu} &= C_{45}\left[\frac{1}{h_1}\frac{\partial U_3^{\lambda\mu}}{\partial y_1} + \frac{\partial U_1^{\lambda\mu}}{\partial z}\right] + C_{44}\left[\frac{1}{h_2}\frac{\partial U_3^{\lambda\mu}}{\partial y_2} + \frac{\partial U_2^{\lambda\mu}}{\partial z}\right] + C_{23\lambda\mu}
\end{aligned}
\qquad [4.30]
$$

To reduce the order of the differential equations of the associated problems, we will now perform a coordinate transformation of the microscopic coordinates $\{y_1, y_2, z\}$ onto $\{\eta_1, \eta_2, \eta_3\}$ as defined by Figure 4-6, so that the η_1 coordinate axis coincides with the longitudinal axis of the reinforcement/actuator and the η_2 coordinate axis is perpendicular to it (in the plane).

From Figure 4-6, the relationship between the two sets of coordinates is given by:

$$\eta_1 = y_1\cos\varphi' + y_2\sin\varphi' \qquad [4.31a]$$

$$\eta_2 = -y_1 \sin\varphi' + y_2 \cos\varphi' \qquad [4.31b]$$

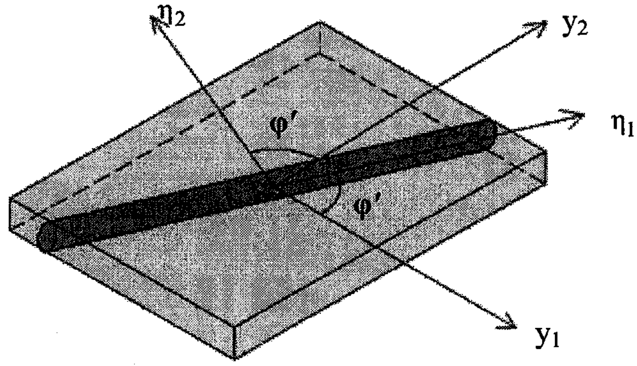

Figure 4-6: Coordinate transformation in the microscopic coordinates

With this choice of local coordinates, it is evident that the problem at hand is now independent of the η_1 coordinate and will only depend on η_2 and z. Consequently, the order of the differential equations is reduced by one, and the analysis of the problem is simplified. Thus, the $b_{ij}^{\lambda\mu}$ functions from Equation [4.30] can be written as:

$$\begin{aligned}
b_{11}^{\lambda\mu} &= -\frac{1}{h_1} C_{11} \sin\varphi' \frac{\partial U_1^{\lambda\mu}}{\partial \eta_2} + \frac{1}{h_2} C_{12} \cos\varphi' \frac{\partial U_2^{\lambda\mu}}{\partial \eta_2} + C_{13} \frac{\partial U_3^{\lambda\mu}}{\partial z} + \\
&\quad C_{16} \left[-\frac{1}{h_1} \sin\varphi' \frac{\partial U_2^{\lambda\mu}}{\partial \eta_2} + \frac{1}{h_2} \cos\varphi' \frac{\partial U_1^{\lambda\mu}}{\partial \eta_2} \right] + C_{11\lambda\mu} \\
b_{22}^{\lambda\mu} &= -\frac{1}{h_1} C_{12} \sin\varphi' \frac{\partial U_1^{\lambda\mu}}{\partial \eta_2} + \frac{1}{h_2} C_{22} \cos\varphi' \frac{\partial U_2^{\lambda\mu}}{\partial \eta_2} + C_{23} \frac{\partial U_3^{\lambda\mu}}{\partial z} + \\
&\quad C_{26} \left[-\frac{1}{h_1} \sin\varphi' \frac{\partial U_2^{\lambda\mu}}{\partial \eta_2} + \frac{1}{h_2} \cos\varphi' \frac{\partial U_1^{\lambda\mu}}{\partial \eta_2} \right] + C_{22\lambda\mu} \\
b_{33}^{\lambda\mu} &= -\frac{1}{h_1} C_{13} \sin\varphi' \frac{\partial U_1^{\lambda\mu}}{\partial \eta_2} + \frac{1}{h_2} C_{23} \cos\varphi' \frac{\partial U_2^{\lambda\mu}}{\partial \eta_2} + C_{33} \frac{\partial U_3^{\lambda\mu}}{\partial z} + \\
&\quad C_{36} \left[-\frac{1}{h_1} \sin\varphi' \frac{\partial U_2^{\lambda\mu}}{\partial \eta_2} + \frac{1}{h_2} \cos\varphi' \frac{\partial U_1^{\lambda\mu}}{\partial \eta_2} \right] + C_{33\lambda\mu}
\end{aligned} \qquad [4.32a]$$

$$b_{12}^{\lambda\mu} = -\frac{1}{h_1}C_{16}\sin\varphi'\frac{\partial U_1^{\lambda\mu}}{\partial\eta_2} + \frac{1}{h_2}C_{26}\cos\varphi'\frac{\partial U_2^{\lambda\mu}}{\partial\eta_2} + C_{36}\frac{\partial U_3^{\lambda\mu}}{\partial z} +$$
$$C_{66}\left[-\frac{1}{h_1}\sin\varphi'\frac{\partial U_2^{\lambda\mu}}{\partial\eta_2} + \frac{1}{h_2}\cos\varphi'\frac{\partial U_1^{\lambda\mu}}{\partial\eta_2}\right] + C_{12\lambda\mu} \qquad [4.32b]$$

$$b_{13}^{\lambda\mu} = C_{55}\left[-\frac{1}{h_1}\sin\varphi'\frac{\partial U_3^{\lambda\mu}}{\partial\eta_2} + \frac{\partial U_1^{\lambda\mu}}{\partial z}\right] + C_{45}\left[\frac{1}{h_2}\cos\varphi'\frac{\partial U_3^{\lambda\mu}}{\partial\eta_2} + \frac{\partial U_2^{\lambda\mu}}{\partial z}\right] + C_{13\lambda\mu}$$

$$b_{23}^{\lambda\mu} = C_{45}\left[-\frac{1}{h_1}\sin\varphi'\frac{\partial U_3^{\lambda\mu}}{\partial\eta_2} + \frac{\partial U_1^{\lambda\mu}}{\partial z}\right] + C_{44}\left[\frac{1}{h_2}\cos\varphi'\frac{\partial U_3^{\lambda\mu}}{\partial\eta_2} + \frac{\partial U_2^{\lambda\mu}}{\partial z}\right] + C_{23\lambda\mu}$$

We subsequently turn our attention to the unit cell problem and associated boundary condition. Rewriting in terms of the coordinates η_2 and z we obtain

$$-\frac{\sin\varphi'}{h_1}\frac{\partial}{\partial\eta_2}b_{i1}^{\lambda\mu} + \frac{\cos\varphi'}{h_2}\frac{\partial}{\partial\eta_2}b_{i2}^{\lambda\mu} + \frac{\partial}{\partial z}b_{i3}^{\lambda\mu} = 0 \qquad [4.33]$$

$$\left[n_2'\left(-\frac{\sin\varphi'}{h_1}b_{i1}^{\lambda\mu} + \frac{\cos\varphi'}{h_2}b_{i2}^{\lambda\mu}\right) + n_3'b_{i3}^{\lambda\mu}\right]\Bigg|_{\Im} = 0 \qquad [4.34]$$

where n_2' and n_3' are the components of the unit vector normal to the lateral surface of the reinforcement with respect to the $\{\eta_1, \eta_2, z\}$ coordinate system, and the suffix "$\Im$" stands for the matrix/reinforcement interphase.

We will solve the system defined by Equation [4.33] and associated boundary condition [4.34] by assuming that the local functions $U_1^{\lambda\mu}$ and $U_2^{\lambda\mu}$ are linear in η_2 and are independent of z, whereas $U_3^{\lambda\mu}$ is linear in z and independent of η_2. That is,

$$U_1^{\lambda\mu} = A^{\lambda\mu}\eta_2$$
$$U_2^{\lambda\mu} = B^{\lambda\mu}\eta_2 \qquad [4.35]$$
$$U_3^{\lambda\mu} = C^{\lambda\mu}z$$

where $A^{\lambda\mu}$, $B^{\lambda\mu}$, $C^{\lambda\mu}$ are yet to be determined constants. It is easily seen that Equation [4.35] will automatically satisfy the unit-cell problem [4.33] in view of the relationships [4.32a] and [43.2b]. The boundary condition [4.34] will be satisfied if:

$$-\frac{\sin\varphi'}{h_1}b_{i1}^{\lambda\mu} + \frac{\cos\varphi'}{h_2}b_{i2}^{\lambda\mu} = 0 \text{ and} \qquad [4.36]$$
$$b_{i3}^{\lambda\mu} = 0$$

Expanding the above equation for i = 1 to 3 gives:

$$-\frac{\sin\varphi'}{h_1}b_{11}^{\lambda\mu} + \frac{\cos\varphi'}{h_2}b_{12}^{\lambda\mu} = 0$$
$$-\frac{\sin\varphi'}{h_1}b_{21}^{\lambda\mu} + \frac{\cos\varphi'}{h_2}b_{22}^{\lambda\mu} = 0 \qquad [4.37]$$
$$b_{13}^{\lambda\mu} = b_{23}^{\lambda\mu} = b_{33}^{\lambda\mu} = 0$$

Substituting Equation [4.35] into the first, second and fourth ($b_{11}^{\lambda\mu}, b_{22}^{\lambda\mu}, b_{12}^{\lambda\mu}$) expressions of Equation [4.32a] and [4.32b] and then the resulting expressions into Equation [4.37] yields the following solution for the constants $A^{\lambda\mu}, B^{\lambda\mu}, C^{\lambda\mu}$ (the procedure is straightforward but algebraically tedious)

$$A^{\lambda\mu} = \frac{\left(C_{12\lambda\mu} - b_{12}^{\lambda\mu}\right)\alpha_4 + \left(C_{11\lambda\mu} - b_{11}^{\lambda\mu}\right)\alpha_5 + \left(C_{22\lambda\mu} - b_{22}^{\lambda\mu}\right)\alpha_6}{\alpha_3}$$

$$B^{\lambda\mu} = A^{\lambda\mu}\left[\frac{\left(\frac{C_{66}c}{h_2} - \frac{C_{16}s}{h_1}\right)}{\left(\frac{C_{66}s}{h_1} - \frac{C_{26}c}{h_2}\right)} - \frac{C_{36}\alpha_1}{\left(\frac{C_{66}s}{h_1} - \frac{C_{26}c}{h_2}\right)\alpha_2}\right] - \frac{C_{36}}{\alpha_2\left(\frac{C_{66}s}{h_1} - \frac{C_{26}c}{h_2}\right)}\left[\left(C_{12\lambda\mu} - b_{12}^{\lambda\mu}\right)\left(\frac{C_{12}c}{h_2} - \frac{C_{16}s}{h_1}\right) + \left(C_{11\lambda\mu} - b_{11}^{\lambda\mu}\right)\left(\frac{C_{66}s}{h_1} - \frac{C_{26}c}{h_2}\right)\right] \tag{4.38}$$

$$C^{\lambda\mu} = \frac{-A^{\lambda\mu}(\alpha_1)}{\alpha_2} - \left[\left(C_{12\lambda\mu} - b_{12}^{\lambda\mu}\right)\left(\frac{C_{12}c}{h_2} - \frac{C_{16}s}{h_1}\right) + \left(C_{11\lambda\mu} - b_{11}^{\lambda\mu}\right)\left(\frac{C_{66}s}{h_1} - \frac{C_{26}c}{h_2}\right)\right]\alpha_2^{-1}$$

Here, we let "c" and "s" stand for $\cos\varphi'$ and $\sin\varphi'$ respectively while the quantities α_1, α_2, …, α_9 are given in Appendix A. The local $b_{ij}^{\lambda\mu}$ functions are then determined from Equations [4.32], [4.35], [4.37] and [4.38] and are:

$$b_{11}^{\lambda\mu} = \frac{C_{12\lambda\mu}\left[\alpha_4\alpha_7 + \alpha_8\alpha_3\right] + C_{11\lambda\mu}\left[\alpha_5\alpha_7 - \alpha_9\alpha_3\right] + C_{22\lambda\mu}\left[\alpha_6\alpha_7\right] + C_{33\lambda\mu}\alpha_3}{\alpha_7\left[\frac{h_2 s}{h_1 c}\alpha_4 + \alpha_5 + \frac{h_2{}^2 s^2}{h_1{}^2 c^2}\alpha_6\right] + \frac{h_2 s}{h_1 c}\left[\alpha_8\alpha_3\right] - \alpha_9\alpha_3}$$

$$b_{22}^{\lambda\mu} = \frac{C_{12\lambda\mu}\left[\alpha_4\alpha_7 + \alpha_8\alpha_3\right] + C_{11\lambda\mu}\left[\alpha_5\alpha_7 - \alpha_9\alpha_3\right] + C_{22\lambda\mu}\left[\alpha_6\alpha_7\right] + C_{33\lambda\mu}\alpha_3}{\alpha_7\left[\frac{h_1 c}{h_2 s}\alpha_4 + \frac{h_1{}^2 c^2}{h_2{}^2 s^2}\alpha_5 + \alpha_6\right] + \frac{h_1 c}{h_2 s}\left[\alpha_8\alpha_3\right] - \frac{h_1{}^2 c^2}{h_2{}^2 s^2}\alpha_9\alpha_3} \tag{4.39}$$

$$b_{12}^{\lambda\mu} = \frac{C_{12\lambda\mu}\left[\alpha_4\alpha_7 + \alpha_8\alpha_3\right] + C_{11\lambda\mu}\left[\alpha_5\alpha_7 - \alpha_9\alpha_3\right] + C_{22\lambda\mu}\left[\alpha_6\alpha_7\right] + C_{33\lambda\mu}\alpha_3}{\alpha_7\left[\alpha_4 + \frac{h_1 c}{h_2 s}\alpha_5 + \frac{h_2 s}{h_1 c}\alpha_6\right] + \left[\alpha_8\alpha_3\right] - \frac{h_1 c}{h_2 s}\alpha_9\alpha_3}$$

$$b_{13}^{\lambda\mu} = b_{23}^{\lambda\mu} = b_{33}^{\lambda\mu} = 0$$

We will now focus on the $b_{ij}^{*\lambda\mu}$ coefficients.

4.4.1.2. Evaluation of $b_{ij}^{*\lambda\mu}$ coefficients for basic unit cell structure

From the Equation [4.18b] and the coordinate transformation [4.31a] and [4.31b], the $b_{ij}^{*\lambda\mu}$ coefficients can be expressed as follows:

$$
\begin{aligned}
b_{11}^{*\lambda\mu} &= -\frac{1}{h_1}C_{11}\sin\varphi'\frac{\partial V_1^{\lambda\mu}}{\partial\eta_2}+\frac{1}{h_2}C_{12}\cos\varphi'\frac{\partial V_2^{\lambda\mu}}{\partial\eta_2}+C_{13}\frac{\partial V_3^{\lambda\mu}}{\partial z}+\\
&\quad C_{16}\left[-\frac{1}{h_1}\sin\varphi'\frac{\partial V_2^{\lambda\mu}}{\partial\eta_2}+\frac{1}{h_2}\cos\varphi'\frac{\partial V_1^{\lambda\mu}}{\partial\eta_2}\right]+zC_{11\lambda\mu}\\
b_{22}^{*\lambda\mu} &= -\frac{1}{h_1}C_{12}\sin\varphi'\frac{\partial V_1^{\lambda\mu}}{\partial\eta_2}+\frac{1}{h_2}C_{22}\cos\varphi'\frac{\partial V_2^{\lambda\mu}}{\partial\eta_2}+C_{23}\frac{\partial V_3^{\lambda\mu}}{\partial z}+\\
&\quad C_{26}\left[-\frac{1}{h_1}\sin\varphi'\frac{\partial V_2^{\lambda\mu}}{\partial\eta_2}+\frac{1}{h_2}\cos\varphi'\frac{\partial V_1^{\lambda\mu}}{\partial\eta_2}\right]+zC_{22\lambda\mu}\\
b_{33}^{*\lambda\mu} &= -\frac{1}{h_1}C_{13}\sin\varphi'\frac{\partial V_1^{\lambda\mu}}{\partial\eta_2}+\frac{1}{h_2}C_{23}\cos\varphi'\frac{\partial V_2^{\lambda\mu}}{\partial\eta_2}+C_{33}\frac{\partial V_3^{\lambda\mu}}{\partial z}+\\
&\quad C_{36}\left[-\frac{1}{h_1}\sin\varphi'\frac{\partial V_2^{\lambda\mu}}{\partial\eta_2}+\frac{1}{h_2}\cos\varphi'\frac{\partial V_1^{\lambda\mu}}{\partial\eta_2}\right]+zC_{33\lambda\mu}\\
b_{12}^{*\lambda\mu} &= -\frac{1}{h_1}C_{16}\sin\varphi'\frac{\partial V_1^{\lambda\mu}}{\partial\eta_2}+\frac{1}{h_2}C_{26}\cos\varphi'\frac{\partial V_2^{\lambda\mu}}{\partial\eta_2}+C_{36}\frac{\partial V_3^{\lambda\mu}}{\partial z}+\\
&\quad C_{66}\left[-\frac{1}{h_1}\sin\varphi'\frac{\partial V_2^{\lambda\mu}}{\partial\eta_2}+\frac{1}{h_2}\cos\varphi'\frac{\partial V_1^{\lambda\mu}}{\partial\eta_2}\right]+zC_{12\lambda\mu}\\
b_{13}^{*\lambda\mu} &= C_{55}\left[-\frac{1}{h_1}\sin\varphi'\frac{\partial V_3^{\lambda\mu}}{\partial\eta_2}+\frac{\partial V_1^{\lambda\mu}}{\partial z}\right]+C_{45}\left[\frac{1}{h_2}\cos\varphi'\frac{\partial V_3^{\lambda\mu}}{\partial\eta_2}+\frac{\partial V_2^{\lambda\mu}}{\partial z}\right]+zC_{13\lambda\mu}\\
b_{23}^{*\lambda\mu} &= C_{45}\left[-\frac{1}{h_1}\sin\varphi'\frac{\partial V_3^{\lambda\mu}}{\partial\eta_2}+\frac{\partial V_1^{\lambda\mu}}{\partial z}\right]+C_{44}\left[\frac{1}{h_2}\cos\varphi'\frac{\partial V_3^{\lambda\mu}}{\partial\eta_2}+\frac{\partial V_2^{\lambda\mu}}{\partial z}\right]+zC_{23\lambda\mu}
\end{aligned}
\qquad [4.40]
$$

As well, rewriting the unit cell problem and the pertinent boundary condition (Equation [4.15b]) in terms of coordinates η_2 and z gives:

$$
\begin{gathered}
-\frac{\sin\varphi'}{h_1}\frac{\partial}{\partial\eta_2}b_{i1}^{*\lambda\mu}+\frac{\cos\varphi'}{h_2}\frac{\partial}{\partial\eta_2}b_{i2}^{*\lambda\mu}+\frac{\partial}{\partial z}b_{i3}^{*\lambda\mu}=0 \\
\left[n_2'\left(-\frac{\sin\varphi'}{h_1}b_{i1}^{*\lambda\mu}+\frac{\cos\varphi'}{h_2}b_{i2}^{*\lambda\mu}\right)+n_3'b_{i3}^{*\lambda\mu}\right]\Bigg|_{\mathfrak{I}}=0
\end{gathered}
\qquad [4.41]
$$

The presence of the z coordinate in the last term of each expression in Equation [4.40] means that the pertinent solution will depend on the shape of the cross-section of the reinforcing bar. This of course is expected because the $b_{ij}^{*\lambda\mu}$ coefficients are associated with out-of-plane deformations. As such, let us assume that the bars have a circular cross-section. We also note from Equation [4.5] that the coordinate transformation from x_1 and x_2 to y_1 and y_2 will transform the circular cross-section into an ellipse (except in the special case when $h_1 = h_2$ when the cross-section remains circular, albeit with a different radius). The value of the eccentricity, e′, of the ellipse is readily determined from Equation [4.42] below and is (derivation of eccentricity, e′ is given in Appendix B):

$$
e'=\left[1-\frac{\left(\sin^2\varphi' h_2{}^2+\cos^2\varphi' h_1{}^2\right)}{h_1{}^2h_2{}^2}\right]^{1/2}=\left[1-\frac{1}{h_1^2\sin^2\varphi+h_2^2\cos^2\varphi}\right]^{1/2} \qquad [4.42]
$$

Furthermore, the components n_2' and n_3' (clearly $n_1'=0$) of the unit vector normal to the bars surface are (Refer to Appendix C):

$$
\begin{gathered}
n_2'=\eta_2\left[1-(e')^2\right]^{-1} \\
\text{and } n_3'=z
\end{gathered}
\qquad [4.43]
$$

The presence of the z coordinate in Equation [4.40] introduces another complication to the solution of this problem. We recall that in the case of the $b_{ij}^{\lambda\mu}$ coefficients, the local

U_i^{jk} functions depended linearly on the η_2 and z coordinates. In the case of the $b_{ij}^{*\lambda\mu}$ coefficients however, a linear dependency of V_i^{jk} on η_2 and z will not satisfy the boundary conditions, but instead, the functions V_i^{jk} must have the following functional form:

$$V_i^{\lambda\mu} = W_{i1}^{\lambda\mu}\eta_2 z + W_{i2}^{\lambda\mu}\frac{\eta_2^{\,2}}{2} + W_{i3}^{\lambda\mu}\frac{z^2}{2} \qquad [4.44]$$

Here, $W_{ij}^{\lambda\mu}$ are constant coefficients which must be determined. To this end and keeping Equations [4.42] and [4.43] in mind, we first substitute Equation [4.44] into Equation [4.40] to give:

$$\begin{aligned}
b_{11}^{*\lambda\mu} &= -\frac{C_{11}}{h_1}\sin\varphi'\left[W_{11}^{\lambda\mu}z + W_{12}^{\lambda\mu}\eta_2\right] + \frac{C_{12}}{h_2}\cos\varphi'\left[W_{21}^{\lambda\mu}z + W_{22}^{\lambda\mu}\eta_2\right] + C_{13}\left[W_{31}^{\lambda\mu}\eta_2 + W_{33}^{\lambda\mu}z\right] \\
&+ C_{16}\left[-\frac{\sin\varphi'}{h_1}\left[W_{21}^{\lambda\mu}z + W_{22}^{\lambda\mu}\eta_2\right] + \frac{\cos\varphi'}{h_2}\left[W_{11}^{\lambda\mu}z + W_{12}^{\lambda\mu}\eta_2\right]\right] + zC_{11\lambda 1} \\
b_{22}^{*\lambda\mu} &= -\frac{C_{12}}{h_1}\sin\varphi'\left[W_{11}^{\lambda\mu}z + W_{12}^{\lambda\mu}\eta_2\right] + \frac{C_{22}}{h_2}\cos\varphi'\left[W_{21}^{\lambda\mu}z + W_{22}^{\lambda\mu}\eta_2\right] + C_{23}\left[W_{31}^{\lambda\mu}\eta_2 + W_{33}^{\lambda\mu}z\right] \\
&+ C_{26}\left[-\frac{\sin\varphi'}{h_1}\left[W_{21}^{\lambda\mu}z + W_{22}^{\lambda\mu}\eta_2\right] + \frac{\cos\varphi'}{h_2}\left[W_{11}^{\lambda\mu}z + W_{12}^{\lambda\mu}\eta_2\right]\right] + zC_{22\lambda 2} \\
b_{33}^{*\lambda\mu} &= -\frac{C_{13}}{h_1}\sin\varphi'\left[W_{11}^{\lambda\mu}z + W_{12}^{\lambda\mu}\eta_2\right] + \frac{C_{23}}{h_2}\cos\varphi'\left[W_{21}^{\lambda\mu}z + W_{22}^{\lambda\mu}\eta_2\right] + C_{33}\left[W_{31}^{\lambda\mu}\eta_2 + W_{33}^{\lambda\mu}z\right] \\
&+ C_{36}\left[-\frac{\sin\varphi'}{h_1}\left[W_{21}^{\lambda\mu}z + W_{22}^{\lambda\mu}\eta_2\right] + \frac{\cos\varphi'}{h_2}\left[W_{11}^{\lambda\mu}z + W_{12}^{\lambda\mu}\eta_2\right]\right] + zC_{33\lambda 3} \\
b_{12}^{*\lambda\mu} &= -\frac{C_{16}}{h_1}\sin\varphi'\left[W_{11}^{\lambda\mu}z + W_{12}^{\lambda\mu}\eta_2\right] + \frac{C_{26}}{h_2}\cos\varphi'\left[W_{21}^{\lambda\mu}z + W_{22}^{\lambda\mu}\eta_2\right] + C_{36}\left[W_{31}^{\lambda\mu}\eta_2 + W_{33}^{\lambda\mu}z\right] \\
&+ C_{66}\left[-\frac{\sin\varphi'}{h_1}\left[W_{21}^{\lambda\mu}z + W_{22}^{\lambda\mu}\eta_2\right] + \frac{\cos\varphi'}{h_2}\left[W_{11}^{\lambda\mu}z + W_{12}^{\lambda\mu}\eta_2\right]\right] + zC_{12\lambda 2}
\end{aligned} \qquad [4.45a]$$

$$b_{13}^{*\lambda\mu} = C_{55}\left[-\frac{\sin\varphi'}{h_1}\left[W_{31}^{\lambda\mu}z + W_{32}^{\lambda\mu}\eta_2\right] + \left[W_{11}^{\lambda\mu}\eta_2 + W_{12}^{\lambda\mu}z\right]\right] +$$
$$C_{45}\left[\frac{\cos\varphi'}{h_2}\left[W_{31}^{\lambda\mu}z + W_{32}^{\lambda\mu}\eta_2\right] + \left[W_{21}^{\lambda\mu}\eta_2 + W_{23}^{\lambda\mu}z\right]\right]$$

[4.45b]

$$b_{23}^{*\lambda\mu} = C_{45}\left[-\frac{\sin\varphi'}{h_1}\left[W_{31}^{\lambda\mu}z + W_{32}^{\lambda\mu}\eta_2\right] + \left[W_{11}^{\lambda\mu}\eta_2 + W_{13}^{\lambda\mu}z\right]\right] +$$
$$C_{44}\left[\frac{\cos\varphi'}{h_2}\left[W_{31}^{\lambda\mu}z + W_{32}^{\lambda\mu}\eta_2\right] + \left[W_{21}^{\lambda\mu}\eta_2 + W_{23}^{\lambda\mu}z\right]\right]$$

We subsequently substitute these expressions into Equation [4.41] and after comparing terms with different power combinations of η_2 and z, we arrive at:

$$W_{12}^{\lambda\mu} = W_{22}^{\lambda\mu} = W_{13}^{\lambda\mu} = W_{23}^{\lambda\mu} = W_{31}^{\lambda\mu} = 0 \qquad [4.46]$$

The remaining four coefficients satisfy the following relationships:

$$\frac{-sC_{13}}{h_1}W_{11}^{\lambda\mu} + \frac{cC_{23}}{h_2}W_{21}^{\lambda\mu} + C_{33}W_{33}^{\lambda\mu} - \frac{sC_{36}}{h_1}W_{21}^{\lambda\mu} + \frac{cC_{36}}{h_2}W_{11}^{\lambda\mu} + C_{33\lambda 3} = 0$$

$$W_{11}^{\lambda\mu}\left[\frac{s^2C_{11}}{h_1{}^2} - \frac{scC_{16}}{h_1h_2} - \frac{scC_{16}}{h_1h_2} + \frac{c^2C_{66}}{h_2{}^2}\right] - W_{21}^{\lambda\mu}\left[\frac{s^2C_{16}}{h_1{}^2} + \frac{c^2C_{26}}{h_2{}^2} - \frac{scC_{12}}{h_1h_2} - \frac{scC_{66}}{h_1h_2}\right] +$$
$$W_{33}^{\lambda\mu}\left[\frac{cC_{36}}{h_2} - \frac{sC_{13}}{h_1}\right] + \frac{cC_{12\lambda\mu}}{h_2} - \frac{sC_{11\lambda\mu}}{h_1} + \qquad [4.47a]$$
$$\left[1-(e')^2\right]\left[\frac{cC_{45}}{h_2}W_{32}^{\lambda\mu} + C_{45}W_{21}^{\lambda\mu} - \frac{sC_{55}}{h_1}W_{32}^{\lambda\mu} + C_{55}W_{11}^{\lambda\mu}\right] = 0$$

$$W_{11}^{\lambda\mu}\left[\frac{s^2C_{16}}{h_1^2}-\frac{scC_{66}}{h_1h_2}-\frac{scC_{12}}{h_1h_2}+\frac{c^2C_{26}}{h_2^2}\right]-W_{21}^{\lambda\mu}\left[\frac{s^2C_{66}}{h_1^2}-2\frac{scC_{26}}{h_1h_2}+\frac{c^2C_{22}}{h_2^2}\right]+$$

$$W_{33}^{\lambda\mu}\left[\frac{cC_{23}}{h_2}-\frac{sC_{36}}{h_1}\right]+\frac{cC_{22\lambda\mu}}{h_2}-\frac{sC_{12\lambda\mu}}{h_1}+$$

$$\left[1-(e')^2\right]\left[-\frac{sC_{45}}{h_1}W_{32}^{\lambda\mu}+C_{45}W_{11}^{\lambda\mu}+\frac{cC_{44}}{h_2}W_{32}^{\lambda\mu}+C_{44}W_{21}^{\lambda\mu}\right]=0 \qquad [4.47b]$$

$$-\frac{scC_{45}}{h_1h_2}W_{32}^{\lambda\mu}-\frac{sC_{45}}{h_1}W_{21}^{\lambda\mu}+\frac{s^2C_{55}}{h_1^2}W_{32}^{\lambda\mu}-\frac{sC_{55}}{h_1}W_{11}^{\lambda\mu}-\frac{scC_{45}}{h_1h_2}W_{32}^{\lambda\mu}+\frac{cC_{45}}{h_2}W_{11}^{\lambda\mu}+$$

$$\frac{c^2C_{44}}{h_2^2}W_{32}^{\lambda\mu}+\frac{cC_{44}}{h_2}W_{21}^{\lambda\mu}=0$$

where we recall the shorthand notations of "s" and "c" for $\sin\varphi'$ and $\cos\varphi'$ respectively. In view of Equation [4.46] the functions V_i^{jk} in Equation [4.44] thus reduce to:

$$\begin{aligned} V_1^{\lambda\mu} &= W_{11}^{\lambda\mu}\eta_2 z \\ V_2^{\lambda\mu} &= W_{21}^{\lambda\mu}\eta_2 z \\ V_3^{\lambda\mu} &= W_{32}^{\lambda\mu}\frac{\eta_2^2}{2}+W_{33}^{\lambda\mu}\frac{z^2}{2} \end{aligned} \qquad [4.48]$$

The solution of the four algebraic equations in [4.47] will give the four unknown $W_{11}^{\lambda\mu}, W_{21}^{\lambda\mu}, W_{32}^{\lambda\mu}, W_{33}^{\lambda\mu}$ functions and then from Equations [4.40] and [4.40] the desired b_{ij}^{*kl} coefficients will be calculated. To derive the expressions for these coefficients in a convenient form, we proceed in the following manner. We first substitute the expressions from Equation [4.46] into Equation [4.45] to obtain:

$$b_{11}^{*\lambda\mu} = z\left[-\frac{sC_{11}}{h_1}W_{11}^{\lambda\mu} + \frac{cC_{12}}{h_2}W_{21}^{\lambda\mu} + C_{13}W_{33}^{\lambda\mu} - \frac{sC_{16}}{h_1}W_{21}^{\lambda\mu} + \frac{cC_{16}}{h_2}W_{11}^{\lambda\mu} + C_{11\lambda\mu}\right]$$

$$b_{22}^{*\lambda\mu} = z\left[-\frac{sC_{12}}{h_1}W_{11}^{\lambda\mu} + \frac{cC_{22}}{h_2}W_{21}^{\lambda\mu} + C_{23}W_{33}^{\lambda\mu} - \frac{sC_{26}}{h_1}W_{21}^{\lambda\mu} + \frac{cC_{26}}{h_2}W_{11}^{\lambda\mu} + C_{22\lambda\mu}\right]$$

$$b_{33}^{*\lambda\mu} = z\left[-\frac{sC_{13}}{h_1}W_{11}^{\lambda\mu} + \frac{cC_{23}}{h_2}W_{21}^{\lambda\mu} + C_{33}W_{33}^{\lambda\mu} - \frac{sC_{36}}{h_1}W_{21}^{\lambda\mu} + \frac{cC_{36}}{h_2}W_{11}^{\lambda\mu} + C_{33\lambda\mu}\right] \quad [4.49]$$

$$b_{12}^{*\lambda\mu} = z\left[-\frac{sC_{16}}{h_1}W_{11}^{\lambda\mu} + \frac{cC_{26}}{h_2}W_{21}^{\lambda\mu} + C_{36}W_{33}^{\lambda\mu} - \frac{sC_{66}}{h_1}W_{21}^{\lambda\mu} + \frac{cC_{66}}{h_2}W_{11}^{\lambda\mu} + C_{12\lambda\mu}\right]$$

$$b_{13}^{*\lambda\mu} = \eta_2\left[\frac{cC_{45}}{h_2}W_{32}^{\lambda\mu} + C_{45}W_{21}^{\lambda\mu} - \frac{sC_{55}}{h_1}W_{32}^{\lambda\mu} + C_{55}W_{11}^{\lambda\mu}\right]$$

$$b_{23}^{*\lambda\mu} = \eta_2\left[-\frac{sC_{45}}{h_1}W_{32}^{\lambda\mu} + C_{45}W_{11}^{\lambda\mu} + \frac{cC_{44}}{h_2}W_{32}^{\lambda\mu} + C_{44}W_{21}^{\lambda\mu}\right]$$

The above equations can be rewritten as

$$b_{11}^{*\lambda\mu} = zB_{11}^{\lambda\mu}; \quad b_{22}^{*\lambda\mu} = zB_{22}^{\lambda\mu}; \quad b_{33}^{*\lambda\mu} = zB_{33}^{\lambda\mu}; \quad b_{12}^{*\lambda\mu} = zB_{12}^{\lambda\mu}$$
$$b_{13}^{*\lambda\mu} = \eta_2 B_{13}^{\lambda\mu}; \quad b_{23}^{*\lambda\mu} = \eta_2 B_{23}^{\lambda\mu} \quad [4.50]$$

where the following definitions are introduced:

$$B_{11}^{\lambda\mu} = -\frac{sC_{11}}{h_1}W_{11}^{\lambda\mu} + \frac{cC_{12}}{h_2}W_{21}^{\lambda\mu} + C_{13}W_{33}^{\lambda\mu} - \frac{sC_{16}}{h_1}W_{21}^{\lambda\mu} + \frac{cC_{16}}{h_2}W_{11}^{\lambda\mu} + C_{11\lambda\mu}$$

$$B_{22}^{\lambda\mu} = -\frac{sC_{12}}{h_1}W_{11}^{\lambda\mu} + \frac{cC_{22}}{h_2}W_{21}^{\lambda\mu} + C_{23}W_{33}^{\lambda\mu} - \frac{sC_{26}}{h_1}W_{21}^{\lambda\mu} + \frac{cC_{26}}{h_2}W_{11}^{\lambda\mu} + C_{22\lambda\mu} \quad [4.51a]$$

$$B_{33}^{\lambda\mu} = -\frac{sC_{13}}{h_1}W_{11}^{\lambda\mu} + \frac{cC_{23}}{h_2}W_{21}^{\lambda\mu} + C_{33}W_{33}^{\lambda\mu} - \frac{sC_{36}}{h_1}W_{21}^{\lambda\mu} + \frac{cC_{36}}{h_2}W_{11}^{\lambda\mu} + C_{33\lambda\mu}$$

$$B_{12}^{\lambda\mu} = -\frac{sC_{16}}{h_1} W_{11}^{\lambda\mu} + \frac{cC_{26}}{h_2} W_{21}^{\lambda\mu} + C_{36} W_{33}^{\lambda\mu} - \frac{sC_{66}}{h_1} W_{21}^{\lambda\mu} + \frac{cC_{66}}{h_2} W_{11}^{\lambda\mu} + C_{12\lambda\mu}$$

$$B_{13}^{\lambda\mu} = \frac{cC_{45}}{h_2} W_{32}^{\lambda\mu} + C_{45} W_{21}^{\lambda\mu} - \frac{sC_{55}}{h_1} W_{32}^{\lambda\mu} + C_{55} W_{11}^{\lambda\mu} \qquad [4.51b]$$

$$B_{23}^{\lambda\mu} = -\frac{sC_{45}}{h_1} W_{32}^{\lambda\mu} + C_{45} W_{11}^{\lambda\mu} + \frac{cC_{44}}{h_2} W_{32}^{\lambda\mu} + C_{44} W_{21}^{\lambda\mu}$$

Substitution of n_2' and n_3' from Equation [4.43] into [4.41] and equating equal powers of η_2 and z results in the following expressions:

$$\begin{gathered} -\frac{s}{h_1} B_{11}^{\lambda\mu} + \frac{c}{h_2} B_{12}^{\lambda\mu} + \left[1 - (e')^2\right] B_{13}^{\lambda\mu} = 0 \\ -\frac{s}{h_1} B_{12}^{\lambda\mu} + \frac{c}{h_2} B_{22}^{\lambda\mu} + \left[1 - (e')^2\right] B_{23}^{\lambda\mu} = 0 \\ -\frac{s}{h_1} B_{13}^{\lambda\mu} + \frac{c}{h_2} B_{23}^{\lambda\mu} = 0 \\ B_{33}^{\lambda\mu} = 0 \end{gathered} \qquad [4.52]$$

From Equations [4.25] and [4.50] it can be observed that we only require $B_{11}^{\lambda\mu}, B_{22}^{\lambda\mu}, B_{12}^{\lambda\mu}$ in order to calculate the effective elastic coefficients of the smart composite layer. Proceeding in a straightforward (although algebraically tedious) manner, we isolate a system of three equations involving only $B_{11}^{\lambda\mu}, B_{22}^{\lambda\mu}, B_{12}^{\lambda\mu}$ from Equations [4.51] and [4.52]. In this process the four unknown $W_{11}^{\lambda\mu}, W_{21}^{\lambda\mu}, W_{32}^{\lambda\mu}, W_{33}^{\lambda\mu}$ functions are given as,

$$W_{21}^{\lambda\mu}=\frac{\Delta_3 h_1 h_2 (cC_{66}h_1 - sC_{16}h_2)}{(sC_{66}h_2 - cC_{26}h_1)\Delta_1 - (cC_{66}h_1 - sC_{16}h_2)\Delta_2}-\frac{\left(B_{12}^{\lambda\mu} - C_{36}W_{33}^{\lambda\mu} - C_{12\lambda\mu}\right)h_1 h_2 \Delta_1}{(sC_{66}h_2 - cC_{26}h_1)\Delta_1 - (cC_{66}h_1 - sC_{16}h_2)\Delta_2}$$

$$W_{11}^{\lambda\mu}=\frac{\left(B_{12}^{\lambda\mu} - C_{36}W_{33}^{\lambda\mu} - C_{12\lambda\mu}\right)h_1 h_2}{(cC_{66}h_1 - sc_{16}h_2)}\left[1-\frac{\Delta_1(sC_{66}h_2 - cC_{26}h_1)}{\Delta_4}\right]+\frac{\Delta_3 h_1 h_2 (sC_{66}h_2 - sC_{26}h_1)}{\Delta_4} \qquad [4.53]$$

$$W_{33}^{\lambda\mu}=\frac{\dfrac{B_{11}^{\lambda\mu} - C_{11\lambda\mu}}{C_{13}} - \dfrac{B_{12}^{\lambda\mu} - C_{12\lambda\mu}}{C_{13}}[\Delta_5]}{1-\dfrac{C_{36}}{C_{13}}\Delta_5}-\frac{\dfrac{\Delta_3}{C_{13}\Delta_4}\left[(sC_{66}h_2 - cC_{26}h_1)(cC_{16}h_1 - sC_{11}h_2)+(cC_{66}h_1 - sC_{16}h_2)(cC_{12}h_1 - sC_{16}h_2)\right]}{1-\dfrac{C_{36}}{C_{13}}\Delta_5}$$

where $\Delta_1 - \Delta_5$ are given in Appendix D.

Finally, the solution of this system is given as:

$$B_{11}^{\lambda\mu}=\frac{\Lambda_5\Lambda_6 - \Lambda_2\Lambda_3}{\Lambda_1\Lambda_2 - \Lambda_4\Lambda_5}$$

$$B_{22}^{\lambda\mu}=\frac{\Lambda_3\Lambda_4 - \Lambda_1\Lambda_6}{\Lambda_1\Lambda_2 - \Lambda_4\Lambda_5} \qquad [4.54]$$

$$B_{12}^{\lambda\mu}=\frac{sh_2}{2h_1 c}B_{11}^{\lambda\mu}+\frac{ch_1}{2sh_2}B_{22}^{\lambda\mu}$$

The quantities $\Lambda_1 - \Lambda_6$ in Equation [4.54] depend on the geometric parameters of the unit cell and the material properties of the orthotropic reinforcement. The explicit expressions for $\Lambda_1, \Lambda_2, \ldots, \Lambda_6$ are provided in Appendix D. It is worth reiterating that in Equations [4.30]-[4.54], as well as in the expressions in the appendices, the elastic coefficients C_{ijkl} are referenced to the $\{x_i\}$ or $\{y_i\}$coordinate system, see Figure 4-5. The relation between these coefficients and the coefficients referred to the principal material coordinate system of the reinforcing bar is expressed by means of the familiar tensor transformation equation for a 4th-order tensor,

$$C_{ijkl} = a_{im} a_{jn} a_{kp} a_{lq} C^{(p)}_{mnqp} \qquad [4.55]$$

where $C^{(p)}_{ijkl}$ represent the elastic coefficients of the reinforcements with respect to their principal material coordinate system and the a_{ij} coefficients are the elements of the transformation tensor T shown in Equation [4.56].

$$[T] = \begin{bmatrix} \cos\varphi & \sin\varphi & 0 \\ -\sin\varphi & \cos\varphi & 0 \\ 0 & 0 & 1 \end{bmatrix} \qquad [4.56]$$

4.4.1.3. Calculation of effective elastic coefficients

The effective moduli for the reinforced composite plate of Figure 4-5 can be calculated by means of Equations [4.39], [4.50], [4.54] and the homogenization Equation [4.14]. Let $\delta^3 V$ be the volume of the reinforcing bar in the unit cell of Figure 4-5. Then, the effective coefficients are (complete derivation is given in Appendix E):

$$\left\langle b^{\lambda\mu}_{ij} \right\rangle = \frac{1}{|\Omega|} \int_{|\Omega|} b^{\lambda\mu}_{ij} dv = \frac{V}{h_1 h_2} b^{\lambda\mu}_{ij} \qquad [4.57a]$$

$$\left\langle zb_{ij}^{\lambda\mu}\right\rangle = \frac{1}{|\Omega|}\int_{|\Omega|} zb_{ij}^{\lambda\mu}dv = 0$$

$$\left\langle b_{ij}^{*\lambda\mu}\right\rangle = 0 \qquad [4.57b]$$

$$\left\langle zb_{ij}^{*\lambda\mu}\right\rangle = \frac{V}{16h_1h_2}B_{ij}^{\lambda\mu}$$

The corresponding results for composites reinforced by more than one family of bars can be obtained from Equation [4.57] by superposition. In doing so, we accept the error incurred due to stress concentrations and other complications at the regions of overlap of the reinforcements. However, this error is small and will not contribute significantly to the integral over the volume of the unit cell. Various examples of network reinforced composite plates will be considered at the end of this chapter.

4.4.1.4. Convergence of model for the particular case of isotropic reinforcements

In the case of isotropic reinforcements, the results converge to those of Kalamkarov [1992] who used the asymptotic homogenization technique and Pshenichnov [1982] who used a different approach based on stress-strain relationships in the reinforcements. The non-vanishing results are:

$$\left\langle b_{11}^{11}\right\rangle = \frac{V}{h_1h_2}E\cos^4\varphi; \quad \left\langle b_{22}^{22}\right\rangle = \frac{V}{h_1h_2}E\sin^4\varphi; \quad \left\langle b_{11}^{12}\right\rangle = \frac{V}{h_1h_2}E\cos^3\varphi\sin\varphi;$$
$$\left\langle b_{22}^{12}\right\rangle = \frac{V}{h_1h_2}E\cos\varphi\sin^3\varphi; \quad \left\langle b_{11}^{22}\right\rangle = \left\langle b_{12}^{12}\right\rangle = \frac{V}{h_1h_2}E\cos^2\varphi\sin^2\varphi; \qquad [4.58a]$$

$$
\begin{aligned}
\left\langle zb_{11}^{*11}\right\rangle &= \frac{V}{16h_1h_2}\frac{E}{1+\nu}\cos^2\varphi\left[\sin^2\varphi+\cos^2\varphi(1+\nu)\right]\\
\left\langle zb_{11}^{*22}\right\rangle &= \frac{V}{16h_1h_2}\frac{E\nu}{1+\nu}\cos^2\varphi\sin^2\varphi\\
\left\langle zb_{11}^{*12}\right\rangle &= \frac{V}{16h_1h_2}\frac{E}{1+\nu}\cos\varphi\sin\varphi\left[\frac{1}{2}\left(\sin^2\varphi-\cos^2\varphi\right)+\cos^2\varphi(1+\nu)\right]\\
\left\langle zb_{12}^{*12}\right\rangle &= \frac{V}{16h_1h_2}\frac{E}{2(1+\nu)}\cos\varphi\sin\varphi\left[\frac{1}{2}\left(\cos^2\varphi-\sin^2\varphi\right)+2\cos^2\varphi\sin^2\varphi(1+\nu)\right]\\
\left\langle zb_{22}^{*12}\right\rangle &= \frac{V}{16h_1h_2}\frac{E}{1+\nu}\cos\varphi\sin\varphi\left[\frac{1}{2}\left(\cos^2\varphi-\sin^2\varphi\right)+\sin^2\varphi(1+\nu)\right]\\
\left\langle zb_{22}^{*22}\right\rangle &= \frac{V}{16h_1h_2}\frac{E}{1+\nu}\sin^2\varphi\left[\cos^2\varphi+\sin^2\varphi(1+\nu)\right]
\end{aligned}
\qquad [4.58b]
$$

In Equation [4.58], E and ν are the Young's modulus and Poisson's ratio respectively of the reinforcement.

4.4.2. Effective Piezoelectric Coefficients

4.4.2.1. Solution of piezoelectric (d_{ij}^{k}) coefficients for simple unit cell structures

We will continue our analysis with the determination of the effective piezoelectric coefficients of the unit cell shown in Figure 4-5. Here we assume that the reinforcements/actuators exhibit piezoelectric characteristics. We recall that this coordinate transformation distorts the shape of the unit cell (since h_1 is not necessarily equal to h_2 and both h_1 and h_2 are larger than unity) and changes the orientation of the orthotropic inclusion from φ to φ' according to Equation [4.27]. We also recall that we are dealing with an off-axis orthotropic reinforcement/actuator. Accordingly, the matrix of piezoelectric coefficients coincides with that of a monoclinic material (see [4.26b]).

Thus the d_{ij}^k coefficients from Equation [4.19a] becomes:

$$
\begin{aligned}
d_{11}^k &= P_{11k} - \frac{1}{h_1} C_{11} \frac{\partial U_1^k}{\partial y_1} - \frac{1}{h_2} C_{12} \frac{\partial U_2^k}{\partial y_2} - C_{13} \frac{\partial U_3^k}{\partial z} - C_{16} \left[\frac{1}{h_1} \frac{\partial U_2^k}{\partial y_1} + \frac{1}{h_2} \frac{\partial U_1^k}{\partial y_2} \right] \\
d_{22}^k &= P_{22k} - \frac{1}{h_1} C_{12} \frac{\partial U_1^k}{\partial y_1} - \frac{1}{h_2} C_{22} \frac{\partial U_2^k}{\partial y_2} - C_{23} \frac{\partial U_3^k}{\partial z} - C_{26} \left[\frac{1}{h_1} \frac{\partial U_2^k}{\partial y_1} + \frac{1}{h_2} \frac{\partial U_1^k}{\partial y_2} \right] \\
d_{33}^k &= P_{33k} - \frac{1}{h_1} C_{13} \frac{\partial U_1^k}{\partial y_1} - \frac{1}{h_2} C_{23} \frac{\partial U_2^k}{\partial y_2} - C_{33} \frac{\partial U_3^k}{\partial z} - C_{36} \left[\frac{1}{h_1} \frac{\partial U_2^k}{\partial y_1} + \frac{1}{h_2} \frac{\partial U_1^k}{\partial y_2} \right] \\
d_{12}^k &= P_{12k} - \frac{1}{h_1} C_{16} \frac{\partial U_1^k}{\partial y_1} - \frac{1}{h_2} C_{26} \frac{\partial U_2^k}{\partial y_2} - C_{36} \frac{\partial U_3^k}{\partial z} - C_{66} \left[\frac{1}{h_1} \frac{\partial U_2^k}{\partial y_1} + \frac{1}{h_2} \frac{\partial U_1^k}{\partial y_2} \right] \\
d_{13}^k &= P_{13k} - C_{55} \left[\frac{1}{h_1} \frac{\partial U_3^k}{\partial y_1} + \frac{\partial U_1^k}{\partial z} \right] - C_{45} \left[\frac{1}{h_2} \frac{\partial U_3^k}{\partial y_2} + \frac{\partial U_2^k}{\partial z} \right] \\
d_{23}^k &= P_{23k} - C_{45} \left[\frac{1}{h_1} \frac{\partial U_3^k}{\partial y_1} + \frac{\partial U_1^k}{\partial z} \right] - C_{44} \left[\frac{1}{h_2} \frac{\partial U_3^k}{\partial y_2} + \frac{\partial U_2^k}{\partial z} \right]
\end{aligned}
\qquad [4.59]
$$

Similarly to the elastic coefficients, we perform the further coordinate transformation of the microscopic coordinates $\{y_1, y_2, z\}$ onto $\{\eta_1, \eta_2, z\}$ as shown in Figure 4-6, so that the η_1 coordinate axis coincides with the direction of the piezoelectric reinforcement. The relationship between the two sets of coordinates is expressed in Equation [4.31].

The pertinent unit cell problem from Equation [4.16a] becomes:

$$
\begin{aligned}
& -\frac{\sin\varphi'}{h_1} \frac{\partial}{\partial \eta_2} d_{i1}^k + \frac{\cos\varphi'}{h_2} \frac{\partial}{\partial \eta_2} d_{i2}^k + \frac{\partial}{\partial z} d_{i3}^k = 0 \\
& \left[n_2' \left(-\frac{\sin\varphi'}{h_1} d_{i1}^k + \frac{\cos\varphi'}{h_2} d_{i2}^k \right) + n_3' d_{i3}^k \right] \Bigg|_{\mho} = 0
\end{aligned}
\qquad [4.60]
$$

As well, the d_{ij}^k coefficients from Equation [4.59] become:

$$d_{11}^k = P_{11k} + \frac{1}{h_1} C_{11} \sin\varphi' \frac{\partial U_1^k}{\partial \eta_2} - \frac{1}{h_2} C_{12} \cos\varphi' \frac{\partial U_2^k}{\partial \eta_2} - C_{13} \frac{\partial U_3^k}{\partial z} - C_{16} \left[-\frac{1}{h_1} \sin\varphi' \frac{\partial U_2^k}{\partial \eta_2} + \frac{1}{h_2} \cos\varphi' \frac{\partial U_1^k}{\partial \eta_2} \right]$$

$$d_{22}^k = P_{22k} + \frac{1}{h_1} C_{12} \sin\varphi' \frac{\partial U_1^k}{\partial \eta_2} - \frac{1}{h_2} C_{22} \cos\varphi' \frac{\partial U_2^k}{\partial \eta_2} - C_{23} \frac{\partial U_3^k}{\partial z} - C_{26} \left[-\frac{1}{h_1} \sin\varphi' \frac{\partial U_2^k}{\partial \eta_2} + \frac{1}{h_2} \cos\varphi' \frac{\partial U_1^k}{\partial \eta_2} \right]$$

$$d_{33}^k = P_{33k} + \frac{1}{h_1} C_{13} \sin\varphi' \frac{\partial U_1^k}{\partial \eta_2} - \frac{1}{h_2} C_{23} \cos\varphi' \frac{\partial U_2^k}{\partial \eta_2} - C_{33} \frac{\partial U_3^k}{\partial z} - C_{36} \left[-\frac{1}{h_1} \sin\varphi' \frac{\partial U_2^k}{\partial \eta_2} + \frac{1}{h_2} \cos\varphi' \frac{\partial U_1^k}{\partial \eta_2} \right] \qquad [4.61]$$

$$d_{12}^k = P_{12k} + \frac{1}{h_1} C_{16} \sin\varphi' \frac{\partial U_1^k}{\partial \eta_2} - \frac{1}{h_2} C_{26} \cos\varphi' \frac{\partial U_2^k}{\partial \eta_2} - C_{36} \frac{\partial U_3^k}{\partial z} - C_{66} \left[-\frac{1}{h_1} \sin\varphi' \frac{\partial U_2^k}{\partial \eta_2} + \frac{1}{h_2} \cos\varphi' \frac{\partial U_1^k}{\partial \eta_2} \right]$$

$$d_{13}^k = P_{13k} - C_{55} \left[-\frac{1}{h_1} \sin\varphi' \frac{\partial U_3^k}{\partial \eta_2} + \frac{\partial U_1^k}{\partial z} \right] - C_{45} \left[\frac{1}{h_2} \cos\varphi' \frac{\partial U_3^k}{\partial \eta_2} + \frac{\partial U_2^k}{\partial z} \right]$$

$$d_{23}^k = P_{23k} - C_{45} \left[-\frac{1}{h_1} \sin\varphi' \frac{\partial U_3^k}{\partial \eta_2} + \frac{\partial U_1^k}{\partial z} \right] - C_{44} \left[\frac{1}{h_2} \cos\varphi' \frac{\partial U_3^k}{\partial \eta_2} + \frac{\partial U_2^k}{\partial z} \right]$$

We will solve Equation [4.61] and associated boundary condition [4.60] by assuming that the local functions U_1^k and U_2^k are linear in η_2 and independent of z while U_3^k is linear in z and independent of η_2. Thus:

$$U_1^k = A^k \eta_2; \quad U_2^k = B^k \eta_2; \quad U_3^k = C^k z; \qquad [4.62]$$

where A^k, B^k, C^k are the algebraic constants to be calculated in the sequel. Substituting Equation [4.62] into [4.61] and the resulting expressions in second of Equation [4.60] results in three algebraic equations for these constants:

$$\begin{aligned}
d_{11}^k &= P_{11k} + A^k\left(\frac{\sin\varphi'}{h_1}C_{11} - \frac{\cos\varphi'}{h_2}C_{16}\right) + B^k\left(-\frac{\cos\varphi'}{h_2}C_{12} + \frac{\sin\varphi'}{h_1}C_{16}\right) - C_{13}C^k \\
d_{22}^k &= P_{22k} + A^k\left(\frac{\sin\varphi'}{h_1}C_{12} - \frac{\cos\varphi'}{h_2}C_{26}\right) + B^k\left(-\frac{\cos\varphi'}{h_2}C_{22} + \frac{\sin\varphi'}{h_1}C_{26}\right) - C_{23}C^k \\
d_{12}^k &= P_{12k} + A^k\left(\frac{\sin\varphi'}{h_1}C_{16} - \frac{\cos\varphi'}{h_2}C_{66}\right) + B^k\left(-\frac{\cos\varphi'}{h_2}C_{26} + \frac{\sin\varphi'}{h_1}C_{66}\right) - C_{36}C^k
\end{aligned} \qquad [4.63]$$

Solving for these constants and back substituting into [4.61] results in the following expressions for the piezoelectric d_{ij}^k coefficients:

$$\begin{aligned}
d_{11}^k &= \frac{P_{12k}[\alpha_4\alpha_7 + \alpha_8\alpha_3] + P_{11k}[\alpha_5\alpha_7 - \alpha_9\alpha_3] + P_{22k}[\alpha_6\alpha_7] + P_{33k}\alpha_3}{\alpha_7\left[\frac{h_2 s}{h_1 c}\alpha_4 + \alpha_5 + \frac{h_2{}^2 s^2}{h_1{}^2 c^2}\alpha_6\right] + \frac{h_2 s}{h_1 c}[\alpha_8\alpha_3] - \alpha_9\alpha_3} \\
d_{22}^k &= \frac{P_{12k}[\alpha_4\alpha_7 + \alpha_8\alpha_3] + P_{11k}[\alpha_5\alpha_7 - \alpha_9\alpha_3] + P_{22k}[\alpha_6\alpha_7] + P_{33k}\alpha_3}{\alpha_7\left[\frac{h_1 c}{h_2 s}\alpha_4 + \frac{h_1{}^2 c^2}{h_2{}^2 s^2}\alpha_5 + \alpha_6\right] + \frac{h_1 c}{h_2 s}[\alpha_8\alpha_3] - \frac{h_1{}^2 c^2}{h_2{}^2 s^2}\alpha_9\alpha_3} \\
d_{12}^k &= \frac{P_{12k}[\alpha_4\alpha_7 + \alpha_8\alpha_3] + P_{11k}[\alpha_5\alpha_7 - \alpha_9\alpha_3] + P_{22k}[\alpha_6\alpha_7] + P_{33k}\alpha_3}{\alpha_7\left[\alpha_4 + \frac{h_1 c}{h_2 s}\alpha_5 + \frac{h_2 s}{h_1 c}\alpha_6\right] + [\alpha_8\alpha_3] - \frac{h_1 c}{h_2 s}\alpha_9\alpha_3} \\
& d_{13}^k = d_{23}^k = d_{33}^k = 0
\end{aligned} \qquad [4.64]$$

where constants α_1- α_9 can be found in Appendix A.

4.4.2.2. Solution of d_{ij}^{*k} coefficients for simple unit cell structure

On account of Equation [4.31], unit cell problem Equation [4.16b] becomes,

$$-\frac{\sin\varphi'}{h_1}\frac{\partial}{\partial\eta_2}d_{i1}^{*k}+\frac{\cos\varphi'}{h_2}\frac{\partial}{\partial\eta_2}d_{i2}^{*k}+\frac{\partial}{\partial z}d_{i3}^{*k}=0$$
$$\left[n_2'\left(-\frac{\sin\varphi'}{h_1}d_{i1}^{*k}+\frac{\cos\varphi'}{h_2}d_{i2}^{*k}\right)+n_3'd_{i3}^{*k}\right]\Bigg|_{\Im}=0 \qquad [4.65]$$

where,

$$d_{11}^{*k}=zP_{11k}+\frac{1}{h_1}C_{11}\sin\varphi'\frac{\partial V_1^k}{\partial\eta_2}-\frac{1}{h_2}C_{12}\cos\varphi'\frac{\partial V_2^k}{\partial\eta_2}-C_{13}\frac{\partial V_3^k}{\partial z}-C_{16}\left[-\frac{1}{h_1}\sin\varphi'\frac{\partial V_2^k}{\partial\eta_2}+\frac{1}{h_2}\cos\varphi'\frac{\partial V_1^k}{\partial\eta_2}\right]$$

$$d_{22}^{*k}=zP_{22k}+\frac{1}{h_1}C_{12}\sin\varphi'\frac{\partial V_1^k}{\partial\eta_2}-\frac{1}{h_2}C_{22}\cos\varphi'\frac{\partial V_2^k}{\partial\eta_2}-C_{23}\frac{\partial V_3^k}{\partial z}-C_{26}\left[-\frac{1}{h_1}\sin\varphi'\frac{\partial V_2^k}{\partial\eta_2}+\frac{1}{h_2}\cos\varphi'\frac{\partial V_1^k}{\partial\eta_2}\right]$$

$$d_{33}^{*k}=zP_{33k}+\frac{1}{h_1}C_{13}\sin\varphi'\frac{\partial V_1^k}{\partial\eta_2}-\frac{1}{h_2}C_{23}\cos\varphi'\frac{\partial V_2^k}{\partial\eta_2}-C_{33}\frac{\partial V_3^k}{\partial z}-C_{36}\left[-\frac{1}{h_1}\sin\varphi'\frac{\partial V_2^k}{\partial\eta_2}+\frac{1}{h_2}\cos\varphi'\frac{\partial V_1^k}{\partial\eta_2}\right] \qquad [4.66a]$$

$$d_{12}^{*k}=zP_{12k}+\frac{1}{h_1}C_{16}\sin\varphi'\frac{\partial V_1^k}{\partial\eta_2}-\frac{1}{h_2}C_{26}\cos\varphi'\frac{\partial V_2^k}{\partial\eta_2}-C_{36}\frac{\partial V_3^k}{\partial z}-C_{66}\left[-\frac{1}{h_1}\sin\varphi'\frac{\partial V_2^k}{\partial\eta_2}+\frac{1}{h_2}\cos\varphi'\frac{\partial V_1^k}{\partial\eta_2}\right]$$

$$d_{13}^{*k} = zP_{13k} - C_{55}\left[-\frac{1}{h_1}\sin\varphi'\frac{\partial V_3^k}{\partial \eta_2} + \frac{\partial V_1^k}{\partial z}\right] - C_{45}\left[\frac{1}{h_2}\cos\varphi'\frac{\partial V_3^k}{\partial \eta_2} + \frac{\partial V_2^k}{\partial z}\right]$$

$$d_{23}^{*k} = zP_{23k} - C_{45}\left[-\frac{1}{h_1}\sin\varphi'\frac{\partial V_3^k}{\partial \eta_2} + \frac{\partial V_1^k}{\partial z}\right] - C_{44}\left[\frac{1}{h_2}\cos\varphi'\frac{\partial V_3^k}{\partial \eta_2} + \frac{\partial V_2^k}{\partial z}\right] \qquad [4.66b]$$

As with the elastic coefficients, the presence of the z coordinate in Equation [4.66a] and [4.66b] means that unlike the case of the d_{ij}^k coefficients, the determination of their d_{ij}^{*k} counterparts will depend on the nature of the cross-section of the piezoelectric reinforcement. Let us now assume that the cross-section of the inclusions is circular. Assume, next that

$$V_i^k = W_{i1}^k \eta_2 z + W_{i2}^k \frac{\eta_2^{\,2}}{2} + W_{i3}^k \frac{z^2}{2} \qquad [4.67]$$

where constants W_{ij} must be determined. To this end, we substitute [4.67] into [4.65] and compare terms with like powers of η_2 and z to arrive at:

$$W_{12}^k = W_{22}^k = W_{13}^k = W_{23}^k = W_{31}^k = 0 \qquad [4.68]$$

The remaining four coefficients satisfy:

$$\begin{aligned}
&W_{11}^k\left[-\frac{s^2c_{11}}{h_1^{\,2}} + \frac{csc_{16}}{h_1h_2} + \frac{csc_{16}}{h_1h_2} - \frac{c^2c_{66}}{h_2^{\,2}}\right] - W_{21}^k\left[-\frac{s^2c_{16}}{h_1^{\,2}} - \frac{c^2c_{26}}{h_2^{\,2}} + \frac{csc_{12}}{h_1h_2} + \frac{csc_{66}}{h_1h_2}\right] - \\
&W_{33}^k\left[\frac{cc_{36}}{h_2} - \frac{sc_{13}}{h_1}\right] + \frac{cP_{12k}}{h_2} - \frac{sP_{11k}}{h_1} - \qquad [4.69a] \\
&\left[1-(e')^2\right]\left[\frac{cc_{45}}{h_2}W_{32}^k + c_{45}W_{21}^k - \frac{sc_{55}}{h_1}W_{32}^k + c_{55}W_{11}^k\right] = 0
\end{aligned}$$

$$W_{11}^{k}\left[-\frac{s^2c_{16}}{h_1^2}+\frac{csc_{66}}{h_1h_2}+\frac{csc_{12}}{h_1h_2}-\frac{c^2c_{26}}{h_2^2}\right]-W_{21}^{k}\left[\frac{s^2c_{66}}{h_1^2}-2\frac{csc_{26}}{h_1h_2}+\frac{c^2c_{22}}{h_2^2}\right]-$$

$$W_{33}^{k}\left[\frac{cc_{23}}{h_2}-\frac{sc_{36}}{h_1}\right]+\frac{cP_{22k}}{h_2}-\frac{sP_{12k}}{h_1}-$$

$$\left[1-(e')^2\right]\left[-\frac{sc_{45}}{h_1}W_{32}^{k}+c_{45}W_{11}^{k}+\frac{cc_{44}}{h_2}W_{32}^{k}+c_{44}W_{21}^{k}\right]=0$$

$$\frac{csc_{45}}{h_1h_2}W_{32}^{k}+\frac{cs_{45}}{h_1}W_{21}^{k}-\frac{s^2c_{55}}{h_1^2}W_{32}^{k}+\frac{cs_{55}}{h_1}W_{11}^{k}+\frac{csc_{45}}{h_1h_2}W_{32}^{k}-\frac{cc_{45}}{h_2}W_{11}^{k}-$$

$$\frac{c^2c_{44}}{h_2^2}W_{32}^{k}-\frac{cc_{44}}{h_2}W_{21}^{k}=0 \qquad [4.69b]$$

$$\frac{sc_{13}}{h_1}W_{11}^{k}-\frac{cc_{23}}{h_2}W_{21}^{k}-C_{33}W_{33}^{k}+\frac{sc_{36}}{h_1}W_{21}^{k}-\frac{cc_{36}}{h_2}W_{11}^{k}+P_{33k}=0$$

Equation [4.69a] and [4.69b] contains four linear algebraic equations in the remaining four unknowns W_{11}^{k}, W_{21}^{k}, W_{32}^{k}, and W_{33}^{k}. Solving for these unknowns and substituting back in Equation [4.67] and then in the expressions in Equation [4.66] gives the following results for the piezoelectric d_{ij}^{*k} coefficients,

$$d_{11}^{*k}=zD_{11}^{k}\ ;\ d_{22}^{*k}=zD_{22}^{k};\ d_{33}^{*k}=zD_{33}^{k}\ ;\ d_{12}^{*k}=zD_{12}^{k} \qquad [4.70]$$

$$d_{13}^{*k}=zP_{13k}-\eta_2D_{13}^{k}\ ;\ d_{23}^{*k}=zP_{23k}-\eta_2D_{23}^{k}$$

where,

$$D_{11}^{k}=\frac{\Lambda_5\Lambda_6-\Lambda_2\Lambda_3}{\Lambda_1\Lambda_2-\Lambda_4\Lambda_5}$$

$$D_{22}^{k}=\frac{\Lambda_3\Lambda_4-\Lambda_1\Lambda_6}{\Lambda_1\Lambda_2-\Lambda_4\Lambda_5} \qquad [4.71]$$

$$D_{12}^{k}=\frac{sh_2}{2h_1c}D_{11}^{k}+\frac{ch_1}{2sh_2}D_{22}^{k}$$

Explicit expressions for the quantities $\Lambda_1, \Lambda_2, \ldots, \Lambda_6$ which depend on the geometric parameters of the unit cell and the elastic and piezoelectric properties of the inclusions can be found from Appendix D by making the following substitution

$$C_{ijkl} \rightarrow P_{ijk} \qquad [4.72]$$

We emphasize here, that the elastic and piezoelectric coefficients in [4.30]-[4.72] as well as in the expressions in Appendices A and D, are a consequence of the basic formulation in [4.2], i.e. are referenced with respect to the $\{x_i\}$ coordinate system, see Figure 4-5. As such, they are, in general, not the principal material coefficients (except in the special case when the actuator/reinforcement is oriented along the x_1 or x_2 directions). The relationship between the two sets of the elastic coefficients is expressed in Equation [4.55] and of the piezoelectric coefficients is expressed in terms of the tensor transformation equation for 3rd order cartesian tensors, i.e.,

$$P_{ijk} = a_{im} a_{jn} a_{kp} P^{(p)}_{mnp} \qquad [4.73]$$

where the superscript (p) denotes the principal material coefficients, and a_{ij} are the elements of the transformation matrix [T] (see also Figure 4-5) as given in Equation [4.56].

4.4.2.3. Effective Piezoelectric Coefficients

The effective piezoelectric coefficients for the smart composite structure of Figure 4-5 can be calculated from [4.64], [4.71] and the homogenization procedure [4.14]. Similar to elastic coefficients, letting the volume of the orthotropic inclusion in Figure 4-5 be $\delta^3 V$, the expressions for the effective piezoelectric coefficients are given by:

$$\left\langle d_{ij}^{k} \right\rangle = \frac{1}{|Y|} \int_{|Y|} d_{ij}^{k} dv = \frac{V}{h_1 h_2} d_{ij}^{k}$$

$$\left\langle z d_{ij}^{*k} \right\rangle = \frac{V}{16 h_1 h_2} D_{ij}^{k} \qquad [4.74]$$

$$\left\langle z d_{ij}^{k} \right\rangle = \left\langle d_{ij}^{*k} \right\rangle = 0$$

These results clearly pertain to thin smart composite plates with a single family of actuators/reinforcements. For structures with more than one family, the results can easily be deduced from Equation [4.74] by means of superposition.

4.4.3. Effective Thermal Expansion Coefficients

4.4.3.1. Solution of Θ_{ij} coefficients for simple unit cell structure

We will now calculate the effective thermal expansion coefficients for the basic unit cell of Figure 4-5. On account of the coordinate transformation [4.31], the unit cell problem in Equation [4.17a] becomes:

$$-\frac{\sin\varphi'}{h_1}\frac{\partial}{\partial \eta_2}\Theta_{i1} + \frac{\cos\varphi'}{h_2}\frac{\partial}{\partial \eta_2}\Theta_{i2} + \frac{\partial}{\partial z}\Theta_{i3} = 0$$

$$\left[n_2'\left(-\frac{\sin\varphi'}{h_1}\Theta_{i1} + \frac{\cos\varphi'}{h_2}\Theta_{i2} \right) + n_3'\Theta_{i3} \right]\Bigg|_{\Im} = 0 \qquad [4.75]$$

As well, the Θ_{ij} coefficients from Equation [4.20a] are given by:

$$\Theta_{ii} = K_{ii} + \frac{1}{h_1} c_{i1} \sin\varphi' \frac{\partial U_1}{\partial \eta_2} - \frac{1}{h_2} c_{i2} \cos\varphi' \frac{\partial U_2}{\partial \eta_2} - c_{i3} \frac{\partial U_3}{\partial z} + \\ -c_{i6}\left[-\frac{1}{h_1} \sin\varphi' \frac{\partial U_2}{\partial \eta_2} + \frac{1}{h_2} \cos\varphi' \frac{\partial U_1}{\partial \eta_2} \right] \quad \text{, no summation on i}$$

$$\Theta_{12} = K_{12} + \frac{1}{h_1} c_{16} \sin\varphi' \frac{\partial U_1}{\partial \eta_2} - \frac{1}{h_2} c_{26} \cos\varphi' \frac{\partial U_2}{\partial \eta_2} - c_{36} \frac{\partial U_3}{\partial z} + \\ -c_{66}\left[-\frac{1}{h_1} \sin\varphi' \frac{\partial U_2}{\partial \eta_2} + \frac{1}{h_2} \cos\varphi' \frac{\partial U_1}{\partial \eta_2} \right] \tag{4.76}$$

$$\Theta_{\alpha 3} = K_{13} - c_{13\alpha 3}\left[-\frac{1}{h_1} \sin\varphi' \frac{\partial U_3}{\partial \eta_2} + \frac{\partial U_1}{\partial z} \right] - c_{23\alpha 3}\left[\frac{1}{h_2} \cos\varphi' \frac{\partial U_3}{\partial \eta_2} + \frac{\partial U_2}{\partial z} \right]$$

Assume next that functions U_1 and U_2 depend only on η_2 and U_3 depends only on z, i.e.

$$U_1 = \lambda_1 \eta_2; \quad U_2 = \lambda_2 \eta_2; \quad U_3 = \lambda_3 z; \tag{4.77}$$

Substitution of [4.77] into [4.76] and the resulting expressions into second expression of Equation [4.75] will yield the results for the constants λ_i. Back substituting the latter into [4.76] results in the following expressions for the Θ_{ij} coefficients:

$$\Theta_{11} = \frac{K_{12}[\alpha_4\alpha_7 + \alpha_8\alpha_3] + K_{11}[\alpha_5\alpha_7 - \alpha_9\alpha_3] + K_{22}[\alpha_6\alpha_7] + K_{33}\alpha_3}{\alpha_7\left[\frac{h_2 s}{h_1 c}\alpha_4 + \alpha_5 + \frac{h_2^2 s^2}{h_1^2 c^2}\alpha_6 \right] + \frac{h_2 s}{h_1 c}[\alpha_8\alpha_3] - \alpha_9\alpha_3}$$

$$\Theta_{22} = \frac{K_{12}[\alpha_4\alpha_7 + \alpha_8\alpha_3] + K_{11}[\alpha_5\alpha_7 - \alpha_9\alpha_3] + K_{22}[\alpha_6\alpha_7] + K_{33}\alpha_3}{\alpha_7\left[\frac{h_1 c}{h_2 s}\alpha_4 + \frac{h_1^2 c^2}{h_2^2 s^2}\alpha_5 + \alpha_6 \right] + \frac{h_1 c}{h_2 s}[\alpha_8\alpha_3] - \frac{h_1^2 c^2}{h_2^2 s^2}\alpha_9\alpha_3} \tag{4.78}$$

$$\Theta_{12} = \frac{K_{12}[\alpha_4\alpha_7 + \alpha_8\alpha_3] + K_{11}[\alpha_5\alpha_7 - \alpha_9\alpha_3] + K_{22}[\alpha_6\alpha_7] + K_{33}\alpha_3}{\alpha_7\left[\alpha_4 + \frac{h_1 c}{h_2 s}\alpha_5 + \frac{h_2 s}{h_1 c}\alpha_6 \right] + [\alpha_8\alpha_3] - \frac{h_1 c}{h_2 s}\alpha_9\alpha_3}$$

$$\Theta_{13} = \Theta_{23} = \Theta_{33} = 0$$

The explicit expressions for constants α_1- α_9 are given in Appendix A.

4.4.3.2. Solution of Θ^*_{ij} coefficients for simple unit cell structure

On account of [4.32], unit cell problem [4.17b] becomes,

$$
\begin{gathered}
-\frac{\sin\varphi'}{h_1}\frac{\partial}{\partial\eta_2}\Theta^*_{i1}+\frac{\cos\varphi'}{h_2}\frac{\partial}{\partial\eta_2}\Theta^*_{i2}+\frac{\partial}{\partial z}\Theta^{*k}_{i3}=0 \\
\left[n_2'\left(-\frac{\sin\varphi'}{h_1}\Theta^*_{i1}+\frac{\cos\varphi'}{h_2}\Theta^*_{i2}\right)+n_3'\Theta^*_{i3}\right]\Bigg|_{\Im}=0
\end{gathered}
\qquad [4.79]
$$

As well, the Θ^*_{ij} coefficients from Equation [4.20b] and [4.31] become:

$$
\begin{aligned}
\Theta^*_{ii} &= zK_{ii}+\frac{1}{h_1}c_{i1}\sin\varphi'\frac{\partial V_1}{\partial\eta_2}-\frac{1}{h_2}c_{i2}\cos\varphi'\frac{\partial V_2}{\partial\eta_2}-c_{i3}\frac{\partial V_3}{\partial z}+ \\
&\quad -c_{i6}\left[-\frac{1}{h_1}\sin\varphi'\frac{\partial V_2}{\partial\eta_2}+\frac{1}{h_2}\cos\varphi'\frac{\partial V_1}{\partial\eta_2}\right] \qquad \text{, no summation on i} \\
\Theta^*_{12} &= zK_{12}+\frac{1}{h_1}c_{16}\sin\varphi'\frac{\partial V_1}{\partial\eta_2}-\frac{1}{h_2}c_{26}\cos\varphi'\frac{\partial V_2}{\partial\eta_2}-c_{36}\frac{\partial V_3}{\partial z}+ \\
&\quad -c_{66}\left[-\frac{1}{h_1}\sin\varphi'\frac{\partial V_2}{\partial\eta_2}+\frac{1}{h_2}\cos\varphi'\frac{\partial V_1}{\partial\eta_2}\right] \\
\Theta^*_{\alpha 3} &= zK_{13}-c_{13\alpha 3}\left[-\frac{1}{h_1}\sin\varphi'\frac{\partial V_3}{\partial\eta_2}+\frac{\partial V_1}{\partial z}\right]-c_{23\alpha 3}\left[\frac{1}{h_2}\cos\varphi'\frac{\partial V_3}{\partial\eta_2}+\frac{\partial V_2}{\partial z}\right]
\end{aligned}
\qquad [4.80]
$$

As in Section 4.4.2.2, we will assume a parabolic variation of the pertinent V_i functions in the variables η_2 and z, i.e.

$$
V_i = W_{i1}\eta_2 z + W_{i2}\frac{\eta_2^{\,2}}{2}+W_{i3}\frac{z^2}{2} \qquad [4.81]
$$

We subsequently substitute [4.81] into [4.79] and compare terms with like powers of η_2 and z to arrive at a set of linear algebraic equations in the constants W_{ij}. Solving for the latter gives, on account of [4.80], the following expressions for the thermal expansion Θ^*_{ij} coefficients,

$$\Theta^*_{11} = zT_{11} \; ; \; \Theta^*_{22} = zT_{22} \; ; \; \Theta^*_{33} = zT_{33}$$
$$; \; \Theta^*_{12} = zT_{12} \qquad [4.82]$$
$$\Theta^*_{13} = zK_{13} - \eta_2 T_{13} \; ; \; \Theta^*_{23} = zK_{23} - \eta_2 T_{23}$$

where,

$$T_{11} = \frac{\Lambda_5\Lambda_6 - \Lambda_2\Lambda_3}{\Lambda_1\Lambda_2 - \Lambda_4\Lambda_5}$$
$$T_{22} = \frac{\Lambda_3\Lambda_4 - \Lambda_1\Lambda_6}{\Lambda_1\Lambda_2 - \Lambda_4\Lambda_5} \qquad [4.83]$$
$$T_{12} = \frac{sh_2}{2h_1 c} T_{11} + \frac{ch_1}{2sh_2} T_{22}$$

Explicit expressions for the quantities Λ_1, Λ_2,..., Λ_6 which depend on the geometric parameters of the unit cell and the elastic and thermal expansion coefficients of the reinforcements be found directly from Appendix D by making the following substitutions:

$$C_{ijkl} \rightarrow K_{ij} \qquad [4.84]$$

We note again that the thermal expansion coefficients given in this chapter are referenced with respect to the $\{x_i\}$ coordinate system shown in Figure 4-5, and will therefore differ from the principal material coefficients. The relationship between the two sets of coefficients is expressed by the following tensor transformation law,

$$K_{ij} = a_{im} a_{jn} K_{mn}^{(p)} \tag{4.85}$$

4.4.3.3. Effective thermal expansion coefficients

Similarly to Section 4.4.2.3, the effective thermal expansion coefficients for the basic smart structure of Figure 4-5 are given by:

$$\begin{aligned} \langle \Theta_{ij} \rangle &= \frac{1}{|Y|} \int_{|Y|} \Theta_{ij} dv = \frac{V}{h_1 h_2} \Theta_{ij} \\ \langle z\Theta_{ij}^* \rangle &= \frac{V}{16 h_1 h_2} T_{ij} \\ \langle z\Theta_{ij} \rangle &= \langle \Theta_{ij}^* \rangle = 0 \end{aligned} \tag{4.86}$$

The effective thermal expansion coefficients of smart structures with more than one family of reinforcements can be readily obtained from Equation [4.86] using superposition.

4.5. Examples and Discussion – Thin networks with orthotropic reinforcements

For illustration purposes we will consider several examples of network reinforced composite plates. Without loss of generality we will assume that all reinforcements have the same (circular) cross-section area and are made of the same material. If desired however, the model allows for each reinforcement family to have unique geometrical and material properties. For the ensuing examples, we will assume that the reinforcements have properties given in Table 4-1 (Gibson, [1994]).

Table 4-1: Reinforcement Properties (Gibson, [1994])

Property	**Value**
E_1	152 GPa
$E_2=E_3$	4.1 GPa
$G_{12}=G_{13}$	2.9 GPa
G_{23}	1.5 GPa
$\nu_{12}=\nu_{13}=\nu_{23}$	0.35

4.5.1. Example 1. Rectangular arrangement

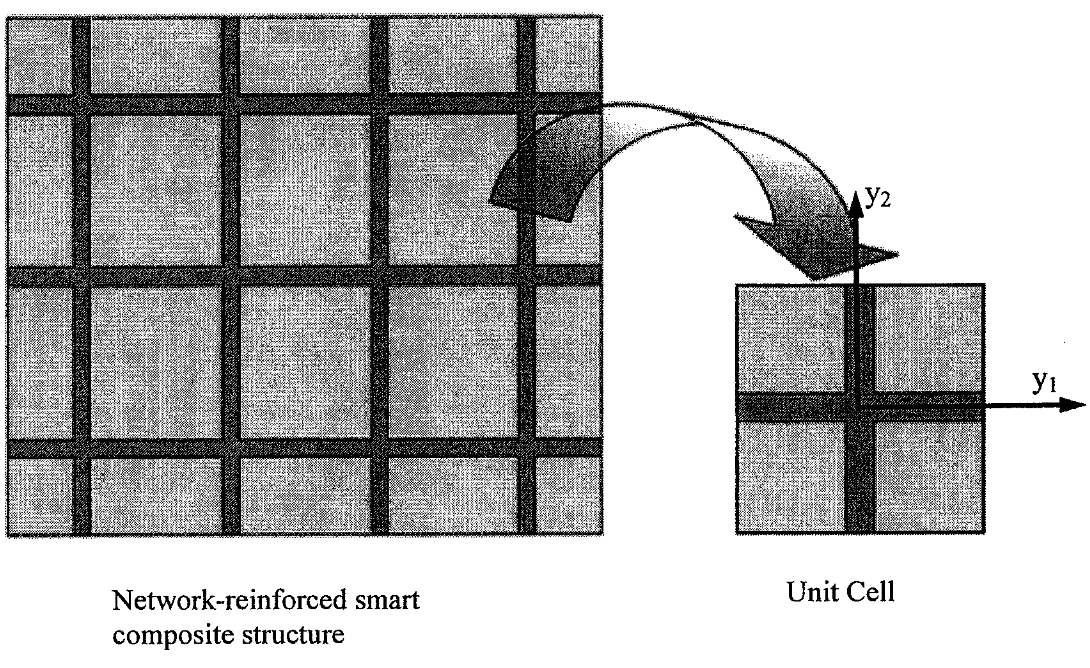

Figure 4-7: Thin smart composite plate with rectangular arrangement of actuators/reinforcements (S1)

The first example to be considered consists of two mutually perpendicular families of orthotropic reinforcements ($\varphi = 0^{o}$ and $\varphi = 90^{o}$) forming a rectangular arrangement as shown in Figure 4-7. The figure also shows the unit cell of the structure. For convenience, this composite plate will be referred to in the sequel as S1. The effective elastic, piezoelectric, thermal expansion coefficients of S1 are readily determined from Equations [4.39], [4.54], [4.57], [4.64], [4.71], [4.74], [4.78], [4.83], and [4.86]. Although the resulting expressions are too lengthy to be reproduced here, some of the effective coefficients will be presented graphically in the next section.

4.5.2. Example 2. Triangular arrangement

The second example (structure S2) represents a composite plate reinforced with three families of orthotropic bars ($\varphi = 30^{o}$, $\varphi = 90^{o}$, $\varphi = 150^{o}$) which intersect to form equilateral triangles as shown in Figure 4-8. The effective coefficients are calculated as for the previous example and some representative results will be shown in the following Sections.

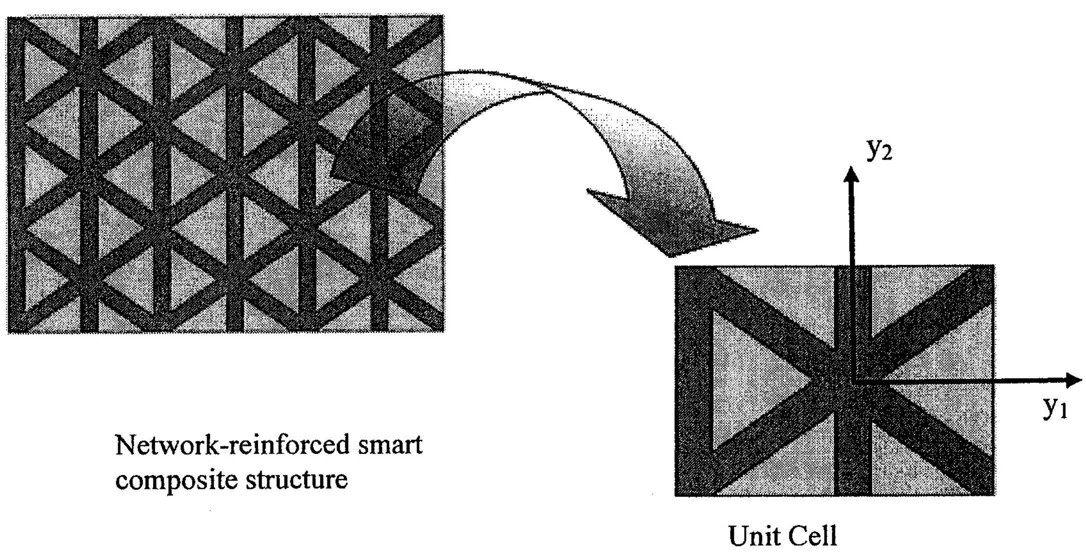

Figure 4-8: Thin smart composite plate with triangular arrangement of actuators/reinforcements (S2)

4.5.2. Example 3. Rhombic arrangement

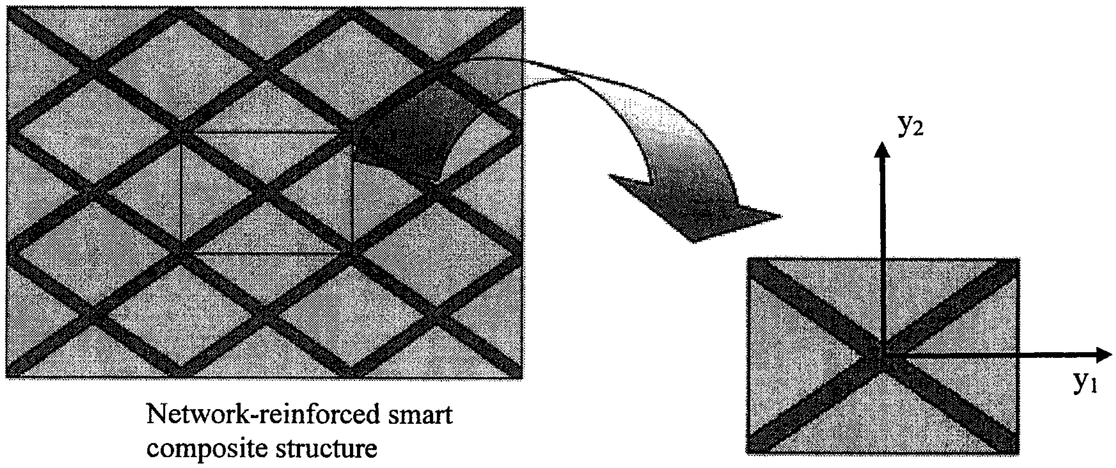

Figure 4-9: Thin smart composite plate with rhombic arrangement of actuators/reinforcements (S3)

The final example (structure S3) pertains to the reinforced plate of Figure 4-9 which consists of two families of reinforcements ($\varphi = 30^o$, $\varphi = 150^o$). Some of the effective coefficients will be shown in the following sections where a comparison will be made of all three structures, S1, S2, and S3.

4.5.4. Plots of effective elastic properties

The mathematical model and methodology presented in Section 4.4 can be used in analysis and design to tailor the effective elastic coefficients of any structure to meet the criteria of a particular application, by selecting the type, number, orientation and size of the reinforcements. In this section typical effective elastic properties of structures S1, S2, and S3 will be computed and plotted. The effective coefficients will be plotted vs. the ratio (R) of the volume of one bar within the unit cell to the volume of the unit cell itself. This ratio equals:

$$R = \frac{\delta^3 V}{\delta^3 h_1 h_2} = \frac{V}{h_1 h_2} \tag{4.87}$$

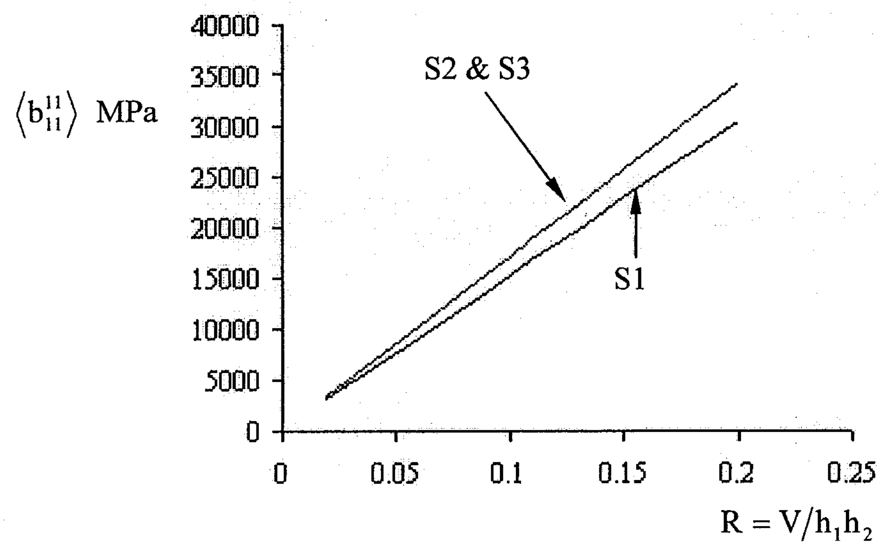

Figure 4-10: Plot of $\langle b_{11}^{11} \rangle$ elastic coefficient vs. V/h_1h_2 for structures S1, S2 and S3

Figure 4-10 shows the variation of $\langle b_{11}^{11} \rangle$ with R for S1, S2, and S3. It can be observed that the stiffness in the y_1 direction is the same for S2 and S3 because of the same number, size and arrangement of reinforcements in that direction. The presence of the extra reinforcements in S2 does not affect the stiffness in the y_1 direction because these reinforcements are oriented entirely in the y_2 direction as shown in Figure 4-8. Both S2 and S3 are stiffer than S1 in the y_1 direction because the former have more reinforcements (even though they are oriented at an angle to y_1) that affect the stiffness in that direction than the latter which only has a single reinforcement which affects the stiffness in the y_1 direction.

Figure 4-11, which is a plot of $\langle b_{22}^{22} \rangle$, shows that S2 is significantly stiffer than S3 in the y_2 direction due to the presence of the extra two reinforcements in the former. For similar reasons, the $\langle b_{22}^{22} \rangle$ value for S1 is larger than that of S3 and smaller than that of S2.

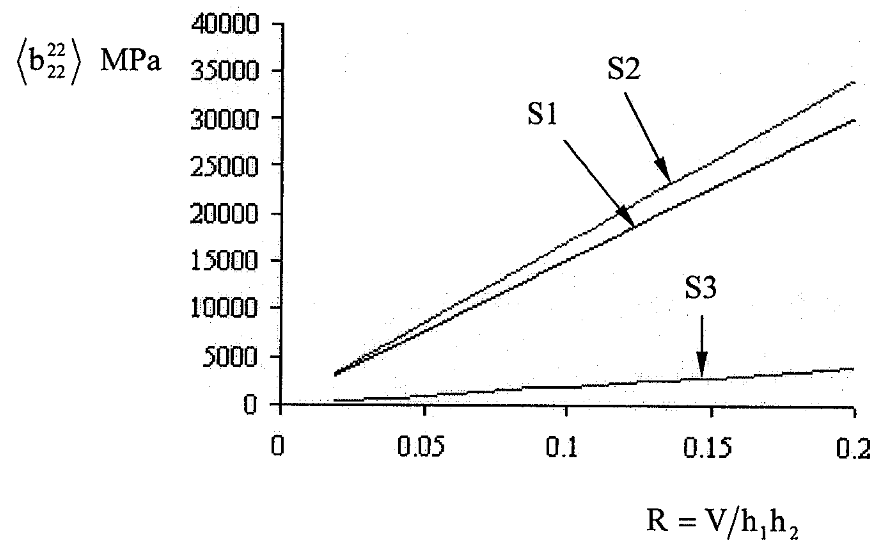

Figure 4-11: Plot of $\langle b_{22}^{22} \rangle$ elastic coefficient vs. V/h_1h_2 for structures S1, S2 and S3

Finally, Figure 4-12 shows the variation of the $\langle zb_{11}^{*11} \rangle$ coefficient with R. We note from Equation [4.13] that this coefficient characterizes the bending stiffness of the composite plate in the y_1-z plane. Since the reinforcing bars which are oriented entirely in the y_2 direction do not affect the bending stiffness in the y_1-z plane, then the value of $\langle zb_{11}^{*11} \rangle$ for structures S2 and S3 is the same. As expected, both structures have a higher bending stiffness than S1. Similar considerations apply to the other effective coefficients. It is evident however, that all of these trends and characteristics can easily be modified by changing the size, type, angular orientation, etc. of the reinforcements so that the desirable elastic coefficients are obtained.

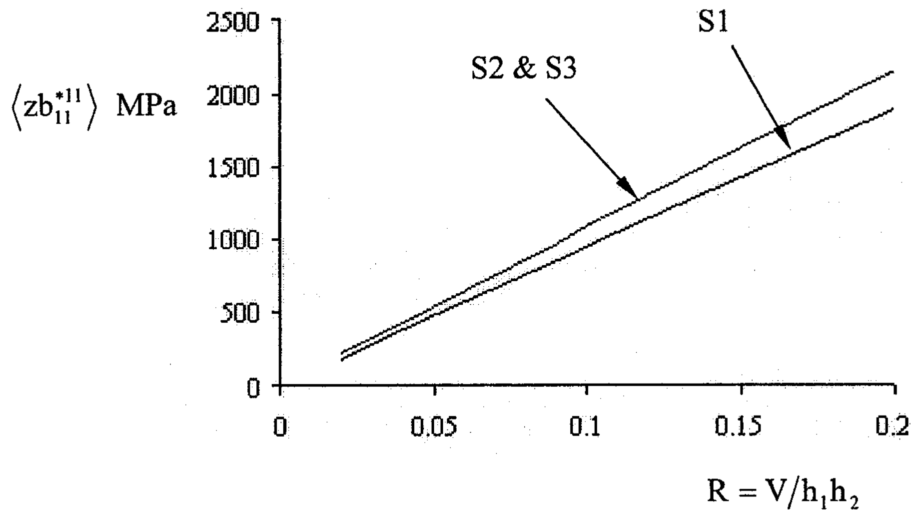

Figure 4-12: Plot of $\langle zb_{11}^{*11} \rangle$ elastic coefficient vs. V/h_1h_2 for structures S1, S2 and S3

4.5.5. Plots of effective piezoelectric coefficients and discussion

We reiterate that the model derived in this paper can be used to tailor the effective coefficients of a network-reinforced smart composite plate (to meet the particular requirements of a given application) by changing some material or geometric parameters of interest such as type or angular orientation of the actuators/reinforcements. For illustration purposes, let us assume that the pertinent material properties are those given in Table 4-2 [Cote et al. 2002]. As well, the effective coefficients will be plotted vs. the ratio (R) of the volume of a single bar within the unit cell to the volume of the unit cell itself as given by Equation [4.87].

Figure 4-13 shows the variation of $\langle d_{11}^{3} \rangle$ with R for S1, S2, and S3. It can be observed that the value of this piezoelectric coefficient is the same for S2 and S3 because they both have the same number, size and arrangements of actuators/reinforcements in the y_1 direction. The presence of the extra elements in S2 does not affect the results because these elements are oriented entirely in the y_2 direction and do not affect the piezoelectric

Table 4-2: Thermopiezoelastic properties of PZT-5A [Cote et al. 2002]

Coefficient	Value
$C_{11}^{(p)} = C_{22}^{(p)}$ (MPa)	119899.13
$C_{33}^{(p)}$ (MPa)	109892.37
$C_{12}^{(p)}$ (MPa)	74732.01
$C_{13}^{(p)} = C_{23}^{(p)}$ (MPa)	74429.92
$C_{44}^{(p)} = C_{55}^{(p)}$ (MPa)	21052.63
$C_{66}^{(p)}$ (MPa)	22573.36
$P_{13}^{(p)} = P_{23}^{(p)}$ (C/mm^2)	-5.45E-6
$P_{33}^{(p)}$ (C/mm^2)	1.56E-5
$P_{42}^{(p)} = P_{51}^{(p)}$ (C/mm^2)	2.46E-5
$\alpha_{11}^{(p)} = \alpha_{22}^{(p)}$ ($/^0$C)	-1.704E-10
$\alpha_{33}^{(p)}$ ($/^0$C)	3.732E-10

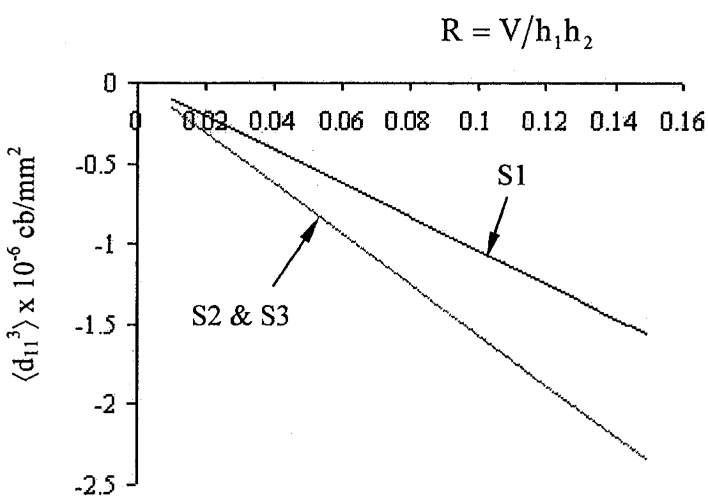

Figure 4-13: Plot of $\langle d_{11}^{3} \rangle$ piezoelectric coefficient vs. V/h_1h_2 for structures S1, S2 and S3

behavior in the y_1 direction. Both S2 and S3 have larger $\langle d_{11}^{3} \rangle$ values than S1 because the former have more actuators (even though they are inclined at angle) that affect the behavior in the y1 direction than S1 which only has a single actuator in that direction.

Figure 4-14 is a plot of $\langle d_{22}^{3} \rangle$ vs. R for the three smart structures. It is seen that S2 exhibits the highest value because it has the largest number of actuators/reinforcements in the y_2 direction. For similar considerations, the $\langle d_{22}^{3} \rangle$ piezoelectric coefficient is a higher for S1 than S2.

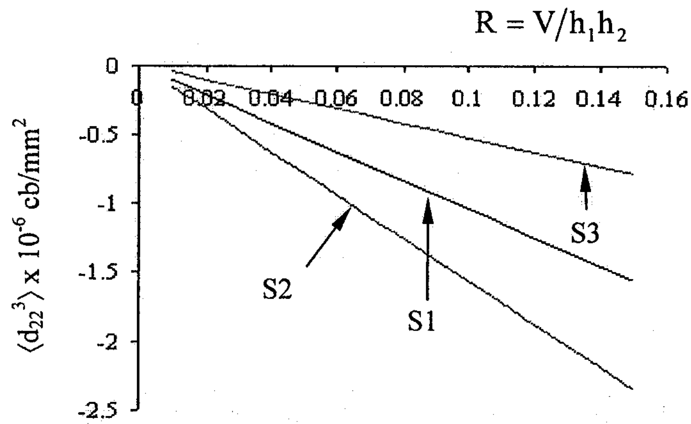

Figure 4-14: Plot of $\langle d_{22}^{3} \rangle$ piezoelectric coefficient vs. V/h_1h_2 for structures S1, S2 and S3

Figure 4-15 shows the variation of $\langle zd_{11}^{*3} \rangle$ vs. R for the three structures. We recall that the $\langle zd_{ij}^{*k} \rangle$ coefficients are related to out-of-plane deformations. Since the actuators oriented in the y_2 direction do not contribute to the deformation in the y_1 direction, the value of $\langle zd_{11}^{*3} \rangle$ for S2 is the same as that of S3 (all other parameters being the same). As expected, both structures exhibit a higher value than S1.

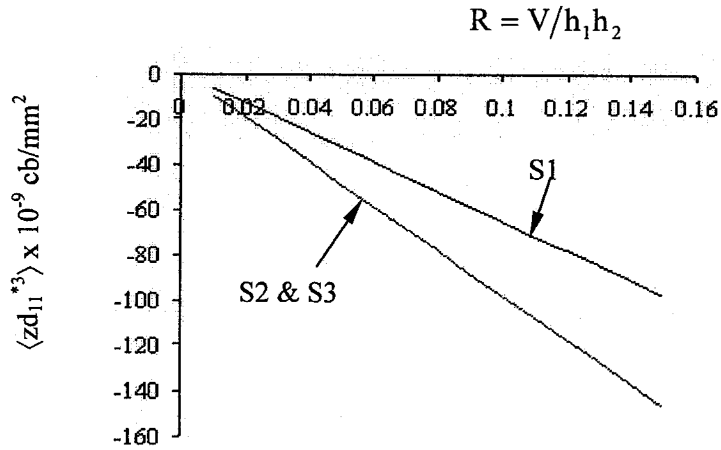

Figure 4-15: Plot of $\langle zd_{11}^{*3}\rangle$ piezoelectric coefficient vs. V/h_1h_2 for structures S1, S2 and S3

4.5.6. Plot of effective thermal expansion coefficients

Similar considerations apply to the case of thermal expansion coefficients. Figure 4-16 is a plot of $\langle \Theta_{11}\rangle$ vs. R and Figure 4-17 a plot of $\langle z\Theta_{22}^{*}\rangle$ vs. R. The reasons for the trends displayed in both figures should be apparent from the discussion above.

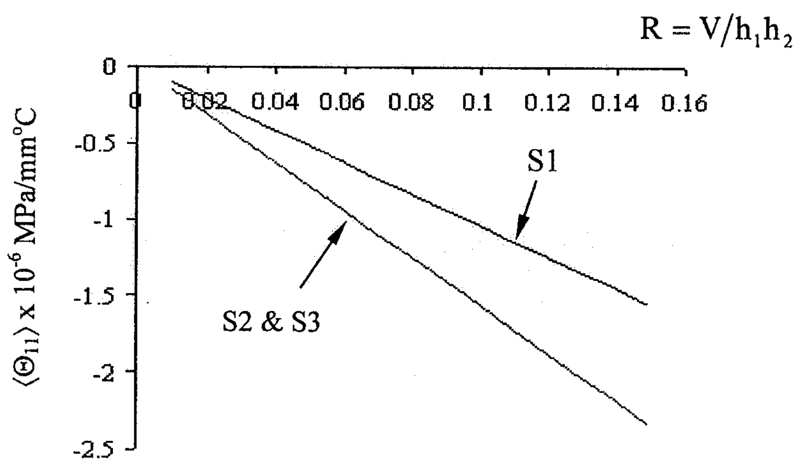

Figure 4-16: Plot of $\langle \Theta_{11}\rangle$ thermal coefficient vs. V/h_1h_2 for structures S1, S2 and S3

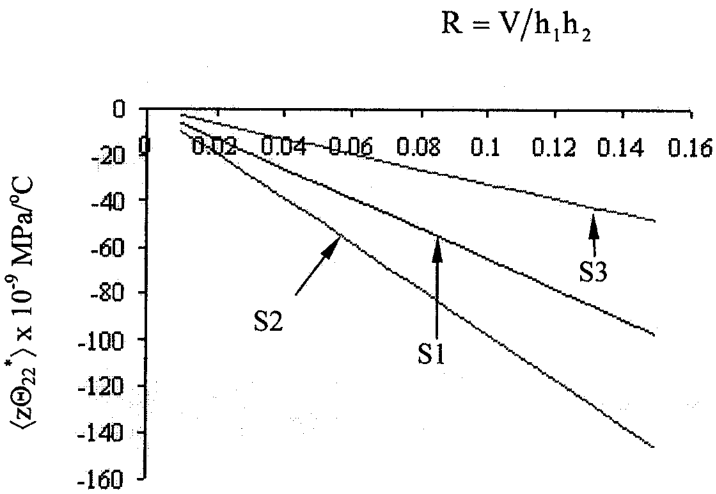

Figure 4-17: Plot of $\langle z\Theta_{22}^{*}\rangle$ thermal coefficient vs. V/h_1h_2 for structures S1, S2 and S3

4.6. Brief Synopsis

The method of asymptotic homogenization was used to obtain the effective coefficients of thin smart composite plates reinforced with a network of orthotropic cylindrical bars. The micromechanical models derived were illustrated by means of several examples which showed that the effective properties can easily be customized to satisfy any application requirements by changing certain geometric and/or material parameters. As such they are useful in design and analysis of smart composite structures.

5. MODELING OF THE THERMOPIEZOELASTIC BEHAVIOR OF PRISMATIC SMART COMPOSITE STRUCTURES MADE OF ORTHOTROPIC MATERIALS

5.1. Introduction

The objective of this chapter is to determine the effective elastic, piezoelectric and thermal expansion coefficients of prismatic smart composite structures with orthotropic characteristics. Examples of structures of interest are shown in Figure 5-1.

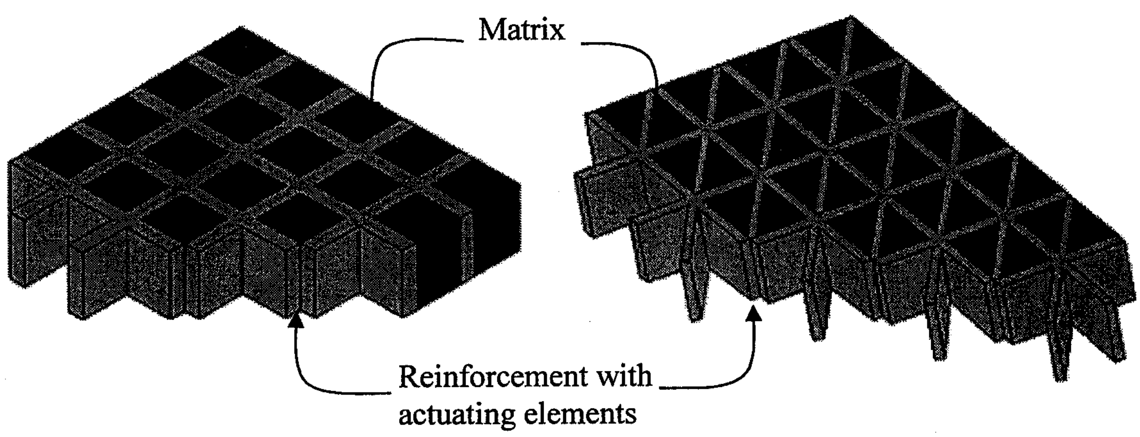

Figure 5-1: Examples of prismatic smart composite structures

Following this section, the basic problem formulation is given in Section 5.2.1 and the important features of the solution methodology are explained in Section 5.2.2. Section 5.2.3 develops the local or unit cell problems. Section 5.3 derives the general model of interest and then uses it to analyze and discuss various practical examples and compare the effective moduli and coefficients of the different smart structures. It is shown in this section that the model developed can be used to tailor the effective properties of any smart structure to meet the specific design criteria pertinent to a particular application.

5.2. Asymptotic Homogenization for Smart Structures

5.2.1. General Model

The general model pertaining to three-dimensional smart composite structure has been previously developed by the authors [Kalamkarov and Georgiades, 2002a]. Here, we summarize the important features of the model in so far as they represent the starting point for the current model. Consider a smart composite structure representing an inhomogeneous solid occupying domain G with boundary ∂G that contains a large number of periodically arranged actuators as shown in Figure 5-2.

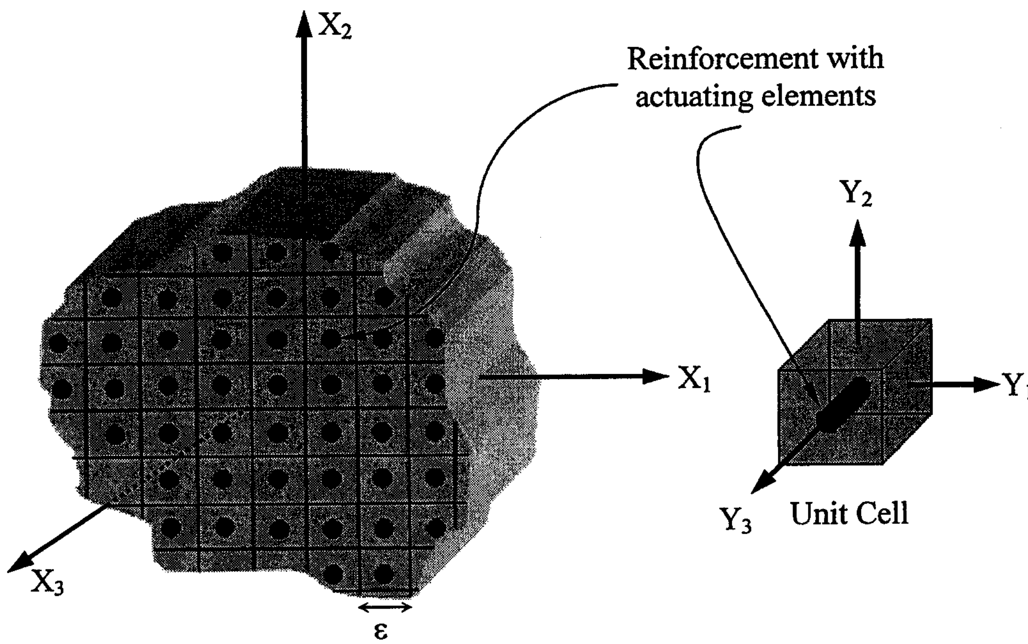

Figure 5-2: Smart composite with periodically arranged actuators and its periodicity cell

The elastic deformation of this smart structure can be described by means of the following system:

$$\frac{\partial \sigma_{ij}^{\varepsilon}\left(\mathbf{x},\frac{\mathbf{x}}{\varepsilon}\right)}{\partial x_j} = f_i \text{ in } G \qquad [5.1]$$

$$u^{\varepsilon}(\mathbf{x},\frac{\mathbf{x}}{\varepsilon}) = 0 \quad \text{on } \partial G$$

$$\sigma_{ij}^{\varepsilon}\left(\mathbf{x},\frac{\mathbf{x}}{\varepsilon}\right) = C_{ijkl}\left(\frac{\mathbf{x}}{\varepsilon}\right)e_{kl}^{\varepsilon}\left(\mathbf{x},\frac{\mathbf{x}}{\varepsilon}\right) - P_{ijk}\left(\frac{\mathbf{x}}{\varepsilon}\right)R_k(\mathbf{x}) - K_{ij}\left(\frac{\mathbf{x}}{\varepsilon}\right)\Theta(\mathbf{x}) \qquad [5.2]$$

$$e_{ij}^{\varepsilon}\left(\mathbf{x},\frac{\mathbf{x}}{\varepsilon}\right) = \frac{1}{2}\left[\frac{\partial u_i}{\partial x_j}\left(\mathbf{x},\frac{\mathbf{x}}{\varepsilon}\right) + \frac{\partial u_j}{\partial x_i}\left(\mathbf{x},\frac{\mathbf{x}}{\varepsilon}\right)\right] \qquad [5.3]$$

Although the variables appearing in Equations [5.1]-[5.3] have been defined before, they will also be given here for the sake of convenience. C_{ijkl}, is the tensor of the elastic coefficients, e_{kl} is the strain tensor, P_{ijk} is a tensor of actuation coefficients describing the effect of a control signal R on the stress field σ, and K_{ij} is the thermal expansion tensor. Finally, Θ represent changes in temperature with respect to some initial state. It is assumed in Equation [5.2] that the C_{ijkl}, P_{ijk}, and K_{ij} coefficients are all periodic with a unit cell Y of characteristic dimension ε, the characteristic distance between the reinforcements (or actuators) as shown in Figure 5-2. Consequently, the smart structure in Figure 5-2 is seen to be made up of a large number of “unit cells” periodically arranged within the domain G.

Substituting Equation [5.3] in [5.2] and interchanging the dummy variables k and l, and recalling the symmetry properties of the elastic coefficients gives:

$$\sigma_{ij}^{\varepsilon}\left(\mathbf{x},\frac{\mathbf{x}}{\varepsilon}\right) = C_{ijkl}\left(\frac{\mathbf{x}}{\varepsilon}\right)\left(\frac{\partial u_k}{\partial x_l}\right) - P_{ijk}\left(\frac{\mathbf{x}}{\varepsilon}\right)R_k(\mathbf{x}) - K_{ij}\left(\frac{\mathbf{x}}{\varepsilon}\right)\Theta(\mathbf{x}) \qquad [5.4]$$

Let us also mention here that, if the physical dimensions of the unit cell in Figure 5-1 are, say, 2ε microns in the x_1 direction, ε microns in the x_2 direction, and 3ε microns in the x_3 direction then upon introduction of the fast variable y, the dimensions of the unit cell become 2 in the y_1 direction, 1 in the y_2 direction, and 3 in the y_3 direction. One may refer to the problem as being 2-periodic in y_1, 1-periodic in y_2 and 3-periodic in y_3, or collectively Y_i-periodic in y_i where it is understood that Y_i may have unequal components.

5.2.2. Two-Scale Asymptotic Expansion

As with the previous model, the nature of the smart structure in Figure 5-2 means that any associated boundary-value problem will be characterized by two different scales, a macroscopic (or slow) scale, x_i, which depends on the global formulation of the problem, and a microscopic (or fast) scale which depends entirely on the structure and geometry of the unit cell. Thus, periodic smart composites of this nature are amenable to treatment by asymptotic homogenization techniques. The first step is to define a new microscopic (fast) variable y_i according to:

$$y_i = \frac{x_i}{\varepsilon} \qquad [5.5]$$

We subsequently expand the displacement and stress fields into infinite series of powers of the small parameter ε as shown below.

$$u^{\varepsilon}(\mathbf{x},\mathbf{y}) = u^{(0)}(\mathbf{x},\mathbf{y}) + \varepsilon u^{(1)}(\mathbf{x},\mathbf{y}) + \varepsilon^2 u^{(2)}(\mathbf{x},\mathbf{y}) + \ldots \qquad [5.6]$$

$$\sigma_{ij}^{\varepsilon}(\mathbf{x},\mathbf{y}) = \sigma_{ij}^{(0)}(\mathbf{x},\mathbf{y}) + \varepsilon\sigma_{ij}^{(1)}(\mathbf{x},\mathbf{y}) + \varepsilon^2\sigma_{ij}^{(2)}(\mathbf{x},\mathbf{y}) + \ldots \qquad [5.7]$$

Similar to previous chapter, the introduction of the fast variable y necessiates the transformation of the derivatives as follows

$$\frac{d}{dx_i} \to \frac{\partial}{\partial x_i} + \frac{\partial}{\partial y_i}\frac{\partial y_i}{\partial x_i} \qquad [5.8]$$

so that in view of Equation [5.5] we arrive at:

$$\frac{d}{dx_i} \to \frac{\partial}{\partial x_i} + \frac{1}{\varepsilon}\frac{\partial}{\partial y_i} \qquad [5.9]$$

Thus

$$\begin{aligned} \frac{\partial \sigma_{ij}^{\varepsilon}}{dx_j} &\to \frac{\partial \sigma_{ij}^{\varepsilon}}{\partial x_j} + \frac{1}{\varepsilon}\frac{\partial \sigma_{ij}^{\varepsilon}}{\partial y_j} \\ \frac{\partial u_k^{\varepsilon}}{dx_l} &\to \frac{\partial u_k^{\varepsilon}}{\partial x_l} + \frac{1}{\varepsilon}\frac{\partial u_k^{\varepsilon}}{\partial y_l} \end{aligned} \qquad [5.10]$$

Accordingly, Equations [5.1] and [5.4] transform to:

$$\begin{aligned} &\frac{\partial \sigma_{ij}^{\varepsilon}}{\partial x_j} + \frac{1}{\varepsilon}\frac{\partial \sigma_{ij}^{\varepsilon}}{\partial y_j} = f_i \quad \text{in } G \\ &u^{\varepsilon}(\mathbf{x},\mathbf{y}) = 0 \quad \text{on } \partial G \end{aligned} \qquad [5.11]$$

and

$$\sigma_{ij}^{\varepsilon}(x,y)=C_{ijkl}(y)\left(\frac{\partial u_k}{\partial x_l}+\frac{1}{\varepsilon}\frac{\partial u_k}{\partial y_l}\right)-P_{ijk}(y)R_k(x)-K_{ij}(y)\Theta(x) \quad [5.12]$$

The substitution of Equation [5.12] into first expression of Equation [5.11] and a consideration of Equation [5.6] reveals that the first term in the asymptotic expansion for the displacement field is independent of **y**.

With this results in mind, Equation [5.6] becomes:

$$u^{\varepsilon}(\mathbf{x},\mathbf{y})=u^{(0)}(\mathbf{x})+\varepsilon u^{(1)}(\mathbf{x},\mathbf{y})+\varepsilon^2 u^{(2)}(\mathbf{x},\mathbf{y})+\ldots \quad [5.13]$$

Subsequently, substituting Equation [5.7] into Equation [5.11] and equating equal powers of ε results in a series of expressions, the first two of which are:

$$\begin{gathered}\frac{\partial\sigma_{ij}^{(0)}(\mathbf{x},\mathbf{y})}{\partial y_j}=0\\ \frac{\partial\sigma_{ij}^{(1)}(\mathbf{x},\mathbf{y})}{\partial y_j}+\frac{\partial\sigma_{ij}^{(0)}(\mathbf{x},\mathbf{y})}{\partial x_j}=f_i\end{gathered} \quad [5.14]$$

where,

$$\begin{gathered}\sigma_{ij}^{(0)}=C_{ijkl}\left(\frac{\partial u_k^{(0)}}{\partial x_l}+\frac{\partial u_k^{(1)}}{\partial y_l}\right)-P_{ijk}R_k-K_{ij}\Theta\\ \sigma_{ij}^{(1)}=C_{ijkl}\left(\frac{\partial u_k^{(1)}}{\partial x_l}+\frac{\partial u_k^{(2)}}{\partial y_l}\right)\end{gathered} \quad [5.15]$$

5.2.3. Governing equations, unit-cell problems and effective coefficients

Substitution of the first expression in Equation [5.15] into the first expression of Equation [5.14] gives:

$$\frac{\partial}{\partial y_j}\left(C_{ijkl}\frac{\partial u_k^{(1)}(\mathbf{x},\mathbf{y})}{\partial y_l}\right)=\frac{\partial P_{ijk}(\mathbf{y})}{\partial y_j}R_k(\mathbf{x})+\frac{\partial K_{ij}(\mathbf{y})}{\partial y_j}\Theta(\mathbf{x})-\frac{\partial C_{ijkl}(\mathbf{y})}{\partial y_j}\frac{\partial u_k^{(0)}(\mathbf{x})}{\partial x_l} \qquad [5.16]$$

The separation of variables in each term on the right-hand-side of [5.16] enables us to write down its solution in the following form,

$$u_n^{(1)}(\mathbf{x},\mathbf{y})=R_k(\mathbf{x})N_n^k(\mathbf{y})+\Theta(\mathbf{x})N_n(\mathbf{y})+\frac{\partial u_k^{(0)}(\mathbf{x})}{\partial x_l}N_n^{kl}(\mathbf{y}) \qquad [5.17]$$

where

$$\begin{aligned}
&\frac{\partial}{\partial y_j}\left(C_{ijml}(\mathbf{y})\frac{\partial N_m^k(\mathbf{y})}{\partial y_l}\right)=\frac{\partial P_{ijk}}{\partial y_j}\\
&\frac{\partial}{\partial y_j}\left(C_{ijml}(\mathbf{y})\frac{\partial N_m(\mathbf{y})}{\partial y_l}\right)=\frac{\partial K_{ij}}{\partial y_j}\\
&\frac{\partial}{\partial y_j}\left(C_{ijmn}(\mathbf{y})\frac{\partial N_m^{kl}(\mathbf{y})}{\partial y_n}\right)=-\frac{\partial C_{ijkl}}{\partial y_j}
\end{aligned} \qquad [5.18]$$

In Equation [5.17] we ignore the homogeneous part of the solution because it does not affect the ensuing analysis. It is observed that the differential equations in Equation [5.18] depend entirely on the fast variable **y** and are thus solved on the domain Y of the unit cell remembering at the same time that all of C_{ijkl}, P_{ijk}, K_{ij}, N_m^{kl} N_m^k, N_m, are periodic in y_i, (with some period Y_i). Thus, the differential equations in [5.18] are appropriately referred to as unit cell problems.

Having determined the first two terms in the asymptotic expression for displacement we will now turn our attention to determine the stress field. To this end, we substitute Equation [5.17] into Equation [5.15] and the resulting expression into Equation [5.14] to get:

$$\frac{\partial \sigma_{ij}^{(1)}(x,y)}{\partial y_j} + C_{ijkl}(y)\frac{\partial^2 u_k^{(0)}(x)}{\partial x_j \partial x_l} + C_{ijmn}(y)\left[\begin{array}{l} \dfrac{\partial N_m^k(y)}{\partial y_n}\dfrac{\partial R_k(x)}{\partial x_j} + \dfrac{\partial M_m(y)}{\partial y_n}\dfrac{\partial \Theta(x)}{\partial x_j} + \\ \dfrac{\partial N_m^{kl}(y)}{\partial y_n}\dfrac{\partial^2 u_k^{(0)}(x)}{\partial x_j \partial x_l} \end{array}\right] \qquad [5.19]$$
$$- P_{ijk}\frac{\partial R_k}{\partial x} - K_{ij}\frac{\partial \Theta}{\partial x} = f_i$$

Equation [5.19] will be used to obtain the governing equations of the problem by averaging over the domain of the unit cell. This is the homogenization procedure and it results in:

$$\frac{1}{|Y|}\int_Y \frac{\partial \sigma_{ij}^{(1)}(x,y)}{\partial y_j} dv + \langle C_{ijkl}\rangle \frac{\partial^2 u_k^{(0)}(x)}{\partial x_j \partial x_l} - \langle P_{ijk}\rangle \frac{\partial R_k(x)}{\partial x_j} - \langle K_{ij}\rangle \frac{\partial \Theta(x)}{\partial x_j} = f_i \qquad [5.20]$$

where

$$\langle C_{ijkl}\rangle = \frac{1}{|Y|}\int_Y \left(C_{ijkl}(y) + C_{ijmn}(y)\frac{\partial N_m^{kl}}{\partial y_n}\right) dv$$
$$\langle P_{ijk}\rangle = \frac{1}{|Y|}\int_Y \left(P_{ijk}(y) - C_{ijmn}(y)\frac{\partial N_m^{k}}{\partial y_n}\right) dv \qquad [5.21]$$
$$\langle K_{ij}\rangle = \frac{1}{|Y|}\int_Y \left(K_{ij}(y) - C_{ijmn}(y)\frac{\partial N_m}{\partial y_n}\right) dv$$

Here $\langle C_{ijkl} \rangle, \langle P_{ijk} \rangle, \langle K_{ij} \rangle$ denote the averaged or homogenized coefficients. Let us now consider the first term in Equation [5.20]. By applying the divergence theorem, it can be wriiten as:

$$\int_Y \frac{\partial \sigma_{ij}^{(1)}(x,y)}{\partial y_j} dv = \int_Y \operatorname{div} \sigma^{(1)} dv = \int_{\partial Y} \sigma^{(1)}(x,y)\, \vec{n}\, dA \qquad [5.22]$$

where **n** is the unit vector normal to the boundary surface ∂Y of the unit cell. Owing to the periodicity of $\sigma^{(1)}(x,y)$, its value at the corresponding points on opposite side of the unit cell are the same but with opposite sign. Hence, the integral vanishies identically, and we are left with:

$$\langle C_{ijkl} \rangle \frac{\partial^2 u_k^{(0)}(x)}{\partial x_j \partial x_l} - \langle P_{ijk} \rangle \frac{\partial R_k(x)}{\partial x_j} - \langle K_{ij} \rangle \frac{\partial \Theta(x)}{\partial x_j} = f_i \qquad [5.23]$$

Similarly, substitution of Equation [5.17] into first expression of Equation [5.15] and then integrating the resulting expression over the domain of the unit cell yields:

$$\langle \sigma_{ij}^{(0)} \rangle = \frac{1}{|Y|} \int_Y \sigma_{ij}^{(0)}(y) dv = \langle C \rangle_{ijkl} \frac{\partial u_k^{(0)}}{\partial x_l} - \langle P_{ijk} \rangle R_k - \langle K_{ij} \rangle \Theta \qquad [5.24]$$

Equations [5.23] and [5.24] represent the homogenized equations for the displacement and stress fields respectively. The coefficients $\langle C_{ijkl} \rangle, \langle P_{ijk} \rangle, \langle K_{ij} \rangle$ will be referred to as the homogenized or effective elastic, piezoelectric, and thermal expansion coefficients. It is observed that these effective coefficients are free from the periodicity complications that characterize the actual material coefficients, and as such, are more amenable to analytical and numerical treatment. They are universal in nature and can be used to study a wide variety of boundary value problems associated with a given smart structure. It should be mentioned at this point that the analysis applies without modification to materials that exhibit magnetostrictive or other effects rather than piezoelectric effects. In fact, the equations derived should be considered to hold equally well if the material in question is associated with some general transduction characteristics that can be used to induce strains and stresses. In that case, the coefficients $\langle P \rangle_{ijk}$ represent the appropriate homogenized material constants (rather than the piezoelectric constants).

In summary, Equations [5.18], [5.21] and [5.23] represent the governing equations of the homogenized model of a smart composite structure with periodically arranged reinforcements and actuators. Equation [5.18] represents the unit cell problems, formulae [5.21] define the effective coefficients, and expression [5.23] provides an asymptotic formula for the local displacement field.

5.3. Prismatic Smart Structures - Current Model

In order to calculate the effective coefficients of the smart structures, the unit cell problems [5.18] must be solved and formulae [5.21] must be applied. We will consider prismatic smart composite structures made of orthotropic material (see Figure 5-1).

5.3.1. Problem Formulation

We begin by introducing the following notations:

$$
\begin{aligned}
b_{ij}^{kl} &= C_{ijkl}\frac{\partial N_m^{kl}(\mathbf{y})}{\partial y_n} + C_{ijkl}(\mathbf{y}) \\
b_{ij}^{k} &= P_{ijk}(\mathbf{y}) - C_{ijml}\frac{\partial N_m^{k}(\mathbf{y})}{\partial y_l} \\
b_{ij} &= K_{ij}(\mathbf{y}) - C_{ijml}\frac{\partial N_m(\mathbf{y})}{\partial y_l}
\end{aligned}
\qquad [5.25]
$$

With these definitions in mind the unit cell problems in Equation [5.18] become:

$$
\begin{aligned}
\frac{\partial}{\partial y_j}\left\{b_{ij}^{kl}\right\} &= 0 \\
\frac{\partial}{\partial y_j}\left\{b_{ij}^{k}\right\} &= 0 \\
\frac{\partial}{\partial y_j}\left\{b_{ij}\right\} &= 0
\end{aligned}
\qquad [5.26]
$$

The structures of interest consist of reinforcing/actuating elements embedded in a matrix. As such, it is necessary to consider the interface conditions that exist between the different constituents of the unit cell. In the sequel, the letters "r", "m", and "s" will denote the inclusion, matrix and inclusion/matrix interface, respectively.

On account of the continuity of the functions $N_m^{kl}(\mathbf{y}), N_m^{k}(\mathbf{y})$, and $N_m(\mathbf{y})$ one naturally arrives at the following set of interface conditions:

$$
\begin{aligned}
N_n^{kl}(r)\big|_s &= N_n^{kl}(m) \\
N_n^{k}(r)\big|_s &= N_n^{k}(m) \\
N_n(r)\big|_s &= N_n(m)
\end{aligned}
\qquad [5.27]
$$

As well, from continuity of the displacement field $u_k^{(0)}$, control signal R_k, and the temperature θ, at the interface, one readily obtains

$$\begin{aligned} b_{ij}^{kl} n_j \big|_r &= b_{ij}^{kl} n_j \big|_m \\ b_{ij}^{k} n_j \big|_r &= b_{ij}^{k} n_j \big|_m \\ b_{ij} n_j \big|_r &= b_{ij} n_j \big|_m \end{aligned} \qquad [5.28]$$

where n_j refer to the components of the unit normal vector at the interface. We will further assume that the structure of interest consists of high modulus reinforcements and "soft" matrix ie E_1^r, E_2^r and $E_3^r >> E^m$. Also, we'll assume that the matrix itself exhibits negligible piezoeletric behaviour. As such $b_{ij}^{kl}(m) \approx 0$, $b_{ij}^{k}(m) \approx 0$ and $b_{ij}(m) \approx 0$. (Clearly, the above relationships become exact for the case of "lattice" structures which do not have any matrix or binder material in the region between the reinforcements). Thus, the interface conditions [5.28] become:

$$\begin{aligned} b_{ij}^{kl} n_j \big|_s &= 0 \\ b_{ij}^{k} n_j \big|_s &= 0 \\ b_{ij} n_j \big|_s &= 0 \end{aligned} \qquad [5.29]$$

In summary, the final problems that must be solved for smart structures similar to those of Figure 5-1 are:

$$\frac{\partial}{\partial y_j}\left\{b_{ij}^{kl}\right\}=0,\quad b_{ij}^{kl}n_j\Big|_s=0$$

$$\frac{\partial}{\partial y_j}\left\{b_{ij}^{k}\right\}=0,\quad b_{ij}^{k}n_j\Big|_s=0 \qquad [5.30]$$

$$\frac{\partial}{\partial y_j}\left\{b_{ij}\right\}=0,\quad b_{ij}n_j\Big|_s=0$$

5.3.2. Coordinate Transformation

In the ensuing examples, we will be primarily concerned with orthotropic materials. As well, the problems in Equation [5.30] will be solved on each inclusion separately, and then the results will be superimposed. Consequently, the analysis will become easier if we define a new coordinate system, $\{\eta_i\}$, so that an arbitrary inclusion will be oriented along one of the coordinate axes of this system. Due to the nature of the smart structures of interest in this chapter, the pertinent rotation will be performed about the y_3 axis as shown in Figure 5-3.

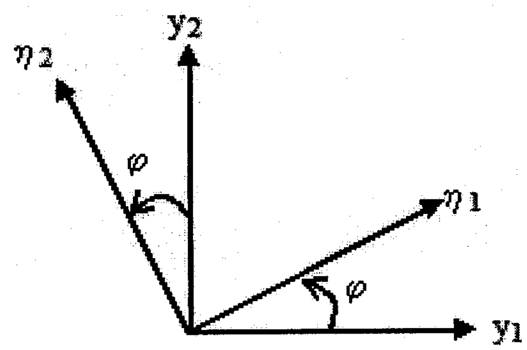

Figure 5-3: Original and rotated coordinate systems

The pertinent transformation matrix [T] is,

$$[T] = \begin{bmatrix} \cos\varphi & \sin\varphi & 0 \\ -\sin\varphi & \cos\varphi & 0 \\ 0 & 0 & 1 \end{bmatrix} \qquad [5.31]$$

and the relationship between the two sets of coordinates is given by:

$$\begin{aligned} \eta_1 &= \cos\varphi y_1 + \sin\varphi y_2 \\ \eta_2 &= -\sin\varphi y_1 + \cos\varphi y_2 \end{aligned} \qquad [5.32]$$

From Equation [5.32], the derivatives transform according to:

$$\begin{aligned} \frac{\partial}{\partial y_1} &= \frac{\partial}{\partial \eta_1}\frac{\partial \eta_1}{\partial y_1} + \frac{\partial}{\partial \eta_2}\frac{\partial \eta_2}{\partial y_1} = \cos\varphi\frac{\partial}{\partial \eta_1} - \sin\frac{\partial}{\partial \eta_2} \\ \frac{\partial}{\partial y_2} &= \frac{\partial}{\partial \eta_1}\frac{\partial \eta_1}{\partial y_2} + \frac{\partial}{\partial \eta_2}\frac{\partial \eta_2}{\partial y_2} = \sin\varphi\frac{\partial}{\partial \eta_1} + \cos\frac{\partial}{\partial \eta_2} \end{aligned} \qquad [5.33]$$

5.3.3. Effective Elastic Coefficients for Prismatic Smart Structures

We are now in a position to solve for the effective elastic, piezoelectric and thermal expansion coefficients of the structures of interest. As shown in Figure 5-1, these structures may consist of many different families of orthotropic reinforcements/actuators, each family oriented in a different direction. As mentioned before, for a given unit cell, we will solve the appropriate differential equations in each reinforcement separately (see Figure 5-4), and then superimpose the results. In doing so, stress concentrations and other complications that arise at the joints will be ignored because they are highly localized and do not contribute significantly to the integrals over the entire unit cell.

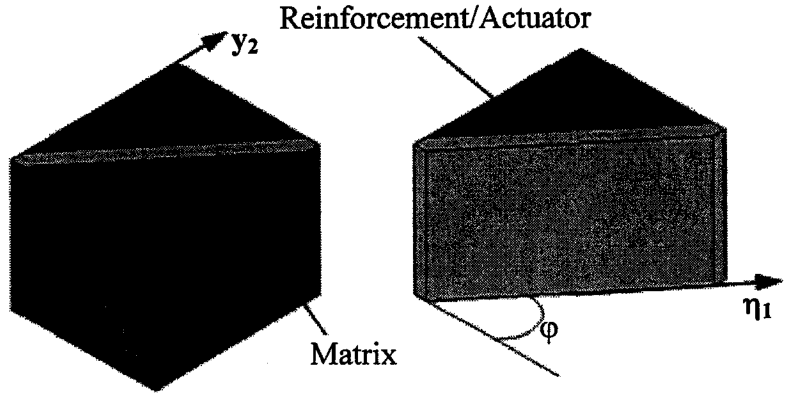

Figure 5-4: Basic unit cell with single arbitrarily-oriented orthotropic inclusion

Due to these considerations, it is prudent to first consider a simpler type of unit cell consisting of only a single arbitrarily oriented inclusion. Referring to Figure 5-4, we begin by rewriting first expression of Equation [5.30] (noting that $\frac{\partial}{\partial y_3} = 0$) as:

$$\begin{aligned} &\frac{\partial b_{i1}^{kl}}{\partial y_1} + \frac{\partial b_{i2}^{kl}}{\partial y_2} = 0, \\ &b_{i1}^{kl} n_1 + b_{i2}^{kl} n_2 \Big|_s = 0 \end{aligned} \qquad [5.34]$$

Since the inclusion is oriented along the η_1 direction, then the problem becomes independent of the $\eta_1$coordinate, and the overall solution is simplified. Accordingly, Equation [5.33] is reduced to:

$$\frac{\partial}{\partial y_1} = -\sin\frac{\partial}{\partial \eta_2}$$
$$\frac{\partial}{\partial y_2} = \cos\frac{\partial}{\partial \eta_2} \qquad [5.35]$$

Rewriting Equation [5.34] in terms of the new coordinates η_2 and z gives:

$$-\sin\varphi\frac{\partial b_{i1}^{kl}}{\partial \eta_2} + \cos\varphi\frac{\partial b_{i2}^{kl}}{\partial \eta_2} = 0$$
$$\sin\varphi\ b_{i1}^{kl} - \cos\varphi\ b_{i2}^{kl}\Big|_s = 0 \qquad [5.36]$$

As well, from Equation [5.25], the elastic coefficients, b_{ij}^{kl}, become (after coordinate transformation):

$$b_{ij}^{kl} = -\sin\varphi\ C_{ijm1}\frac{\partial N_m^{kl}}{\partial \eta_2} + \cos\varphi\ C_{ijm2}\frac{\partial N_m^{kl}}{\partial \eta_2} + C_{ijkl} \qquad [5.37]$$

It is worthwhile to reiterate here that as with the model presented in the previous chapter, when an orthotropic material is not referred to its principal material coordinate system, the number and location of the non-zero terms in the matrix of elastic coefficients coincide with those of a monoclinic material. This matrix has the form shown in Equation [4.30a], where C_{ijkl} are the stiffness values referred to the original $\{y_i\}$ coordinate system.

On account of Equation [4.30a], Equation [5.37] can be expanded as:

$$b_{11}^{kl} = -\sin\varphi\left\{C_{1111}\frac{\partial N_1^{kl}}{\partial\eta_2} + C_{1121}\frac{\partial N_2^{kl}}{\partial\eta_2}\right\} + \cos\varphi\left\{C_{1112}\frac{\partial N_1^{kl}}{\partial\eta_2} + C_{1122}\frac{\partial N_2^{kl}}{\partial\eta_2}\right\} + C_{11kl}$$

$$b_{22}^{kl} = -\sin\varphi\left\{C_{2211}\frac{\partial N_1^{kl}}{\partial\eta_2} + C_{2221}\frac{\partial N_2^{kl}}{\partial\eta_2}\right\} + \cos\varphi\left\{C_{2212}\frac{\partial N_1^{kl}}{\partial\eta_2} + C_{2222}\frac{\partial N_2^{kl}}{\partial\eta_2}\right\} + C_{22kl}$$

$$b_{12}^{kl} = b_{21}^{kl} = -\sin\varphi\left\{C_{2111}\frac{\partial N_1^{kl}}{\partial\eta_2} + C_{2121}\frac{\partial N_2^{kl}}{\partial\eta_2}\right\} + \cos\varphi\left\{C_{2112}\frac{\partial N_1^{kl}}{\partial\eta_2} + C_{2122}\frac{\partial N_2^{kl}}{\partial\eta_2}\right\} + C_{21kl} \qquad [5.38]$$

$$b_{13}^{kl} = b_{31}^{kl} = -\sin\varphi\, C_{3131}\frac{\partial N_3^{kl}}{\partial\eta_2} + \cos\varphi\, C_{3132}\frac{\partial N_3^{kl}}{\partial\eta_2} + C_{31kl}$$

$$b_{23}^{kl} = b_{32}^{kl} = -\sin\varphi\, C_{3231}\frac{\partial N_3^{kl}}{\partial\eta_2} + \cos\varphi\, C_{3232}\frac{\partial N_3^{kl}}{\partial\eta_2} + C_{32kl}$$

We will subsequently assume a linear variation of the N_i^{kl} functions in Equation [5.38], i.e.

$$\begin{aligned} N_1^{kl} &= \lambda_1^{kl}\eta_2, \\ N_2^{kl} &= \lambda_2^{kl}\eta_2, \\ N_3^{kl} &= \lambda_3^{kl}\eta_2 \end{aligned} \qquad [5.39]$$

where λ_i^{kl} are constants, which will be determined in the sequel. Thus, the elastic coefficients in Equation [5.38] can be expressed in terms of these constants as:

$$\begin{aligned} b_{11}^{kl} &= -\sin\varphi\left\{C_{11}\lambda_1^{kl} + C_{16}\lambda_2^{kl}\right\} + \cos\varphi\left\{C_{16}\lambda_1^{kl} + C_{12}\lambda_2^{kl}\right\} + C_{11kl} \\ b_{22}^{kl} &= -\sin\varphi\left\{C_{12}\lambda_1^{kl} + C_{26}\lambda_2^{kl}\right\} + \cos\varphi\left\{C_{26}\lambda_1^{kl} + C_{22}\lambda_2^{kl}\right\} + C_{22kl} \\ b_{12}^{kl} = b_{21}^{kl} &= -\sin\varphi\left\{C_{16}\lambda_1^{kl} + C_{66}\lambda_2^{kl}\right\} + \cos\varphi\left\{C_{66}\lambda_1^{kl} + C_{26}\lambda_2^{kl}\right\} + C_{21kl} \\ b_{13}^{kl} = b_{31}^{kl} &= -\sin\varphi\, C_{55}\lambda_3^{kl} + \cos\varphi\, C_{45}\lambda_3^{kl} + C_{31kl} \\ b_{23}^{kl} = b_{32}^{kl} &= -\sin\varphi\, C_{45}\lambda_3^{kl} + \cos\varphi\, C_{44}\lambda_3^{kl} + C_{32kl} \end{aligned} \qquad [5.40]$$

After introducing the following definitions,

$$
\begin{gathered}
A_1 = -C_{11}\sin\varphi + C_{16}\cos\varphi,\ \ A_2 = -C_{16}\ \sin\varphi + C_{12}\ \cos\varphi,\ \ A_3 = C_{11kl} \\
A_4 = -C_{12}\sin\varphi + C_{26}\cos\varphi\ ,\ A_5 = -C_{26}\sin\varphi + C_{22}\cos\varphi,\ \ A_6 = C_{22kl} \\
A_7 = -C_{16}\sin\varphi + C_{66}\cos\varphi\ ,\ A_8 = -C_{66}\sin\varphi + C_{26}\cos\varphi,\ \ A_9 = C_{12kl} \\
A_{10} = -C_{55}\ \sin\varphi + C_{45}\cos\varphi\ , A_{11} = C_{13kl} \\
A_{12} = -C_{45}\sin\varphi + C_{44}\cos\varphi,\ \ A_{13} = C_{23kl}
\end{gathered}
\qquad [5.41]
$$

Equation [5.40] becomes:

$$
\begin{gathered}
b_{11}^{kl} = \lambda_1 A_1 + \lambda_2 A_2 + A_3 \\
b_{22}^{kl} = \lambda_1\ A_4 + \lambda_2\ A_5 + A_6 \\
b_{12}^{kl} = b_{21}^{kl} = \lambda_1\ A_7 + \lambda_2 A_8 + A_9 \\
b_{13}^{kl} = b_{31}^{kl} = \lambda_3 A_{10} + A_{11} \\
b_{23}^{kl} = b_{32}^{kl} = \lambda_3 A_{12} + A_{13}
\end{gathered}
\qquad [5.42]
$$

Expanding the interface conditions for i = 1, 2, and 3 in second expression of Equation [5.36], one obtains:

$$
\begin{gathered}
\sin\varphi\ b_{11}^{kl} - \cos\varphi\ b_{12}^{kl} = 0 \\
\sin\varphi\ b_{21}^{kl} - \cos\varphi\ b_{22}^{kl} = 0 \\
\sin\varphi\ b_{31}^{kl} - \cos\varphi\ b_{32}^{kl} = 0
\end{gathered}
\qquad [5.43]
$$

Solving Equations [5.42] and [5.43], for λ_i^{kl}, is straight forward and results in:

$$\lambda_1^{kl} = \frac{\begin{array}{c}\left(s\,C_{12kl} - c\,C_{22kl}\right)\left(scC_{12} + scC_{66} - s^2C_{16} - c^2C_{26}\right) - \\ \left(sC_{11kl} - cC_{12kl}\right)\left(2scC_{26} - s^2C_{66} - c^2C_{22}\right)\end{array}}{\left(\begin{array}{l}s^4C_{11}C_{66} + s^2c^2C_{11}C_{22} - 2s^3cC_{11}C_{26} + c^4C_{66}C_{22} - 2sc^3C_{16}C_{22} + 2s^2c^2C_{16}C_{26} \\ - s^4C_{16}{}^2 + 2s^3cC_{16}C_{12} - c^4C_{26}{}^2 + 2sc^3C_{12}C_{26} - s^2c^2C_{12}{}^2 - 2s^2c^2C_{12}C_{66}\end{array}\right)}$$

$$\lambda_2^{kl} = \frac{\begin{array}{c}\left(s\,C_{12kl} - c\,C_{22kl}\right)\left(2scC_{16} - s^2C_{11} - c^2C_{66}\right) - \\ \left(sC_{11kl} - cC_{12kl}\right)\left(scC_{12} + scC_{66} - s^2C_{16} - c^2C_{26}\right)\end{array}}{\left(\begin{array}{l}- s^4C_{11}C_{66} - s^2c^2C_{11}C_{22} + 2s^3cC_{11}C_{26} - c^4C_{66}C_{22} + 2sc^3C_{16}C_{22} - 2s^2c^2C_{16}C_{26} \\ + s^4C_{16}{}^2 - 2s^3cC_{16}C_{12} + c^4C_{26}{}^2 - 2sc^3C_{12}C_{26} + s^2c^2C_{12}{}^2 + 2s^2c^2C_{12}C_{66}\end{array}\right)} \qquad [5.44]$$

$$\lambda_3^{kl} = -\frac{\left(sC_{13kl} - cC_{23kl}\right)}{\left(2scC_{45} - s^2C_{55} - c^2C_{44}\right)}$$

Here we use the shorthand notations of "s" and "c" to denote sinφ and cosφ respectively. For an inclusion oriented in a given direction φ, one calculates $\lambda_1^{kl}, \lambda_2^{kl}, \lambda_3^{kl}$. The results are then substituted in Equation [5.40] to calculate b_{ij}^{kl}. This is repeated for each inclusion in the unit cell and finally the effective elastic coefficients for the entire structure are obtained from Equation [5.21]. Some examples will be considered next.

5.3.3.1. Examples of Structures; Effective Elastic Coefficients

5.3.3.1.1. Example 1

This example pertains to the first smart structure of Figure 5-1. Isometric and top views of this structure are shown in Figure 5-5. The unit cell for this structure is shown in Figure 5-6. The unit cell problem will be solved approximately for each element Ω_1 and Ω_2 of the unit-cell and then the results will be superimposed.

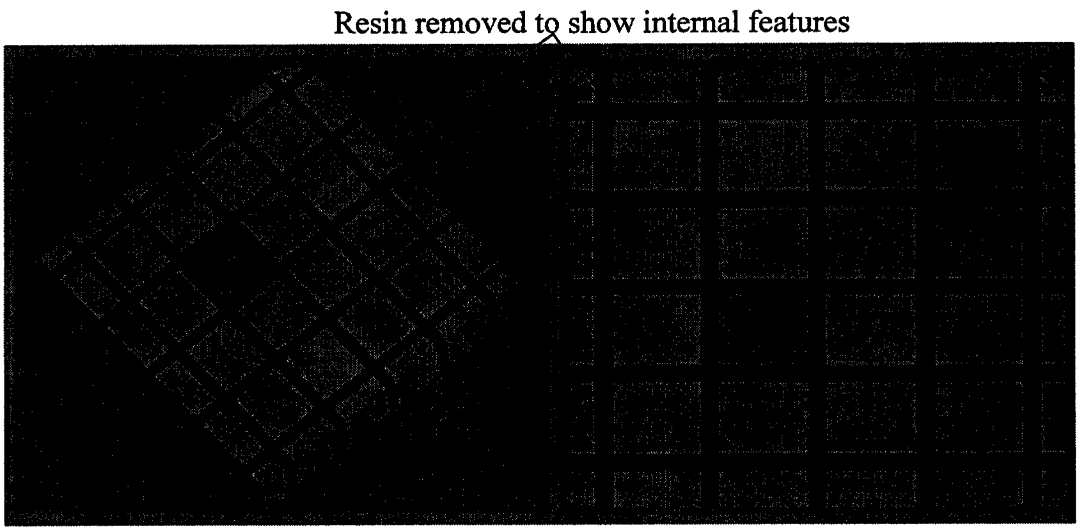

Figure 5-5: Isometric and top view of smart structure with orientations in 0° and 90°

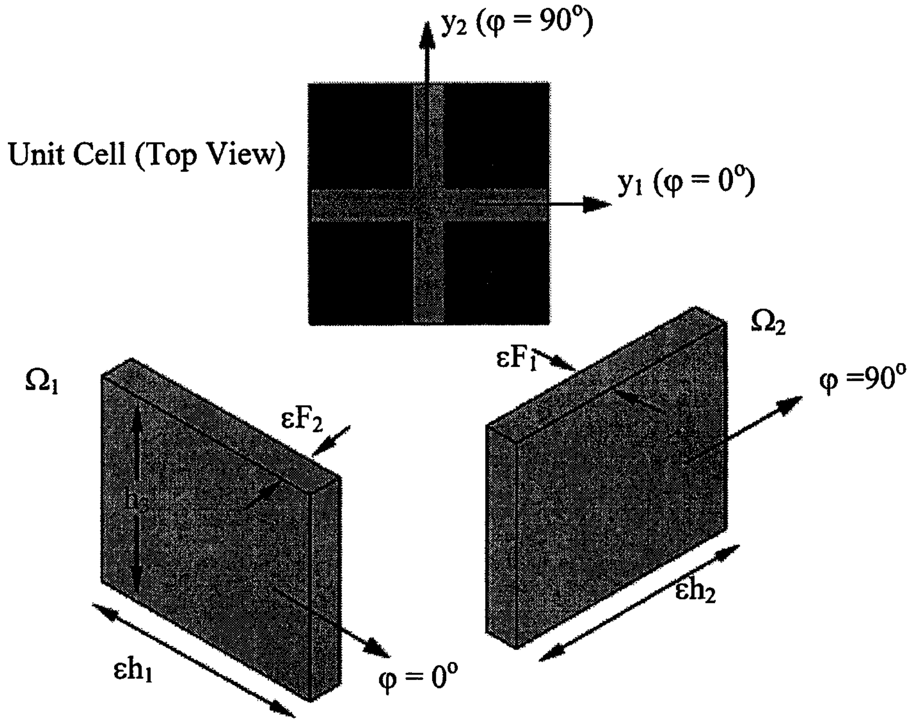

Figure 5-6: Smart structure with orientation of reinforcements in 0° and 90°

(a) Region Ω_1 ($\varphi = 0^o$):

Solving for λ_i^{kl} from Equation [5.44] gives,

$$\lambda_1 = -\frac{C_{12kl}}{C_{66}}, \ \lambda_2 = -\frac{C_{22kl}}{C_{22}}, \ \lambda_3 = -\frac{C_{23kl}}{C_{44}} \qquad [5.45]$$

and then substituting the results in Equation [5.40] gives the following expressions for the non-vanishing elastic coefficients:

$$b_{11}^{11} = C_{11} - \frac{{C_{12}}^2}{C_{22}}; \ b_{33}^{11} = C_{13} - \frac{C_{23}C_{12}}{C_{22}}; \ b_{33}^{33} = C_{33} - \frac{{C_{23}}^2}{C_{22}}; \ b_{13}^{13} = C_{55} \qquad [5.46]$$

(b) Region Ω_2 ($\varphi = 90^o$):

Repeating the procedure results in:

$$b_{22}^{22} = C_{22} - \frac{{C_{12}}^2}{C_{11}}; \ b_{33}^{22} = C_{23} - \frac{C_{13}C_{12}}{C_{11}}; \ b_{33}^{33} = C_{33} - \frac{{C_{13}}^2}{C_{11}}; \ b_{23}^{23} = C_{44} \qquad [5.47]$$

We are now ready to compute the effective elastic coefficients. To this end, we note from Figure 5-6 that the volumes of elements Ω_1, Ω_2 and the entire unit cell are $\varepsilon^2 F_2 h_1 h_3$, $\varepsilon^2 F_1 h_2 h_3$ and $\varepsilon^2 h_1 h_2 h_3$ respectively, where εF_1 and εF_2 are the thicknesses of the reinforcements Ω_2 and Ω_1. Thus, from Equation [5.21] the effective elastic coefficients for this structure are computed as:

$$\left\langle C_{ijkl} \right\rangle = \frac{1}{|Y|} \int_{|Y|} b_{ij}^{kl} dv$$

$$\therefore \left\langle C_{ijkl} \right\rangle = \frac{F_2}{h_2} b_{ij}^{kl} \Big|_{\Omega_1} + \frac{F_1}{h_1} b_{ij}^{kl} \Big|_{\Omega_2} \qquad [5.48]$$

Before we can express these elastic coefficients in terms of the engineering constants, we need to make use of the familiar tensor transformation equation for a 4th-order tensor,

$$C_{ijkl} = a_{im} a_{jn} a_{kp} a_{lq} C_{mnpq}^{(p)} \qquad [5.49a]$$

where the a_{ij} coefficients are the elements of the transformation matrix in Equation [5.31] and $C_{mnpq}^{(p)}$ represent the elastic coefficients of the reinforcements with respect to their principal material coordinate system. Equation [5.49b] and [5.49c] below is the expanded form of Equation [5.49a].

$$\begin{aligned}
C_{11} &= C_{11}^{(p)} c^4 - 4C_{16}^{(p)} c^3 s + 2\left(C_{12}^{(p)} + 2C_{66}^{(p)}\right) c^2 s^2 - 4C_{26}^{(p)} cs^3 + C_{22}^{(p)} s^4 \\
C_{12} &= C_{12}^{(p)} c^4 + 2\left(C_{16}^{(p)} - C_{26}^{(p)}\right) c^3 s + \left(C_{11}^{(p)} + C_{22}^{(p)} - 4C_{66}^{(p)}\right) c^2 s^2 + \\
&\quad 2\left(C_{26}^{(p)} - C_{16}^{(p)}\right) cs^3 + C_{12}^{(p)} s^4 \\
C_{13} &= C_{13}^{(p)} c^2 - 2C_{36}^{(p)} cs + C_{23}^{(p)} s^2 \\
C_{16} &= C_{16}^{(p)} c^4 + \left(C_{11}^{(p)} - C_{12}^{(p)} - 2C_{66}^{(p)}\right) c^3 s + 3\left(C_{26}^{(p)} - C_{16}^{(p)}\right) c^2 s^2 + \\
&\quad \left(2C_{66}^{(p)} + C_{12}^{(p)} - C_{22}^{(p)}\right) cs^3 - C_{26}^{(p)} s^4 \\
C_{22} &= C_{22}^{(p)} c^4 + 4C_{26}^{(p)} c^3 s + 2\left(C_{12}^{(p)} + 2C_{66}^{(p)}\right) c^2 s^2 + 4C_{16}^{(p)} cs^3 + C_{11}^{(p)} s^4 \\
C_{23} &= C_{23}^{(p)} c^2 - 2C_{36}^{(p)} cs + C_{13}^{(p)} s^2 \\
C_{26} &= C_{66}^{(p)} c^4 + \left(C_{12}^{(p)} - C_{22}^{(p)} - 2C_{66}^{(p)}\right) c^3 s + 3\left(C_{16}^{(p)} - C_{26}^{(p)}\right) c^2 s^2 + \\
&\quad \left(C_{11}^{(p)} - 2C_{66}^{(p)} - C_{12}^{(p)}\right) cs^3 - C_{16}^{(p)} s^4
\end{aligned} \qquad [5.49b]$$

$$C_{33} = C_{33}^{(p)}$$

$$C_{36} = \left(C_{13}^{(p)} - C_{23}^{(p)}\right)cs + C_{36}^{(p)}\left(c^2 - s^2\right)$$

$$C_{66} = 2\left(C_{16}^{(p)} - C_{26}^{(p)}\right)c^3 s + \left(C_{11}^{(p)} + C_{22}^{(p)} - 2C_{12}^{(p)} - 2C_{66}^{(p)}\right)c^2 s^2 + 2\left(C_{26}^{(p)} - C_{16}^{(p)}\right)cs^3 + C_{66}^{(p)}\left(c^4 + s^4\right) \qquad [5.49c]$$

$$C_{44} = C_{44}^{(p)}c^2 + C_{55}^{(p)}s^2 + 2C_{45}^{(p)}cs$$

$$C_{45} = C_{45}^{(p)}\left(c^2 - s^2\right) + \left(C_{55}^{(p)} - C_{44}^{(p)}\right)cs$$

$$C_{55} = C_{55}^{(p)}c^2 + C_{44}^{(p)}s^2 - 2C_{45}^{(p)}cs$$

Next, assuming (without loss of generality) that both reinforcements are made of the same orthotropic material, the non-vanishing effective elastic coefficients for the smart structure of Figure 5-6 are obtained from Equations [5.48] and [5.49a] and are:

$$\begin{aligned}
\langle C_{11} \rangle &= \frac{F_2}{h_2}\left(\frac{E_1^{(P)}}{1 - \upsilon_{13}^{(P)}\upsilon_{31}^{(P)}}\right), \\
\langle C_{22} \rangle &= \frac{F_1}{h_1}\left(\frac{E_1^{(P)}}{1 - \upsilon_{13}^{(P)}\upsilon_{31}^{(P)}}\right), \\
\langle C_{13} \rangle = \langle C_{31} \rangle &= \frac{F_2}{h_2}\left(\frac{\upsilon_{13}^{(P)}E_3^{(P)}}{1 - \upsilon_{13}^{(P)}\upsilon_{31}^{(P)}}\right), \\
\langle C_{23} \rangle = \langle C_{32} \rangle &= \frac{F_1}{h_1}\left(\frac{\upsilon_{13}^{(P)}E_3^{(P)}}{1 - \upsilon_{13}^{(P)}\upsilon_{31}^{(P)}}\right), \\
\langle C_{33} \rangle &= \frac{F_2}{h_2}\left(\frac{E_3^{(P)}}{1 - \upsilon_{13}^{(P)}\upsilon_{31}^{(P)}}\right) + \frac{F_1}{h_1}\left(\frac{E_3^{(P)}}{1 - \upsilon_{13}^{(P)}\upsilon_{31}^{(P)}}\right), \\
\langle C_{44} \rangle &= \frac{F_1}{h_1}G_{13}^{(P)}, \\
\langle C_{55} \rangle &= \frac{F_2}{h_2}G_{13}^{(P)}
\end{aligned} \qquad [5.50]$$

Here, $E_i^{(p)}, G_{ij}^{(p)}, v_{ij}^{(p)}$ represent the principal elastic moduli, shear moduli, and Poisson's ratios for the reinforcement. We also note that in arriving at Equation [5.50] we made use of the well-known relationships between the C_{ijkl} coefficients and the engineering constants, see e.g. Reddy [1997].

5.3.3.1.2. Example 2

This example pertains to the second smart structure of Figure 5-1. Figure 5-7 shows the enlarged isometric view of this structure. The unit cell for this structure is shown in Figure 5-8. This structure is composed of three families of reinforcements, each family oriented in a different direction. Each reinforcement can be made of a different orthotropic material and can have a different thickness. The distance between the two neighboring reinforcements of the same family is εa.

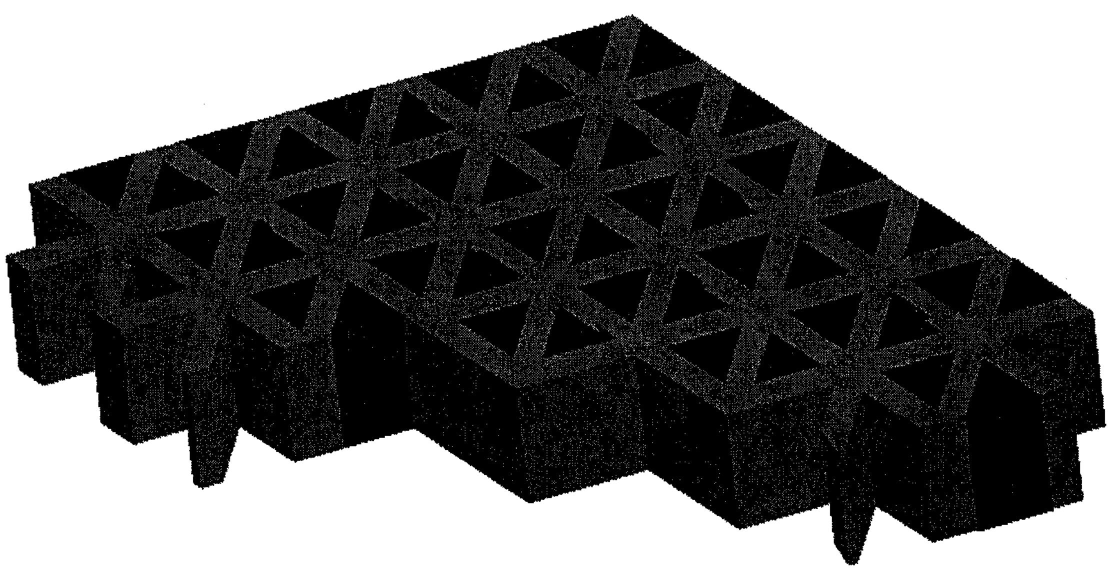

Figure 5-7: Isometric view of Smart structure with reinforcements at 30°, 90°, and 150°

Following the same methodology as for the previous example, the elastic b_{ij}^{kl} constants are readily calculated. Here, we provide the final values for λ_i^{kl} and b_{ij}^{kl} constants.

(a) Region Ω_1 (φ = 90°):

The elastic coefficients for the region 1 are given in the Equation [5.47], and will not be repeated.

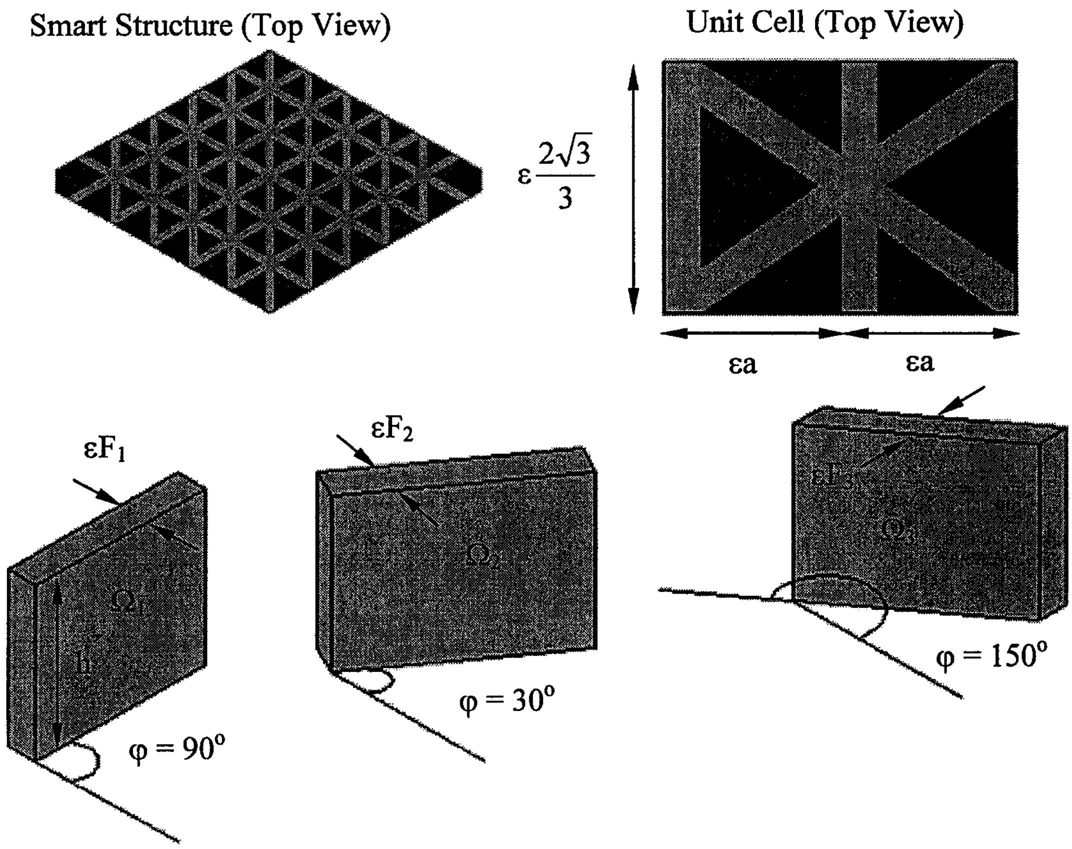

Figure 5-8: Smart structure with reinforcements at 30°, 90°, and 150°

(b) Region Ω_2 (φ = 30°):

From Equation [5.44]; λ's are calculated as:

$$\lambda_1 = \frac{\begin{pmatrix}(0.5\,C_{12kl} - 0.866\,C_{22kl})(-0.25C_{16} - 0.75C_{26} + 0.433C_{12} + 0.433C_{66}) - \\ (0.5C_{11kl} - 0.866C_{12kl})(-0.25C_{66} - 0.75C_{22} + 0.866C_{26})\end{pmatrix}}{\begin{pmatrix}0.0625C_{11}C_{66} + 0.1875C_{11}C_{22} - 0.2165C_{11}C_{26} + 0.5625C_{66}C_{22} - \\ 0.6495C_{16}C_{22} + 0.375C_{16}C_{26} - 0.0625C_{16}{}^2 + 0.2165C_{16}C_{12} \\ -0.5625C_{26}{}^2 + 0.6495C_{12}C_{26} - 0.1875C_{12}{}^2 - 0.375C_{12}C_{66}\end{pmatrix}}$$

$$\lambda_2 = \frac{\begin{pmatrix}(0.5\,C_{12kl} - 0.866\,C_{22kl})(-0.25C_{11} - 0.75C_{66} + 0.866C_{16}) - \\ (0.5C_{11kl} - 0.866C_{12kl})(-0.25C_{16} - 0.75C_{26} + 0.433C_{12} + 0.433C_{66})\end{pmatrix}}{\begin{pmatrix}-0.0625C_{11}C_{66} - 0.1875C_{11}C_{22} + 0.2165C_{11}C_{26} - 0.5625C_{66}C_{22} \\ +0.6495C_{16}C_{22} - 0.375C_{16}C_{26} + 0.0625C_{16}{}^2 - 0.2165C_{16}C_{12} + \\ 0.5625C_{26}{}^2 - 0.6495C_{12}C_{26} + 0.1875C_{12}{}^2 + 0.375C_{12}C_{66}\end{pmatrix}} \quad [5.51]$$

$$\lambda_3 = -\frac{(0.5C_{13kl} - 0.866C_{23kl})}{(-0.25C_{55} - 0.75C_{44} + 0.866C_{45})}$$

Subsequently, the elastic coefficients for the region Ω_2 are:

$$b_{11}^{11} = \frac{(-0.5C_{11} + 0.866C_{16})\begin{pmatrix}(0.5\,C_{16} - 0.866\,C_{12})(-0.25C_{16} - 0.75C_{26} + 0.433C_{12} + 0.433C_{66}) - \\ (0.5C_{11} - 0.866C_{16})(-0.25C_{66} - 0.75C_{22} + 0.866C_{26})\end{pmatrix}}{\Delta}$$
$$\frac{-(-0.5C_{16} + 0.866C_{12})\begin{pmatrix}(0.5\,C_{16} - 0.866\,C_{12})(-0.25C_{11} - 0.75C_{66} + 0.866C_{16}) - \\ (0.5C_{11} - 0.866C_{16})(-0.25C_{16} - 0.75C_{26} + 0.433C_{12} + 0.433C_{66})\end{pmatrix}}{\Delta} + C_{11}$$

[5.52a]

$$b_{11}^{22} = \frac{(-0.5C_{11} + 0.866C_{16})\begin{pmatrix}(0.5\,C_{26} - 0.866\,C_{22})(-0.25C_{16} - 0.75C_{26} + 0.433C_{12} + 0.433C_{66}) - \\ (0.5C_{12} - 0.866C_{26})(-0.25C_{66} - 0.75C_{22} + 0.866C_{26})\end{pmatrix}}{\Delta}$$
$$\frac{-(-0.5C_{16} + 0.866C_{12})\begin{pmatrix}(0.5\,C_{26} - 0.866\,C_{22})(-0.25C_{11} - 0.75C_{66} + 0.866C_{16}) - \\ (0.5C_{12} - 0.866C_{26})(-0.25C_{16} - 0.75C_{26} + 0.433C_{12} + 0.433C_{66})\end{pmatrix}}{\Delta} + C_{12}$$

$$b_{11}^{33}=\frac{\left(-0.5C_{11}+0.866C_{16}\right)\begin{pmatrix}(0.5\,C_{36}-0.866\,C_{23})(-0.25C_{16}-0.75C_{26}+0.433C_{12}+0.433C_{66})-\\(0.5C_{13}-0.866C_{36})(-0.25C_{66}-0.75C_{22}+0.866C_{26})\end{pmatrix}}{\Delta}$$

$$\frac{-\left(-0.5C_{16}+0.866C_{12}\right)\begin{pmatrix}(0.5\,C_{36}-0.866\,C_{23})(-0.25C_{11}-0.75C_{66}+0.866C_{16})-\\(0.5C_{13}-0.866C_{36})(-0.25C_{16}-0.75C_{26}+0.433C_{12}+0.433C_{66})\end{pmatrix}}{\Delta}+C_{13}$$

$$b_{11}^{13}=b_{13}^{11}=0$$

$$b_{11}^{23}=b_{23}^{11}=0$$

$$b_{11}^{12}=\frac{\left(-0.5C_{11}+0.866C_{16}\right)\begin{pmatrix}(0.5\,C_{66}-0.866\,C_{26})(-0.25C_{16}-0.75C_{26}+0.433C_{12}+0.433C_{66})-\\(0.5C_{16}-0.866C_{66})(-0.25C_{66}-0.75C_{22}+0.866C_{26})\end{pmatrix}}{\Delta}$$

$$\frac{-\left(-0.5C_{16}+0.866C_{12}\right)\begin{pmatrix}(0.5\,C_{66}-0.866\,C_{26})(-0.25C_{11}-0.75C_{66}+0.866C_{16})-\\(0.5C_{16}-0.866C_{66})(-0.25C_{16}-0.75C_{26}+0.433C_{12}+0.433C_{66})\end{pmatrix}}{\Delta}+C_{16}$$

$$b_{22}^{22}=\frac{\left(-0.5C_{12}+0.866C_{26}\right)\begin{pmatrix}(0.5\,C_{26}-0.866\,C_{22})(-0.25C_{16}-0.75C_{26}+0.433C_{12}+0.433C_{66})-\\(0.5C_{12}-0.866C_{26})(-0.25C_{66}-0.75C_{22}+0.866C_{26})\end{pmatrix}}{\Delta} \qquad [5.52b]$$

$$\frac{-\left(-0.5C_{26}+0.866C_{22}\right)\begin{pmatrix}(0.5\,C_{26}-0.866C_{22})(-0.25C_{11}-0.75C_{66}+0.866C_{16})-\\(0.5C_{12}-0.866C_{26})(-0.25C_{16}-0.75C_{26}+0.433C_{12}+0.433C_{66})\end{pmatrix}}{\Delta}+C_{22}$$

$$b_{22}^{13}=b_{13}^{22}=0$$

$$b_{22}^{23}=b_{23}^{22}=0$$

$$b_{22}^{12}=\frac{\left(-0.5C_{12}+0.866C_{26}\right)\begin{pmatrix}(0.5\,C_{66}-0.866\,C_{26})(-0.25C_{16}-0.75C_{26}+0.433C_{12}+0.433C_{66})-\\(0.5C_{16}-0.866C_{66})(-0.25C_{66}-0.75C_{22}+0.866C_{26})\end{pmatrix}}{\Delta}$$

$$\frac{-\left(-0.5C_{26}+0.866C_{22}\right)\begin{pmatrix}(0.5\,C_{66}-0.866\,C_{26})(-0.25C_{11}-0.75C_{66}+0.866C_{16})-\\(0.5C_{16}-0.866C_{66})(-0.25C_{16}-0.75C_{26}+0.433C_{12}+0.433C_{66})\end{pmatrix}}{\Delta}+C_{26}$$

$$b_{33}^{22}=\frac{\left(-0.5C_{13}+0.866C_{36}\right)\begin{pmatrix}(0.5C_{26}-0.866\,C_{22})(-0.25C_{16}-0.75C_{26}+0.433C_{12}+0.433C_{66})-\\(0.5C_{12}-0.866C_{26})(-0.25C_{66}-0.7C_{22}+0.866C_{26})\end{pmatrix}}{\Delta}$$

$$\frac{-\left(-0.5C_{36}+0.866C_{23}\right)\begin{pmatrix}(0.5\,C_{26}-0.866\,C_{22})(-0.25C_{11}-0.75C_{66}+0.866C_{16})-\\(0.5C_{12}-0.866C_{26})(-0.25C_{16}-0.75C_{26}+0.433C_{12}+0.433C_{66})\end{pmatrix}}{\Delta}+C_{32}$$

$$b_{33}^{33}=\frac{\left(-0.5C_{13}+0.866C_{36}\right)\begin{pmatrix}\left(0.5\,C_{36}-0.866\,C_{23}\right)\left(-0.25C_{16}-0.75C_{26}+0.433C_{12}+0.433C_{66}\right)-\\\left(0.5C_{13}-0.866C_{36}\right)\left(-0.25C_{66}-0.75C_{22}+0.866C_{26}\right)\end{pmatrix}}{\Delta}$$

$$\frac{-\left(-0.5C_{36}+0.866C_{32}\right)\begin{pmatrix}\left(0.5\,C_{36}-0.866\,C_{23}\right)\left(-0.25C_{11}-0.75C_{66}+0.866C_{16}\right)-\\\left(0.5C_{13}-0.866C_{36}\right)\left(-0.25C_{16}-0.75C_{26}+0.433C_{12}+0.433C_{66}\right)\end{pmatrix}}{\Delta}+C_{33}$$

$$b_{33}^{13}=b_{13}^{33}=0$$

$$b_{33}^{23}=b_{23}^{33}=0$$

$$b_{33}^{12}=\frac{\left(-0.5C_{13}+0.866C_{36}\right)\begin{pmatrix}\left(0.5\,C_{66}-0.866\,C_{26}\right)\left(-0.25C_{16}-0.75C_{26}+0.433C_{12}+0.433C_{66}\right)-\\\left(0.5C_{16}-0.866C_{66}\right)\left(-0.25C_{66}-0.75C_{22}+0.866C_{26}\right)\end{pmatrix}}{\Delta}$$

$$\frac{-\left(-0.5C_{36}+0.866C_{23}\right)\begin{pmatrix}\left(0.5\,C_{66}-0.866\,C_{26}\right)\left(-0.25C_{11}-0.75C_{66}+0.866C_{16}\right)-\\\left(0.5C_{16}-0.866C_{66}\right)\left(-0.25C_{16}-0.75C_{26}+0.433C_{12}+0.433C_{66}\right)\end{pmatrix}}{\Delta}+C_{36}$$

$$b_{12}^{12}=\frac{\left(-0.5C_{16}+0.866C_{66}\right)\begin{pmatrix}\left(0.5\,C_{66}-0.866\,C_{26}\right)\left(-0.25C_{16}-0.75C_{26}+0.433C_{12}+0.433C_{66}\right)-\\\left(0.5C_{16}-0.866C_{66}\right)\left(-0.25C_{66}-0.75C_{22}+0.866C_{26}\right)\end{pmatrix}}{\Delta} \qquad [5.52c]$$

$$\frac{-\left(-0.5C_{66}+0.866C_{26}\right)\begin{pmatrix}\left(0.5\,C_{66}-0.866\,C_{26}\right)\left(-0.25C_{11}-0.75C_{66}+0.866C_{16}\right)-\\\left(0.5C_{16}-0.866C_{66}\right)\left(-0.25C_{16}-0.75C_{26}+0.433C_{12}+0.433C_{66}\right)\end{pmatrix}}{\Delta}+C_{66}$$

$$b_{23}^{23}=-\frac{\left(0.5C_{45}-0.866C_{44}\right)}{\left(-0.25C_{55}-0.75C_{44}+0.866C_{45}\right)}\left(-0.5C_{45}+0.866C_{44}\right)+C_{44}$$

$$b_{23}^{13}=-\frac{\left(0.5C_{55}-0.866C_{45}\right)}{\left(-0.25C_{55}-0.75C_{44}+0.866C_{45}\right)}\left(-0.5C_{45}+0.866C_{44}\right)+C_{45}$$

$$b_{23}^{12}=b_{12}^{23}=0$$

$$b_{13}^{23}=-\frac{\left(0.5C_{45}-0.866C_{44}\right)}{\left(-0.25C_{55}-0.75C_{44}+0.866C_{45}\right)}\left(-0.5C_{55}+0.866C_{45}\right)+C_{45}$$

$$b_{13}^{13}=-\frac{\left(0.5C_{55}-0.866C_{45}\right)}{\left(-0.25C_{55}-0.75C_{44}+0.866C_{45}\right)}\left(-0.5C_{55}+0.866C_{45}\right)+C_{55}$$

$$b_{13}^{12}=b_{12}^{13}=0$$

where

$$\begin{aligned}\Delta = {} & 0.0625C_{11}C_{66} + 0.1875C_{11}C_{22} - 0.2165C_{11}C_{26} + 0.5625C_{66}C_{22} - \\ & 0.6495C_{16}C_{22} + 0.375C_{16}C_{26} - 0.0625C_{16}{}^{2} + 0.2165C_{16}C_{12} \\ & -0.5625C_{26}{}^{2} + 0.6495C_{12}C_{26} - 0.1875C_{12}{}^{2} - 0.375C_{12}C_{66}\end{aligned} \qquad [5.52d]$$

(c) Region Ω_3 (φ = 150°):

Similarly the λ's for the region 3 are calculated as given below

$$\lambda_1 = \frac{\begin{pmatrix}(0.5\,C_{12kl} + 0.866\,C_{22kl})(-0.433C_{12} - 0.433C_{66} - 0.25C_{16} - 0.75C_{26}) - \\ (0.5C_{11kl} + 0.866C_{12kl})(-0.25C_{66} - 0.75C_{22} - 0.866C_{26})\end{pmatrix}}{\begin{pmatrix}0.0625C_{11}C_{66} + 0.1875C_{11}C_{22} + 0.2165C_{11}C_{26} + 0.5625C_{66}C_{22} + \\ 0.6495C_{16}C_{22} + 0.375C_{16}C_{26} - 0.0625C_{16}{}^{2} - 0.2165C_{16}C_{12} \\ -0.5625C_{26}{}^{2} - 0.6495C_{12}C_{26} - 0.1875C_{12}{}^{2} - 0.375C_{12}C_{66}\end{pmatrix}}$$

$$\lambda_2 = \frac{\begin{matrix}(0.5\,C_{12kl} + 0.866\,C_{22kl})(-0.25C_{11} - 0.75C_{66} - 0.866C_{16}) - \\ (0.5C_{11kl} + 0.866C_{12kl})(-0.433C_{12} - 0.433C_{66} - 0.25C_{16} - 0.75C_{26})\end{matrix}}{\begin{pmatrix}-0.0625C_{11}C_{66} - 0.1875C_{11}C_{22} - 0.2165C_{11}C_{26} - 0.5625C_{66}C_{22} - \\ 0.6495C_{16}C_{22} - 0.375C_{16}C_{26} + 0.0625C_{16}{}^{2} + 0.2165C_{16}C_{12} \\ +0.5625C_{26}{}^{2} + 0.6495C_{12}C_{26} + 0.1875C_{12}{}^{2} + 0.375C_{12}C_{66}\end{pmatrix}} \qquad [5.53]$$

$$\lambda_3 = -\frac{(0.5C_{13kl} + 0.866C_{23kl})}{(-0.25C_{55} - 0.75C_{44} - 0.866C_{45})}$$

And the elastic coefficients are given as

$$b_{11}^{11} = \frac{-(0.5C_{11} + 0.866C_{16})\begin{pmatrix}(0.5\,C_{16} + 0.866\,C_{12})(-0.433C_{12} - 0.433C_{66} - 0.25C_{16} - 0.75C_{26}) - \\ (0.5C_{11} + 0.866C_{16})(-0.25C_{66} - 0.75C_{22} - 0.866C_{26})\end{pmatrix}}{\Delta^*} \qquad [5.54a]$$

$$\frac{+(0.5C_{16} + 0.866C_{12})\begin{pmatrix}(0.5\,C_{16} + 0.866\,C_{12})(-0.25C_{11} - 0.75C_{66} - 0.866C_{16}) - \\ (0.5C_{11} + 0.866C_{16})(-0.433C_{12} - 0.433C_{66} - 0.25C_{16} - 0.75C_{26})\end{pmatrix}}{\Delta^*} + C_{11}$$

$$b_{11}^{22} = \frac{-\left(0.5C_{11} + 0.866C_{16}\right)\begin{pmatrix}\left(0.5\,C_{26} + 0.866\,C_{22}\right)\left(-0.433C_{12} - 0.433C_{66} - 0.25C_{16} - 0.75C_{26}\right) - \\ \left(0.5C_{12} + 0.866C_{26}\right)\left(-0.25C_{66} - 0.75C_{22} - 0.866C_{26}\right)\end{pmatrix}}{\Delta^*}$$

$$\frac{+\left(0.5C_{16} + 0.866C_{12}\right)\begin{pmatrix}\left(0.5\,C_{26} + 0.866C_{22}\right)\left(-0.25C_{11} - 0.75C_{66} - 0.866C_{16}\right) - \\ \left(0.5C_{12} + 0.866C_{26}\right)\left(-0.433C_{12} - 0.433C_{66} - 0.25C_{16} - 0.75C_{26}\right)\end{pmatrix}}{\Delta^*} + C_{12}$$

$$b_{11}^{33} = \frac{-\left(0.5C_{11} + 0.866C_{16}\right)\begin{pmatrix}\left(0.5\,C_{36} + 0.866\,C_{23}\right)\left(-0.433C_{12} - 0.433C_{66} - 0.25C_{16} - 0.75C_{26}\right) - \\ \left(0.5C_{13} + 0.866C_{36}\right)\left(-0.25C_{66} - 0.75C_{22} - 0.866C_{26}\right)\end{pmatrix}}{\Delta^*}$$

$$\frac{+\left(0.5C_{16} + 0.866C_{12}\right)\begin{pmatrix}\left(0.5\,C_{36} + 0.866\,C_{23}\right)\left(-0.25C_{11} - 0.75C_{66} - 0.866C_{16}\right) - \\ \left(0.5C_{13} + 0.866C_{36}\right)\left(-0.433C_{12} - 0.433C_{66} - 0.25C_{16} - 0.75C_{26}\right)\end{pmatrix}}{\Delta^*} + C_{13}$$

$$b_{11}^{13} = b_{13}^{11} = 0$$

$$b_{11}^{23} = b_{23}^{11} = 0 \qquad [5.54b]$$

$$b_{11}^{12} = \frac{-\left(0.5C_{11} + 0.866C_{16}\right)\begin{pmatrix}\left(0.5\,C_{66} + 0.866\,C_{26}\right)\left(-0.433C_{12} - 0.433C_{66} - 0.25C_{16} - 0.75C_{26}\right) - \\ \left(0.5C_{16} + 0.866C_{66}\right)\left(-0.25C_{66} - 0.75C_{22} - 0.866C_{26}\right)\end{pmatrix}}{\Delta^*}$$

$$\frac{+\left(0.5C_{16} + 0.866C_{12}\right)\begin{pmatrix}\left(0.5\,C_{66} + 0.866\,C_{26}\right)\left(-0.25C_{11} - 0.75C_{66} - 0.866C_{16}\right) - \\ \left(0.5C_{16} + 0.866C_{66}\right)\left(-0.433C_{12} - 0.433C_{66} - 0.25C_{16} - 0.75C_{26}\right)\end{pmatrix}}{\Delta^*} + C_{16}$$

$$b_{22}^{22} = \frac{-\left(0.5C_{12} + 0.866C_{26}\right)\begin{pmatrix}\left(0.5\,C_{26} + 0.866\,C_{22}\right)\left(-0.433C_{12} - 0.433C_{66} - 0.25C_{16} - 0.75C_{26}\right) - \\ \left(0.5C_{12} + 0.866C_{26}\right)\left(-0.25C_{66} - 0.75C_{22} - 0.866C_{26}\right)\end{pmatrix}}{\Delta^*}$$

$$\frac{+\left(0.5C_{26} + 0.866C_{22}\right)\begin{pmatrix}\left(0.5C_{26} + 0.866\,C_{22}\right)\left(-0.25C_{11} - 0.75C_{66} - 0.866C_{16}\right) - \\ \left(0.5C_{12} + 0.866C_{26}\right)\left(-0.433C_{12} - 0.433C_{66} - 0.25C_{16} - 0.75C_{26}\right)\end{pmatrix}}{\Delta^*} + C_{22}$$

$$b_{22}^{13} = b_{13}^{22} = 0$$

$$b_{22}^{23} = b_{23}^{22} = 0$$

$$b_{22}^{12}=\frac{-\left(0.5C_{12}+0.866C_{26}\right)\begin{pmatrix}\left(0.5\,C_{66}+0.866\,C_{26}\right)\left(-0.433C_{12}-0.433C_{66}-0.25C_{16}-0.75C_{26}\right)-\\ \left(0.5C_{16}+0.866C_{66}\right)\left(-0.25C_{66}-0.75C_{22}-0.866C_{26}\right)\end{pmatrix}}{\Delta^{*}}$$
$$\frac{+\left(0.5C_{26}+0.866C_{22}\right)\begin{pmatrix}\left(0.5\,C_{66}+0.866\,C_{26}\right)\left(-0.25C_{11}-0.75C_{66}-0.866C_{16}\right)-\\ \left(0.5C_{16}+0.866C_{66}\right)\left(-0.433C_{12}-0.433C_{66}-0.25C_{16}-0.75C_{26}\right)\end{pmatrix}}{\Delta^{*}}+C_{26}$$

$$b_{33}^{22}=\frac{-\left(0.5C_{13}+0.866C_{36}\right)\begin{pmatrix}\left(0.5C_{26}+0.866\,C_{22}\right)\left(-0.433C_{12}-0.433C_{66}-0.25C_{16}-0.75C_{26}\right)-\\ \left(0.5C_{12}+0.866C_{26}\right)\left(-0.25C_{66}-0.75C_{22}-0.866C_{26}\right)\end{pmatrix}}{\Delta^{*}}$$
$$\frac{+\left(0.5C_{36}+0.866C_{23}\right)\begin{pmatrix}\left(0.5\,C_{26}+0.866\,C_{22}\right)\left(-0.25C_{11}-0.75C_{66}-0.866C_{16}\right)-\\ \left(0.5C_{12}+0.866C_{26}\right)\left(-0.433C_{12}-0.433C_{66}-0.25C_{16}-0.75C_{26}\right)\end{pmatrix}}{\Delta^{*}}+C_{32}$$

$$b_{33}^{33}=\frac{-\left(0.5C_{13}+0.866C_{36}\right)\begin{pmatrix}\left(0.5\,C_{36}+0.866\,C_{23}\right)\left(-0.433C_{12}-0.433C_{66}-0.25C_{16}-0.75C_{26}\right)-\\ \left(0.5C_{13}+0.866C_{36}\right)\left(-0.25C_{66}-0.75C_{22}-0.866C_{26}\right)\end{pmatrix}}{\Delta^{*}}$$
$$\frac{+\left(0.5C_{36}+0.866C_{23}\right)\begin{pmatrix}\left(0.5\,C_{36}+0.866\,C_{23}\right)\left(-0.25C_{11}-0.75C_{66}-0.866C_{16}\right)-\\ \left(0.5C_{13}+0.866C_{36}\right)\left(-0.433C_{12}-0.433C_{66}-0.25C_{16}-0.75C_{26}\right)\end{pmatrix}}{\Delta^{*}}+C_{33} \qquad [5.54c]$$

$$b_{33}^{13}=b_{13}^{33}=0$$

$$b_{33}^{23}=b_{23}^{33}=0$$

$$b_{33}^{12}=\frac{-\left(0.5C_{13}+0.866C_{36}\right)\begin{pmatrix}\left(0.5\,C_{66}+0.866C_{26}\right)\left(-0.433C_{12}-0.433C_{66}-0.25C_{16}-0.75C_{26}\right)-\\ \left(0.5C_{16}+0.866C_{66}\right)\left(-0.25C_{66}-0.75C_{22}-0.866C_{26}\right)\end{pmatrix}}{\Delta^{*}}$$
$$\frac{+\left(0.5C_{36}+0.866C_{23}\right)\begin{pmatrix}\left(0.5\,C_{66}+0.866\,C_{26}\right)\left(-0.25C_{11}-0.75C_{66}-0.866C_{16}\right)-\\ \left(0.5C_{16}+0.866C_{66}\right)\left(-0.433C_{12}-0.433C_{66}-0.25C_{16}-0.75C_{26}\right)\end{pmatrix}}{\Delta^{*}}+C_{36}$$

$$b_{12}^{12}=\frac{-\left(0.5C_{16}+0.866C_{66}\right)\begin{pmatrix}\left(0.5\,C_{66}+0.866\,C_{26}\right)\left(-0.433C_{12}-0.433C_{66}-0.25C_{16}-0.75C_{26}\right)-\\ \left(0.5C_{16}+0.866C_{66}\right)\left(-0.25C_{66}-0.75C_{22}-0.866C_{26}\right)\end{pmatrix}}{\Delta^{*}}$$
$$\frac{+\left(0.5C_{66}+0.866C_{26}\right)\begin{pmatrix}\left(0.5\,C_{66}+0.866\,C_{26}\right)\left(-0.25C_{11}-0.75C_{66}-0.866C_{16}\right)-\\ \left(0.5C_{16}+0.866C_{66}\right)\left(-0.433C_{12}-0.433C_{66}-0.25C_{16}-0.75C_{26}\right)\end{pmatrix}}{\Delta^{*}}+C_{66}$$

$$b_{23}^{23}=\frac{\left(0.5C_{45}+0.866C_{44}\right)}{\left(-0.25C_{55}-0.75C_{44}-0.866C_{45}\right)}\left(0.5C_{45}+0.866C_{44}\right)+C_{44}$$

$$b_{23}^{13} = \frac{(0.5C_{55} + 0.866C_{45})}{(-0.25C_{55} - 0.75C_{44} - 0.866C_{45})}(0.5C_{45} + 0.866C_{44}) + C_{45}$$

$$b_{23}^{12} = b_{12}^{23} = 0$$

$$b_{13}^{23} = \frac{(0.5C_{45} + 0.866C_{44})}{(-0.25C_{55} - 0.75C_{44} - 0.866C_{45})}(0.5C_{55} + 0.866C_{45}) + C_{55} \qquad [5.54d]$$

$$b_{13}^{13} = \frac{(0.5C_{55} + 0.866C_{45})}{(-0.25C_{55} - 0.75C_{44} - 0.866C_{45})}(0.5C_{55} + 0.866C_{45}) + C_{45}$$

$$b_{13}^{12} = b_{12}^{13} = 0$$

where Δ^* is defined by

$$\begin{aligned}\Delta^* = {} & 0.0625C_{11}C_{66} + 0.1875C_{11}C_{22} + 0.2165C_{11}C_{26} + 0.5625C_{66}C_{22} + \\ & 0.6495C_{16}C_{22} + 0.375C_{16}C_{26} - 0.0625C_{16}{}^2 - 0.2165C_{16}C_{12} \\ & -0.5625C_{26}{}^2 - 0.6495C_{12}C_{26} - 0.1875C_{12}{}^2 - 0.375C_{12}C_{66}\end{aligned} \qquad [5.54e]$$

Inspection of Figure 5-8 reveals that the volume of the unit cell is $(4\sqrt{3}/3)\varepsilon a^2 h$ and the volumes of the reinforcements Ω_1, Ω_2, and Ω_3 are $(4\sqrt{3}/3)\varepsilon^2 aF_1 h$, $(4\sqrt{3}/3)\varepsilon^2 aF_2 h$, and $(4\sqrt{3}/3)\varepsilon^2 aF_3 h$ respectively, where εF_1, εF_2 and εF_3 are the corresponding thicknesses. The effective elastic coefficients for this structure are calculated as:

$$\langle C_{ijkl} \rangle = \frac{F_1}{a} b_{ij}^{kl}\Big|_{\Omega_1} + \frac{F_2}{a} b_{ij}^{kl}\Big|_{\Omega_2} + \frac{F_3}{a} b_{ij}^{kl}\Big|_{\Omega_3} \qquad [5.55]$$

The expressions for the elastic coefficients in terms of the engineering constants are too lengthy to be reproduced here (although straight-forward). For illustration purposes, let us consider a material with properties given in Table 5-1 [Daniel, 1994].

Table 5-1: Properties of E-glass/Epoxy [Daniel, 1994]

Coefficient	**E-Glass/epoxy**
E_1 (MPa)	39000
E_2 (MPa)	8600
G_{12}(MPa)	3800
α_{11} ($10^{-6}/^0C$)	7.0
α_{22} ($10^{-6}/^0C$)	21
α_{33} ($10^{-6}/^0C$)	21

The effective elastic coefficients (in GPa) are then calculated to be:

$$\begin{aligned}
&\langle C_{11}\rangle = 22.3\frac{F_1}{a} + 22.3\frac{F_2}{a}; \langle C_{12}\rangle = 7.4\frac{F_1}{a} + 7.4\frac{F_2}{a}; \langle C_{13}\rangle = 1.9\frac{F_1}{a} + 1.9\frac{F_2}{a};\\
&\langle C_{16}\rangle = 12.9\frac{F_1}{a} - 12.9\frac{F_2}{a}; \langle C_{22}\rangle = 2.5\frac{F_1}{a} + 2.5\frac{F_2}{a} + 39.7\frac{F_3}{a};\\
&\langle C_{26}\rangle = 4.3\frac{F_1}{a} - 4.3\frac{F_2}{a}; \langle C_{36}\rangle = 1.1\frac{F_1}{a} - 1.1\frac{F_2}{a}; \langle C_{23}\rangle = 0.6\frac{F_1}{a} + 0.6\frac{F_2}{a} + 2.4\frac{F_3}{a};\\
&\langle C_{33}\rangle = 9.0\frac{F_1}{a} + 9.0\frac{F_2}{a} + 8.8\frac{F_3}{a}; \langle C_{44}\rangle = 1.0\frac{F_1}{a} + 1.0\frac{F_2}{a} + 3.8\frac{F_3}{a};\\
&\langle C_{45}\rangle = 1.6\frac{F_1}{a} - 1.6\frac{F_2}{a}; \langle C_{55}\rangle = 2.8\frac{F_1}{a} + 2.8\frac{F_2}{a}; \langle C_{66}\rangle = 7.4\frac{F_1}{a} + 7.4\frac{F_2}{a};
\end{aligned} \qquad [5.56]$$

5.3.3.1.3. Example 3

Let us now consider a prismatic structure with a rhombic configuration, as shown in Figure 5-9. The prismatic structure is composed of two families of mutually parallel orthotropic reinforcements. The distance between the two neighboring reinforcements of the same family is εa. The effective elastic coefficients for this structure can be easily derived from those of the previous example and will not be repeated here.

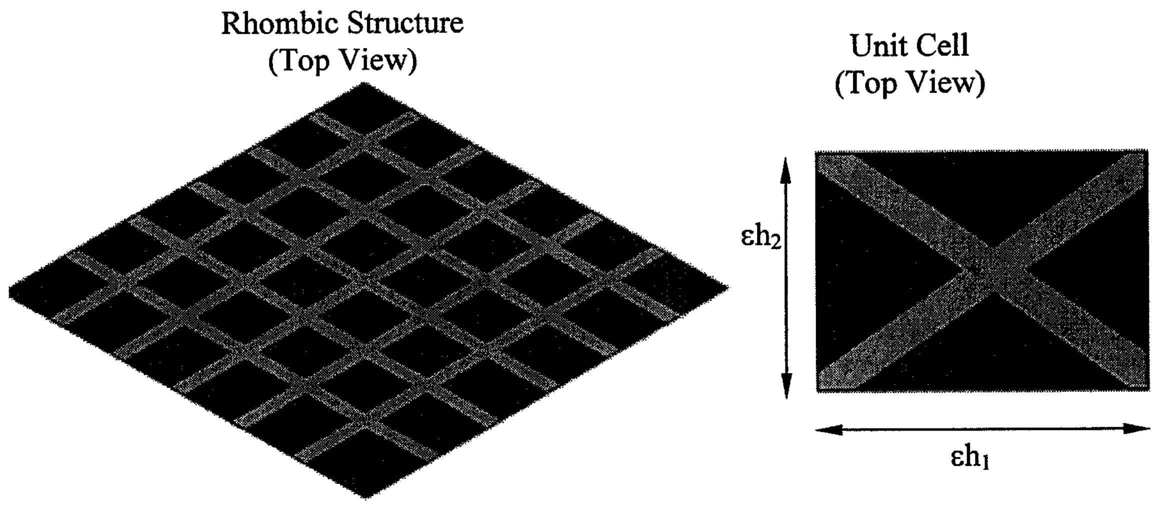

Figure 5-9: Rhombic smart structure with reinforcements at 30° and 150°

5.3.3.2. Plots of Effective Properties and Discussion

The mathematical model and methodology presented in Section 5.3.3 can be used in analysis and design to tailor the effective elastic coefficients of any structure to meet the criteria pertaining to a particular application, by selecting the type, number, orientation and size of the reinforcements. In this section typical elastic properties of the structures in Section 5.3.3.1 will be computed and plotted vs. some geometrical parameters of interest. For the sake of efficiency the structures in Figure 5-6, Figure 5-8 and Figure 5-9 will be referred to as S1, S2 and S3 respectively. We will assume in each case that the reinforcements have the same thickness and are made of the same material with properties given in Table 5-1 [Daniel, 1994]. In the first case we will compare the elastic coefficients for the three smart structures by varying the lengths of the unit cell and keeping the thickness F of the reinforcements fixed. That is, we will take $\varepsilon h_1 = \varepsilon h_2 =$ constant value in S1, S2, and S3. Figure 5-10 and Figure 5-11 show plots of the variation of $\langle C_{11} \rangle$ and $\langle C_{22} \rangle$ vs. εh_1 or εh_2. We note again that the 1, 2, 3 indices in $\langle C_{ij} \rangle$ refer to the y_1, y_2 and y_3 directions respectively, see Figure 5-2.

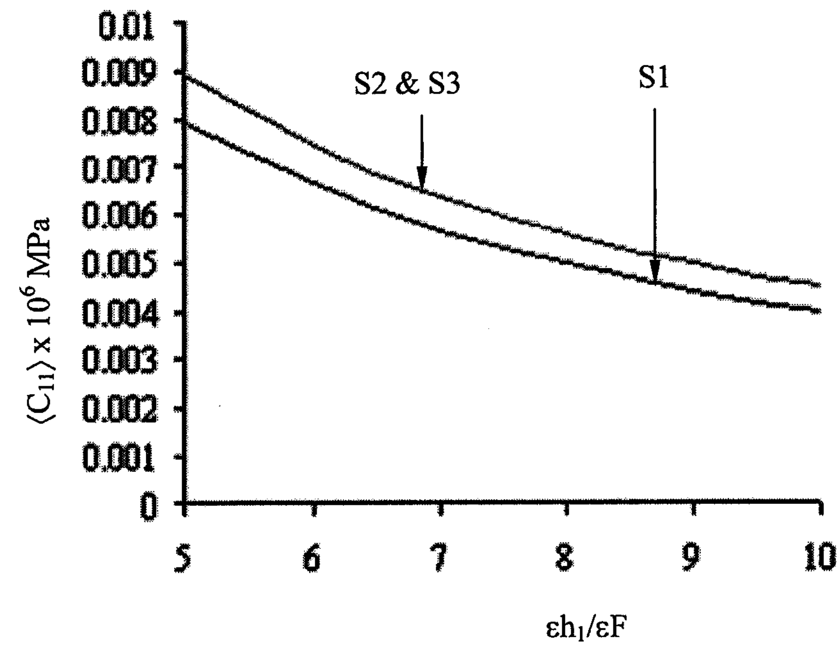

Figure 5-10: Plot of the $\langle C_{11}\rangle$ effective coefficient vs. $\varepsilon h_l/\varepsilon F$ for S1, S2, S3

It can be observed in Figure 5-10 that the stiffness in the y_1 direction is the same for S2 and S3 because of the same number, size and arrangement of reinforcements in that direction. The presence of the extra reinforcements in S2 does not affect the stiffness in the y_1 direction because these reinforcements are oriented entirely in the y_2 direction. Both S2 and S3 are a little stiffer than S1 in the y_1 direction because the former have more reinforcements (even though they are oriented at an angle to y_1) that affect the stiffness in that direction than the latter which only has a single reinforcement which affects the stiffness in the y_1 direction.

Figure 5-11 shows that S2 is significantly stiffer than S3 in the y_2 direction due to the presence of the extra 2 reinforcements in the former. For similar reasons, the $\langle C_{22}\rangle$ value for S1 is larger than that of S3 and smaller than that of S2. Of course, all of these trends and characteristics can easily be modified by changing the thickness, type, etc. of the reinforcements so that the desirable elastic coefficients are obtained.

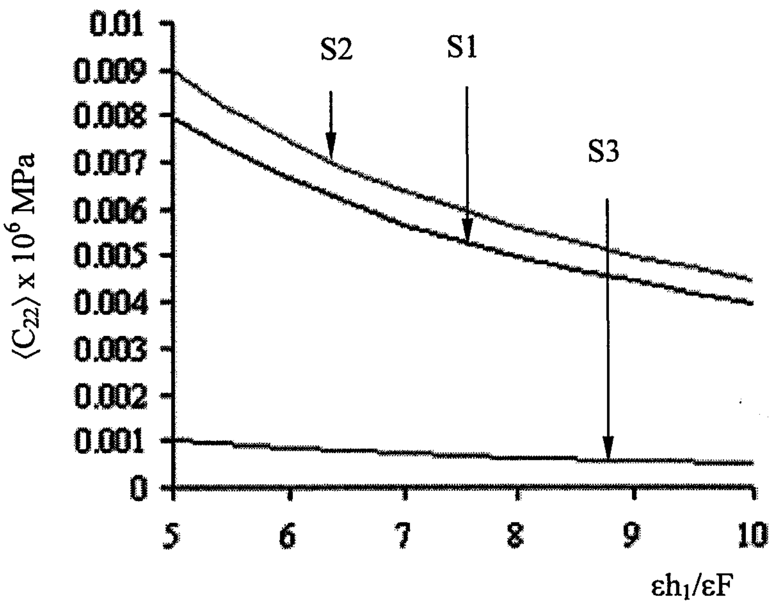

Figure 5-11: Plot of the $\langle C_{22}\rangle$ effective coefficient vs. $\varepsilon h_l/\varepsilon F$ for S1, S2, S3

In the second case we will vary the thickness of the inclusion keeping the length of the unit cell constant and assume that the thickness of the all the inclusions are the same. That is, we will take $\varepsilon F_1 = \varepsilon F_2 = \varepsilon a$ in S1, S3 and $= 0.5\varepsilon a$ in S2. Figure 5-12 and Figure 5-13 show plots of the variation of $\langle C_{11}\rangle$ and $\langle C_{22}\rangle$ vs. εF/εh.

For reasons explained above, we observed in Figure 5-12 that the stiffness in the y_1 direction is the same for S2 and S3 and is a little higher than S1. Figure 5-13 shows that S2 is significantly stiffer than S3 and S1 in the y_2 direction due to the presence of the extra two reinforcements in the former, than in the latter two structures.

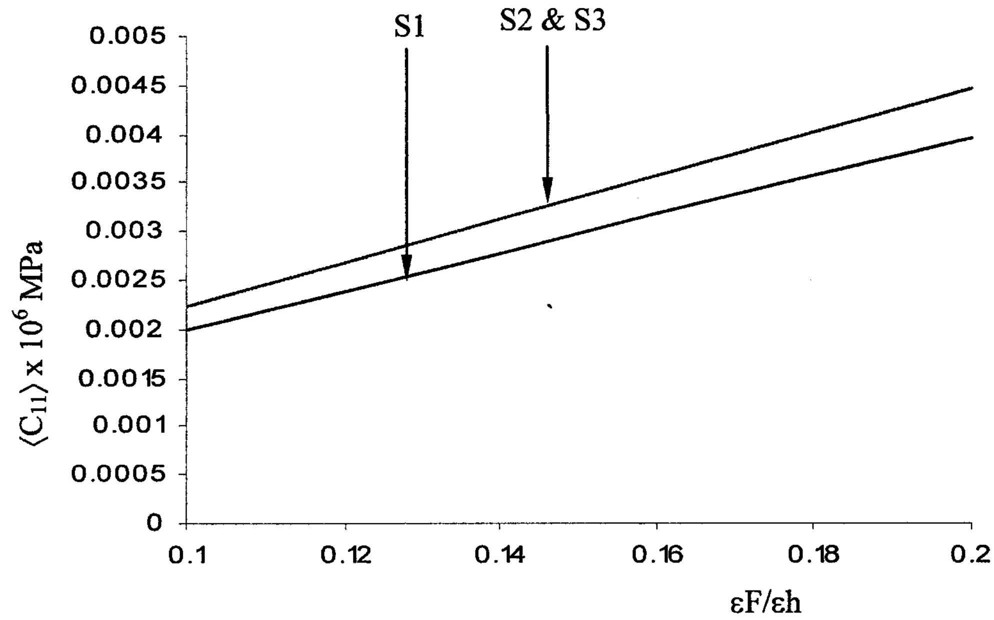

Figure 5-12: Plot of the $\langle C_{11}\rangle$ effective coefficient vs. εF/εh for S1, S2, S3

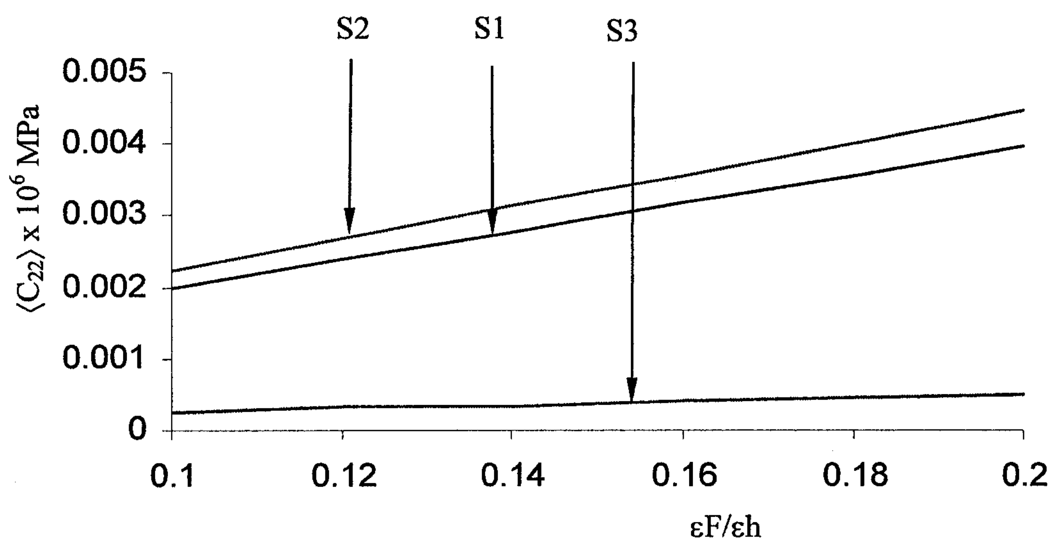

Figure 5-13: Plot of the $\langle C_{22}\rangle$ effective coefficient vs. εF/εh for S1, S2, S3

5.3.4. Effective Piezoelectric Coefficients for Prismatic Smart Structures

We now turn our attention to smart structures reinforced with stiffeners that also exhibit piezoelectric behavior.

Referring to Figure 5-4, we begin by rewriting the pertinent unit cell problem given by second expression in Equation [5.30] in terms of the new coordinates (see Figure 5-3) η_2 and z as,

$$\begin{aligned} &-\sin\varphi \frac{\partial b_{i1}^{k}}{\partial \eta_2} + \cos\varphi \frac{\partial b_{i2}^{k}}{\partial \eta_2} = 0 \\ &\sin\varphi\, b_{i1}^{k} - \cos\varphi\, b_{i2}^{k}\Big|_{s} = 0 \end{aligned} \qquad [5.57]$$

where the piezoelectric coefficients as given by Equations [5.25] and [5.33] are:

$$b_{ij}^{k} = P_{ijk} + \sin\varphi\, C_{ijm1} \frac{\partial N_m^k}{\partial \eta_2} - \cos\varphi\, C_{ijm2} \frac{\partial N_m^k}{\partial \eta_2} \qquad [5.58]$$

We note again that the matrix of the piezoelectric coefficients of an orthotropic material with respect to a coordinate system rotated by an arbitrary angle φ (in the y_1-y_2 plane) from the principle material system has the following form [Reddy, 1997].

$$\begin{bmatrix} 0 & 0 & P_{113} \\ 0 & 0 & P_{223} \\ 0 & 0 & P_{333} \\ P_{231} & P_{232} & 0 \\ P_{311} & P_{312} & 0 \\ 0 & 0 & P_{123} \end{bmatrix} = \begin{bmatrix} 0 & 0 & P_{13} \\ 0 & 0 & P_{23} \\ 0 & 0 & P_{33} \\ P_{41} & P_{42} & 0 \\ P_{51} & P_{52} & 0 \\ 0 & 0 & P_{63} \end{bmatrix} \qquad [5.59]$$

Next, we assume a linear dependency of N_i^k functions on η_2, i.e.

$$N_i^k = \mu_i^k \eta_2 \qquad [5.60]$$

Substituting Equation [5.58] into the three interface conditions in Equation [5.57] gives three linear algebraic equations in the constants μ_i^k, the solution of which is given by:

$$\mu_1^k = \frac{\begin{gathered}\left(s\,P_{21k} - c\,P_{22k}\right)\left(s^2C_{16} + c^2C_{26} - scC_{12} - scC_{66}\right) - \\ \left(sP_{11k} - cP_{21k}\right)\left(s^2C_{66} + c^2C_{22} - 2scC_{26}\right)\end{gathered}}{\left(\begin{gathered}s^4C_{11}C_{66} + s^2c^2C_{11}C_{22} - 2s^3cC_{11}C_{26} + c^4C_{66}C_{22} - 2sc^3C_{16}C_{22} + 2s^2c^2C_{16}C_{26} \\ - s^4C_{16}{}^2 + 2s^3cC_{16}C_{12} - c^4C_{26}{}^2 + 2sc^3C_{12}C_{26} - s^2c^2C_{12}{}^2 - 2s^2c^2C_{12}C_{66}\end{gathered}\right)}$$

$$\mu_2^k = \frac{\begin{gathered}\left(s\,P_{21k} - c\,P_{22k}\right)\left(s^2C_{11} + c^2C_{66} - 2scC_{16}\right) - \\ \left(sP_{11k} - cP_{21k}\right)\left(s^2C_{16} + c^2C_{26} - scC_{12} - scC_{66}\right)\end{gathered}}{\left(\begin{gathered}- s^4C_{11}C_{66} - s^2c^2C_{11}C_{22} + 2s^3cC_{11}C_{26} - c^4C_{66}C_{22} + 2sc^3C_{16}C_{22} - 2s^2c^2C_{16}C_{26} \\ + s^4C_{16}{}^2 - 2s^3cC_{16}C_{12} + c^4C_{26}{}^2 - 2sc^3C_{12}C_{26} + s^2c^2C_{12}{}^2 + 2s^2c^2C_{12}C_{66}\end{gathered}\right)} \qquad [5.61]$$

$$\mu_3^k = -\frac{\left(sP_{31k} - cP_{32k}\right)}{\left(s^2C_{55} + c^2C_{44} - 2scC_{45}\right)}$$

As with the elastic coefficients, for an actuator oriented in a given direction φ, one calculates $\mu_1^k, \mu_2^k, \mu_3^k$. The results are then substituted in Equation [5.58] to calculate b_{ij}^k. This is repeated for each inclusion in the unit cell and finally the effective piezoelectric coefficients for the entire structure are obtained from second expression of Equation [5.21]. Some examples will be considered next.

5.3.4.1. Examples of Structures; Effective Piezoelectric Coefficients

5.3.4.1.1. Example 1

This example pertains to structure S1 in Figure 5-6. Solving for μ_i^k from Equation [5.61] and then substituting the results in Equation [5.58] gives the following expressions for the non-vanishing piezoelectric coefficients for actuator Ω_1:

$$b_{11}^3 = P_{31} - \frac{C_{12}P_{32}}{C_{22}}, \quad b_{31}^1 = P_{15}, \quad b_{31}^2 = P_{25}, \quad b_{33}^3 = P_{33} - \frac{C_{23}P_{32}}{C_{22}} \qquad [5.62]$$

Repeating the procedure for actuator Ω_2 results in:

$$b_{22}^3 = P_{32} - \frac{C_{12}P_{31}}{C_{11}}, \quad b_{33}^3 = P_{33} - \frac{C_{13}P_{31}}{C_{11}}, \quad b_{32}^1 = P_{14}, \quad b_{32}^2 = P_{24} \qquad [5.63]$$

With these results, the effective piezoelectric coefficients are given from Equation [5.21] as:

$$\langle P_{ijk} \rangle = \frac{F_2}{h_2} b_{ij}^k \Big|_{\Omega_1} + \frac{F_1}{h_1} b_{ij}^k \Big|_{\Omega_2} \qquad [5.64]$$

In order to express these coefficients in terms of the piezoelectric constants referred to the principal material coordinate system, (to be identified, as before, with a superscript "p") we need to make use of Equation [5.49a] as well as the tensor transformation law for a 3rd-order tensor,

$$P_{ijk} = a_{im} a_{jn} a_{kp} P^{(p)}_{mnp} \qquad [5.65a]$$

which when written in full has the form:

$$\begin{aligned}
P_{13} &= P^{(p)}_{13} c^2 + P^{(p)}_{23} s^2 \\
P_{23} &= P^{(p)}_{13} s^2 + C^{(p)}_{23} c^2 \\
P_{33} &= P^{(p)}_{33} c \\
P_{41} &= -P^{(p)}_{51} sc + P^{(p)}_{42} cs \\
P_{42} &= P^{(p)}_{51} s^2 + P^{(p)}_{42} c^2 \\
P_{51} &= P^{(p)}_{51} c^2 + P^{(p)}_{42} s^2 \\
P_{52} &= -P^{(p)}_{51} sc + P^{(p)}_{42} cs \\
P_{63} &= -P^{(p)}_{13} sc + P^{(p)}_{23} cs
\end{aligned} \qquad [5.65b]$$

Next, assuming (without loss of generality) that both actuators are made of the same orthotropic material, the non-vanishing effective piezoelectric coefficients for the smart structure of Figure 5-6 are obtained from Equations [5.62]-[5.65a] and are:

$$\langle P_{13}\rangle = \frac{F_2}{h_2}\left(P_{31}^{(p)} - \frac{\left(\upsilon_{21}^{(p)} + \upsilon_{31}^{(p)}\upsilon_{23}^{(p)}\right)E_1^{(p)}}{\left(1-\upsilon_{13}^{(p)}\upsilon_{31}^{(p)}\right)E_2^{(p)}}P_{32}^{(p)}\right);$$

$$\langle P_{23}\rangle = \frac{F_2}{h_2}\left(P_{31}^{(p)} - \frac{\left(\upsilon_{21}^{(p)} + \upsilon_{31}^{(p)}\upsilon_{23}^{(p)}\right)E_1^{(p)}}{\left(1-\upsilon_{13}^{(p)}\upsilon_{31}^{(p)}\right)E_2^{(p)}}P_{32}^{(p)}\right) \qquad [5.66]$$

$$\langle P_{33}\rangle = \frac{F_2}{h_2}\left(P_{33}^{(p)} - \frac{\left(\upsilon_{23}^{(p)} + \upsilon_{21}^{(p)}\upsilon_{13}^{(p)}\right)E_3^{(p)}}{\left(1-\upsilon_{13}^{(p)}\upsilon_{31}^{(p)}\right)E_2^{(p)}}P_{32}^{(p)}\right) + \frac{F_1}{h_1}\left(P_{33}^{(p)} - \frac{\left(\upsilon_{23}^{(p)} + \upsilon_{21}^{(p)}\upsilon_{13}^{(p)}\right)E_3^{(p)}}{\left(1-\upsilon_{13}^{(p)}\upsilon_{31}^{(p)}\right)E_2^{(p)}}P_{32}^{(p)}\right)$$

$$\langle P_{24}\rangle = \frac{F_1}{h_1}P_{15}^{(p)};\ \langle P_{15}\rangle = \frac{F_2}{h_2}P_{15}^{(p)}$$

5.3.4.1.2. Example 2

We will now consider the structure S2 of Figure 5-8. Following the same methodology as for the previous example, the piezoelectric constants in each actuator region are determined as:

(a) Region Ω_1:

The piezoelectric coefficients for the region 1 ($\varphi = 90^o$) are given in Equation [5.63].

(b) Region Ω_2:

The piezoelectric coefficients for the reinforcement/inclusion in the $\varphi = 30^o$ direction is given as:

$$b_{11}^1 = 0$$

$$b_{11}^2 = 0 \qquad [5.67a]$$

$$b_{11}^3 = \frac{(0.5C_{11} - 0.866C_{16})\begin{pmatrix}(0.5P_{36} - 0.866P_{32})(0.25C_{16} + 0.75C_{26} - 0.433C_{12} - 0.433C_{66}) - \\ (0.5P_{13} - 0.866P_{36})(0.25C_{66} + 0.75C_{22} - 0.866C_{26})\end{pmatrix}}{\Delta}$$

$$\frac{-(0.5C_{16} - 0.866C_{12})\begin{pmatrix}(0.5P_{36} - 0.866P_{32})(0.25C_{11} + 0.75C_{66} - 0.866C_{16}) - \\ (0.5P_{13} - 0.866P_{36})(0.25C_{16} + 0.75C_{26} - 0.433C_{12} - 0.433C_{66})\end{pmatrix}}{\Delta} + P_{31}$$

$$b_{22}^1 = b_{22}^2 = 0$$

$$b_{22}^3 = \frac{(0.5C_{12} - 0.866C_{26})\begin{pmatrix}(0.5P_{36} - 0.866P_{32})(0.25C_{16} + 0.75C_{26} - 0.433C_{12} - 0.433C_{66}) - \\ (0.5P_{13} - 0.866P_{36})(0.25C_{66} + 0.75C_{22} - 0.866C_{26})\end{pmatrix}}{\Delta}$$

$$\frac{-(0.5C_{26} - 0.866C_{22})\begin{pmatrix}(0.5P_{36} - 0.866P_{32})(0.25C_{11} + 0.75C_{66} - 0.866C_{16}) - \\ (0.5P_{13} - 0.866P_{36})(0.25C_{16} + 0.75C_{26} - 0.433C_{12} - 0.433C_{66})\end{pmatrix}}{\Delta} + P_{32}$$

$$b_{21}^1 = b_{21}^2 = 0$$

$$b_{21}^3 = \frac{(0.5C_{16} - 0.866C_{66})\begin{pmatrix}(0.5P_{36} - 0.866P_{32})(0.25C_{16} + 0.75C_{26} - 0.433C_{12} - 0.433C_{66}) - \\ (0.5P_{13} - 0.866P_{36})(0.25C_{66} + 0.75C_{22} - 0.866C_{26})\end{pmatrix}}{\Delta}$$

$$\frac{-(0.5C_{66} - 0.866C_{26})\begin{pmatrix}(0.5P_{36} - 0.866P_{32})(0.25C_{11} + 0.75C_{66} - 0.866C_{16}) - \\ (0.5P_{13} - 0.866P_{36})(0.25C_{16} + 0.75C_{26} - 0.433C_{12} - 0.433C_{66})\end{pmatrix}}{\Delta} + P_{36} \qquad [5.67b]$$

$$b_{31}^1 = P_{15} - (0.5C_{55} - 0.866C_{45})\left(\frac{0.5P_{15} - 0.866P_{14}}{0.25C_{55} + 0.75C_{44} - 0.866C_{45}}\right)$$

$$b_{31}^2 = P_{25} - (0.5C_{55} - 0.866C_{45})\left(\frac{0.5P_{25} - 0.866P_{24}}{0.25C_{55} + 0.75C_{44} - 0.866C_{45}}\right)$$

$$b_{31}^3 = 0$$

$$b_{32}^1 = P_{14} - (0.5C_{45} - 0.866C_{44})\left(\frac{0.5P_{15} - 0.866P_{14}}{0.25C_{55} + 0.75C_{44} - 0.866C_{45}}\right)$$

$$b_{32}^2 = P_{24} - (0.5C_{45} - 0.866C_{44})\left(\frac{0.5P_{25} - 0.866P_{24}}{0.25C_{55} + 0.75C_{44} - 0.866C_{45}}\right)$$

$$b_{32}^3 = 0$$

$$b_{33}^1 = b_{33}^2 = 0$$

$$b_{33}^{3}=\frac{\left(0.5C_{13}-0.866C_{36}\right)\begin{pmatrix}\left(0.5\,P_{36}-0.866\,P_{32}\right)\left(0.25C_{16}+0.75C_{26}-0.433C_{12}-0.433C_{66}\right)-\\ \left(0.5P_{13}-0.866P_{36}\right)\left(0.25C_{66}+0.75C_{22}-0.866C_{26}\right)\end{pmatrix}}{\Delta}$$
$$\frac{-\left(0.5C_{36}-0.866C_{23}\right)\begin{pmatrix}\left(0.5\,P_{36}-0.866\,P_{32}\right)\left(0.25C_{11}+0.75C_{66}-0.866C_{16}\right)-\\ \left(0.5P_{13}-0.866P_{36}\right)\left(0.25C_{16}+0.75C_{26}-0.433C_{12}-0.433C_{66}\right)\end{pmatrix}}{\Delta}+P_{33} \qquad [5.67c]$$

Where Δ is given by the Equation [5.52d]

(c) Region Ω_3:

Similarly the piezoelectric coefficients for reinforcements in φ = 150° are given by:

$$b_{11}^{1}=0$$

$$b_{11}^{2}=0$$

$$b_{11}^{3}=\frac{\left(0.5C_{11}+0.866C_{16}\right)\begin{pmatrix}\left(0.5\,P_{36}-0.866\,P_{32}\right)\left(0.25C_{16}+0.75C_{26}-0.433C_{12}-0.433C_{66}\right)-\\ \left(0.5P_{13}-0.866P_{36}\right)\left(0.25C_{66}+0.75C_{22}-0.866C_{26}\right)\end{pmatrix}}{\Delta^{*}}$$
$$\frac{-\left(0.5C_{16}+0.866C_{12}\right)\begin{pmatrix}\left(0.5\,P_{36}-0.866\,P_{32}\right)\left(0.25C_{11}+0.75C_{66}-0.866C_{16}\right)-\\ \left(0.5P_{13}-0.866P_{36}\right)\left(0.25C_{16}+0.75C_{26}-0.433C_{12}-0.433C_{66}\right)\end{pmatrix}}{\Delta^{*}}+P_{31}$$

[5.68a]

$$b_{22}^{1}=b_{22}^{2}=0$$

$$b_{22}^{3}=\frac{\left(0.5C_{12}+0.866C_{26}\right)\begin{pmatrix}\left(0.5\,P_{36}-0.866\,P_{32}\right)\left(0.25C_{16}+0.75C_{26}-0.433C_{12}-0.433C_{66}\right)-\\ \left(0.5P_{13}-0.866P_{36}\right)\left(0.25C_{66}+0.75C_{22}-0.866C_{26}\right)\end{pmatrix}}{\Delta^{*}}$$
$$\frac{-\left(0.5C_{26}+0.866C_{22}\right)\begin{pmatrix}\left(0.5\,P_{36}-0.866\,P_{32}\right)\left(0.25C_{11}+0.75C_{66}-0.866C_{16}\right)-\\ \left(0.5P_{13}-0.866P_{36}\right)\left(0.25C_{16}+0.75C_{26}-0.433C_{12}-0.433C_{66}\right)\end{pmatrix}}{\Delta^{*}}+P_{32}$$

$$b_{21}^{1}=b_{21}^{2}=0$$

$$b_{21}^3 = \frac{(0.5C_{16}+0.866C_{66})\begin{pmatrix}(0.5P_{36}-0.866P_{32})(0.25C_{16}+0.75C_{26}-0.433C_{12}-0.433C_{66})-\\(0.5P_{13}-0.866P_{36})(0.25C_{66}+0.75C_{22}-0.866C_{26})\end{pmatrix}}{\Delta^*}$$

$$\frac{-(0.5C_{66}+0.866C_{26})\begin{pmatrix}(0.5P_{36}-0.866P_{32})(0.25C_{11}+0.75C_{66}-0.866C_{16})-\\(0.5P_{13}-0.866P_{36})(0.25C_{16}+0.75C_{26}-0.433C_{12}-0.433C_{66})\end{pmatrix}}{\Delta^*}+P_{36}$$

$$b_{31}^1 = P_{15}-(0.5C_{55}+0.866C_{45})\left(\frac{0.5P_{15}-0.866P_{14}}{0.25C_{55}+0.75C_{44}-0.866C_{45}}\right)$$

$$b_{31}^2 = P_{25}-(0.5C_{55}+0.866C_{45})\left(\frac{0.5P_{25}-0.866P_{24}}{0.25C_{55}+0.75C_{44}-0.866C_{45}}\right)$$

$$b_{31}^3 = 0 \qquad [5.68b]$$

$$b_{32}^1 = P_{14}-(0.5C_{45}+0.866C_{44})\left(\frac{0.5P_{15}-0.866P_{14}}{0.25C_{55}+0.75C_{44}-0.866C_{45}}\right)$$

$$b_{32}^2 = P_{24}-(0.5C_{45}+0.866C_{44})\left(\frac{0.5P_{25}-0.866P_{24}}{0.25C_{55}+0.75C_{44}-0.866C_{45}}\right)$$

$$b_{32}^3 = 0$$

$$b_{33}^1 = b_{33}^2 = 0$$

$$b_{33}^3 = \frac{(0.5C_{13}+0.866C_{36})\begin{pmatrix}(0.5P_{36}-0.866P_{32})(0.25C_{16}+0.75C_{26}-0.433C_{12}-0.433C_{66})-\\(0.5P_{13}-0.866P_{36})(0.25C_{66}+0.75C_{22}-0.866C_{26})\end{pmatrix}}{\Delta^*}$$

$$\frac{-(0.5C_{36}+0.866C_{23})\begin{pmatrix}(0.5P_{36}-0.866P_{32})(0.25C_{11}+0.75C_{66}-0.866C_{16})-\\(0.5P_{13}-0.866P_{36})(0.25C_{16}+0.75C_{26}-0.433C_{12}-0.433C_{66})\end{pmatrix}}{\Delta^*}+P_{33}$$

where Δ^* is given by Equation [5.54e]. The results are finally superimposed according to the second expression of Equation [5.21] and are:

$$\langle P_{ijk}\rangle = \frac{F_1}{a}b_{ij}^k\Big|_{\Omega_1}+\frac{F_2}{a}b_{ij}^k\Big|_{\Omega_2}+\frac{F_3}{a}b_{ij}^k\Big|_{\Omega_3} \qquad [5.69]$$

Since the general expressions for the effective coefficients in terms of the principal piezoelectric constants are too lengthy to be reproduced here, we will present them numerically for a specific example, namely the material PZT-5A with properties shown in Table 5-2 [Cote et al. 2002]. Assuming that all reinforcements are made of the same orthotropic material, the effective piezoelectric coefficients (in c/mm^2) are calculated to be:

$$\begin{aligned}
&\langle P_{13}\rangle = -1.6\text{x}10^{-6}\left(\frac{F_1}{a}+\frac{F_2}{a}\right); \langle P_{23}\rangle = -5.5\text{x}10^{-7}\left(\frac{F_1}{a}+\frac{F_2}{a}\right) - 2.1\text{x}10^{-6}\frac{F_3}{a} \\
&\langle P_{63}\rangle = -9.4\text{x}10^{-7}\left(\frac{F_1}{a}+\frac{F_2}{a}\right); \langle P_{51}\rangle = -1.8\text{x}10^{-5}\left(\frac{F_1}{a}+\frac{F_2}{a}\right); \\
&\langle P_{52}\rangle = 1.1\text{x}10^{-5}\left(\frac{F_1}{a}-\frac{F_2}{a}\right) \\
&\langle P_{42}\rangle = 6.1\text{x}10^{-6}\left(\frac{F_1}{a}+\frac{F_2}{a}\right) + 2.5\text{x}10^{-5}\frac{F_3}{a} \\
&\langle P_{33}\rangle = 1.8\text{x}10^{-5}\left(\frac{F_1}{a}+\frac{F_2}{a}\right) + 1.9\text{x}10^{-5}\frac{F_3}{a}
\end{aligned} \qquad [5.70]$$

5.3.4.1.3. Example 3

The effective piezoelectric coefficients of the smart structure S3 of Figure 5-9 can be derived from those of S2 and will not be given here. However, some of these coefficients will be presented graphically in the next section when a comparison between all three structures is made.

5.3.4.2. Plots of Effective Properties and Discussion

The mathematical models derived in Sections 5.3.3 and 5.3.4 can be used in the design of a smart structure with a desirable combination of elastic and piezoelectric properties by carefully selecting the type, orientation, and geometric characteristics of the actuators/reinforcements. In Section 5.3.3.2, some of the effective elastic coefficients pertaining to structures S1-S3 were plotted and compared. In this section we will repeat this for the case of the piezoelectric coefficients.

Table 5-2: Piezoelastic properties of PZT-5A [Cote et al. 2002]

Coefficient	**Value**
$C_{11}^{(p)} = C_{22}^{(p)}$ (MPa)	119899.13
$C_{33}^{(p)}$ (MPa)	109892.37
$C_{12}^{(p)}$ (MPa)	74732.01
$C_{23}^{(p)}$ (MPa)	74429.92
$C_{13}^{(p)}$ (MPa)	74429.92
$C_{44}^{(p)}$ (MPa)	21052.63
$C_{55}^{(p)}$ (MPa)	21052.63
$C_{66}^{(p)}$ (MPa)	22573.36
$P_{13}^{(p)}$ (C/mm^2)	-5.45E-6
$P_{23}^{(p)}$ (C/mm^2)	-5.45E-6
$P_{33}^{(p)}$ (C/mm^2)	1.56E-5
$P_{42}^{(p)}$ (C/mm^2)	2.46E-5
$P_{51}^{(p)}$ (C/mm^2)	2.46E-5

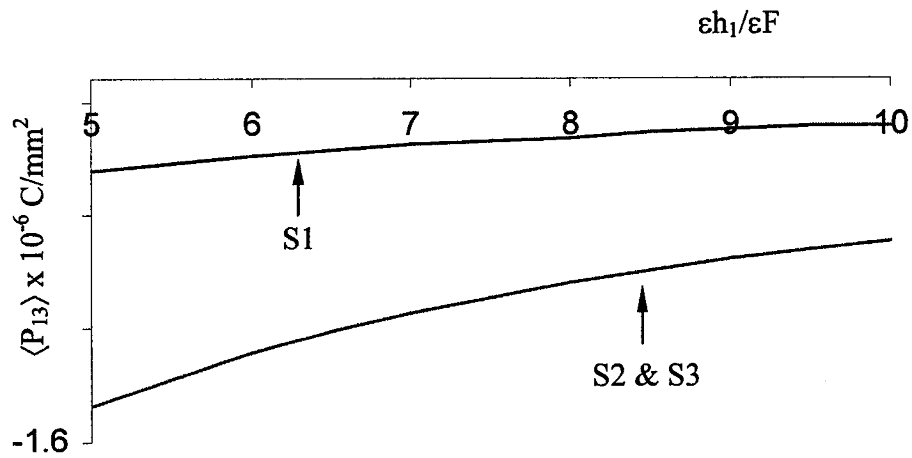

Figure 5-14: Plot of the $\langle P_{13} \rangle$ effective coefficient vs. $\varepsilon h_1/\varepsilon F$ for S1, S2, S3

Without loss of generality we will assume that the actuators have the same thickness and are made of the same material with properties given in Table 5-2 [Cote et al. 2002]. As in Section 5.3.3.2, we will vary the lengths of the unit cell for all the three structures and keep the thickness F of the reinforcements fixed. That is, we will take $\varepsilon h_1 = \varepsilon h_2 =$ constant value in S1, S2, and S3. Figure 5-14, and Figure 5-15, show plots of the variation of $\langle P13 \rangle$, and $\langle P51 \rangle$ vs. εh_1 or εh_2. Figure 5-14 shows the variation of $\langle P_{13} \rangle$ vs. h_1. It is observed that this coefficient has the same magnitude for S2 and S3 because of the same number, size and arrangement of the actuators in the y_1 direction. As expected, the presence of the extra actuators in S2 does not the affect the value of $\langle P_{13} \rangle$ because these actuators are oriented in the y_2 direction and do not contribute to the y_1 direction. The magnitude of $\langle P_{13} \rangle$ is larger for S2 and S3 than S1 because the former have more actuators that affect the strain/stress in the y_1 direction (even though they are oriented at an angle to y_1) than the latter which only has a single actuator in the y_1 direction. Similar considerations apply for the $\langle P_{51} \rangle$ coefficient shown in Figure 5-15.

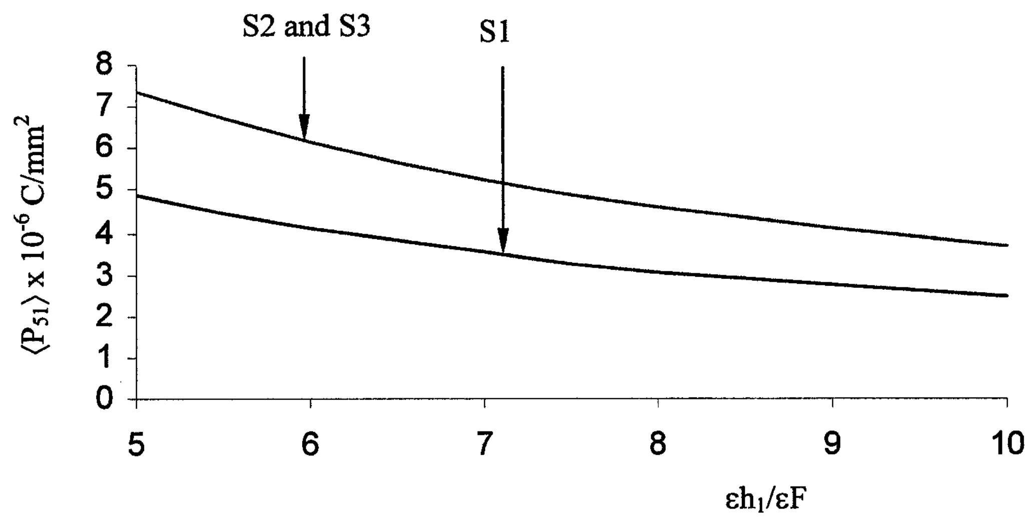

Figure 5-15: Plot of the $\langle P_{51} \rangle$ effective coefficient vs. $\varepsilon h_l/\varepsilon F$ for S1, S2, S3

As a further illustration, we will allow the thickness F of the actuators to vary but keep the length of the unit cell fixed. This means that $\varepsilon h_1 = \varepsilon h_2 = \varepsilon\alpha$ in S1 and S3 $= 2\varepsilon\alpha$ in S2 = constant. Figure 5-16 shows the variation of $\langle P_{13} \rangle$ vs. $\varepsilon F/\varepsilon h$. Similar to the above case, we observe that the magnitude of the coefficients for S2 and S3 is larger than for S1. Finally Figure 5-17 shows the variation of $\langle P_{51} \rangle$ vs. $\varepsilon F/\varepsilon h$.

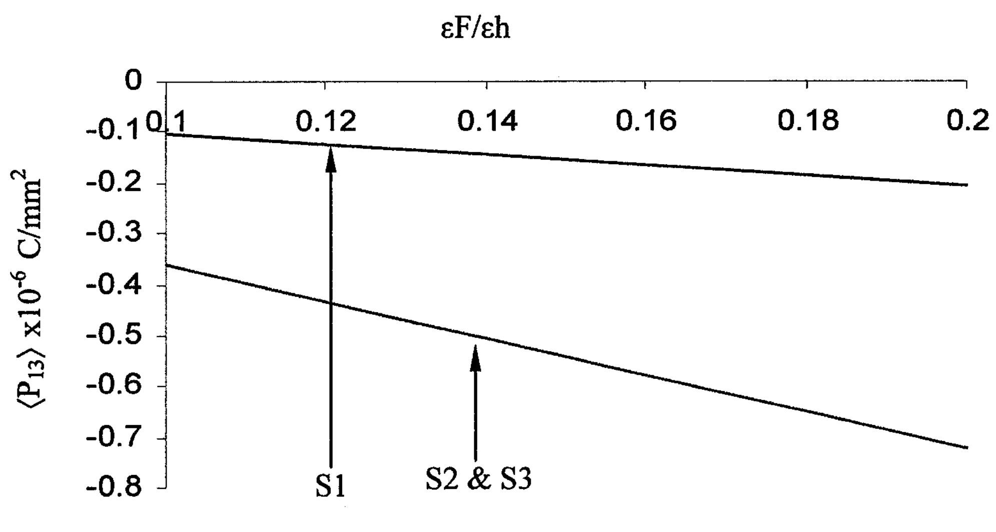

Figure 5-16: Plot of effective elastic coefficients vs $\varepsilon F/\varepsilon h$ for Structures S1, S2 and S3

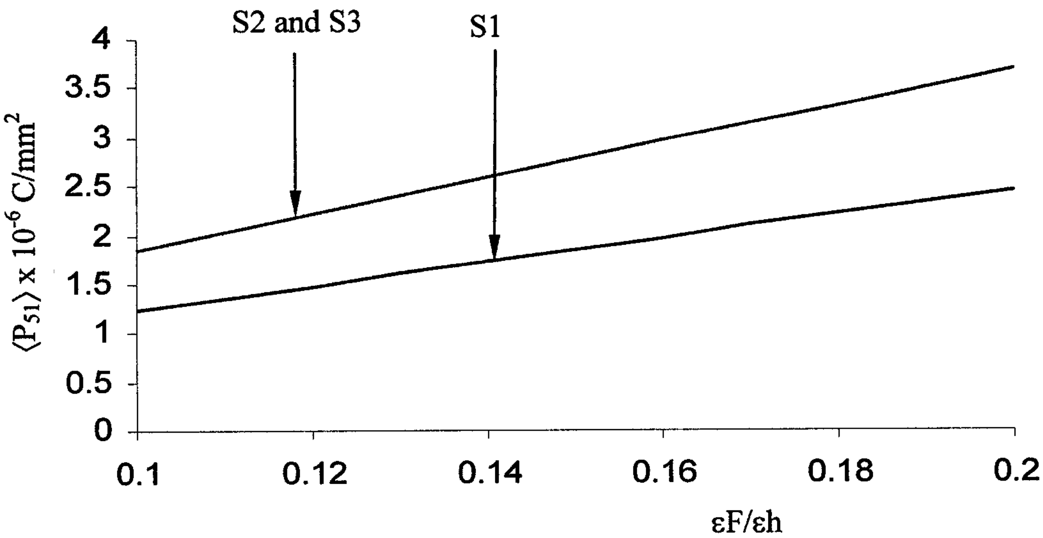

Figure 5-17: Plot of effective elastic coefficients vs εF/εh for Structures S1, S2 and S3

5.3.5. Effective Thermal Expansion Coefficients for Prismatic Smart Structures

We will finally consider the thermal expansion coefficients. Referring to Figure 5-4, we begin by rewriting the appropriate unit cell problem given Equation [5.30] in terms of the new coordinates η_2 and z as,

$$
\begin{aligned}
&-\sin\varphi\frac{\partial b_{i1}}{\partial\eta_2}+\cos\varphi\frac{\partial b_{i2}}{\partial\eta_2}=0 \\
&\sin\varphi\ b_{i1}-\cos\varphi\ b_{i2}\big|_s=0
\end{aligned}
\qquad [5.71]
$$

where the thermal expansion coefficients as given by third expression of Equation [5.25] are:

$$b_{ij} = K_{ij} + \sin\varphi\, C_{ijm1} \frac{\partial N_m}{\partial \eta_2} - \cos\varphi\, C_{ijm2} \frac{\partial N_m}{\partial \eta_2} \tag{5.72}$$

We note that the matrix of the thermal expansion coefficients of an orthotropic material with respect to a coordinate system rotated by an arbitrary angle φ in the y_1-y_2 plane from the principle material system has the following form [Reddy, 1997].

$$\begin{bmatrix} K_{11} & K_{12} & 0 \\ K_{12} & K_{22} & 0 \\ 0 & 0 & K_{33} \end{bmatrix} = \begin{bmatrix} K_{11} \\ K_{22} \\ K_{33} \\ 0 \\ 0 \\ K_{12} \end{bmatrix} = \begin{bmatrix} K_{1} \\ K_{2} \\ K_{3} \\ 0 \\ 0 \\ K_{6} \end{bmatrix} \tag{5.73}$$

Next, we assume a linear dependency of N_i function on η_2, i.e.

$$N_i = \xi_i \eta_2 \tag{5.74}$$

Substituting Equations [5.72] and [5.74] into the interface conditions in Equation [5.71] gives three linear algebraic equations in the constants ξ_i, the solution of which is given by the following equations:

$$\xi_1 = \frac{\begin{matrix}(sK_6 - cK_2)(s^2C_{16} + c^2C_{26} - scC_{12} - scC_{66}) - \\ (sK_1 - cK_6)(s^2C_{66} + c^2C_{22} - 2scC_{26})\end{matrix}}{\begin{pmatrix}s^4C_{11}C_{66} + s^2c^2C_{11}C_{22} - 2s^3cC_{11}C_{26} + c^4C_{66}C_{22} - 2sc^3C_{16}C_{22} + 2s^2c^2C_{16}C_{26} \\ - s^4C_{16}{}^2 + 2s^3cC_{16}C_{12} - c^4C_{26}{}^2 + 2sc^3C_{12}C_{26} - s^2c^2C_{12}{}^2 - 2s^2c^2C_{12}C_{66}\end{pmatrix}}$$

$$\xi_2 = \frac{\begin{matrix}(sK_6 - cK_2)(s^2C_{11} + c^2C_{66} - 2scC_{16}) - \\ (sK_1 - cK_6)(s^2C_{16} + c^2C_{26} - scC_{12} - scC_{66})\end{matrix}}{\begin{pmatrix}- s^4C_{11}C_{66} - s^2c^2C_{11}C_{22} + 2s^3cC_{11}C_{26} - c^4C_{66}C_{22} + 2sc^3C_{16}C_{22} - 2s^2c^2C_{16}C_{26} \\ + s^4C_{16}{}^2 - 2s^3cC_{16}C_{12} + c^4C_{26}{}^2 - 2sc^3C_{12}C_{26} + s^2c^2C_{12}{}^2 + 2s^2c^2C_{12}C_{66}\end{pmatrix}} \quad [5.75]$$

$$\xi_3 = -\frac{(sK_5 - cK_4)}{(s^2C_{55} + c^2C_{44} - 2scC_{45})}$$

As with the elastic and piezoelectric coefficients, for a reinforcement/actuator oriented in a given direction φ, one calculates ξ_1, ξ_2, ξ_3. The results are then substituted in Equation [5.72] to calculate b_{ij}. This is repeated for each inclusion in the unit cell and finally the effective thermal expansion coefficients for the entire structure are obtained from third expression of Equation [5.21]. Some examples will be considered next.

5.3.5.1. Examples of Structures; Effective Thermal Expansion Coefficients

5.3.5.1.1. Example 1

We will again consider structure S1 in Figure 5-6. Solving for ξ_i from Equation [5.75] and then substituting the results in Equation [5.72] gives the following expressions for the non-vanishing thermal expansion coefficients for reinforcement Ω_1

$$b_{11} = K_1 - \frac{C_{12}K_2}{C_{22}}; \; b_{33} = K_{33} - \frac{C_{23}K_2}{C_{22}} \quad [5.76]$$

Repeating the procedure for reinforcement Ω_2 results in the following:

$$b_{22} = K_2 - \frac{C_{12}K_1}{C_{11}};\ b_{33} = K_{33} - \frac{C_{13}K_1}{C_{11}} \tag{5.77}$$

With these results, the effective thermal expansion coefficients as given from Equation [5.21] are:

$$\langle K_{ij} \rangle = \frac{F_2}{h_2} b_{ij}\Big|_{\Omega_1} + \frac{F_1}{h_1} b_{ij}\Big|_{\Omega_2} \tag{5.78}$$

We will now express these coefficients in terms of the thermal expansion constants referred to the principal material coordinate system using the familiar tensor transformation law:

$$K_{ij} = a_{im} a_{jn} K^{(p)}_{mn} \tag{5.79}$$

Assuming that both reinforcements are made of the same orthotropic material, the non-vanishing effective thermal expansion coefficients for S1 are:

$$\begin{aligned}
\langle K_1 \rangle &= \frac{F_2}{h_2}\left(K_1^{(P)} - \frac{\left(\upsilon_{21}^{(p)} + \upsilon_{31}^{(p)}\upsilon_{23}^{(p)}\right)E_1^{(p)}}{\left(1 - \upsilon_{13}^{(p)}\upsilon_{31}^{(p)}\right)E_2^{(p)}} K_2^{(P)} \right), \\
\langle K_2 \rangle &= \frac{F_1}{h_1}\left(K_1^{(P)} - \frac{\left(\upsilon_{21}^{(p)} + \upsilon_{31}^{(p)}\upsilon_{23}^{(p)}\right)E_1^{(p)}}{\left(1 - \upsilon_{13}^{(p)}\upsilon_{31}^{(p)}\right)E_2^{(p)}} K_2^{(P)} \right) \\
\langle K_3 \rangle &= \frac{F_1}{h_1}\left(K_3^{(p)} - \frac{\left(\upsilon_{23}^{(p)} + \upsilon_{21}^{(p)}\upsilon_{13}^{(p)}\right)E_3^{(p)}}{\left(1 - \upsilon_{13}^{(p)}\upsilon_{31}^{(p)}\right)E_2^{(p)}} K_2^{(p)} \right)
\end{aligned} \tag{5.80}$$

5.3.5.1.2. Example 2

Let us now consider structure S2 of Figure 5-8. Following the same methodology as before, the effective thermal expansion coefficients in each reinforcement region are determined and the results are finally superimposed according to third expression of Equation [5.21]:

$$\langle P_{ijk} \rangle = \frac{F_1}{a} b_{ij}\Big|_{\Omega_1} + \frac{F_2}{a} b_{ij}\Big|_{\Omega_2} + \frac{F_3}{a} b_{ij}\Big|_{\Omega_3} \qquad [5.81]$$

As for the case of the elastic and piezoelectric coefficients, the expressions for the effective thermal expansion coefficients in terms of the material (principal) constants are too lengthy to be conveniently shown here, and as such, we will evaluate them numerically for a specific material. Thus, assuming all reinforcements are made of E-glass/Epoxy with properties given in Table 5-1 [Daniel, 1994] the effective thermal expansion coefficients (in MPa/^{o}C) are calculated to be:

$$\begin{aligned} &\langle K_1 \rangle = 0.14\frac{F_1}{a} + 0.14\frac{F_2}{a}; \langle K_2 \rangle = 0.23\frac{F_1}{a} + 0.23\frac{F_2}{a} + 0.33\frac{F_3}{a} \\ &\langle K_6 \rangle = 0.08\frac{F_1}{a} - 0.08\frac{F_2}{a}; \langle K_3 \rangle = 0.19\frac{F_1}{a} + 0.19\frac{F_2}{a} + 0.20\frac{F_3}{a} \end{aligned} \qquad [5.82]$$

5.3.5.1.3. Example 3

The effective thermal expansion coefficients of the structure S3 of Figure 5-9 can easily be derived from those of S2. Some of these coefficients will be presented graphically in the next section when a comparison between all three structures is made.

5.3.5.2. Plots of Effective Properties and Discussion

As was done previously for the case of elastic and piezoelectric coefficients, we will now compare typical effective thermal expansion coefficients for structures S1, S2 and S3. We will assume that the reinforcements have the same thickness and are made of the same material with properties given in Table 5-1 [Daniel, 1994].

Similar to the above examples, in the first case we will vary the length of the unit cell keeping thickness constant. Figure 5-18 and Figure 5-19 plot the variation of $\langle K_1 \rangle$ and $\langle K_2 \rangle$ vs. $\varepsilon h_1/\varepsilon F$ respectively. The trends in these plots should be clear on account of the discussion in sections 5.3.3.2 and 5.4.3.2. Similarly, considerations apply to Figure 5-20 and Figure 5-21 which plot, respectively, $\langle K_1 \rangle$ and $\langle K_2 \rangle$ vs. $\varepsilon F/\varepsilon h_1$ respectively.

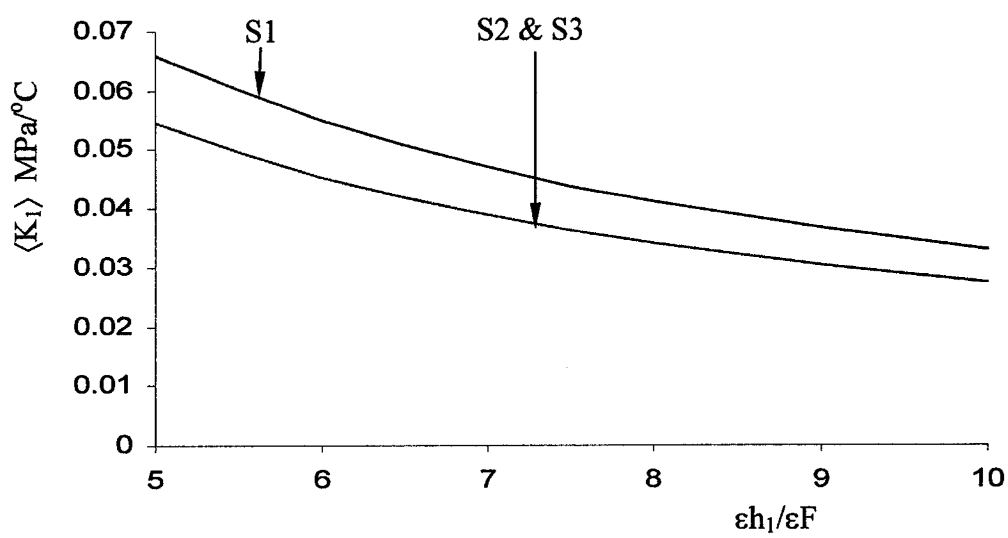

Figure 5-18: Plot of $\langle K_1 \rangle$ effective coefficients vs $\varepsilon h_1/\varepsilon F$ for Structures S1, S2 and S3

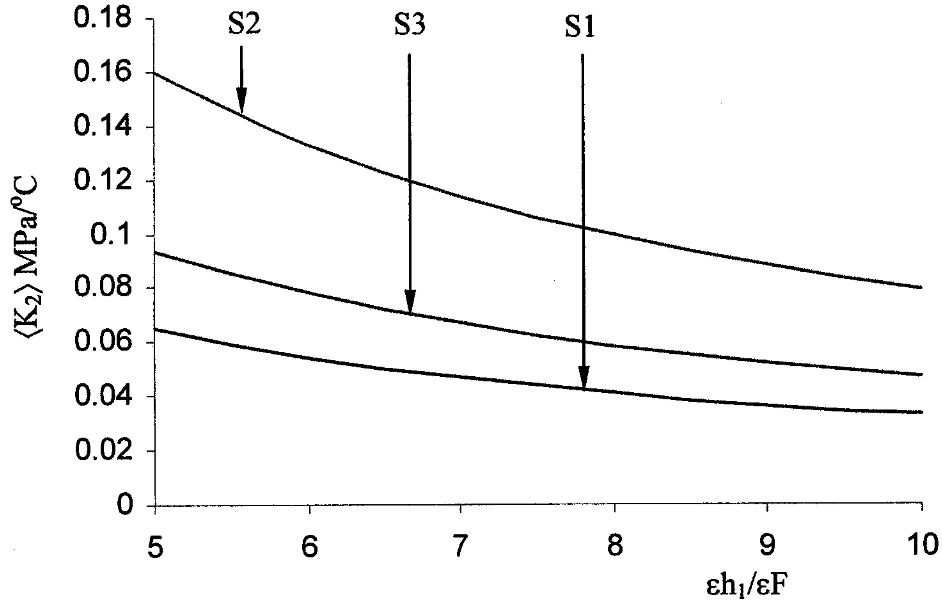

Figure 5-19: Plot of the $\langle K_2 \rangle$ effective coefficient vs. $\varepsilon h_l/\varepsilon F$ for S1, S2, S3

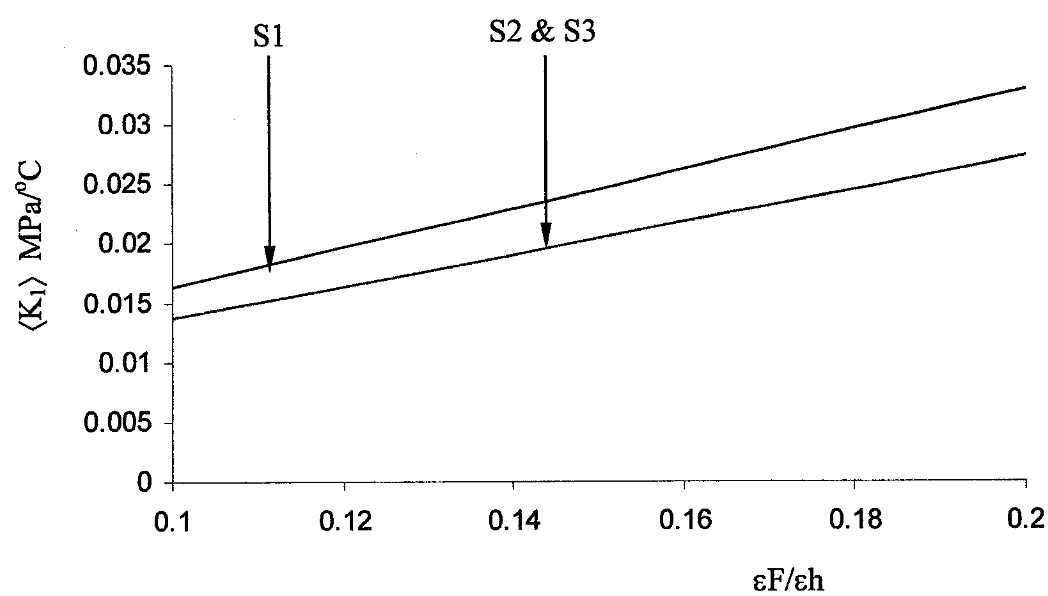

Figure 5-20: Plot of $\langle K_1 \rangle$ effective coefficients vs $\varepsilon F/\varepsilon h$ for Structures S1, S2 and S3

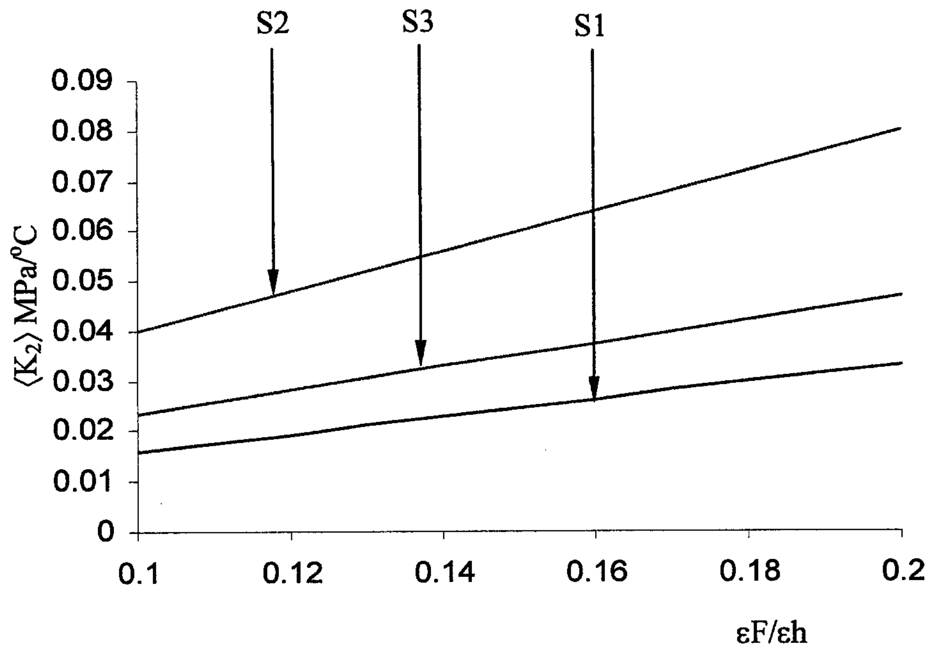

Figure 5-21: Plot of the $\langle K_2 \rangle$ effective coefficient vs. $\varepsilon F/\varepsilon h$ for S1, S2, S3

5.4. Conclusions

The method of asymptotic homogenization was used to analyze a prismatic smart composite structure with orthotropic constituents, through the development of a suitable micromechanical model.

The derived model was applied to three different structures of practical interest (with rectangular, hexagonal, and rhombic configurations) consisting of orthotropic reinforcements and/or actuators. The effective elastic, piezoelectric and thermal expansion coefficients for these structures were determined and then compared graphically for the three structures. The usefulness of the presented methodology lies in the fact that the derived model can be used in design and analysis to tailor the effective coefficients of any structure to meet the engineering criteria pertaining to a particular application, by selecting the type, number, orientation, and size of the reinforcements.

6. ASYMPTOTIC HOMOGENIZATION MODEL FOR THREE-DIMENSIONAL NETWORK REINFORCED COMPOSITE STRUCTURES

6.1. Introduction

The present chapter develops a novel asymptotic homogenization model for three-dimensional network reinforced composite structures (Figure 6-1). In this model, the composite structure is made of periodically arranged families of isotropic reinforcements and, if desired, each family may have different mechanical properties.

The rest of the chapter is organized as follows: The basic problem formulation and model development is presented in Section 6.2. Section 6.3 derives the general model for three-dimensional network reinforced composite structures and uses it to analyze and discuss various examples. Finally section 6.4 gives a brief conclusion.

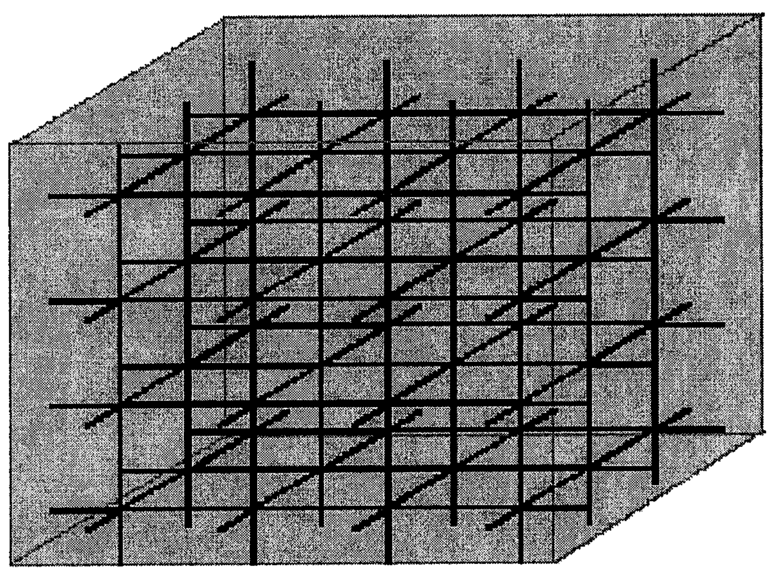

Figure 6-1: Three-Dimensional Network Reinforced Composite Structure

6.2. Homogenization Model for Three-Dimensional Structures

6.2.1. General Model

The micromechanical model for a three-dimensional network reinforced composite structure will be developed from the general model (modified slightly since no actuation or thermal expansion effects will be considered here) presented in the previous chapter. For the sake of convenience the main results of that model will be repeated here since they provide the motivation for the development of the new model of interest.

Consider a general composite structure representing an inhomogeneous solid occupying domain G with boundary ∂G that contains a large number of periodically arranged reinforcements as shown in Figure 6-2.

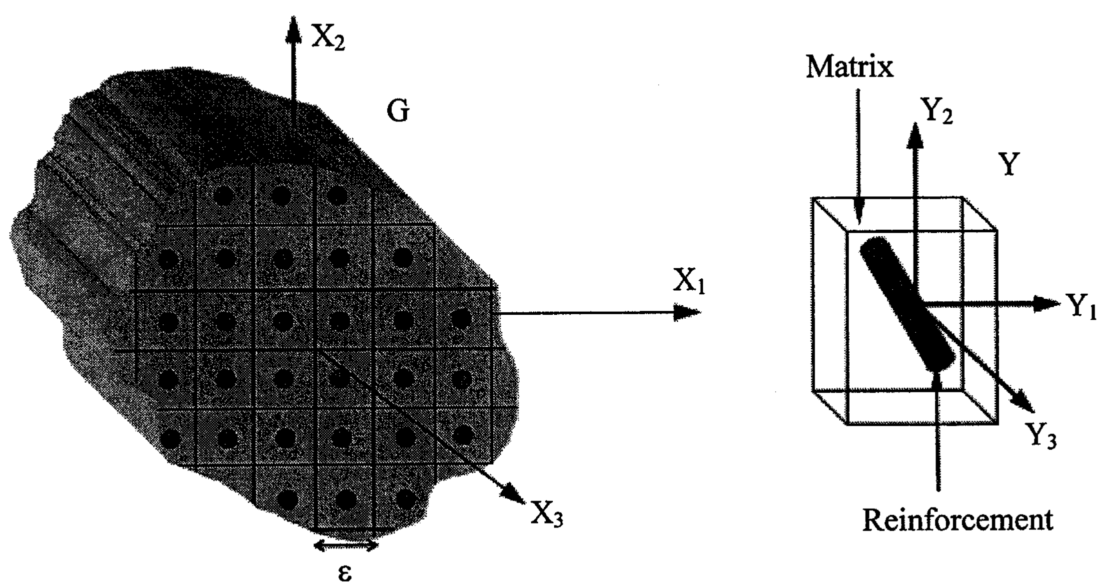

Figure 6-2: Three-Dimensional composite structure with its periodicity (unit) cell

The elastic deformation of this structure can be described by means of the following set of equations:

$$\frac{\partial \sigma_{ij}^{\varepsilon}}{\partial x_j} = f_i \text{ in } G$$
$$u^{\varepsilon}(x) = 0 \quad \text{on } \partial G \tag{6.1}$$

where,

$$\sigma_{ij}^{\varepsilon}\left(\mathbf{x}, \frac{\mathbf{x}}{\varepsilon}\right) = C_{ijkl}\left(\frac{\mathbf{x}}{\varepsilon}\right) e_{kl}^{\varepsilon}\left(\mathbf{x}, \frac{\mathbf{x}}{\varepsilon}\right) \tag{6.2}$$

$$e_{ij}^{\varepsilon}\left(\mathbf{x}, \frac{\mathbf{x}}{\varepsilon}\right) = \frac{1}{2}\left[\frac{\partial u_i}{\partial x_j}\left(\mathbf{x}, \frac{\mathbf{x}}{\varepsilon}\right) + \frac{\partial u_j}{\partial x_i}\left(\mathbf{x}, \frac{\mathbf{x}}{\varepsilon}\right)\right] \tag{6.3}$$

The various field variables in Equations [6.1]-[6.3] have been defined in sections 4.3.1. and 5.2.1. The periodic composite structure in Figure 6-2 is seen to be made up of a large number of "unit cell" periodically arranged with the domain G.

6.2.2. Asymptotic expansion, Governing equation, and unit cell problem

In view of the introduction of "fast" variable **y** according to,

$$y_i = \frac{x_i}{\varepsilon} \tag{6.4}$$

the boundary value problem in Equation [6.1] transforms to:

$$\frac{\partial \sigma_{ij}^{\varepsilon}}{\partial x_j} + \frac{1}{\varepsilon}\frac{\partial \sigma_{ij}^{\varepsilon}}{\partial y_j} = f_i \quad \text{in } G$$

$$u^{\varepsilon} = 0 \quad \text{on } \partial G \tag{6.5}$$

The displacement and stress fields are subsequently expressed as infinite power series in terms of the small parameter ε,

$$\mathbf{u}^{\varepsilon}(\mathbf{x},\mathbf{y}) = \mathbf{u}^{(0)}(\mathbf{x}) + \varepsilon \mathbf{u}^{(1)}(\mathbf{x},\mathbf{y}) + \varepsilon^2 \mathbf{u}^{(2)}(\mathbf{x},\mathbf{y}) + \ldots \tag{6.6}$$

$$\sigma_{ij}^{\varepsilon}(\mathbf{x},\mathbf{y}) = \sigma_{ij}^{(0)}(\mathbf{x},\mathbf{y}) + \varepsilon \sigma_{ij}^{(1)}(\mathbf{x},\mathbf{y}) + \varepsilon^2 \sigma_{ij}^{(2)}(\mathbf{x},\mathbf{y}) + \ldots \tag{6.7}$$

where,

$$\frac{\partial \sigma_{ij}^{(0)}}{\partial y_j} = 0$$

$$\frac{\partial \sigma_{ij}^{(1)}}{\partial y_j} + \frac{\partial \sigma_{ij}^{(0)}}{\partial x_j} = f_i \tag{6.8}$$

and

$$\sigma_{ij}^{(0)} = C_{ijkl}\left(\frac{\partial u_k^{(0)}}{\partial x_l} + \frac{\partial u_k^{(1)}}{\partial y_l}\right)$$

$$\sigma_{ij}^{(1)} = C_{ijkl}\left(\frac{\partial u_k^{(1)}}{\partial x_l} + \frac{\partial u_k^{(2)}}{\partial y_l}\right) \tag{6.9}$$

while,

$$u_n^{(1)}(\mathbf{x},\mathbf{y}) = V_n(\mathbf{x}) + \frac{\partial u_k^{(0)}(\mathbf{x})}{\partial x_l} N_n^{kl}(\mathbf{y}) \tag{6.10}$$

Functions N_m^{kl} In Equation [6.10] are periodic in y and they satisfy the following equation:

$$\frac{\partial}{\partial y_j}\left(C_{ijmn}(\mathbf{y})\frac{\partial N_m^{kl}(\mathbf{y})}{\partial y_n}\right)=-\frac{\partial C_{ijkl}}{\partial y_j} \qquad [6.11]$$

It is seen that Equation [6.11] depends entirely on the fast variable **y** and is thus solved on the domain Y of the unit cell remembering at the same time the periodicity of C_{ijkl}, N_m^{kl} in y_i. Consequently, Equation [6.11] is appropriately referred to as the "unit-cell" problem.

Finally, from Equations [6.8]-[6.11] and after averaging over the domain Y of the unit cell with volume $|Y|$ (homogenization process) we arrive at:

$$\tilde{C}_{ijkl}\frac{\partial^2 u_k^{(0)}(\mathbf{x})}{\partial x_j \partial x_l}=f_i \qquad [6.12]$$

where

$$\tilde{C}_{ijkl}=\frac{1}{|Y|}\int_Y\left(C_{ijkl}(\mathbf{y})+C_{ijmn}(\mathbf{y})\frac{\partial N_m^{kl}}{\partial y_n}\right)dv \qquad [6.13]$$

The coefficients $\tilde{C}_{ijkl}$ are of-course the effective elastic coefficients. We reiterate that the effective elastic coefficients are free from the periodicity complications that characterize their actual material counterparts, C_{ijkl}, and as such, are more amenable to analytical and numerical treatment.

6.3. Three-Dimensional Network Reinforced Composite Structures

For the problem at hand, we turn our attention to a general macroscopically anisotropic three-dimensional composite structure reinforced with N families of reinforcements or bars, see for example Figure 6-1, where a particular case of 3 families of reinforcements is shown. The members of each family are made of generally different isotropic materials and are oriented at angles $\varphi_1^n, \varphi_2^n, \varphi_3^n$ (where n = 1, 2, …., N) with the y_1, y_2, y_3 axes respectively. Furthermore, they are assumed to be much stiffer than the surrounding matrix so that we are justified in neglecting the contribution of the latter in the ensuing analysis. For the particular case of framework or lattice network structures the surrounding matrix is absent and this is modeled by assuming zero matrix rigidity. The nature of the network structure of Figure 6-1 is such that it would be more efficient if we first considered a simpler type of unit cell made of only a single reinforcement as shown in Figure 6-3. Having solved this, the effective elastic coefficients of more general structures with several families of reinforcements can readily be determined by superposition of solution for each family found separately. In doing so, we accept of course the error incurred at the regions of intersection between the reinforcements, but this error is localized and will not add significantly to the integral over the unit cell. In order to calculate the effective coefficients for the simpler structure of Figure 6-3, one must first solve the unit cell problem Equation [6.11] and then apply the formula in Equation [6.13].

6.3.1. Problem Formulation

We begin the problem formulation for the structure of Figure 6-3 by introducing the following notation:

$$b_{ij}^{kl} = C_{ijkl}(y)\frac{\partial N_m^{kl}(y)}{\partial y_n} + C_{ijkl} \qquad [6.14]$$

With this definition in mind, the unit cell problem of Equation [6.11] becomes:

$$\frac{\partial}{\partial y_j}\left\{b_{ij}^{kl}\right\} = 0 \qquad [6.15]$$

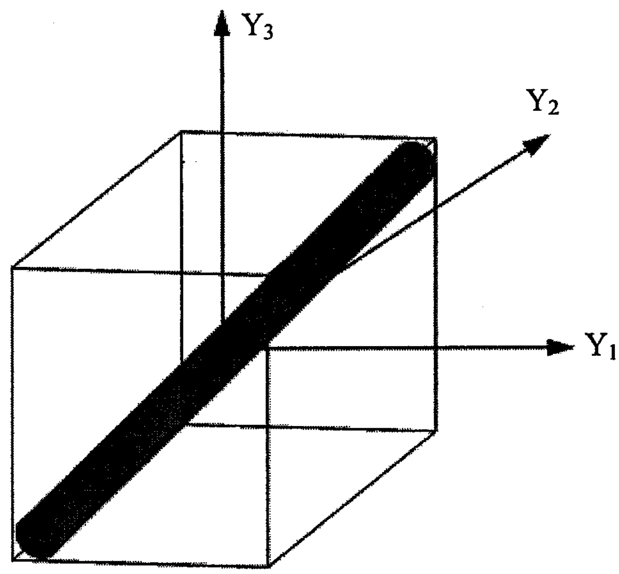

Figure 6-3: Unit cell of composite network reinforced with a single reinforcement family

Because of the multiconstituent nature of the network structures under consideration, it is prudent to also consider the interfacial conditions that exist between the matrix and the reinforcements. The first such condition is a direct consequence of the continuity of the $N_m^{kl}(y)$ functions and may be stated as:

$$N_n^{kl}(r)\Big|_s = N_n^{kl}(m) \qquad [6.16]$$

Furthermore, continuity of the displacement field leads to:

$$b_{ij}^{kl} n_j \Big|_r = b_{ij}^{kl} n_j \Big|_m \qquad [6.17]$$

In Equation [6.16] and [6.17] the suffixes "s", "r" and "m" stand for "interface", "reinforcement" and "matrix" respectively. As well, n_j are the components of the unit normal vector to the interface. As mentioned earlier on, we will further assume that the structure of interest is made of high modulus reinforcements and "soft" matrix. As such, we may take $b_{ij}^{kl}(m) \approx 0$ and thus, condition [6.17] becomes:

$$b_{ij}^{kl} n_j \Big|_s = 0 \qquad [6.18]$$

In summary, the final problem that must be solved for the three-dimensional network structure reinforced with a single family of isotropic bars is:

$$\frac{\partial}{\partial y_j}\left\{b_{ij}^{kl}\right\} = 0 \qquad [6.19]$$

$$b_{ij}^{kl} n_j \Big|_s = 0 \qquad [6.20]$$

6.3.2. Coordinate Transformation

Before proceeding to the solution of the unit cell problem given in Equations [6.19] and [6.20], we perform a coordinate transformation of the microscopic coordinates $\{y_1, y_2, y_3\}$ onto $\{\eta_1, \eta_2, \eta_3\}$ as shown in Figure 6-4. The coordinate transformation is carried out in such a way that the η_1 coordinate axis coincides with the direction of the reinforcement and η_2, η_3 are perpendicular to the reinforcement (and each other).

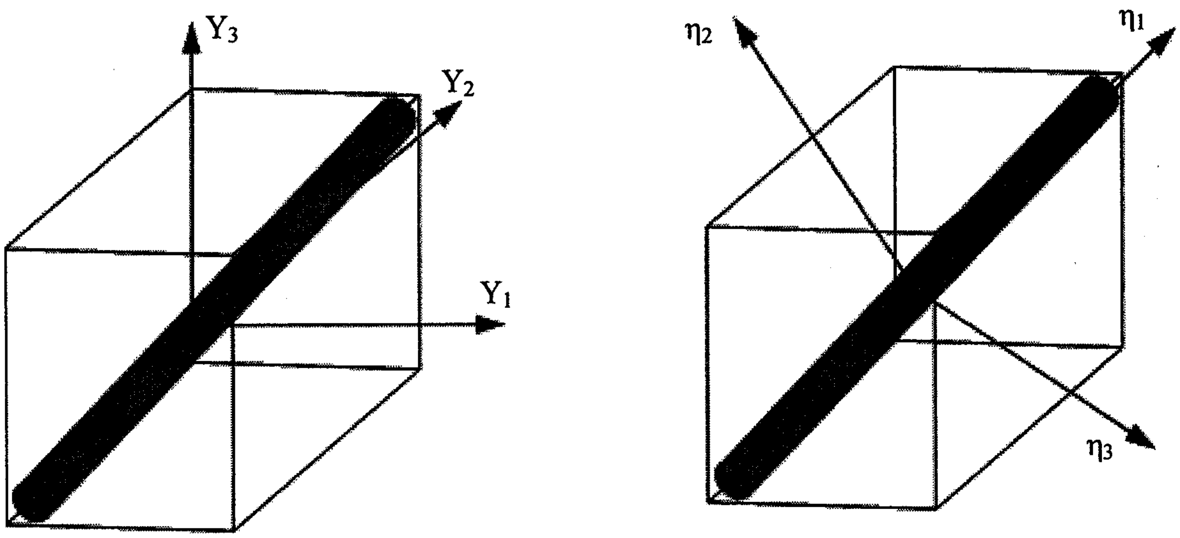

Figure 6-4: Unit cell in original and rotated macroscopic coordinates

Thus, derivatives transform according to:

$$\frac{\partial}{\partial y_i} = q_{ij} \frac{\partial}{\partial \eta_i} \qquad [6.21]$$

where q_{ij} are the components of the matrix of direction cosines characterizing the axis rotation.

With this choice of coordinate system, it is evident that the problem [6.19]-[6.20] will be independent of η_1 and will only depend on η_2 and η_3. Consequently, the order of the differential equations is reduced by one, and the analysis of the problem is simplified.

6.3.3. Determination of Elastic Coefficients

With reference to Figure 6-4, we begin by rewriting Equations [6.19] and [6.20] in terms of the η_i coordinates to get:

$$
\begin{aligned}
& b_{ij}^{kl} = C_{ijmn} q_{np} \frac{\partial N_m^{kl}}{\partial \eta_p} + C_{ijkl} \\
& b_{ij}^{kl} q_{i2} n_2' + b_{ij}^{kl} q_{i3} n_3' \Big|_s = 0
\end{aligned}
\qquad [6.22]
$$

Here, n_i' represent the components of the unit normal vector expressed in terms of the new coordinates. Expanding first expression of Equation [6.22] remembering at the same time the independency of the problem on η_1 gives:

$$
\begin{aligned}
b_{ij}^{kl} = C_{ijkl} &+ C_{ijm1} q_{21} \frac{\partial N_m^{kl}}{\partial \eta_2} + C_{ijm2} q_{22} \frac{\partial N_m^{kl}}{\partial \eta_2} + C_{ijm3} q_{23} \frac{\partial N_m^{kl}}{\partial \eta_2} + \\
& C_{ijm1} q_{31} \frac{\partial N_m^{kl}}{\partial \eta_3} + C_{ijm2} q_{32} \frac{\partial N_m^{kl}}{\partial \eta_3} + C_{ijm3} q_{33} \frac{\partial N_m^{kl}}{\partial \eta_3}
\end{aligned}
\qquad [6.23]
$$

It is possible to solve the system [6.22] by assuming a linear variation of the N_i^{kl} functions in η_2 and η_3, i.e.

$$
\begin{aligned}
N_1^{kl} &= \lambda_1 \eta_2 + \lambda_2 \eta_3 \\
N_2^{kl} &= \lambda_3 \eta_2 + \lambda_4 \eta_3 \\
N_3^{kl} &= \lambda_5 \eta_2 + \lambda_6 \eta_3
\end{aligned}
\qquad [6.24]
$$

where λ_i are constants to be determined from the boundary conditions. From Equations [6.23] and [6.24], the elastic b_{ij}^{kl} coefficients may be written as follows:

$$
\begin{aligned}
b_{11}^{kl} &= C_{11kl} + C_{11}q_{21}\lambda_1 + C_{11}q_{31}\lambda_2 + C_{12}q_{22}\lambda_3 + C_{12}q_{32}\lambda_4 + C_{13}q_{23}\lambda_5 + C_{13}q_{33}\lambda_6 \\
b_{22}^{kl} &= C_{22kl} + C_{12}q_{21}\lambda_1 + C_{12}q_{31}\lambda_2 + C_{22}q_{22}\lambda_3 + C_{22}q_{32}\lambda_4 + C_{23}q_{23}\lambda_5 + C_{23}q_{33}\lambda_6 \\
b_{33}^{kl} &= C_{33kl} + C_{13}q_{21}\lambda_1 + C_{13}q_{31}\lambda_2 + C_{23}q_{22}\lambda_3 + C_{23}q_{32}\lambda_4 + C_{33}q_{23}\lambda_5 + C_{33}q_{33}\lambda_6 \\
b_{23}^{kl} &= C_{23kl} + C_{44}q_{23}\lambda_3 + C_{44}q_{33}\lambda_4 + C_{44}q_{22}\lambda_5 + C_{44}q_{33}\lambda_6 \\
b_{13}^{kl} &= C_{13kl} + C_{55}q_{23}\lambda_1 + C_{55}q_{33}\lambda_2 + C_{55}q_{21}\lambda_5 + C_{55}q_{31}\lambda_6 \\
b_{12}^{kl} &= C_{12kl} + C_{66}q_{22}\lambda_1 + C_{66}q_{32}\lambda_2 + C_{66}q_{21}\lambda_3 + C_{66}q_{31}\lambda_6
\end{aligned}
\qquad [6.25]
$$

Here C_{ij} are the elastic coefficients of the reinforcements in the contacted notation (see e.g. Reddy, 1997). Substituting Equation [6.25] into the second expression of Equation [6.22] and letting j take on the values 1, 2, 3 results in 6 linear algebraic equations in λ_i, i=1, 2, ……, 6;

$$
\begin{aligned}
A_1\lambda_1 + A_2\lambda_2 + A_3\lambda_3 + A_4\lambda_4 + A_5\lambda_5 + A_6\lambda_6 + A_7 &= 0 \\
A_8\lambda_1 + A_9\lambda_2 + A_{10}\lambda_3 + A_{11}\lambda_4 + A_{12}\lambda_5 + A_{13}\lambda_6 + A_{14} &= 0 \\
A_{15}\lambda_1 + A_{16}\lambda_2 + A_{17}\lambda_3 + A_{18}\lambda_4 + A_{19}\lambda_5 + A_{20}\lambda_6 + A_{21} &= 0 \\
A_{22}\lambda_1 + A_{23}\lambda_2 + A_{24}\lambda_3 + A_{25}\lambda_4 + A_{26}\lambda_5 + A_{27}\lambda_6 + A_{28} &= 0 \\
A_{29}\lambda_1 + A_{30}\lambda_2 + A_{31}\lambda_3 + A_{32}\lambda_4 + A_{33}\lambda_5 + A_{34}\lambda_6 + A_{35} &= 0 \\
A_{36}\lambda_1 + A_{37}\lambda_2 + A_{38}\lambda_3 + A_{39}\lambda_4 + A_{40}\lambda_5 + A_{41}\lambda_6 + A_{42} &= 0
\end{aligned}
\qquad [6.26]
$$

where A_i are constants which depend on the direction of the reinforcement as well as its mechanical properties. The explicit expressions for these constants are given in Appendix F. Once the system of Equations [6.26] is solved, the determined λ_i coefficients are substituted back into Equation [6.25] to solve for the b_{ij}^{kl} coefficients. In turn, these are used to calculate the effective elastic coefficients of the structure of Figure 6-3 by integrating over the volume of the unit cell as explained below in Section 6.3.4.

6.3.4. Effective Elastic Coefficients

The effective elastic coefficients of the network composite structure of Figure 6-3 are obtained by means of Equation [6.13], which, on account of notation [6.14] becomes:

$$\widetilde{C}_{ijkl} = \frac{1}{|Y|} \int_Y b_{ij}^{kl} dv \qquad [6.27]$$

Assuming that the length (within unit cell) and cross-sectional area of the reinforcement in coordinates $\{y_1, y_2, y_3\}$ are L and A respectively, and that the volume of the unit cell is V in the same coordinates $\{y_1, y_2, y_3\}$, then the effective elastic coefficients are,

$$\widetilde{C}_{ijkl} = \frac{AL}{V} b_{ij}^{kl} = V_f b_{ij}^{kl} \qquad [6.28]$$

where b_{ij}^{kl} is constant and V_f is the volume fraction of the reinforcement within the unit cell.

For network structures with more than a single family of reinforcements, the effective coefficients can be determined by superposition ignoring stress concentration and other local complications at the regions of intersections. For example, for a network composite structure with N families of isotropic reinforcements, the effective elastic coefficients will be given by,

$$\widetilde{C}_{ijkl} = \sum_{n=1}^{N} V_f^{(n)} b_{ij}^{(n)kl} \qquad [6.29]$$

where the superscript (n) represents the n^{th} reinforcement family.

6.3.5. Examples of network structures

Let us now apply above developed theory to the analysis of some examples.

6.3.5.1. Example 1-Convergence of Model for the Case of 2D Composite Network

For the purposes of the first example, we will verify the validity of our model for the case of 2D network structures whereby the reinforcements lie entirely in the Y_1-Y_2 plane. The pertinent unit cell for such a structure is shown in Figure 6-5.

Solving Equation [6.26] for λ_i and substituting the results into Equation [6.25] gives the following expressions for the non-zero elastic coefficients.

$$b_{11}^{11} = E\cos^4\theta,\ b_{11}^{12} = E\cos^3\theta\sin\theta,\ b_{11}^{22} = b_{12}^{12} = E\cos^2\theta\sin^2\theta \qquad [6.30]$$
$$b_{22}^{12} = E\cos\theta\cos^3\theta,\ b_{22}^{22} = E\sin^4\theta,\ b_{ij}^{kl} = b_{kl}^{ij}$$

Here, E stands for the Young's Modulus of the reinforcing material. These results are the same as those obtained earlier by Kalamkarov [1992] who developed an asymptotic homogenization model for a thin flat network-reinforced composite plates.

6.3.5.2. Example 2

The second example pertains to the cubic structure of Figure 6-6. This composite structure has three families of reinforcements, each family oriented along one of the coordinate axes.

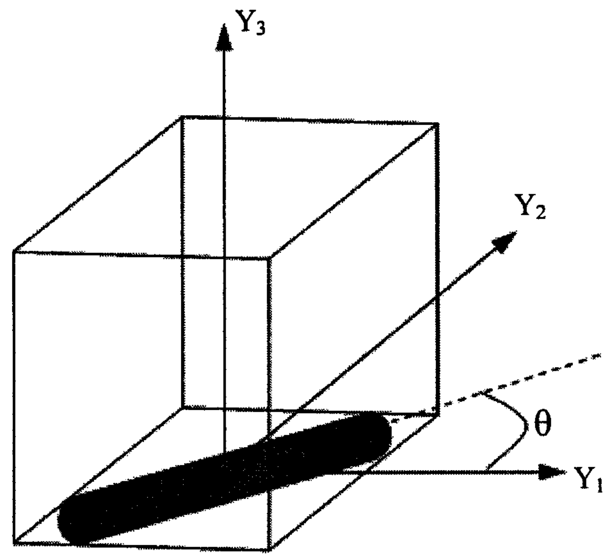

Figure 6-5: Unit cell for (2D) structure with reinforcements in the Y_1-Y_2 plane

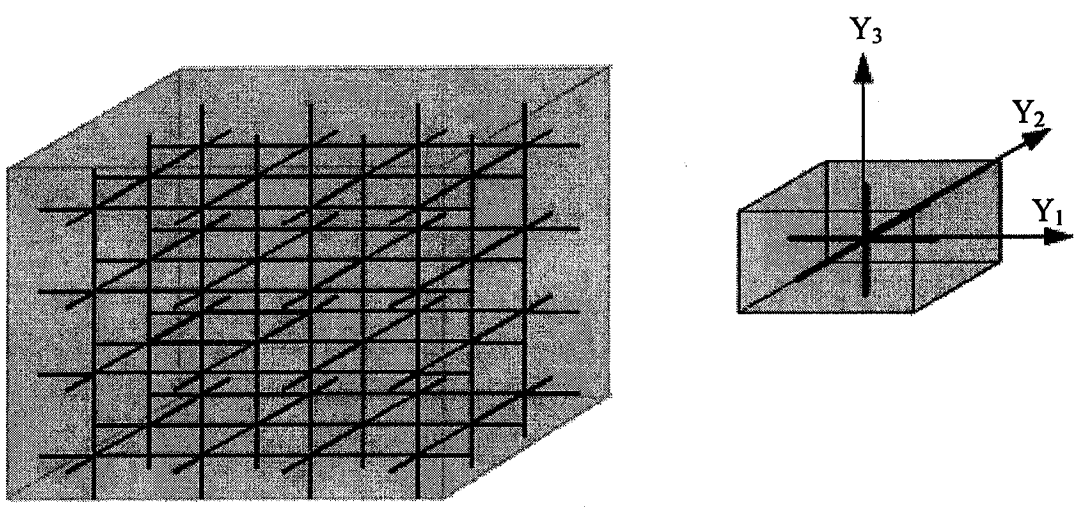

Figure 6-6: Cubic network structure with reinforcements in Y_1, Y_2, Y_3 directions

Noting that $q_{ij} = \delta_{ij}$, where δ_{ij} are the components of the identity tensor, the values of λ_i for the reinforcement in the Y_1 direction are readily obtained from Equation [6.26] to be as follows:

$$\lambda_1 = \frac{-C_{12kl}}{C_{66}}, \lambda_2 = \frac{-C_{13kl}}{C_{55}}, \lambda_3 = \frac{C_{33}C_{22kl} - C_{23}C_{33kl}}{C_{23}{}^2 - C_{22}C_{33}},$$
$$\lambda_4 + \lambda_5 = \frac{-C_{23kl}}{C_{44}}, \lambda_6 = \frac{C_{22}C_{33kl} - C_{23}C_{22kl}}{C_{23}{}^2 - C_{22}C_{33}} \qquad [6.31]$$

From Equation [6.25], the b_{ij}^{kl} coefficients are given by:

$$b_{11}^{kl} = C_{11kl} + \frac{[C_{12}C_{33} - C_{13}C_{23}]C_{22kl} + [C_{13}C_{22} - C_{12}C_{23}]C_{33kl}}{C_{23}^2 - C_{22}C_{33}} \qquad [6.32]$$

After substituting expressions for elastic coefficients we obtain:

$$\begin{aligned} &b_{11}^{11} = E \\ &b_{11}^{22} = b_{11}^{33} = b_{11}^{23} = b_{11}^{13} = b_{11}^{12} = 0 \\ &b_{22}^{kl} = b_{33}^{kl} = b_{23}^{kl} = b_{13}^{kl} = b_{12}^{kl} = 0 \end{aligned} \qquad [6.33]$$

Repeating the procedure for the reinforcement in the Y_2 direction yields:

$$\begin{aligned} &b_{22}^{22} = E \\ &b_{22}^{11} = b_{22}^{33} = b_{22}^{23} = b_{22}^{13} = b_{22}^{12} = 0 \\ &b_{11}^{kl} = b_{33}^{kl} = b_{23}^{kl} = b_{13}^{kl} = b_{12}^{kl} = 0 \end{aligned} \qquad [6.34]$$

Finally, for the reinforcement in the Y3 direction, the results are:

$$\begin{aligned} &b_{33}^{33} = E \\ &b_{33}^{11} = b_{33}^{22} = b_{33}^{23} = b_{33}^{13} = b_{33}^{12} = 0 \\ &b_{11}^{kl} = b_{22}^{kl} = b_{23}^{kl} = b_{13}^{kl} = b_{12}^{kl} = 0 \end{aligned} \qquad [6.35]$$

We are now ready to compute the effective elastic coefficients of the cubic network structures shown in Figure 6-6. Let the length (within unit cell) and cross-sectional area of the i^{th} reinforcement in the Y_i direction be L_i and A_i respectively (in coordinates y_1, y_2, y_3). Also let us assume that E_i is the Young's modulus of the reinforcement in the Y_i direction. Then, for a unit cell of volume V, the corresponding volume fraction v_i is given by $v_i = A_i L_i / V$. Thus, from Equations [6.29], [6.33] and [6.35] the non-zero effective elastic coefficients for the composite network structure of Figure 6-6 are,

$$\begin{aligned}\tilde{C}_{11} &= \frac{A_1 L_1}{V} E_{(1)} = v_1 E_{(1)}; \\ \tilde{C}_{22} &= \frac{A_2 L_2}{V} E_{(2)} = v_2 E_{(2)}; \\ \tilde{C}_{33} &= \frac{A_3 L_3}{V} E_{(3)} = v_3 E_{(3)}\end{aligned} \qquad [6.36]$$

where $E_{(i)}$ is the young's modulus of the i^{th} reinforcement. In the case where the reinforcements have the same material properties (namely Young's modulus, E) the expression in Equation [6.36] become,

$$\tilde{C}_{11} = \frac{A_1}{V} E = v_1 E; \quad \tilde{C}_{22} = \frac{A_2}{V} E = v_2 E; \quad \tilde{C}_{33} = \frac{A_3}{V} E = v_3 E \qquad [6.37]$$

6.3.5.3. Example 3

This example pertains to a composite network structure with a conical arrangement of isotropic reinforcements. In this example (to be referred to as structure S_1) the unit cell is made of three reinforcements oriented as shown in Figure 6-7. The expressions for the effective coefficients are readily determined from Equation [6.25], [6.26] and [6.29].

Although the expressions are too lengthy to be reproduced here, some of these coefficients will be presented graphically in the next section.

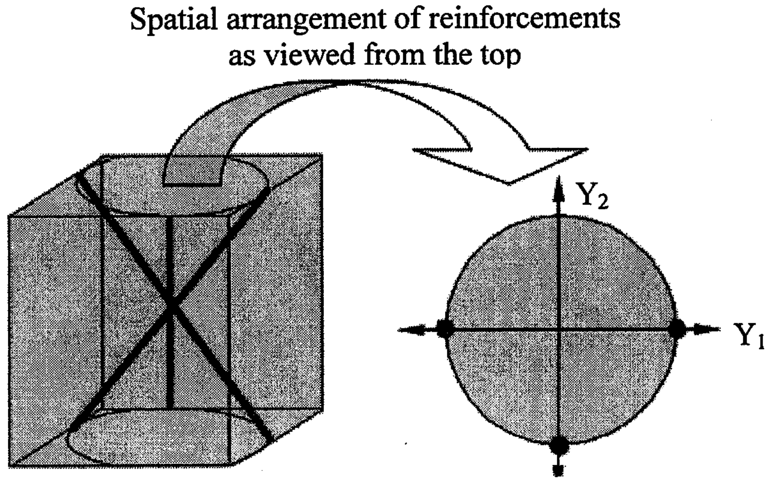

Figure 6-7: Unit cell for composite network structure with conical arrangement of isotropic reinforcements (Structure S_1)

6.3.5.4. Example 4

In this example let us consider a general unit cell (S_2) as shown in Figure 6-8. The general unit cell consists of three reinforcements two of which span from different corners of the unit cell to the diametrically opposite ones and the third reinforcement is oriented from the middle of the bottom edge to the middle of the top edge on the opposite face.

The effective coefficients for this structure are calculated in the same manner as for the ones in the previous examples. The resulting expressions are too lengthy to be reproduced here. However as an illustration some of the effective coefficients are plotted vs. the height of the unit-cell in the following section.

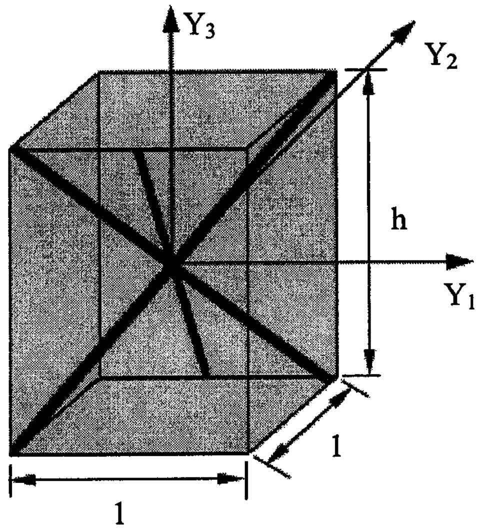

Figure 6-8: Structure S_2

6.3.6. Plots of Effective properties and discussion

The mathematical model and methodology presented in Sections 6.3-6.3.4 can be used in analysis and design to tailor the effective elastic coefficients of any three-dimensional composite network structure by changing the material, number, orientation and/or cross-sectional area and material selection of the reinforcements. In this Section typical effective coefficients will be computed and plotted. For illustration purposes, we will assume that the reinforcements have a Young's Modulus and Poisson's Ratio equal to 200 GPa and 0.3, respectively.

We will begin with the plot of some of the effective coefficients for the structure S1 shown in Figure 6-7. The effective coefficients will be plotted vs. the total volume fraction of the reinforcements within the unit cell. As expected, the effective coefficients increase with an increase in the overall reinforcement volume fraction, as shown in Figure 6-9 and Figure 6-10.

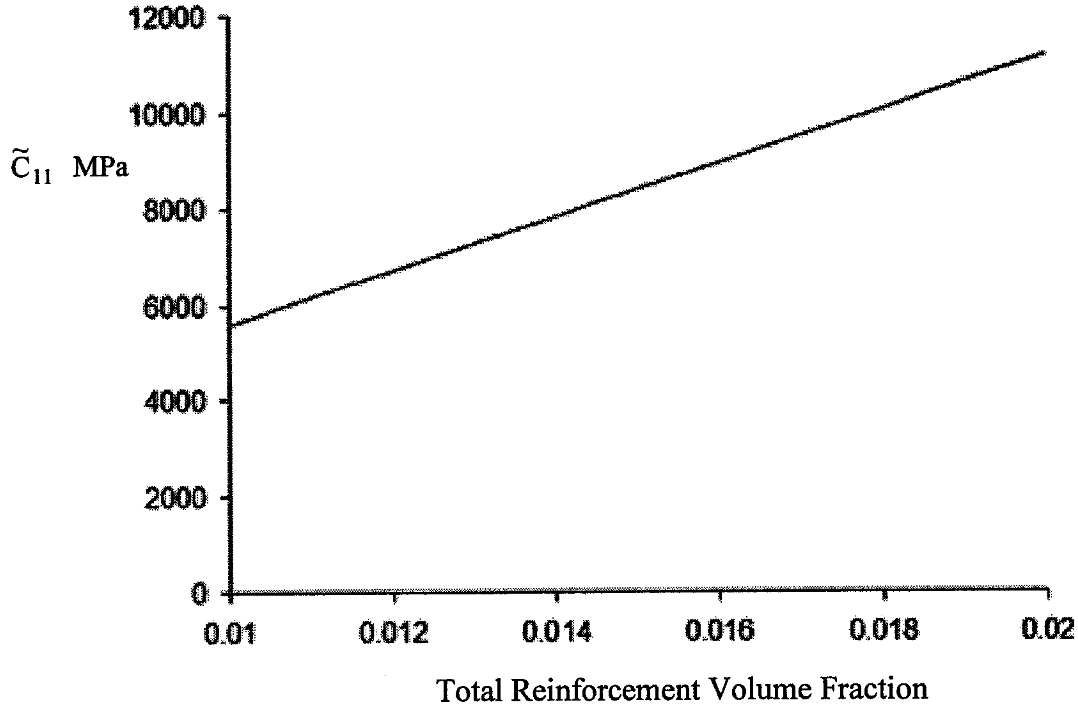

Figure 6-9: Plot of $\tilde{C}_{11}$ vs. reinforcement volume fraction for structure S_1

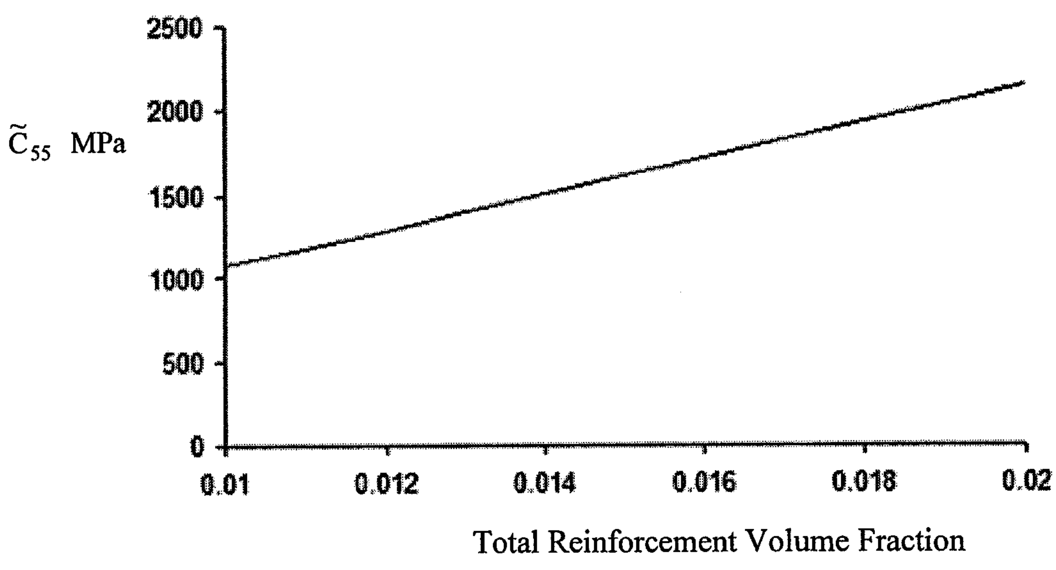

Figure 6-10: Plot of $\tilde{C}_{55}$ vs. reinforcement volume fraction for structure S_1

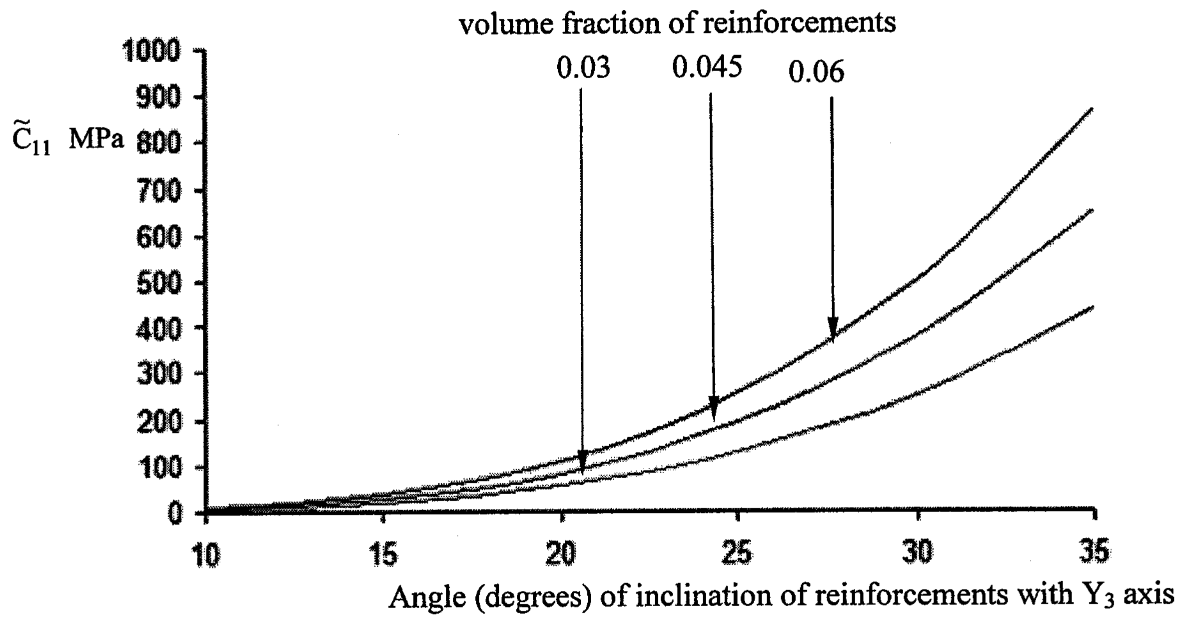

Figure 6-11: Plot of the $\widetilde{C}_{11}$ effective coefficient vs. inclination of reinforcements with the Y_3 axis pertaining to structure S_1 for reinforcement volume fractions equal to 0.03, 0.045, and 0.06

It would also be of interest to plot the variation of some of the effective coefficients of structure S_1 with the angle of inclination of the reinforcements to the Y_3 axis. As this angle increases, the reinforcements are oriented progressively closer to the Y_1 and Y_2 axis and the stiffness in these directions is expected to increase. Indeed a reference to Figure 6-11 and Figure 6-12 shows precisely that. On the contrary, (see Figure 6-13) at the same time as the stiffness in the Y_1 and Y_2 directions increases, the corresponding value in the Y_3 direction decreases because the reinforcements are oriented further away from the Y_3 axis.

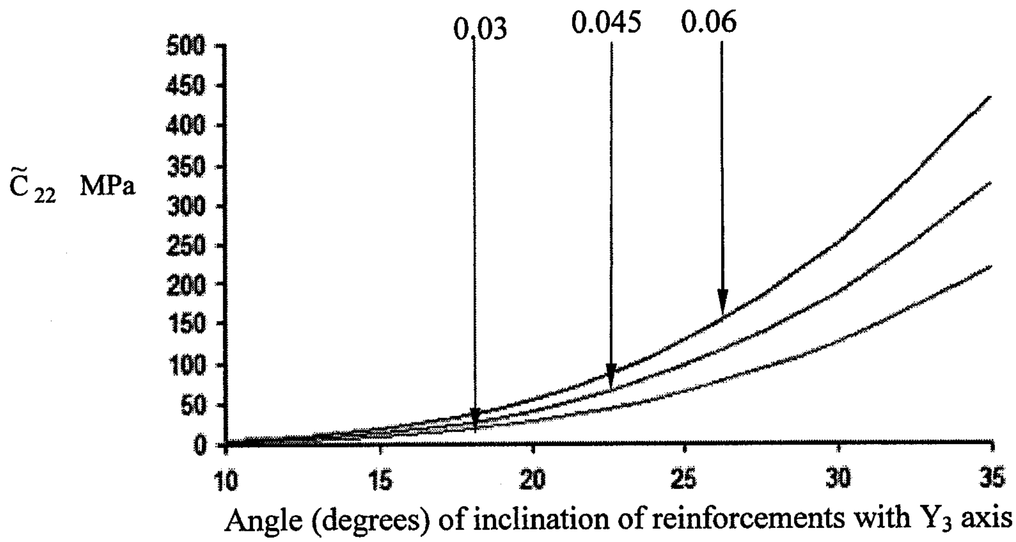

Figure 6-12: Plot of the $\tilde{C}_{22}$ effective coefficient vs. inclination of reinforcements with the Y_3 axis pertaining to structure S_1 for reinforcement volume fractions equal to 0.03, 0.045, and 0.06

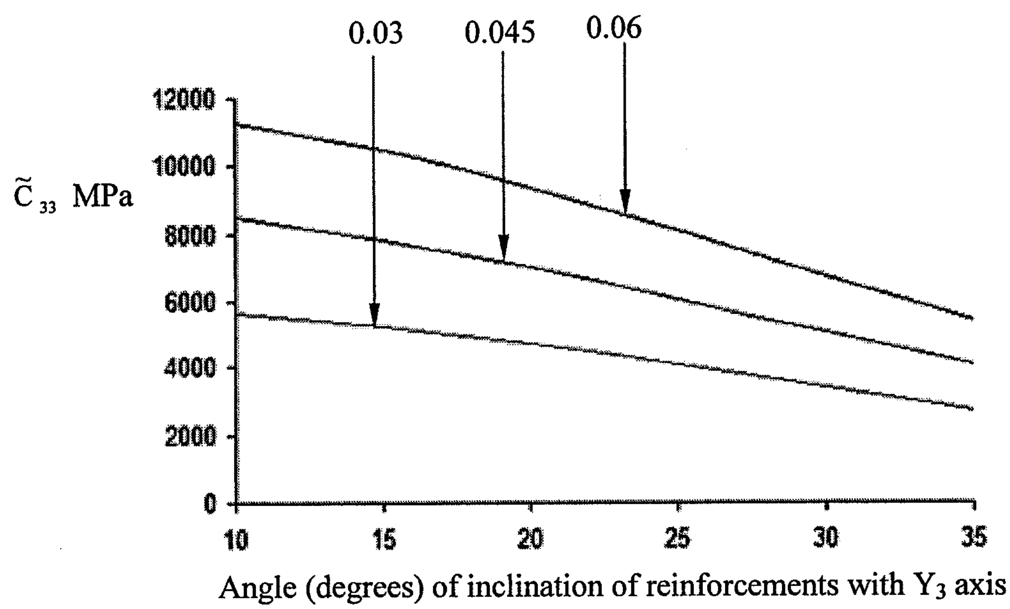

Figure 6-13: Plot of the $\tilde{C}_{33}$ effective coefficient vs. inclination of reinforcements with the Y_3 axis pertaining to structure S_1 for reinforcement volume fractions equal to 0.03, 0.045, and 0.06

We now turn our attention to the S_2 composite structure (Figure 6-8) and plot some of the effective coefficients by varying the height of the unit cell but keeping the other dimensions as well as the cross-sectional area of the reinforcements constant. It is noted that as the height of the unit cell is varied, the lengths and orientations of the reinforcements change.

Figure 6-14 shows a plot of the effective coefficients $\tilde{C}_{11}$, $\tilde{C}_{22}$, $\tilde{C}_{33}$, and $\tilde{C}_{55}$ vs. the height of the unit cell. As the height of the unit-cell increases, the volume fraction of the reinforcements decreases and at the same time the reinforcements are oriented closer to the Y_3 axis and further away from Y_1, and Y_2 axis. Both of these effects contribute to the stiffness in the Y_1, and Y_2 direction decreasing. However, $\tilde{C}_{33}$ increases because the increase in stiffness due to a smaller angle of inclination with the Y_3 axis dominates the decrease in stiffness due to the reinforcements volume fraction decreasing.

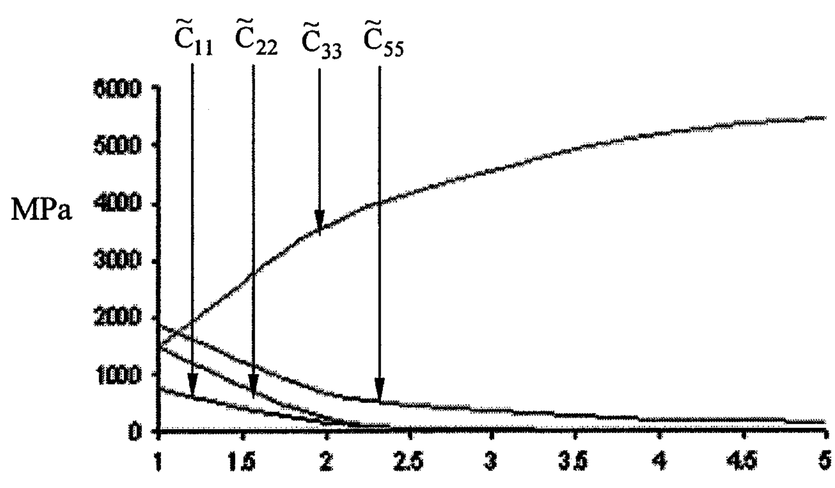

Figure 6-14: Plot of $\tilde{C}_{11}$, $\tilde{C}_{22}$, $\tilde{C}_{33}$, and $\tilde{C}_{55}$ effective coefficient vs. height of the unit cell for S_2 structure shown in Figure 6-8

Finally, we are interested in comparing the effective coefficients of structures S_1 (Figure 6-7) and S_2 (Figure 6-8) by varying the volume fraction. The volume fraction for structure S_1 is varied by varying the reinforcement cross-sectional properties and for structure S_2 by varying the height (h) of the unit cell. From the Figure 6-15 we see that $\tilde{C}_{33}$ for S_1 increases as the volume fraction increases and at the same time for S_2 it decreases because the fibers in the latter are oriented progressively further away from the Y_3 axis as the volume fraction increases. Beyond a certain volume fraction, S_1 is stiffer in the Y_3 direction. Of course these trends can be easily changed. For example, if the volume fraction of the reinforcements of S_2 is changed by keeping all dimensions of unit cell constant (i.e. direction cosines pertinent to reinforcements unchanged) and changing its cross-sectional properties then, increasing the volume fractions would increase $\tilde{C}_{33}$, and the relative stiffness between the two structures would be different than that depicted in Figure 6-15. What's important is to realize that the model allows for complete flexibility in designing a structure with desirable mechanical and geometrical characteristics.

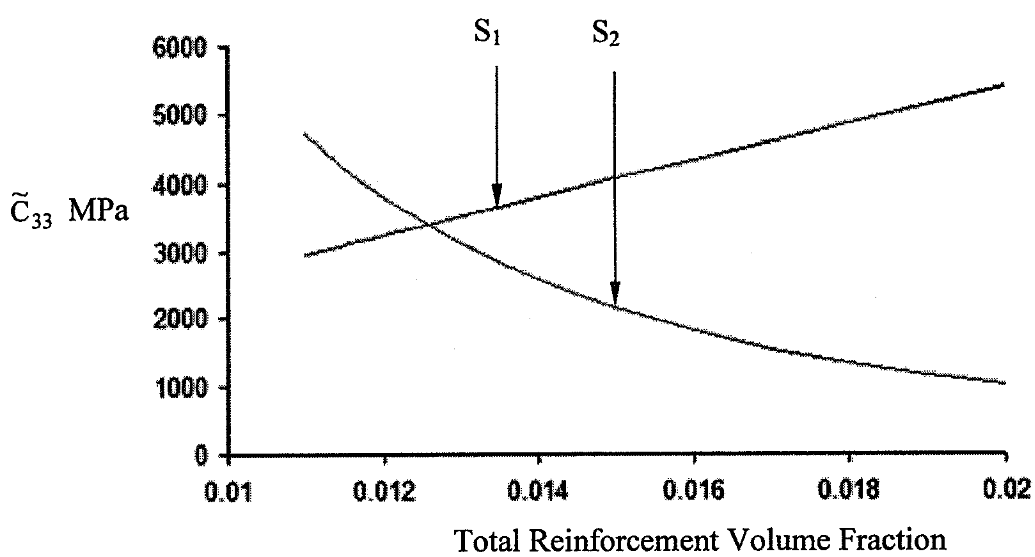

Figure 6-15: Plot of $\tilde{C}_{33}$ vs. total volume fraction for structures S_1 (Figure 6-7) and S_2 (Figure 6-8)

6.4. Conclusions

A general three-dimensional micromechanical model pertaining to globally anisotropic periodic composite structures reinforced with a spatial network of isotropic reinforcements is developed. The derived model is illustrated by means of different composite structures with cubic or conical configurations of reinforcements. The usefulness of this work lies in the fact that the model can be used to tailor the effective coefficients of any three-dimensional composite structure to meet the requirements of a particular application by changing such geometric or material parameters as the type, number, cross-sectional dimensions, and relative angular orientation of the reinforcements.

7. CONCLUSIONS

The first mathematical model developed applied a general 3-dimensional micromechanical model pertaining to smart composite layers with wavy boundaries to the case of thin smart plates reinforced with a network of generally orthotropic bars that may also exhibit piezoelectric behavior. The method used for the development of the model is that of asymptotic homogenization which reduces the original boundary value problem into a set of three decoupled problems each problem characterized by two differential equations. These three sets of differential equations, referred to as "unit cell problems", deal, separately, with the elastic, piezoelectric, and thermal expansion behavior of the network reinforced smart composite plates. The solution of the unit cell problems yields expressions for effective elastic, piezoelectric and thermal expansion coefficients. These coefficients are universal in nature and can be used to study a wide variety of boundary value problems associated with a smart structure of a given geometry.

The developed model is illustrated by means of three different smart structures, with orthotropic actuators/reinforcements oriented in a rectangular, triangular or rhombic manner. The effective coefficients pertinent to these structures were calculated and presented graphically. It is shown in this work that the effective coefficients of any network-reinforced smart composite plate can be customized to meet the requirements of a particular application by changing certain material or geometric parameters of interest such as size, type, angular orientation, etc. of the actuators/reinforcements so that the desirable properties are obtained.

The second mathematical model developed was used to analyze a prismatic smart composite structure with orthotropic constituents. The original boundary value problem which is characterized by rapidly oscillating material coefficients and is therefore difficult to solve, is transformed to a similar problem with effective coefficients which are independent of the microscopic variables. Consequently, this problem is much more amenable to analytical (or numerical) techniques.

Once the general model is derived and the governing equations including the appropriate interface conditions are determined, the effective elastic, actuation, and thermal expansion coefficients can be calculated. The actuation coefficients characterize the intrinsic transducer nature of active smart materials that can be used to induce strains and stresses in a controlled manner. The analysis presented was applied to piezoelectric materials, but the equations derived should be considered to hold equally well if the material in question exhibits for example magnetostrictive characteristics, or is associated with some general transduction characteristics that can be used to induce residual strains and stresses.

The derived model was applied to three different structures of practical interest (with rectangular, hexagonal, or rhombic configurations) consisting of orthotropic reinforcements and/or actuators. The effective elastic, piezoelectric and thermal expansion coefficients for these structures were determined and then compared graphically for the three structures. The usefulness of the presented methodology lies in the fact that the derived models can be used in design and analysis to tailor the effective coefficients of any structure to meet the engineering criteria pertaining to a particular application, by selecting the type, number, orientation, and size of the reinforcements.

The third and final mathematical model developed is used to analyze 3-D globally anisotropic periodic composite structures reinforced with a spatial network of isotropic reinforcements is developed. The model, which is developed using the asymptotic homogenization technique, transforms the original boundary value problem into a simpler one that is characterized by some effective elastic coefficients. The effective coefficients are shown to depend only on the pertinent geometric and material characteristics of the periodicity cell and are therefore independent of the global formulation of the problem.

The derived model is illustrated by means of different composite structures with cubic or conical configurations of reinforcements. As with the previous model, the usefulness of this work lies in the fact that the model can be used to tailor the effective coefficients of any three-dimensional composite structure to meet the requirements of a particular application by changing such geometric or material parameters as the type, number, cross-sectional dimensions, and relative angular orientation of the reinforcements. In the particular case in which the reinforcements form only a two-dimensional (planar) network, the results are shown to converge to previous models developed by Kalamkarov (1992) who also used the asymptotic homogenization technique and Pshenichnov (1982) who used stress-strain relationships in the reinforcements.

8. REFERENCES

Adachi, Y., Unjoh, S., Kondoh, M. Development of shape memory alloy damper for intelligent bridge systems, *Proceeding of the International Symposium on Shape memory materials*, Kanazawa, Japan, 31-34, 1999

Adali, S., Bruch Jr, J. C., Sadek, I.S., and Sloss, J.M. Robust shape control of beams with load uncertainties by optimally placed piezoelectric actuators, *Struct. Multidisc. Optim*, vol. 19, pp. 274-281, 2000

AEROFIT$_{INC}$, (2002), SMA hysteresis [online]
Available:
http://www.aerofit.com/sma/hysteresis.htm

American Composite Manufacturers Association, Technical Recourses [online]
Available:
www.acmanet.org [2006]

Andrianov, I.V., Lesnichaya, V.A., and Manevich, L.I. Homogenization methods in the statics and dynamics of ribbed shells, Nauka, Moscow, 1985

APC International Limited, (1999) Piezoelectric ceramics [online]
Available:
www.americanpiezo.com [2002]

Artola, M. and Duvaut, G. Homogenization d'une plaque reinforce, *C. R. Acad. Aci., Ser. A*, vol. 284, pp. 707-710, 1977

AZoM Pvt. Ltd. (2004), Thermosetting composite-article, Azom.com, [online].
Available:
http://www.azom.com/work/47wEj793H71F6t8kntY2_files/image003.gif [2004]

Bakhvalov, N. and Panasenko, G. Homogenisation: Averaging processes in periodic media, Kluwer Academic Publishers, Netherlands, 1984

Barboni, R., Mannini, A., Fantini, F., and Gaudenzi, P. Optimal placement of PZT actuators for the control of beam dynamics, *Smart Mater. Struct*, vol. 9, pp. 110-120, 2000

Bensoussan, A., Lions, J.L., and Papanicolaou, G. Asymptotic analysis for periodic structures, North-Holland Publ. Comp, Amsterdam, 1978

Bent, A. and Hagood, N.W. Piezoelectric Fiber Composites with Interdigital Electrodes, *J. Intell. Mater. Syst. and Struct*, Vol. 8, No. 11, pp 903-919, 1997

Berryman, J.G. Single-scatterng approximations for coefficients in Biot's equatons of poroelasticity, *J. Acoust. Soc. Am,* vol. 91, pp. 551-571, 1992

Berryman, J.G. Long-wavelength propagation in composite elastic media, *J. Acoust. Soc. Am*, vol. 69, pp.416–24, 1980

Bi, J. and Anjanappa, M. Investigation of active vibration damping using magnetostrictive mini actuators, *Proc of the SPIE conference on smart structures and materials: smart structures and intelligent systems*, Feb 14-16, Orlando, Florida, 171-180, 1994

Bob, S.S., Tracy, Mike., Roh, Youn-Seo., and Chang Fu-Kuo. Built-in piezoelectric for processing and health monitoring of composite structures, Stanford University, 2002

Bruant, I., Coffignal, G., Lene, F., Verge, M. A methodology for determination of piezoelectric actuator and sensor location on beam structures, *J. Sound Vib,* vol. 243(5), 861-882, 2001

Budiansky, B. On the elastic moduli of some heterogeneous materials, *J. Mech. Phys. Solids*, vol.13, pp. 223-227, 1965

Caillerie, D. Thin elastic and periodic plates, *Math. Appl. Sci*, vol. 6, pp. 159-191, 1984

Challagulla, K., Georgiades, A.V., and Kalamkarov, A.L. Asymptotic homogenization modeling of thin network structures, *Compos. Struct*, In press, 2006

Challagulla, K.S., Georgiades, A.V., and Kalamkarov, A.L. Asymptotic homogenization model for Three-Dimensional network reinforced composite structures, *Journal of Mechanics of Materials and Structures*, Submitted 2006

Challagulla, K.S., Georgiades, A.V., and Kalamkarov, A.L. Micromechanical Analysis of Smart Composite Plates, *Proceedings of the Fifth Structural Engineering Convention*, Bangalore, India, 2005

Challagulla, K.S. Experimental and Theoretical Studies of Smart Composite Structures, M.A.Sc. Thesis, Dalhousie University, Halifax, Nova Scotia, 2003

Chawla, K.K. Ceramic matrix composites, Chapman & Hall, London, 1993

Chen, P.C. and Chopra, I. Induced strain actuation of composite beams and rotor blades with embedded piezoelectric elements, *Proc. Of the SPIE Conference on Smart Structures and Materials: Smart Structures and Intelligent Systems*, Feb 14-16, Orlando, Florida, pp. 38-51, 1994

Chen, S.M. and Wei, C.G. Experimental study of the rheological behavior of electrorheological fluids, *Smart Mater. Struct*, vol. 15, pp. 371–377, 2006

Chen, X. and Anjanappa, M. Health monitoring of composites embedded with magnetostrictive thick film without disassembly, *Smart Mater. Struct*, vol. 15, pp. 20–32, 2006

Christensen, R.M. A critical evaluation for a class for a class of micromechanics models, *J Mech. Phys. Solids*, vol. 38, pp. 379-404, 1990

Ciarlet, P.G. Plates and Junctions in Elastic Multi-Structures: An Asymptotic Analysis, Vol. 14, Masson, Paris, 1990

Cioranescu, D. and Donato, P. An Introduction to homogenization, Oxford University Press, Oxford, United Kingdom, 1999

Cote, F., Masson, P., and Mrad, N. Dynamic and static assessment of piezoelectric embedded composites, *Proc SPIE*, vol. 4701, pp. 316-325, 2002

Daniel, I.M. and Ishai, O. Engineering mechanics of composite materials, Oxford University press, Inc., New York, 1994

Design inSite, http://www.designinsite.dk/ [online]
Available:
www.designinsite.dk/gifs/pb0102.jpg [2006]

Devries, F., Dumontet, H., Duvaut, G., and Lene, F. Homogenization and damage for composite structures, *Internat J. for Numer. Methods Engrg*, vol. 27, pp. 285-298, 1989

Drugan, W. J. and. Willis, J. R. A micromechanics-based nonlocal constitutive equation and estimates of representative volume element size for elastic composites, *J. Mech. Phys. Solids*, vol. 44:4, pp. 497-524, 1996

Duvaut, G. Analyse fonctionnelle et méchanique des milieux continues, *Proceeding of the 14th IUTAM Congress*, Delft, pp. 119-132, 1976

Engineering materials handbook, Volume 1: Composites, ASM International, Metals Park, Ohio, 1987

Eshelby, J.D, The determination of the elastic field of an ellipsoidal inclusion, and related problems, *Proc. R. Soc. Lond*, vol. A241, pp. 376-396, 1957

Fenn, R. and Gever, M.J. Passive damping and velocity sensing using magnetostrictive transduction, *Proc of the SPIE Conference on Smart structures and materials: Smart structures and Intelligent systems*, Feb 14-16, Orlando, Florida, 216-227, 1994

Flint, E.M., Rogers, C.A., and Liang, C. Electro-dynamic Transduction Equations for piezoelectric stack actuators, Adaptive structural and composite materials: Analysis and Applications, *ASME 1994 International Mechanical Engineering Congress and Exposition*, Chicago, Illinois, Nov 6-11, pp. 2001-210, 1994

Fukunaga, H., Hu, N., and Chang F. Structural damage identification using piezoelectric sensors, *Int. J. Solids Struct*, vol. 34, pp. 393–418, 2002

Georgiades, A.V., Challagulla, K., and Kalamkarov, A.L. Modeling of the thermopiezoelectric behavior of prismatic smart composite structures made of orthotropic materials, *Composites Part B: Engineering*, In Press, 2006

Georgiades, A.V., Kalamkarov, A.L., Challagulla, K.S., Asymptotic homogenization model for smart network composite reinforced plates, *Smart Mater. Struct*, vol. 15, pp. 1197-1210, 2006

Georgiades, A.V. and Kalamkarov, A.L. Asymptotic homogenization models for smart composite plates with rapidly varying thickness: Part - II Applications, *Int. J. Mult. Comp. Eng*, vol. 2(1), pp. 149-172, 2004

Georgiades, A.V., Kalamkarov, A.L., and Challagulla, K. Micromechanical analysis of smart composite structures with a periodic array of embedded actuators, *CAN/COM 2003*, Ottawa, Canada, CD-ROM ID 063, July 2003

Georgiades, A.V. Experimental and Analytical Studies of Smart Composite Reinforcements and Structures, PhD. Thesis, Dalhousie University, Halifax, Nova Scotia, 2002

Ghosh, D.P. and Gopalakrishnan, S. Coupled analysis of composite laminate with embedded magnetostrictive patches, *Smart Mater. Struct*, vol. 14, pp. 1462–1473, 2005

Gibson, R.F. Principles of composite materials mechanics, McGraw-Hill, Inc., 1994

Guedes, J.M. and Kikuchi, N. Preprocessing and postprocessing for materials based on the homogenization method with adaptive finite element methods, *Comput. Methods Appl. Mech. Engrg*, vol. 83, pp. 143-198, 1990

Hashin, Z. Analysis of composite materials: a survey, *J. Appl. Mech*, vol. 50, pp. 481-505, 1983

Hashin, Z. Theory of fiber reinforced materials. *NASA CR-1974*

Hashin, Z. The elastic moduli of heterogeneous materials, *J. Appl. Mech*, vol. 29, pp. 143-150, 1962

Hashin, Z. and Rosen, B. W. The elastic moduli of fiber-reinforced materials, *J. Appl. Mech*, vol. 31, pp. 223-232, 1964

Hashin, Z. and Shtrikman, S. A variational approach to the theory of elastic behavior of multiphase materials, J. *Mech. Phys. Solids*, vol. 11, pp. 127-140, 1963a

Hashin, Z. and Shtrikman, S. Conductivity of polycrystals, *Phys. Rev*, vol. 130 (1), pp. 129-133, 1963b

Hershey, A.V. The elasticity of an isotropic aggregate of anisotropic cubic crystals, *J. Appl. Mech*, vol. 21, pp. 236-240, 1954

Heverly, II. D.E., Wang, K.W., and Smith, E.C., An Optimal Actuator Placement Methodology for Active Control of Helicopter Airframe Vibration, *Journal of the American Helicopter Society*, vol. 46 (4), pp. 251 – 261, 2001

Heyliger, P. Two-Dimensional Static Field in Magneto-electro-elastic Laminates, *J. Intell. Mater. Syst. and Struct*, Vol. 15, pp. 689-709, 2004

Hexcel Composites Inc., [2001] [online]
Available:
www.hexcelcomposites.com [2001]

Hill, R. Elastic properties of reinforced solids, *J. Mech. Phys. Solids*, vol. 11, pp. 357-372, 1963

Hill, R. A self-consistent mechanics of composite materials, *J. Mech. Phys. Solids*, vol. 13, pp. 213-222, 1965

Hollister, S. and Kikuchi, N. Comparison of homogenization and standard mechanics analyses for periodic porous composites, *Comput. Mech*, vol. 10, pp. 73-95, 1992

Holmes H, Mark. Introduction to Perturbation Methods, Springer-Verlag, Berlin, 1995

Holzapfel, G. A. Nonlinear Solid mechanics, John Wiley & Sons, 2000

Humbeeck, J.V. and Kustov, S. Active and passive damping of noise and vibrations through shape memory alloys: applications and mechanisms, *Smart Mater. Struct*, vol. 14, pp. S171–S185, 2005

Jain, A.K. and Sirkis, J.S. Continuum damage mechanics in piezoelectric ceramics *Adaptive Structures and Composite Materials: Analysis and Application*, pp. 47-58, 1994

Jansson, S. Homogenized nonlinear constitutive properties and local stress concentrations for composites with periodic internal structure, *Int. J. Solids Struct*, vol. 29, pp. 2181–200, 1992

Jordan, T.L. and Ounaies, Z. Piezoelectric ceramic characterization, *NASA Langley Research Center*, September 2001

Kalamkarov, A.L., Georgiades, A.V., Challagulla, K., and Saha, G. Micromechanics of smart composite plates with periodically embedded actuators and rapidly varying thickness, *Journal of Thermoplastic Composite Materials*, vol. 19, pp. 251-276, 2006

Kalamkarov AL, Georgiades AV. Asymptotic homogenization models for smart composite plates with rapidly varying thicknesses: part I – theory. *Int. J. Mult. Comp. Eng*, vol. **2**(1), pp. 133-148, 2004

Kalamkarov, A.L., Georgiades, A.V., Challagulla, K., and Saha, G. Thermal and Actuation Micromechanical Modeling of Smart Composite Structures, *5th International Congress on Thermal Stresses*, Virginia Polytechnic Institute and State University, Blacksburg, Virginia, Vol. 2, pp. WA-6-5-1 – WA-6-5-4, June 2003

Kalamkarov, A.L. Georgiades, A.V. Modeling of Smart Composites on Account of Actuation, Thermal Conductivity and Hygroscopic Absorption. *Composites part B: Engineering*, vol. 33, pp. 141-152, 2002a

Kalamkarov, A.L. and Georgiades, A.V. Micromechanical Modeling of Smart Composite Structures, *Smart Mater. Struct*, vol. 11, pp. 423-434, 2002b

Kalamkarov, A.L. and Kolpakov, A.G. A new asymptotic model for a composite piezoelastic plate, *Int. J. Solids Struct*, vol. 38, pp. 6027-6044, 2001

Kalamkarov, A.L., Liu., H.Q., and MacDonald, D.O. Experimental and analytical studies of smart composite reinforcements, *Composites part B: Engineering*, vol. 29B(1), pp. 21-30, 1998a

Kalamkarov, A.L. and Liu, H,Q. A new model for a multiphase fiber-matrix composite materials, *Composites Part B: Engineering*, vol. 29B (5), pp. 643-653, 1998b

Kalamkarov, A.L. and Kolpakov, A.G. Analysis, design and optimization of composite structures, Wiley, Chichester, UK, 1997

Kalamkarov, A.L. Composite and Reinforced Elements of Construction, Chichetser: Wiley, 1992

Kannan, K.S. and Dasgupta, A. Finite element modeling of Multi-Functional composite with embedded magnetostrictive devices, Adaptive structures and composite materials: analysis and application, *International mechanical engineering congress and exposition: ASME 1994*, Chicago, Illimois, Nov 6-11, 21-28, 1994

Kaw, A. K. Mechanics of Composite Materials, CRC Press, New York, 1997

Kevin, K Tseng, and Liangsheng, Wang. Smart piezoelectric transducers for *in situ* health monitoring of concrete, *Smart Mater. Struct*, vol. 13, pp. 1017–1024, 2004

Kim, K,Y., Park, K,H., Park, H,C., Goo, N,S., and Yoon K,J. Performance evaluation of lightweight piezo-composite actuators, *Sensors Actuators : A*, vol. 120, pp. 123–9, 2005

Kohn, R.V. and Vogelius, M.A new model for thin plates with rapidly varying thickness, III: Comparison of different scalings, *Quart .J. Appl. Math*, vol. 44, pp. 35-48, 1986

Kohn, R.V. and Vogelius, M.A new model for thin plates with rapidly varying thickness, II: A convergence proof, *Quart. J. Appl. Math*, vol. 43, pp. 1-22, 1985

Kohn, RV. and Vogelius, M.A new model for thin plates with rapidly varying thickness, *Int. J. Solids Struct*, vol. 20, pp. 333-350, 1984

Kolpakov, A.G. and Kolpakova, I.G. Design of laminated composites possessing specified homogenized characteristics, *Comput. Struct*, vol. 57:4, pp. 599-604, 1995

Krishnamurthy, A,V., Anjanappa, M., Wang, Z., and Chen, Z. Sensing of delaminations in composite laminates using embedded magnetostrictive particle layers, *J. Intell. Mater. Syst. and Struct*, vol. 10, pp. 825–35, 1999

Lee, H-G. and Choi, S-B. Dynamic properties of an ER fluid under shear and flow modes, *Mater. Design*, vol. 23, pp. 69–76, 2002

Lene, F. and Leguillon, D. Homogenized constitutive law for a partially cohesive composite material, *Int. J. Solids Struct*, vol. 18:5, pp. 443-458, 1982

Mallick, P.K. Fiber reinforced composites: Materials, manufacturing, and design, Marcel Dekker, Inc., 1988

Marcelo, J.D., Ralph, C.S., and Alison, B.F, Structural Magnetic Strain Model for Magnetostrictive Transducers, IEEE transactions on magnetics, vol. 36(3), 2000

Mavko, G., Mukerji, T., and Dvorkin, J. The rock physics handbook, Cambridge University Press, Cambridge, 1998

Matthews, F.L. and Rawlings, R.D. Composite Materials: Engineering and Science, Chapman & Hall, London, 1994

Michel, J.C., Moulinec, H., and Suquet, P. Effective properties of composite materials with periodic microstructure: a computational approach, *Comput. Methods Appl. Mech. Engrg,* vol. 172, pp. 109-143, 1999

Milton, G.W. Bounds on the elastic and transport properties of two-component composites, *J. Mech. Phys. Solids*, vol. 30, pp. 177-191, 1982

Milton, G.W. Bounds on the electromagnetic, elastic, and other properties of two-component composites, *Phys. Rev. Lett.*, vol. 46, pp. 542-545, 1981

Milton, G.W. and Kohn, R.V. Variational bounds on the effective moduli of anisotropic composites, *J. Mech. Phys. Solids*, vol. 36, pp. 597-629, 1988

Mori, T. and Tanaka, K. Average stress in matrix and average energy of materials with misfitting inclusions, *Acta Metallurgica et Materialia*, vol. 21, pp. 571-574, 1973

Nagai, H. and Oishi, R. Shape memory alloys as strain sensors in composites, *Smart Mater. Struct*, vol. 15, pp. 493–498, 2006

Nayfeh, A. Perturbation methods, John Wiley & Sons, New York, 1973

Nemat-Nasser, S. and Hori, M. Micromechanics overall properties of heterogeneous solids, Amsterdam: Elsevier, 1993

Ogisu, T., Shimanuki, M., Kiyoshima, S., Takaki, J., Taketa, I., and Takeda, N. Damage behavior analysis of smart composites with embedded pre-strained SMA foils, *Smart Mater. Struct*, vol. 15, pp. 41–50, 2006

Park, S., Yun, C-B., Roh, Y., and Lee J-J. Health monitoring of steel structures using impedance of thickness modes at PZT patches, *Smart Struct. Systems*, vol. 1, pp. 339–53, 2005

Pshenichnov, G.I. Theory of thin elastic network plates and shells, Moscow: Nauka, 1982

Reddy, J.N. Mechanics of laminated composite plates, New York, CRC Press, 1997

Rees, D., Chiu, W.K., and Jones, R.A numerical study of crack monitoring in patched structures using a piezoelectric sensor, *Smart Mater. Struct*, vol. 1, pp. 202-205, 1992

Russel, W.B. On the effective moduli of composite materials: effect of fiber length and geometry at dilute concentrations, *Z Angew. Math. Phys*, vol. 24, pp. 581-600, 1973

Saadat, S., Davoodi, H., Hou, Z., Suzuki, Y., and Masouda, A. Using NiTi SMA tendons for vibration control of coastal structures, *Smart Mater. Struct*, vol. 10, pp. 697-704, 2001

Saidha, E., Naik, G.N., and Gopalakrishnan, S. An experimental investigation of a smart laminated composite beam with magnetostrictive patch for health monitoring applications, *Struct. Health Monitoring*, vol. 2, pp. 273–92, 2003

Samak, D.K., and Chopra, I., Design of High force, high displacement actuators for helicopter rotors, *Proc of the SPIE conference on Smart structures and materials: Smart Structures and Intelligent Systems*, Feb 14-16, Orlando, Florida, pp. 86-98, 2004

Sanchez-Palencia, E. Non-Homogeneous media and vibration theory. Lecture Notes in Physics, Springer-Verlag, Berlin, 1980

Schwartz, M.M. Composite materials, Volume I: Properties, nondestructive testing, and repair, Prentice Hall, 1997a

Schwartz, M.M. Composite materials, Volume II: Processing, Fabrication and Applications, Prentice Hall, 1997b

Schwartz, M.M. Composite materials Handbook, McGraw-Hill, Inc. 1992

Sendeckyj, G.P. Elastic behavior of composites. Composite Materials, Vol. 2: Mechanics of composite materials, Academic Press, New York, 1974

Seth, S, Kessler. Piezoelectric-Based In-Situ Damage Detection of Composite Materials for Structural Health Monitoring Systems, PhD. Thesis, Massachusetts Institute Of Technology, U.S.A, 2002

Seunghee ,Park., Chung-Bang, Yun., Yongrae, Roh., and Jong-Jae, Lee. PZT-based active damage detection techniques for steel bridge components, *Smart Mater. Struct*, vol. 15, pp. 957–966, 2006

Sevostianov, I., Yilmaz, N., Kushch, V., and Levin, V. Effective elastic properties of matrix composites with transversely-isotropic phases, *Int. J. Solids Struct*, vol. 42, pp. 455-476, 2005

Sevostianov, I. and Kachanov, M. Correlations between elastic moduli and thermal conductivities of anisotropic short fiber reinforced thermoplastics: theory and experimental verification, *Mater. Sci. Eng., A-360,* pp. 339-344. 2003

Sevostianov, I., Verijenko, V.E., and Kachanov, M. Cross-property correlations for short fiber reinforced composites with damage and their experimental verification, *Composites Part B*, vol. 33, pp. 205-213. 2002

Shahin, A.R., Mecki, P.H., and Hones, J.D. Vibration control using shape memory alloy wires, Adaptive structures and composite materials: Analysis and Applications, *International mechanical Engineering Congress and Exposition, ASME 1994*, Chicago, Illinois, Nov. 6-11, 227-234, 1994

Shakeri, C., Noori, M.N., and Hou, Z. Smart materials and structures: a review, *Proceeding of the 4th Materials Engineering Conference*, Vol. 2, Washington, D. C., Nov 10-14, pp. 863-876, 1996

Song, G., Qiao, P.Z., Binienda, W.K., and Zou, G.P. Active vibration damping of composite beam using smart sensors and actuators, *J. Aerosp. Engrg*, vol. 15(3), pp. 97-103, 2002

Song, O. and Librescu, L. Adaptive vibration control of rotating helicopter blades carrying a tip mass, *Proc. Of the SPIE Conference on Smart Structures and Materials: Smart Structures and Intelligent Systems*, Feb 14-16, Orlando, Florida, pp. 52-63, 1994

Sumant, P.S. and Maiti, S.K. Crack detection in a beam using PZT sensors, *Smart Mater. Struct*, vol. 15, pp. 695–703, 2006

Technical Insights, Smart Materials: Emerging Markets for Intelligent Gels, Ceramics, Alloys, and Polymer, John Wiley & Sons Inc, 1999

Teply, J.L. and Dvorak, G.J. Bounds on overall instantaneous properties of elastic-plastic composites, *J. Mech. Phys. Solid*, vol. 36, pp. 29-58, 1988

Torquato, S. Random heterogeneous media: Microstructure and improved bounds on effective properties, *Appl. Mech. Rev*, vol. 44(2), pp. 37-76, 1991

Torquato, S. and Stell, G. Microstructure of two-phase random media, *J. Chem. Phys*, vol. 82(2), pp. 980-987, 1985

Trovillion, J., Kamphaus, J., Quattrone, R., and Berman, J. Structural Integrity Monitoring Using Smart Magnetostrictive Composites, *Proceedings of International Composites EXPO'99*, Cincinnati, OH, session 22-D, pp. 1-6, 1999

Tsai, S.W. Theory of Composites Design. Dayton, OH, 1992

Vasiliev, V.V. Mechanics of composite structures, Taylor & Francis Washington, DC, 1993

Vasiliev, V.V. and Tarnopol'skii, YuM. Composite materials. Mashinostroenie, Moscow (in Russian) 1990

Vinson, J.R. The behavior of shells composed of isotropic and composite materials, Dordrecht, Kluwer, 1993

Vinson, J.R, and Sierokowski, R.L. The behavior of structures composed of composite materials, Nijhoff, Dordrecht: Kluwer Academic Publishers, 1986

Weng, G.J., Taya, M., Abé H, Eds. Micromechanics and Inhomogeneity-The T. Mura 65th Anniversary Volume, New York: Springer; 1990

Xu, Y., Otsuka, K., Toyama, N., Yoshida, H., Nagai. H., and Kishi. T. A Novel Technique for Fabricating SMA/CFRP Adaptive Composites using Ultrathin TiNi Wires, *Smart Mater. Struct*, vol. 13(1), pp. 196-202, 2004

Zeman, J. and Šejnoha, M. Numerical Evaluation of effective elastic properties of graphite fiber tow impregnated by polymer matrix, *J. Mech. Phys. Solids*, vol. 49, pp. 69-90, 2001

Zheng, X.J. and Liu, X.E. A nonlinear constitutive model for Terfenol-D rods, *J. Appl. Phys*, vol. 97(5), pp. 053901-8, 2005

Zhou, H.M., Zheng, X.J., and Zhou, Y.H. Active vibration control of nonlinear giant magnetostrictive actuators, *Smart Mater. Struct*, vol. 15, pp. 792–798, 2006

APPENDIX

Appendix A. Quantities that enter Equation [4.39], [4.64], and [4.78]

We give here the expressions for the constants α_1-α_9 that are needed to calculate the elastic ($b_{ij}^{\lambda\mu}$), piezoelectric (d_{ij}^{k}) and thermal expansion coefficients (Θ_{ij})for the unit cell of Figure 4-6. They are:

$$\alpha_1 = \frac{scC_{11}C_{26}}{h_1h_2} - \frac{s^2C_{11}C_{66}}{h_1^2} - \frac{c^2C_{16}C_{26}}{h_2^2} - \frac{scC_{12}C_{16}}{h_1h_2} + \frac{c^2C_{12}C_{66}}{h_2^2} + \frac{s^2C_{16}^2}{h_1^2}$$

$$\alpha_2 = C_{36}\left(\frac{cC_{12}}{h_2} - \frac{sC_{16}}{h_1}\right) - C_{13}\left(\frac{cC_{26}}{h_2} - \frac{sC_{66}}{h_1}\right)$$

$$\begin{aligned}
\alpha_3 = &-\frac{cC_{26}^2C_{11}C_{23}}{C_{66}h_1h_2^2} + \frac{2sC_{11}C_{26}C_{23}}{h_1^2h_2} + \frac{cC_{11}C_{26}C_{36}C_{22}}{C_{66}h_1h_2^2} - \frac{sC_{11}C_{26}^2C_{36}}{C_{66}h_1^2h_2} \\
&-\frac{s^2C_{11}C_{66}C_{23}}{ch_1^3} - \frac{sC_{11}C_{36}C_{22}}{h_1^2h_2} + \frac{s^2C_{11}C_{36}C_{26}}{ch_1^3} + \frac{c^2C_{26}^2C_{16}C_{23}}{sC_{66}h_2^3} \\
&-\frac{cC_{16}C_{26}C_{23}}{h_1h_2^2} - \frac{c^2C_{16}C_{26}C_{36}C_{22}}{sC_{66}h_2^3} + \frac{cC_{12}C_{16}C_{23}C_{26}}{C_{66}h_1h_2^2} - \frac{sC_{12}C_{16}C_{23}}{h_1^2h_2} \\
&+\frac{sC_{12}C_{16}C_{36}C_{26}}{C_{66}h_1^2h_2} - \frac{c^2C_{12}C_{23}C_{26}}{sh_2^3} + \frac{cC_{12}C_{66}C_{23}}{h_1h_2^2} - \frac{cC_{12}C_{36}C_{26}}{h_1h_2^2} \\
&-\frac{sC_{16}^2C_{23}C_{26}}{C_{66}h_1^2h_2} + \frac{s^2C_{16}^2C_{23}}{ch_1^3} + \frac{cC_{12}C_{26}^2C_{13}}{C_{66}h_1h_2^2} - \frac{2sC_{12}C_{26}C_{13}}{h_1^2h_2} - \frac{cC_{12}^2C_{26}C_{36}}{C_{66}h_1h_2^2} \\
&+\frac{s^2C_{12}C_{66}C_{13}}{ch_1^3} + \frac{sC_{12}^2C_{36}}{h_1^2h_2} - \frac{s^2C_{12}C_{36}C_{16}}{ch_1^3} - \frac{c^2C_{13}C_{26}^3}{sC_{66}h_2^3} + \frac{cC_{13}C_{26}^2}{h_1h_2^2} \\
&+\frac{c^2C_{26}^2C_{36}C_{12}}{sC_{66}h_2^3} - \frac{cC_{22}C_{16}C_{13}C_{26}}{C_{66}h_1h_2^2} + \frac{sC_{22}C_{16}C_{13}}{h_1^2h_2} + \frac{c^2C_{22}C_{13}C_{26}}{sh_2^3} \\
&-\frac{cC_{22}C_{66}C_{13}}{h_1h_2^2} + \frac{cC_{22}C_{36}c_{16}}{h_1h_2^2} + \frac{sC_{26}^2C_{16}C_{13}}{C_{66}h_1^2h_2} - \frac{s^2C_{26}C_{16}C_{13}}{ch_1^3}
\end{aligned} \quad \text{[A.1a]}$$

$$\alpha_4 = \frac{cC_{23}C_{26}C_{12}}{sC_{66}h_2^{\,2}} - \frac{C_{12}C_{23}}{h_1h_2} - \frac{C_{16}C_{23}C_{26}}{C_{66}h_1h_2} + \frac{sC_{16}C_{23}}{ch_1^{\,2}} - \frac{cC_{22}C_{13}C_{26}}{sC_{66}h_2^{\,2}} + \frac{C_{22}C_{13}}{h_1h_2} + \frac{C_{13}C_{26}^{\,2}}{C_{66}h_1h_2} - \frac{sC_{26}C_{13}}{ch_1^{\,2}}$$

$$\alpha_5 = -\frac{cC_{26}^{\,2}C_{23}}{sC_{66}h_2^{\,2}} + \frac{C_{26}C_{23}}{h_1h_2} + \frac{cC_{26}C_{22}C_{36}}{sh_2^{\,2}C_{66}} - \frac{C_{26}^{\,2}C_{36}}{C_{66}h_1h_2} + \frac{C_{23}C_{26}}{h_1h_2} - \frac{sC_{23}C_{66}}{ch_1^{\,2}} - \frac{C_{22}C_{36}}{h_1h_2} + \frac{sC_{26}C_{36}}{ch_1^{\,2}}$$

$$\alpha_6 = \frac{cC_{26}^{\,2}C_{13}}{sC_{66}h_2^{\,2}} - \frac{C_{13}C_{26}}{h_1h_2} - \frac{cC_{26}C_{36}C_{12}}{sC_{66}h_2^{\,2}} + \frac{C_{26}C_{36}C_{16}}{C_{66}h_1h_2} - \frac{C_{13}C_{26}}{h_1h_2} + \frac{sC_{13}C_{66}}{ch_1^{\,2}} + \frac{C_{36}C_{12}}{h_1h_2} - \frac{sC_{36}C_{16}}{ch_1^{\,2}} \qquad \text{[A.1b]}$$

$$\alpha_7 = \left(\frac{cC_{36}}{h_2} - \frac{sC_{13}}{h_1}\right) + \frac{\left(\frac{cC_{23}}{h_2} - \frac{sC_{36}}{h_1}\right)}{\left(\frac{sC_{66}}{h_1} - \frac{cC_{26}}{h_2}\right)}\left[\left(\frac{cC_{66}}{h_2} - \frac{sC_{16}}{h_1}\right) - \frac{C_{36}\alpha_1}{\alpha_2}\right] - C_{33}\frac{\alpha_1}{\alpha_2}$$

$$\alpha_8 = \frac{\left(\frac{cC_{23}}{h_2} - \frac{sC_{36}}{h_1}\right)}{\left(\frac{sC_{66}}{h_1} - \frac{cC_{26}}{h_2}\right)} - \frac{C_{36}\left(\frac{cC_{12}}{h_2} - \frac{sC_{16}}{h_1}\right)\left(\frac{cC_{23}}{h_2} - \frac{sC_{36}}{h_1}\right)}{\alpha_2\left(\frac{sC_{66}}{h_1} - \frac{cC_{26}}{h_2}\right)} - \frac{C_{33}\left(\frac{cC_{12}}{h_2} - \frac{sC_{16}}{h_1}\right)}{\alpha_2}$$

$$\alpha_9 = \frac{C_{36}\left(\frac{cC_{23}}{h_2} - \frac{sC_{36}}{h_1}\right)}{\alpha_2} + \frac{C_{33}\left(\frac{sC_{66}}{h_1} - \frac{cC_{26}}{h_2}\right)}{\alpha_2}$$

Appendix B. Derivation of eccentricity, e′[4.42]

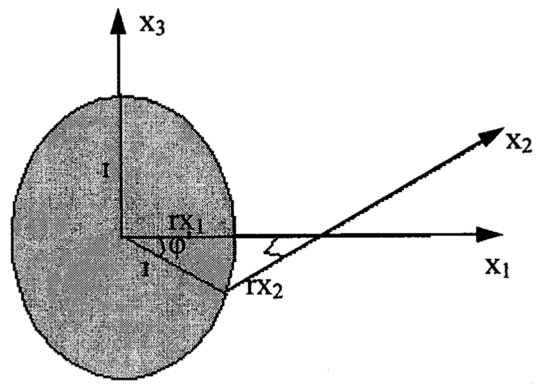

Figure A-1: Cross-sectional view of reinforcement/actuators

From the above figure, coordinates of the radius in the x_1, x_2, and x_3 direction are:

$$\begin{aligned} rx_1 &= r\sin\varphi', \\ rx_2 &= r\cos\varphi', \\ rx_3 &= r. \end{aligned} \qquad [A.2]$$

According to the microscopic scale, the above equation transforms into:

$$\begin{aligned} ry_1 &= \frac{r\sin\varphi'}{\delta h_1}, \\ ry_2 &= \frac{r\cos\varphi'}{\delta h_2}, \\ ry_3 &= \frac{r}{\delta}. \end{aligned} \qquad [A.3]$$

and the minor radius is calculated as:

$$\left(r'\right)^2 = \frac{r^2\sin^2\varphi'}{\delta^2 h_1^2} + \frac{r^2\cos^2\varphi'}{\delta^2 h_2^2} \qquad [A.4]$$

We recall that the coordinate transformation from x_1 and x_2 to y_1 and y_2 will transform the circular cross-section into an ellipse and the minor axis to major axis is given by:

$$\left(\frac{\text{minor}}{\text{major}}\right)^2 = \sqrt{1-e'^2} \qquad \text{[A.5]}$$

From Equations [A.4] and [A.5] the eccentricity of an ellipse can be determined as:

$$e' = \left[1 - \frac{\left(\sin^2\varphi' h_2^2 + \cos^2\varphi' h_1^2\right)}{h_1^2 h_2^2}\right]^{\frac{1}{2}} \qquad \text{[A.6]}$$

Appendix C. Derivation of Equation [4.43]

Equation [4.43] will be derived in a rather heuristic manner, ignoring some of the formal mathematical details.

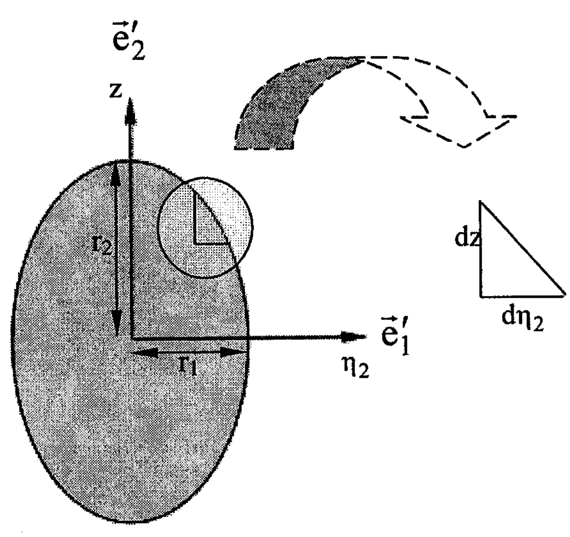

Figure A-2: Cross-sectional view of reinforcement/actuators after coordinate transformation

The equation of ellipse in terms of coordinates η_1, η_2, z is given by

$$\frac{\eta_2^2}{r_1^2} + \frac{z^2}{r_2^2} = 1 \tag{A.7}$$

Let

$$\mu = \frac{\eta_2^2}{r_1^2} + \frac{z^2}{r_2^2} \tag{A.8}$$

where μ is constant anywhere on the circumference of the ellipse. From chain rule, we write,

$$d\mu = \frac{\partial \mu}{\partial z} dz + \frac{\partial \mu}{\partial \eta_2} d\eta_2 = 0 \tag{A.9}$$

which may be expressed as:

$$d\mu = \left(\frac{\partial \mu}{\partial \eta_2} \vec{e}'_1 + \frac{\partial \mu}{\partial z} \vec{e}'_2 \right) . \left(d\eta_2 \vec{e}'_1 + dz \vec{e}'_2 \right) = 0 \tag{A.10}$$

Here,

$\frac{\partial \mu}{\partial \eta_2} \vec{e}'_1 + \frac{\partial \mu}{\partial z} \vec{e}'_2$ is a vector tangent to circumference [A.11]

and

$\partial \eta_2 \vec{e}'_1 + \partial z \vec{e}'_2$ is a vector normal to circumference. [A.12]

Thus, from Equation [A.12] the unit normal vector is calculated as:

$$\vec{n} = \frac{\frac{\partial\mu}{\partial\eta_2}\vec{e}'_1 + \frac{\partial\mu}{\partial z}\vec{e}'_2}{\left|\frac{\partial\mu}{\partial\eta_2}\vec{e}'_1 + \frac{\partial\mu}{\partial z}\vec{e}'_2\right|} = \frac{\frac{2\eta_2}{r_1^2}\vec{e}'_1 + \frac{2z}{r_2^2}\vec{e}'_2}{\sqrt{\frac{4\eta_2^2}{r_1^4} + \frac{4z^2}{r_2^4}}} \qquad [A.13]$$

After some algebraic manipulations we get:

$$\vec{n} = \frac{\frac{\eta_2}{r_1^2/r_2^2}\vec{e}'_1 + z\vec{e}'_2}{\sqrt{\frac{\eta_2^2}{r_1^4/r_2^4} + z^2}} \qquad [A.14]$$

Solving the above equation in accordance to the relationship $\left(\frac{r_1}{r_2}\right)^2 = 1 - e'^2$ and for $r_2 =$ 0.5 gives

$$n_2' = \eta_2\left[1 - (e')^2\right]^{-1}, \text{ and } n_3' = z \qquad [A.15]$$

Appendix D. Quantities that enter Equation [4.54], [4.71], and [4.83]

We give here the expressions for the constants $\Lambda_1 - \Lambda_6$ that are needed to calculate the $b_{ij}^{*\lambda\mu}$ functions for the unit cell of Figure 4-3 They are:

$$\Lambda_1 = -\frac{s^2c}{h_1{}^2h_2} + \Delta_7 A_1 + A_2\Delta_7 + \frac{\Delta_9 A_3}{\Delta_4} + [A_4\Delta_7 - A_5\Delta_9]A_6 + \frac{2scC_{23}\Delta_{12}}{C_{13}\Delta_4\Delta_{13}}[A_4\Delta_7 - A_5\Delta_9]$$

$$\Lambda_2 = A_8\Delta_{10} - A_9\Delta_{10} - \frac{\Delta_{11}A_{10}}{\Delta_4} + [A_4\Delta_{10} - A_5\Delta_{11}]A_{11} - \frac{C_{33}A_{12}}{h_2}$$

$$\Lambda_3 = A_{13}\Delta_7 - A_{14}\Delta_7 + A_{15}\Delta_9 + A_{16}\Delta_9 - [A_{17}\Delta_7 - A_{18}\Delta_9]A_{19}$$

$$\Lambda_4 = \Delta_{10}A_1 + A_2\Delta_{10} + \frac{\Delta_{11}A_3}{\Delta_4} + [A_4\Delta_{10} - A_5\Delta_{11}]A_6 - \frac{C_{33}A_7}{h_1} + \frac{2scC_{23}\Delta_{12}}{C_{13}\Delta_4\Delta_{13}}[A_4\Delta_{10} - A_5\Delta_{11}] - \frac{2scC_{23}\Delta_{12}}{C_{13}\Delta_4\Delta_{13}}\left[\frac{C_{33}}{h_1h_2}\right] \qquad [A.16]$$

$$\Lambda_5 = A_8\Delta_7 - A_9\Delta_7 - \frac{\Delta_9 A_{10}}{\Delta_4} + [A_4\Delta_7 - A_5\Delta_9]A_{11} + \frac{c^3}{h_2{}^3}$$

$$\Lambda_6 = \Delta_{10}A_{13} - A_{14}\Delta_{10} + A_{15}\Delta_{11} + A_{16}\Delta_{11} - [A_{17}\Delta_{10} - A_{18}\Delta_{11}]A_{19} + \frac{2scC_{33}A_{19}}{h_1h_2} + \frac{2scC_{33\lambda\mu}}{h_1h_2}$$

where

$$\Delta_1 = C_{23}(cC_{16}h_1 - sC_{11}h_2) - C_{13}(cC_{26}h_1 - sC_{12}h_2)$$

$$\Delta_2 = C_{23}(cC_{12}h_1 - sC_{16}h_2) - C_{13}(cC_{22}h_1 - sC_{26}h_2)$$

$$\Delta_3 = C_{23}B_{11}^{\lambda\mu} - C_{13}B_{22}^{\lambda\mu} - C_{23}C_{11\lambda\mu} + C_{13}C_{22\lambda\mu}$$

$$\Delta_4 = \Delta_1(sC_{66}h_2 - cC_{26}h_1) + \Delta_2(cC_{66}h_1 - sC_{16}h_2) \qquad [A.17a]$$

$$\Delta_5 = \frac{cC_{16}h_1 - sC_{11}h_2}{cC_{66}h_1 - sC_{16}h_2} - \frac{\Delta_1(sC_{66}h_2 - cC_{26}h_1)(cC_{16}h_1 - sC_{11}h_2)}{\Delta_4(cC_{66}h_1 - sC_{16}h_2)} - \frac{\Delta_1(cC_{12}h_1 - sC_{16}h_2)}{\Delta_4}$$

$$\Delta_6 = -\frac{scC_{45}}{h_1 h_2} + \frac{s^2 C_{55}}{h_1{}^2} - \frac{scC_{45}}{h_1 h_2} + \frac{c^2 C_{44}}{h_2{}^2}$$

$$\Delta_7 = \left[C_{55} + \left(\frac{cC_{45}h_1 - sC_{55}h_2}{h_1^2 h_2^2}\right)\left(\frac{sC_{55}h_2 - cC_{45}h_1}{\Delta_6}\right)\right]\left[1 - (e')^2\right]$$

$$\Delta_8 = 1 - \frac{\Delta_1 (sC_{66}h_2 - cC_{26}h_1)}{\Delta_4}$$

$$\Delta_9 = \left[C_{45} + \left(\frac{cC_{45}h_1 - sC_{55}h_2}{h_1^2 h_2^2}\right)\left(\frac{sC_{45}h_2 - cC_{44}h_1}{\Delta_6}\right)\right]\left[1 - (e')^2\right]$$

$$\Delta_{10} = \frac{cC_{36}h_1 - sC_{13}h_2}{h_1 h_2} \; ; \; \Delta_{11} = \frac{cC_{23}h_1 - sC_{36}h_2}{h_1 h_2}$$

$$\Delta_{12} = (sC_{66}h_2 - cC_{26}h_1)(cC_{16}h_1 - sC_{11}h_2) + (cC_{66}h_1 - sC_{16}h_2)(cC_{12}h_1 - sC_{16}h_2)$$

$$\Delta_{13} = 1 - \frac{c_{36}\Delta_5}{c_{13}} \; ; \; \Delta_{14} = sC_{66}h_2 - cC_{26}h_1 \; ; \; \Delta_{15} = cC_{66}h_1 - sC_{16}h_2$$

[A.17b]

$$A_1 = \frac{s^2 h_2 \Delta_8}{h_1 \Delta_{15}} \; ; \; A_2 = \frac{2scC_{23}\Delta_{14}}{\Delta_4} \; ; \; A_3 = 2scC_{23}\Delta_{15} - \frac{s^2 \Delta_1 h_2}{h_1} \; ;$$

$$A_4 = \frac{C_{36}\Delta_8}{\Delta_{15}}$$

$$A_5 = \frac{C_{36}\Delta_1}{\Delta_4} \; ; \; A_6 = \frac{s^2 h_2 \Delta_5}{h_1 C_{13}\Delta_{13}} - \frac{2sc}{C_{13}\Delta_{13}} \; ; \; A_7 = \frac{s^2 \Delta_5}{h_1 C_{13}\Delta_{13}} - \frac{2sc}{h_2 C_{13}\Delta_{13}}$$

$$A_8 = \frac{c^2 h_1 \Delta_8}{h_2 \Delta_{15}} \; ; \; A_9 = \frac{2scC_{13}\Delta_{14}}{\Delta_4} \; ; \; A_{10} = 2scC_{13}\Delta_{15} + \frac{c^2 \Delta_1 h_1}{h_2}$$

$$A_{11} = \frac{c^2 \Delta_5 h_1}{h_2 C_{13}\Delta_{13}} - \frac{2sc\Delta_{12}}{\Delta_{13}\Delta_4} \; ; \; A_{12} = \frac{c^2 \Delta_5}{h_2 C_{13}\Delta_{13}} - \frac{2sc\Delta_{12}}{h_1 \Delta_{13}\Delta_4}$$

$$A_{13} = \frac{(-C_{23}C_{11\lambda\mu} + C_{13}C_{22\lambda\mu})2sc\Delta_{14}}{\Delta_4} \; ; \; A_{14} = \frac{2sc\Delta_8 C_{12\lambda\mu}}{\Delta_{15}}$$

$$A_{15} = \frac{(-C_{23}C_{11\lambda\mu} + C_{13}C_{22\lambda\mu})2sc\Delta_{15}}{\Delta_4} \; ; \; A_{16} = \frac{2sc\Delta_1 C_{12\lambda\mu}}{\Delta_4} \; ;$$

$$A_{17} = \frac{2sc\Delta_8 C_{36}}{\Delta_{15}}$$

$$A_{18} = \frac{2sc\Delta_1 C_{36}}{\Delta_4} \; ; \; A_{19} = -\frac{C_{11\lambda\mu}}{C_{13}\Delta_{13}} + \frac{\Delta_5 C_{12\lambda\mu}}{C_{13}\Delta_{13}} + \frac{(C_{23}C_{11\lambda\mu} - C_{13}C_{22\lambda\mu})\Delta_{12}}{C_{13}\Delta_4\Delta_{13}} \qquad \text{[A.17c]}$$

Appendix E. Derivation of Equation [4.57], [4.74], and [4.86]

The effective coefficients of the homogenized plate are obtained through the integration over the volume of the entire unit cell Ω_δ (with volume equal to $|\Omega|$) according to Equation [4.14]. Let $\delta^3 V$ be the volume of the reinforcing bar within the unit cell (Figure 4-5). The volume of the unit cell can be readily calculated from Figure 4-5 as $\delta^3 h_1 h_2$. Then, the $\langle b_{ij}^{\lambda\mu} \rangle$ effective coefficients are calculated from:

$$\langle b_{ij}^{\lambda\mu} \rangle = \frac{1}{|\Omega|} \int_{|\Omega|} b_{ij}^{\lambda\mu} dv \qquad \text{[A.18]}$$

where $\int_{|\Omega|} b_{ij}^{kl} dv$ is the volume of the reinforcing bar. Substituting the volume of the unit cell and reinforcing bar in the above equation gives

$$\langle b_{ij}^{\lambda\mu} \rangle = \frac{V}{h_1 h_2} b_{ij}^{\lambda\mu} \qquad \text{[A.19]}$$

Note that due to the symmetry of the circular cross-section with respect to the shell middle surface, the skew-symmetrical coefficients $\langle zb_{ij}^{\lambda\mu} \rangle$, $\langle b_{ij}^{*\lambda\mu} \rangle$ vanishes.

Let us now derive the equation to find the effective coefficients for $\left\langle zb_{ij}^{*\lambda\mu}\right\rangle$ problem. The $\left\langle zb_{ij}^{*\lambda\mu}\right\rangle$ effective can be calculated from

$$\left\langle zb_{ij}^{*\lambda\mu}\right\rangle = \frac{1}{|\Omega|}\int_{|\Omega|} zb_{ij}^{*\lambda\mu} dv = \frac{1}{|\Omega|}\left[\int_{|\Omega|} zb_{ij}^{*\lambda\mu} dv\right] \qquad \text{[A.20]}$$

First we will consider the term within the bracket of Equation [A.20]. Rewriting this term in terms of length (L) of the fiber and area gives:

$$B_{ij}^{\lambda\mu} L \int_{area} z^2 da, \text{ where } L = \frac{4\delta V}{\Pi} \qquad \text{[A.21]}$$

Substituting Equation [A.21] into [A.20] results in:

$$\left\langle zb_{ij}^{*\lambda\mu}\right\rangle = \frac{1}{|\Omega|}\frac{4\delta V}{\Pi} B_{ij}^{\lambda\mu} \int_{area} z^2 da \qquad \text{[A.22]}$$

The above equation can be rewritten using Equation [4.5] as:

$$\left\langle zb_{ij}^{*\lambda\mu}\right\rangle = \frac{1}{|\Omega|}\frac{4V}{\Pi\delta} B_{ij}^{\lambda\mu} \int_0^{\delta/2}\int_0^{2\Pi} r^2 \sin^2\theta (r dr d\theta) \qquad \text{[A.23]}$$

Solving Equation [A.23] gives the effective coefficients as:

$$\left\langle zb_{ij}^{*\lambda\mu}\right\rangle = \frac{V}{16h_1h_2} B_{ij}^{\lambda\mu} \qquad \text{[A.24]}$$

Appendix F. Quantities that enter Equation [6.26]

$$
\begin{aligned}
A_1 &= q_{21}^2 C_{11} + q_{22}^2 C_{66} + q_{23}^2 C_{55} \\
A_2 &= q_{21} q_{31} C_{11} + q_{22} q_{32} C_{66} + q_{23} q_{33} C_{55} \\
A_3 &= q_{21} q_{22} C_{12} + q_{21} q_{22} C_{66} \\
A_4 &= q_{21} q_{32} C_{12} + q_{22} q_{31} C_{66} \\
A_5 &= q_{21} q_{23} C_{13} + q_{21} q_{23} C_{55} \\
A_6 &= q_{21} q_{33} C_{13} + q_{23} q_{31} C_{55} \\
A_7 &= q_{21} C_{11kl} + q_{22} C_{12kl} + q_{23} C_{13kl} \\
A_8 &= q_{21} q_{31} C_{11} + q_{22} q_{32} C_{66} + q_{23} q_{33} C_{55} \\
A_9 &= q_{31}^2 C_{11} + q_{32}^2 C_{66} + q_{33}^2 C_{55} \\
A_{10} &= q_{31} q_{22} C_{12} + q_{21} q_{32} C_{66} \\
A_{11} &= q_{31} q_{32} C_{12} + q_{32} q_{31} C_{66} \\
A_{12} &= q_{31} q_{23} C_{13} + q_{21} q_{33} C_{55} \\
A_{13} &= q_{31} q_{33} C_{13} + q_{33} q_{31} C_{55} \\
A_{14} &= q_{31} C_{11kl} + q_{32} C_{12kl} + q_{33} C_{13kl} \\
A_{15} &= q_{21} q_{22} C_{66} + q_{21} q_{22} C_{12} \\
A_{16} &= q_{21} q_{32} C_{66} + q_{22} q_{31} C_{12} \\
A_{17} &= q_{21}^2 C_{66} + q_{22}^2 C_{22} + q_{23}^2 C_{44} \\
A_{18} &= q_{21} q_{31} C_{66} + q_{22} q_{32} C_{22} + q_{23} q_{33} C_{44} \\
A_{19} &= q_{22} q_{23} C_{23} + q_{22} q_{23} C_{44} \\
A_{20} &= q_{22} q_{33} C_{23} + q_{23} q_{32} C_{44} \\
A_{21} &= q_{21} C_{12kl} + q_{22} C_{22kl} + q_{23} C_{23kl} \\
A_{22} &= q_{31} q_{22} C_{66} + q_{21} q_{32} C_{12} \\
A_{23} &= q_{31} q_{32} C_{66} + q_{32} q_{31} C_{12} \\
A_{24} &= q_{21} q_{31} C_{66} + q_{22} q_{32} C_{22} + q_{23} q_{33} C_{44} \\
A_{25} &= q_{31}^2 C_{66} + q_{32}^2 C_{22} + q_{33}^2 C_{44} \\
A_{26} &= q_{32} q_{23} C_{23} + q_{22} q_{33} C_{44} \\
A_{27} &= q_{32} q_{33} C_{23} + q_{33} q_{32} C_{44} \\
A_{28} &= q_{31} C_{12kl} + q_{32} C_{22kl} + q_{33} C_{23kl} \\
A_{29} &= q_{21} q_{23} C_{55} + q_{21} q_{23} C_{13} \\
A_{30} &= q_{21} q_{33} C_{55} + q_{23} q_{31} C_{13}
\end{aligned}
\qquad \text{[A25a]}
$$

$$
\begin{aligned}
A_{31} &= q_{22}q_{23}C_{44} + q_{22}q_{23}C_{23} \\
A_{32} &= q_{22}q_{33}C_{44} + q_{23}q_{32}C_{23} \\
A_{33} &= q_{21}{}^{2}C_{55} + q_{22}{}^{2}C_{44} + q_{23}{}^{2}C_{33} \\
A_{34} &= q_{21}q_{31}C_{55} + q_{22}q_{32}C_{44} + q_{23}q_{33}C_{33} \\
A_{35} &= q_{21}C_{13kl} + q_{22}C_{23kl} + q_{23}C_{33kl} \\
A_{36} &= q_{31}q_{23}C_{55} + q_{21}q_{33}C_{13} \\
A_{37} &= q_{31}q_{33}C_{55} + q_{33}q_{31}C_{13} \\
A_{38} &= q_{23}q_{32}C_{44} + q_{22}q_{33}C_{23} \\
A_{39} &= q_{32}q_{33}C_{44} + q_{33}q_{32}C_{23} \\
A_{40} &= q_{21}q_{31}C_{55} + q_{22}q_{32}C_{44} + q_{23}q_{33}C_{33} \\
A_{41} &= q_{31}{}^{2}C_{55} + q_{32}{}^{2}C_{44} + q_{33}{}^{2}C_{33} \\
A_{42} &= q_{31}C_{13kl} + q_{32}C_{23kl} + q_{33}C_{33kl}
\end{aligned}
\qquad \text{[A25b]}
$$